The vulnerability of low-arsenic aquifers in Bangladesh: a multi-scale geochemical and hydrologic approach

Ivan Mihajlov

Submitted in partial fulfillment of the
requirements for the degree of
Doctor of Philosophy
in the Graduate School of Arts and Sciences

COLUMBIA UNIVERSITY

2014

ABSTRACT

The vulnerability of low-arsenic aquifers in Bangladesh:

a multi-scale geochemical and hydrologic approach

Ivan Mihajlov

The worldwide natural occurrence of high levels of arsenic (As) in groundwater and its deleterious effects on human health have inspired a great amount of related research in public health and geosciences internationally. With >100 million people in South and Southeast Asia exposed to >10 μg/L As in shallow groundwater that they use for drinking, the installation of deeper, low-As wells has emerged as a major strategy for lowering the exposure. As the magnitude of deep pumping continues to increase, this work focuses on the geochemical and hydrologic questions surrounding the vulnerability and sustainability of low-As aquifers in Bangladesh, the country most affected by As crisis. In an effort to better understand the residence time of groundwater in low-As aquifers at depth, radiocarbon (^{14}C) and ^{13}C in dissolved inorganic carbon, tritium (^{3}H), stable isotopes of hydrogen (^{2}H) and oxygen (^{18}O), and noble gas concentrations were measured across a ~25 km^2 area of Araihazar, ~30 km east of Dhaka. Groundwater from >120 m depth is shown to be ~10,000 years old and its isotopic signatures indicate that recharge occurred at the time of changing climate from the late Pleistocene to early Holocene, with little recharge occurring since. In contrast, the intermediate depth low-As aquifers (<120 m) have a heterogeneous distribution of groundwater chemistry and ages, and contain groundwater recharged <60 years ago in certain locations. In one such area surrounding a small village, the effects that subsurface clay layer distribution has on

recharge patterns and redox status of the intermediate aquifer was investigated. The relevant hydrogeologic and geochemical processes that led to documented failures of a community well at the site were assessed using a combination of solid and water phase geochemistry with tritium-helium ($^3H/^3He$) dating, hydraulic head monitoring, and pumping tests. Organic matter seeping from a compressible clay layer, which is subject to a pumping-induced, downward hydraulic gradient, reduces iron oxides and helps release As in the grey, upper part of the intermediate aquifer. No recent recharge was detected by ^3H measurements in the upper, grey sand layer, however a layer of orange sand beneath it contains groundwater that was recharged 10-60 years ago. This groundwater laterally bypasses the confining clay layer to recharge the middle of the aquifer and contains dissolved As levels of <10 μg/L. In this particular case, the pore water that leaches from clay layers contributes to As contamination, whereas the lateral recharge with shallow groundwater coincides with the low-As depth. Thus, clay layers may not always protect the low-As aquifers from As contamination, even if they can block direct vertical recharge with shallow groundwater enriched in As and organics. Finally, the adsorption of As to aquifer sediments, as a natural mechanism of the low-As aquifer defense against contamination, was assessed in the field via a column study. The column experiments were conducted by pumping shallow, high-As groundwater through freshly collected sediment cores to quantify the retardation of As transport through the aquifer. This study demonstrated an elegant method of assessing contaminant transport under nearly *in situ* conditions that resulted in sorption estimates similar to those made by field studies using more challenging methods or located at hard-to-find sites with convenient flow patterns. My work, therefore, contributed to a better understanding of low-As aquifers in

Bangladesh from the perspectives of both the groundwater flow and water-sediment interactions on various scales, and it integrated methods that can be employed elsewhere to characterize aquifers and study contaminant transport.

Table of Contents

List of Figures

List of Tables

Acknowledgements

I owe the most gratitude and appreciation to my scientific advisers, Martin Stute, Alexander van Geen, Benjamín Bostick, Peter Schlosser, and Yan Zheng, for their support and guidance throughout the past six years. They had to put up with a great deal of indecisiveness on my part, tolerate my last-minute work style, and occasionally remind me of what matters the most in research and life. I was truly blessed to work with such a diverse group of individuals, who are not only good scientists with unique points of view, but also caring and kind people. They were there for me in tough moments, and I was very lucky to have traveled the world with most of them. Martin accompanied me in almost all of my field trips to Bangladesh, introduced me to fieldwork, and taught me hydrology and mechanical skills. He was always a great source of advice and support; I just wish he could have delighted more in the culinary aspects of our Bangladesh experience. Lex had a way like no one else to motivate me to research deeper into every question, intuitively suggest field and lab work that I looked over, and get me excited to think, re-analyze and write. Ben brought an all-round and refreshing point of view on geochemical aspects of my work when he joined the group, and working with him has been the most fun, whether sampling street food or staying up all night at the synchrotron. Peter always amazed me with his ability to home in quickly on the most important aspects of my research, to provide insightful comments, and to raise the questions I needed to address better. When I was just starting with my research, Yan was there to guide my experiments, bring life to our discussions, and teach me laboratory work.

None of this work would have been possible without the generous support of the Columbia Superfund Research Program (SRP) funded by the National Institute of Environmental Health and Safety (NIEHS) and led by Joseph Graziano. The Columbia SRP has worked in Bangladesh for over a decade and funded my entire PhD career. The participation of our collaborator from Dhaka University, Kazi Matin Ahmed, ensured that our projects would run smoothly and safely. I would also like to thank my defense committee members, Steven Chillrud and Zoltan Szabo, for their commitment of attention and time to discuss my findings.

There were many people responsible for this dissertation becoming a reality, and I can only mention but a few here. Karrie Radloff is responsible for the success of my earliest field trips to Bangladesh; she helped me walk the ropes of fieldwork, and deserves the title of an honorary adviser for the care and concern she showed when I was trying to figure out what I was doing. The involvement of Brian Mailloux was just as important, as he provided thoughtful and often subtle advice in navigating the waters of analysis, research communication, and writing. When it came to running the dreadful ICP-MS, fixing the lab equipment, and discussing just about anything, Jacob Mey was a ready and helpful partner. Many of the lab hours became shorter with my friends, Jing Sun, Stephen Barten, Masha Pitiranggon, Lynnette Pitcher, and Rajib Mozumder.

When I think about how I came to get involved in my projects and pursue a doctorate in the first place, I must say it was really the prospect of impacting the quality of water supply in Bangladesh that motivated me, and the support of my dear friends that helped me go on. The travel and work in Bangladesh was an exciting, pleasant, and humbling experience for me, and all the effort makes sense when I remember the happy

faces of Shahidullah Shahud and his wife and three boys, the excitement of Peter Knappett on my first trip, the philosophy of Imtiaz Choudhury, the care of Babu Bhai, and the helping hands of Md. “Palash” Rezaul Huq, Majibul “Shoikat” Hosain, Md. “Liton” Jahangir Alam, Milon, and Razzak. Stanislav Presolski and Vu Hong are guilty of my going to graduate school in the first place, while Truett Lee Vaigneur, Jr., Miguel Torres Carlos, and Guleed Ali provided a constant encouragement and made life in NYC so much more beautiful.

Dedication

My dearest Dad,

supportive and proud,

You must be smiling

from a light cloud

Chapter 1:
Introduction

1.1 Exposure to arsenic in groundwater

Arsenic is a toxic metalloid and a widespread contaminant of drinking water causing public health problems in South and Southeast Asia, China and Taiwan, Chile, Argentina, Mexico, and the USA (Argos et al., 2010). In South and Southeast Asia, including Bangladesh, India, Pakistan, Nepal, Myanmar, China, Cambodia and Vietnam, the number of people drinking shallow groundwater with arsenic (As) levels >10 μg/L, the World Health Organization limit, has been estimated at >100 million, (Ravenscroft et al., 2009). In Bangladesh alone, being the most severely affected country, an estimated 57 million people, comprising 46% of the total population in 1999, were exposed to >10 μg/L in groundwater from shallow tubewells (BGS and DPHE, 2001). The proliferation of PVC-cased, hand-pumped, shallow tubewells (~5-20 m deep), relatively inexpensive and simple to install, occurred since the 1970s when UNICEF concentrated its efforts on providing pathogen-free water to prevent water-borne diseases associated with drinking surface water from rivers and ponds. The resulting installation of >10 million shallow tubewells in Bangladesh prompted, due to the exposure to As, what has been called "the largest mass poisoning of a population in human history" (Smith et al., 2000). The effects of exposure to As include skin lesions, liver problems, cancers of skin and internal organs such as kidney, bladder, and lung, increased overall mortality rate, cardiovascular disease, diabetes, and neurological issues, including effects on intellectual development of children (Argos et al., 2010; Smith et al., 2000; Wasserman et al., 2007; Yu et al., 2003).

The primary route of exposure is via drinking water, but exposure through eating rice with elevated As concentrations in the grain can also be significant in the regional cuisines where rice is a major source of daily carbohydrates (Duxbury et al., 2003; Meharg and Rahman, 2003; Panaullah et al., 2009). Eating rice can in fact be a dominant source of As exposure if the concentrations of As in drinking water are <50-100 μg/L (Meharg and Rahman, 2003; Panaullah et al., 2009; van Geen et al., 2006). Pumping of the same high-As shallow groundwater used for drinking to irrigate winter rice crops during dry season has been responsible for the "green revolution", which allowed Bangladesh to be largely self-sufficient in food production, given that rice and other crops could be harvested multiple times a year from the same field. However, due to irrigation with high-As groundwater, soils in irrigated fields have been progressively accumulating As (Dittmar et al., 2010), reaching up to 45-70 ppm in the most affected zones (Meharg and Rahman, 2003; Panaullah et al., 2009). Despite the release by monsoonal flooding of 13-62% of As added to the paddy soil during irrigation (Roberts et al., 2010), the net accumulation of As in the soils continues and has been shown to reduce rice yields by >50% in highly affected soil and greatly increase As content in the rice-straw used to feed cattle (Panaullah et al., 2009). The reductions in rice yields and increases in As content of food, therefore, call the sustainability of irrigation by shallow groundwater into question (Ravenscroft et al., 2013).

1.2 Mechanisms of As release

The regions of South and Southeast Asia affected by high As in shallow groundwater coincide with low-lying, topographically flat river floodplains and deltas of

major Himalayan rivers, including the Ganges, the Brahmaputra, the Meghna, the Mekong, the Irrawaddy and the Red River, where major aquifers made of unconsolidated sediments were deposited in the early Holocene (Fendorf et al., 2010; Ravenscroft et al., 2009; Winkel et al., 2011). These sediments are not particularly high in total As content compared to other locations in the world, but it is rather the specific geochemical conditions that dictate the mobilization of As from sediment to groundwater (BGS and DPHE, 2001; Fendorf et al., 2010). The primary source of As in the Himalayan rocks are likely coal seams and sulfide minerals (Acharyya et al., 1999) that become oxidized when exposed to the atmosphere and transfer their As to secondary mineral phases, such as Fe oxides that coat sediment grains and accumulate especially in the fine-grained fraction (BGS and DPHE, 2001; Dowling et al., 2002; Fendorf et al., 2010; Welch and Lico, 1998). Once deposited with riverine and deltaic sediments, these As-rich Fe oxides are within an environment where groundwater flow is very slow due to the flat topography and oxygen can be quickly depleted if sufficient organic matter is present to drive microbial respiration. Under reducing conditions, As release is thought to occur by microbial reduction of Fe oxides coupled to oxidation of available organic matter (BGS and DPHE, 2001; Harvey et al., 2002; Islam et al., 2004; McArthur et al., 2001; Nickson et al., 2000). High As in groundwater does not necessarily always correlate with high dissolved Fe, possibly due to the formation of new Fe phases that preferentially retain Fe or As (Horneman et al., 2004; Tufano and Fendorf, 2008; van Geen et al., 2004). The release of As may also be enhanced by concomitant reduction of As(V) to more mobile As(III) (BGS and DPHE, 2001; Fendorf et al., 2010; Kocar et al., 2006; Tufano et al., 2008), and by the release of PO_4 from Fe oxides that can compete with As for the

remaining sorption sites (BGS and DPHE, 2001; Fendorf et al., 2010; McArthur et al., 2004; Stollenwerk et al., 2007). Other sources of As supply to groundwater directly, or to the Fe oxides in aquifer sediments, might also include the oxidation of detrital and authigenic As-bearing sulfides from surface soils (Polizzotto et al., 2006), and weathering of micas (Dowling et al., 2002), or biotite in particular (Itai et al., 2008).

The primary As release mechanism by reductive dissolution of Fe oxyhydroxides requires a source of organic matter (OM) to sustain reduction, and the exact source of this OM has been a matter of contention. Internal sources included OM deposited at the same time as the sediment. Although old OM co-deposited with the sediment can be recalcitrant because the labile OM is preferentially metabolized, a number of researchers identified organic-rich peat layers as a likely source of OM that drives reductive processes in shallow aquifers (Dowling et al., 2002; McArthur et al., 2004; McArthur et al., 2001; Meharg et al., 2006; Nickson et al., 1998; Nickson et al., 2000; Zheng et al., 2004). Rowland et al. (2006) postulated that the organics associated with petroleum deposits seeping from deeper, thermally mature sediments as a potential source of microbial food. Other researchers pointed to the possibility of advection of organic carbon from organic-rich environments at the surface, such as wetlands and ponds, which might have been accelerated by irrigation pumping over the past 20-30 years (Harvey et al., 2002; Neumann et al., 2010; Polizzotto et al., 2008), thus underscoring the anthropogenic influence on high As levels in groundwater. Such a view has been disputed by others seeing little or no correlation of subsurface As peak to the markers of recent recharge, such as bomb-released ^{14}C and ^{3}H, or a solid correlation between pond water stable isotopes and groundwater at depth of peaking As concentrations (Aggarwal et al.,

2003; Klump et al., 2006; Sengupta et al., 2008; van Geen et al., 2003b). A recent study of ^{14}C in microbial DNA by Mailloux et al. (2013) demonstrated that OM advected from the surface is preferentially metabolized by microbes, but the transport of organics appears slow and bomb ^{14}C-labeled OM has not yet reached the depth of maximum As levels, thus the release of As predates human interference. Ultimately, it is likely that multiple different sources of OM are present in Holocene aquifers and that their relative importance varies between different study locations, thus it may be incorrect to make a generalizing conclusion for the whole basin from a few points at one site. In that context, the human impact via irrigation and pond construction could have exacerbated the groundwater As problem in shallow aquifer at certain locations, but not elsewhere.

At least two other important processes control the distribution of As in the subsurface, known to be highly heterogeneous even on village scales (van Geen et al., 2003c). First, the occurrence of As in sulfide minerals has been identified in field samples (Lowers et al., 2007; Polizzotto et al., 2006), and enhanced incorporation of As into mixed Fe(II)/Fe(III) phases has been observed under sulfate-reducing conditions in the laboratory (Kocar et al., 2006; Saalfield and Bostick, 2009). The release of As is likely to be inhibited, therefore, by SO_4 reduction in the areas where enough SO_4 supply to the groundwater exists, as inferred by Buschmann and Berg (2009). Second, the velocity of groundwater flow is likely to control the amount of As in the dissolved phase by limiting the As accumulation time in groundwater and/or by reducing the pool of labile As in the sediment with repeated flushing, both of which might have resulted in the observed correlation of shallow groundwater age with As concentrations in our field area (Stute et al., 2007). The occurrence of lower As levels in areas of higher hydraulic conductivity of

surface sediments (Aziz et al., 2008), and therefore greater recharge, corroborates this evidence, as does the co-location of higher groundwater As concentrations with the clay-capped areas (Weinman et al., 2008). On a larger scale, countrywide As distribution might be controlled by the amount of groundwater flow that progressively flushes aquifers of their As, as illustrated by van Geen et al. (2008) under an assumption of As sorption equilibrium. This could also help explain the relatively lower As concentrations in the north of Bangladesh, where both the larger grain sizes and steeper topography allow faster groundwater flow, compared to the higher concentrations in the very flat south of the country (BGS and DPHE, 2001).

1.3 Deeper, low-As aquifers to mitigate As crisis

The efforts to reduce As exposure via drinking and cooking water have involved the construction of shallow dug wells, piped water systems, arsenic removal units/filters, rainwater collection, well switching to a safe (low-As) shallow well, and deep community well installation. Whilst none of these intervention methods have thus far succeeded in protecting the majority of people, the two mitigation strategies currently reaching the greatest number of people, based on available surveys (Ahmed et al., 2006; Opar et al., 2007), are simple well switching and deep community well construction. For example, when informed about the As status of their well and the adverse health effects of As, the largest proportion (29-36%) of households with unsafe wells in the study areas switched to an alternative, low-As well within walking distance, or installed a new well. This rate of well switching may not, however, be generalizable to the non-study areas, and the replacement of existing wells by new wells with unknown levels of As is ongoing at the

same or higher rate, thus potentially undermining the efforts to reduce mass poisoning with arsenic.

The amount of well switching depended in part on the availability of low-As wells in the vicinity, but there are villages where such wells were scarce. The alternative, and recently increasingly popular, method of reducing As exposure has been the installation of deeper, shared wells often referred to as “community wells”. By 2006, an estimated 12% of the exposed population had switched to tens of thousands of installed community well for drinking water supply (Ahmed et al., 2006). The users of community wells are willing to walk up to 150 m distance to fetch water several times a day despite the availability of a (high As) shallow well in their yard (van Geen et al., 2003a). Deeper wells, both in the intermediate depth range (35-150 m) and deeper than 150 m, have been shown to provide groundwater of stable quality and low in As over a period of 5-13 years, thus justifying the major efforts by government and non-governmental organizations to install more wells (Ravenscroft et al., 2013; van Geen et al., 2007). Current estimates indicate that 100,000-200,000 community wells at depth >150 m have been installed in Bangladesh (JICA and DPHE, 2010). Ravenscroft et al. (2013) argue that the exploitation of deeper aquifers should be further expanded to include crop irrigation supply, as well as more widespread mechanized pumping systems for household supply. Such a development would be ethically justifiable if it provided safe drinking water and harvests of sufficient yield and crop quality in the short term, thus putting a stop on the current mass poisoning and buying some time until alternative water supply solutions can be found.

Deeper aquifers, despite what their name might suggest, are not well defined by depth, as the vertical extent of the shallow, Holocene aquifer varies largely across Bangladesh and the larger Bengal basin (Aggarwal et al., 2000; BGS and DPHE, 2001; Burgess et al., 2010). Instead, "deeper" aquifers are often defined by being low in As and by additional characteristics such as their sediment age, geochemical, or hydrologic properties. In terms of sediment age, aquifers of Pleistocene age normally host low-As groundwater and their upper boundary can vary from the present-day land surface to several 100s of meters below ground level (bgl). The famous Barind and Madhupur tracts, or Pleistocene terraces, located in northern and central Bangladesh, represent Pleistocene sediment that was not eroded by the Ganges or the Brahmaputra during the sea level lowstand, and have likely been uplifted by tectonic activity (BGS and DPHE, 2001; Burgess et al., 2010; Goodbred and Kuehl, 2000b; Khandoker, 1987; Ravenscroft et al., 2005). Both host aquifers with low dissolved As. The Madhupur terrace underlies the capital of Bangladesh, Dhaka, and its surface outcrop terminates just north of our field area of Araihazar upazila (one out of ~500 "counties" in Bangladesh).

In terms of sediment geochemistry, although shallow and deeper sediments contain a similar amount of total As, the deeper sediment has a low amount (<1 mg/kg) of easily desorbed, mobilizable As (Dhar et al., 2011; Zheng et al., 2005), which translates into a correspondingly low groundwater As content due to the sorption equilibrium between the adsorbed and dissolved As (Radloff et al., 2011; van Geen et al., 2008). If in the Pleistocene sediment, the low amount of readily available As is thought to have resulted from higher hydraulic gradients at times of lower sea level. Higher groundwater flow velocities under such a hydrologic regime would have flushed

dissolved As out, and depleted the sediment of its labile As and organic C pools (BGS and DPHE, 2001; McArthur et al., 2008; Ravenscroft et al., 2005). Faster flows, as well as the subaerial exposure of sediment, also brought more oxygen into the system and are thus responsible for the telltale orange or brown color the Pleistocene sediment, often targeted by the local drillers for the installation of low-As wells (McArthur et al., 2008; van Geen et al., 2007; Zheng et al., 2005). Orange, more oxidized sands owe their color to the ferric iron coating of sand grains (BGS and DPHE, 2001; Horneman et al., 2004; van Geen et al., 2004). Grey sands of Holocene, Pleistocene, and older ages are also common in deeper, low-As aquifers (BGS and DPHE, 2001; Burgess et al., 2010; Zheng et al., 2005) and can contain As sequestered in authigenic pyrite (Lowers et al., 2007).

Little is known about the residence times and flowpaths in deep aquifers of the Bengal basin. No clear patterns related to the depth or ages of groundwater have emerged in water stable isotopic content ($^{2}H/^{1}H$ and $^{18}O/^{16}O$) of deep groundwater (Aggarwal et al., 2000; Hoque and Burgess, 2012; Mukherjee et al., 2007). Estimates based on the ^{14}C age of dissolved inorganic carbon (DIC) place groundwater ages in the Bangladeshi Pleistocene aquifers deeper than 100 m at ~10,000 yr before present (BP), but the data are sparse and no flowpaths have been inferred (Aggarwal et al., 2000; BGS and DPHE, 2001; Fendorf et al., 2010; Zheng et al., 2005). A recent study by Hoque and Burgess (2012) proposed a recharge flowpath from the eastern edge of the Basin in the Tripura hills towards central Bangladesh based on a weak east-west trend in their ^{14}C DIC ages, but it could be an artifact of the applied ^{14}C corrections and/or a few outliers in the data. The fact that much of the deep groundwater has been dated to ~10 kyr BP or older points to the potentially stagnant groundwater with little or no recharge since the Pleistocene,

which could have implications for the sustainability of abstractions in the future (Aggarwal et al., 2000).

1.4 Concerns about low-As aquifer sustainability

The installation of community wells tapping deeper, Pleistocene aquifers continues at a fast pace (JICA and DPHE, 2010), and ever increasing mechanized withdrawals from these aquifers occur for urban supply near multiple cities of South and Southeast Asia, e.g. Hanoi (Berg et al., 2008; Winkel et al., 2011), Ho Chi Minh City (Erban et al., 2013), Kolkata (Mukherjee et al., 2011), and Dhaka (Hoque et al., 2007). Thus, the issue of sustainability of low-As aquifer extractions has been raised by a number of studies (Burgess et al., 2010; Harvey et al., 2002; Michael and Voss, 2008; Radloff et al., 2011). The general concern is that lowering hydraulic heads at depths below the peaking As concentrations of the shallow aquifer would induce a downward leakage of shallow, high-As groundwater into the low-As aquifers, causing As contamination and providing a source of organic matter that could drive reduction processes and additional As release. The reported scale of contamination can range from point failures of individual deep wells due to mechanical/installation problems, such as cracked well casings, screens at multiple depths, or flow along the well annulus (Aggarwal et al., 2000; van Geen et al., 2007), to broader basin-wide contamination of water supply wells in the Pleistocene aquifer, so far documented in Vietnam (Erban et al., 2013; Winkel et al., 2011) and asserted in West Bengal (Mukherjee et al., 2011) where the history of large groundwater abstractions is considerably longer. Somewhere in between these two physical scales, site-specific studies covering the 0.5-5 km scale have

reported contamination of local low-As aquifers due to the inflow of shallow, high-As groundwater vertically or laterally into the areas that lack confinement (McArthur et al., 2010; McArthur et al., 2011; McArthur et al., 2008; van Geen et al., 2013), or even across implied clay layers (Berg et al., 2008; Norrman et al., 2008). Where clay layers were implicated, their exact role was not directly assessed.

The evaluation and prediction of deeper aquifer sustainability has relied upon models of regional groundwater flow and the studies of deeper aquifer sediment properties. Groundwater flow models of the entire Bengal basin, using scaled up values of aquifer hydraulic properties and aquitard distribution based on available driller logs, hydraulic heads, and ^{14}C groundwater ages (Michael and Voss, 2009a, b) have addressed various scenarios of deeper aquifer usage. Their results based on uniform aquifer properties have suggested that pumping the deeper aquifer for domestic water supply only would likely be sustainable for hundreds of years; however switching the irrigation pumping (0.21 m/yr) to the deeper aquifer, which has approximately one order of magnitude higher pumping rates than domestic supply withdrawals, would significantly shorten the flowpaths to 150-200 m depth and contaminate large portions of the aquifer (Michael and Voss, 2008). Many such examples exist in the United States where contaminants are introduced to deeper aquifers as a result of extensive irrigation pumping (Landon et al., 2008). In Bengal basin, these models assume that natural, pre-development flowpaths to 175 m depth are ~100 km long and originate at the basin edges, therefore implying that active flow occurs from recharge areas at higher elevation; however these flowpaths have not been confirmed by field studies or geochemical evidence.

Other recent studies have focused on the evaluation of deeper aquifer sediments' capacity to adsorb As and retard its transport in the aquifer. Stollenwerk et al. (2007) showed in batch reactor studies coupled to a sophisticated surface complexation model that the brown/orange sediments collected from low-As aquifers have a substantial, but ultimately limited, capacity to remove As from groundwater. This finding was confirmed by an intricate *in situ* study of As sorption (Radloff et al., 2011) that produced a range of As partitioning coefficients between 1.7 and 28.7 L/kg, depending on the conceptualization of the pore-scale sorption reactions. The findings of this study were incorporated into the flow models of Michael and Voss to reflect the retardation of As transport, resulting in more optimistic prognoses of deeper aquifer sustainability (Radloff et al., 2011), but still emphasized the potential dangers in case large-scale irrigation were to switch to deep wells. Furthermore, when a supply of organic matter and/or metal reducing bacteria was procured to the orange low-As aquifer sediment, releases of As and Fe, greying of the sediment, and/or the re-partitioning of As into a more mobilizable phase were observed (Dhar et al., 2011; Robinson et al., 2011), suggesting that the sediment would be at additional risk when shallow groundwater loaded with organic matter would intrude. Therefore, facile and accurate evaluation of the local hydrostratigraphy, organic matter loading, and the sediment capacity to attenuate As intrusion appears to be crucial in predicting and evaluating the vulnerability of local low-As aquifers across the affected basins.

1.5 Questions explored and chapter summaries

Despite the significant advances that have been made in the understanding of low-As aquifer sustainability in Bangladesh and elsewhere in South and Southeast Asia, quite a few open questions and concerns remain that this work explores further. Little is known about the background, pre-development residence time and age of groundwater in deeper, low-As aquifers around Dhaka, where large and increasing abstraction of deep groundwater is now occurring (Hoque et al., 2007). The relative importance of vertical recharge from the shallow aquifer compared to distal recharge from the basin boundaries could have implications over the long-term As status of the deeper aquifer. As we observe a steady decline in hydraulic heads at depth over the past decade in our field area of Araihazar upazilla, the stage is set for shallow groundwater intrusion to intermediate-depth low-As aquifers, an important source of low-As groundwater that can be tapped by less costly wells installed by local drillers. The distribution of clay layers, their vertical conductivities and impact on groundwater chemistry are likely to significantly modulate the effects shallow groundwater intrusion will have on aquifer As status and overall geochemistry, and previous studies have not focused on this aspect in detail. Finally, the effect that the adsorption by aquifer sands has on transport of As through the low-As aquifers will likely need to be assessed at various locations, but an easily executable, field-based method, accurately approximating the *in situ* conditions, has not been available.

In Chapter 2, the results of a regional tracer survey of low-As wells (largely <10 μg/L As) from across Araihazar upazilla are presented, including ^{14}C and ^{13}C in dissolved inorganic carbon (DIC), noble gases, and stable isotopes of the water molecule (^{2}H and

^{18}O). A geochemical evaluation of groundwater chemistry is coupled to the radiocarbon and C isotopic data to arrive at groundwater age/residence time estimates for the intermediate (35-120 m bgl) and deep (>120 m bgl) aquifer in the area. The radiogenic helium content of groundwater, estimated by a model fit of dissolved noble gas concentrations, is used to double-check the validity of ^{14}C ages. This approach also allowed us to investigate other issues, such as the paleoclimate record retained in groundwater ^{2}H, ^{18}O, and $^{13}C_{DIC}$. The observed $^{13}C_{DIC}$ signature and the estimated ^{14}C ages are, thus, examined in the context of regional climate change that occurred during last deglaciation.

A village-scale investigation of an intermediate-depth (40-75 m bgl) low-As aquifer is described in Chapter 3. The aquifer was tapped by several community well installations that failed to produced low-As groundwater, with sudden occurrences of As >25 µg/L not related to well mechanics. The role that a compressible confining unit plays in promoting reduction processes in this aquifer under a downward vertical hydraulic gradient, ultimately resulting in the reported well failures, is explored by evaluating the hydraulic properties and pore water chemistry of the clay unit, as well as those of the intermediate aquifer and its redox-stratified sediment and groundwater. The notion that clay units, as often assumed, protect deeper aquifers from As contamination is challenged here. In addition, the impact of a lateral discontinuity in the clay layer, allowing for the arrival of recently recharged groundwater (10-50 yr ago) to the aquifer, is assessed in the context of aquifer redox chemistry, and yet another notion (that recharge from shallow aquifer causes As contamination) is challenged.

Lastly, a series of column experiments performed in the field with freshly cored low-As brown sediment through which shallow, high-As groundwater is pumped at various pore velocities is reported in Chapter 4. The transport of As in these 10-cm columns is modeled by a simple, 1D advection-dispersion analytical model calibrated for dispersion by the breakthrough of bromide tracer. The estimates of As partitioning constants and retardation coefficients obtained in such a straight-forward manner and under nearly *in situ* conditions are compared to other recent studies to demonstrate their relevance and relative simplicity. Kinetic limitations of the experiment and the reversibility of As sorption are also investigated by means of batch experiments, sediment extractions, and flushing of the columns in the field with low-As groundwater. A discussion of the impact that the observed reductive changes on the sediment have on As retention is also offered.

The work presented here, therefore, addresses the issues surrounding the sustainability and vulnerability of low-As aquifers in Bangladesh by combining geochemical and hydrologic tools across several physical scales of investigation: 1-10 km (Ch. 2), 0.1-1 km (Ch. 3), and 10 cm (Ch. 4). As the exploitation of these aquifers continues at increasing pace and provides a relatively easy solution to the arsenic crisis, it is important to understand the accompanying risks, even if taking these risks is inevitable. The hope is that the observations and insights presented here can guide resource management and might also be applicable to other aquifers affected by reductive release of toxic contaminants in South and Southeast Asia, and elsewhere in the world.

1.6 References

Acharyya, S.K., Chakraborty, P., Lahiri, S., Raymahashay, B.C., Guha, S., Bhowmik, A., 1999. Arsenic poisoning in the Ganges delta. Nature 401, 545-545.

Aggarwal, P.K., Basu, A.R., Kulkarni, K.M., 2003. Comment on "Arsenic mobility and groundwater extraction in Bangladesh" (I). Science 300, 584B-U581.

Aggarwal, P.K., Basu, A.R., Poreda, R.J., Kulkarni, K.M., Froehlich, K., Tarafdar, S.A., Ali, M., Ahmed, N., Hussain, A., Rahman, M., Ahmed, S.R., 2000. Isotope hydrology of groundwater in Bangladesh: Implications for characterization and mitigation of arsenic in groundwater, IAEA-TC Project (BGD/8/016). International Atomic Energy Agency.

Ahmed, M.F., Ahuja, S., Alauddin, M., Hug, S.J., Lloyd, J.R., Pfaff, A., Pichler, T., Saltikov, C., Stute, M., van Geen, A., 2006. Epidemiology - Ensuring safe drinking water in Bangladesh. Science 314, 1687-1688.

Argos, M., Kalra, T., Rathouz, P.J., Chen, Y., Pierce, B., Parvez, F., Islam, T., Ahmed, A., Rakibuz-Zaman, M., Hasan, R., Sarwar, G., Slavkovich, V., van Geen, A., Graziano, J., Ahsan, H., 2010. Arsenic exposure from drinking water, and all-cause and chronic-disease mortalities in Bangladesh (HEALS): a prospective cohort study. Lancet 376, 252-258.

Aziz, Z., van Geen, A., Stute, M., Versteeg, R., Horneman, A., Zheng, Y., Goodbred, S., Steckler, M., Weinman, B., Gavrieli, I., Hoque, M.A., Shamsudduha, M., Ahmed, K.M., 2008. Impact of local recharge on arsenic concentrations in shallow aquifers inferred from the electromagnetic conductivity of soils in Araihazar, Bangladesh. Water Resources Research 44.

Berg, M., Trang, P.T.K., Stengel, C., Buschmann, J., Viet, P.H., Van Dan, N., Giger, W., Stueben, D., 2008. Hydrological and sedimentary controls leading to arsenic contamination of groundwater in the Hanoi area, Vietnam: The impact of iron-arsenic ratios, peat, river bank deposits, and excessive groundwater abstraction. Chemical Geology 249, 91-112.

BGS and DPHE, 2001. Arsenic Contamination of Groundwater in Bangladesh, in: Kinniburgh, D.G., Smedley, P.L. (Eds.). British Geological Survey and Department of Public Health Engineering, BGS Technical Report WC/00/19. British Geological Survey, Keyworth, UK.

Burgess, W.G., Hoque, M.A., Michael, H.A., Voss, C.I., Breit, G.N., Ahmed, K.M., 2010. Vulnerability of deep groundwater in the Bengal Aquifer System to contamination by arsenic. Nature Geoscience 3, 83-87.

Buschmann, J., Berg, M., 2009. Impact of sulfate reduction on the scale of arsenic contamination in groundwater of the Mekong, Bengal and Red River deltas. Applied Geochemistry 24, 1278-1286.

Dhar, R.K., Zheng, Y., Saltikov, C.W., Radloff, K.A., Mailloux, B.J., Ahmed, K.M., van Geen, A., 2011. Microbes Enhance Mobility of Arsenic in Pleistocene Aquifer Sand from Bangladesh. Environmental Science & Technology 45, 2648-2654.

Dittmar, J., Voegelin, A., Roberts, L.C., Hug, S.J., Saha, G.C., Ali, M.A., Badruzzaman, A.B.M., Kretzschmar, R., 2010. Arsenic Accumulation in a Paddy Field in Bangladesh: Seasonal Dynamics and Trends over a Three-Year Monitoring Period. Environmental Science & Technology 44, 2925-2931.

Dowling, C.B., Poreda, R.J., Basu, A.R., Peters, S.L., Aggarwal, P.K., 2002. Geochemical study of arsenic release mechanisms in the Bengal Basin groundwater. Water Resources Research 38.

Duxbury, J.M., Mayer, A.B., Lauren, J.G., Hassan, N., 2003. Food chain aspects of arsenic contamination in Bangladesh: Effects on quality and productivity of rice. Journal of Environmental Science and Health Part a-Toxic/Hazardous Substances & Environmental Engineering 38, 61-69.

Erban, L.E., Gorelick, S.M., Zebker, H.A., Fendorf, S., 2013. Release of arsenic to deep groundwater in the Mekong Delta, Vietnam, linked to pumping-induced land subsidence. Proceedings of the National Academy of Sciences of the United States of America 110, 13751-13756.

Fendorf, S., Michael, H.A., van Geen, A., 2010. Spatial and Temporal Variations of Groundwater Arsenic in South and Southeast Asia. Science 328, 1123-1127.

Goodbred, S.L., Kuehl, S.A., 2000. The significance of large sediment supply, active tectonism, and eustasy on margin sequence development: Late Quaternary stratigraphy and evolution of the Ganges-Brahmaputra delta. Sedimentary Geology 133, 227-248.

Harvey, C.F., Swartz, C.H., Badruzzaman, A.B.M., Keon-Blute, N., Yu, W., Ali, M.A., Jay, J., Beckie, R., Niedan, V., Brabander, D., Oates, P.M., Ashfaque, K.N., Islam, S., Hemond, H.F., Ahmed, M.F., 2002. Arsenic mobility and groundwater extraction in Bangladesh. Science 298, 1602-1606.

Hoque, M.A., Burgess, W.G., 2012. C-14 dating of deep groundwater in the Bengal Aquifer System, Bangladesh: Implications for aquifer anisotropy, recharge sources and sustainability. Journal of Hydrology 444, 209-220.

Hoque, M.A., Hoque, M.M., Ahmed, K.M., 2007. Declining groundwater level and aquifer dewatering in Dhaka metropolitan area, Bangladesh: causes and quantification. Hydrogeology Journal 15, 1523-1534.

Horneman, A., Van Geen, A., Kent, D.V., Mathe, P.E., Zheng, Y., Dhar, R.K., O'Connell, S., Hoque, M.A., Aziz, Z., Shamsudduha, M., Seddique, A.A., Ahmed, K.M., 2004. Decoupling of As and Fe release to Bangladesh groundwater under reducing conditions. Part 1: Evidence from sediment profiles. Geochimica Et Cosmochimica Acta 68, 3459-3473.

Islam, F.S., Gault, A.G., Boothman, C., Polya, D.A., Charnock, J.M., Chatterjee, D., Lloyd, J.R., 2004. Role of metal-reducing bacteria in arsenic release from Bengal delta sediments. Nature 430, 68-71.

Itai, T., Masuda, H., Seddique, A.A., Mitamura, M., Maruoka, T., Li, X., Kusakabe, M., Dipak, B.K., Farooqi, A., Yamanaka, T., Nakaya, S., Matsuda, J.-i., Ahmed, K.M., 2008. Hydrological and geochemical constraints on the mechanism of formation of arsenic contaminated groundwater in Sonargaon, Bangladesh. Applied Geochemistry 23, 3155-3176.

JICA and DPHE, 2010. Report on Situation Analysis of Arsenic Mitigation, 2009. Dept. of Public Health Engineering, Bangladesh and Japan International Cooperation Agency, Local Government Division, Government of Bangladesh, DPHE, JICA.

Khandoker, R.A., 1987. Origin of elevated Barin-Madhupur areas, Bengal Basin: Result of neotectonic activities. Bangladesh Journal of Geology 6, 1-9.

Klump, S., Kipfer, R., Cirpka, O.A., Harvey, C.F., Brennwald, M.S., Ashfaque, K.N., Badruzzaman, A.B.M., Hug, S.J., Imboden, D.M., 2006. Groundwater dynamics and arsenic mobilization in Bangladesh assessed using noble gases and tritium. Environmental Science & Technology 40, 243-250.

Kocar, B.D., Herbel, M.J., Tufano, K.J., Fendorf, S., 2006. Contrasting effects of dissimilatory iron(III) and arsenic(V) reduction on arsenic retention and transport. Environmental Science & Technology 40, 6715-6721.

Landon, M.K., Clark, B.R., McMahon, P.B., McGuire, V.L., Turco, M.J., 2008. Hydrogeology, chemical characteristics, and transport processes in the zone of contribution of a public-supply well in York, Nebraska. U. S. Geological Survey Scientific Investigations Report 2008-5050.

Lowers, H.A., Breit, G.N., Foster, A.L., Whitney, J., Yount, J., Uddin, N., Muneem, A., 2007. Arsenic incorporation into authigenic pyrite, bengal basin sediment, Bangladesh. Geochimica Et Cosmochimica Acta 71, 2699-2717.

Mailloux, B.J., Trembath-Reichert, E., Cheung, J., Watson, M., Stute, M., Freyer, G.A., Ferguson, A.S., Ahmed, K.M., Alam, M.J., Buchholz, B.A., Thomas, J., Layton, A.C., Zheng, Y., Bostick, B.C., van Geen, A., 2013. Advection of surface-derived organic carbon fuels microbial reduction in Bangladesh groundwater. Proceedings of the National Academy of Sciences of the United States of America 110, 5331-5335.

McArthur, J.M., Banerjee, D.M., Hudson-Edwards, K.A., Mishra, R., Purohit, R., Ravenscroft, P., Cronin, A., Howarth, R.J., Chatterjee, A., Talukder, T., Lowry, D., Houghton, S., Chadha, D.K., 2004. Natural organic matter in sedimentary basins and its relation to arsenic in anoxic ground water: the example of West Bengal and its worldwide implications. Applied Geochemistry 19.

McArthur, J.M., Banerjee, D.M., Sengupta, S., Ravenscroft, P., Klump, S., Sarkar, A., Disch, B., Kipfer, R., 2010. Migration of As, and H-3/(3) He ages, in groundwater from West Bengal: Implications for monitoring. Water Research 44, 4171-4185.

McArthur, J.M., Nath, B., Banerjee, D.M., Purohit, R., Grassineau, N., 2011. Palaeosol Control on Groundwater Flow and Pollutant Distribution: The Example of Arsenic. Environmental Science & Technology 45, 1376-1383.

McArthur, J.M., Ravenscroft, P., Banerjee, D.M., Milsom, J., Hudson-Edwards, K.A., Sengupta, S., Bristow, C., Sarkar, A., Tonkin, S., Purohit, R., 2008. How paleosols influence groundwater flow and arsenic pollution: A model from the Bengal Basin and its worldwide implication. Water Resources Research 44.

McArthur, J.M., Ravenscroft, P., Safiulla, S., Thirlwall, M.F., 2001. Arsenic in groundwater: Testing pollution mechanisms for sedimentary aquifers in Bangladesh. Water Resources Research 37, 109-117.

Meharg, A.A., Rahman, M., 2003. Arsenic contamination of Bangladesh paddy field soils: Implications for rice contribution to arsenic consumption. Environmental Science & Technology 37, 229-234.

Meharg, A.A., Scrimgeour, C., Hossain, S.A., Fuller, K., Cruickshank, K., Williams, P.N., Kinniburgh, D.G., 2006. Codeposition of organic carbon and arsenic in Bengal Delta aquifers. Environmental Science & Technology 40, 4928-4935.

Michael, H.A., Voss, C.I., 2008. Evaluation of the sustainability of deep groundwater as an arsenic-safe resource in the Bengal Basin. Proceedings of the National Academy of Sciences of the United States of America 105, 8531-8536.

Michael, H.A., Voss, C.I., 2009a. Controls on groundwater flow in the Bengal Basin of India and Bangladesh: regional modeling analysis. Hydrogeology Journal 17, 1561-1577.

Michael, H.A., Voss, C.I., 2009b. Estimation of regional-scale groundwater flow properties in the Bengal Basin of India and Bangladesh. Hydrogeology Journal 17, 1329-1346.

Mukherjee, A., Fryar, A.E., Rowe, H.D., 2007. Regional-scale stable isotopic signatures of recharge and deep groundwater in the arsenic affected areas of West Bengal, India. Journal of Hydrology 334, 151-161.

Mukherjee, A., Fryar, A.E., Scanlon, B.R., Bhattacharya, P., Bhattacharya, A., 2011. Elevated arsenic in deeper groundwater of the western Bengal basin, India: Extent and controls from regional to local scale. Applied Geochemistry 26, 600-613.

Neumann, R.B., Ashfaque, K.N., Badruzzaman, A.B.M., Ali, M.A., Shoemaker, J.K., Harvey, C.F., 2010. Anthropogenic influences on groundwater arsenic concentrations in Bangladesh. Nature Geoscience 3, 46-52.

Nickson, R., McArthur, J., Burgess, W., Ahmed, K.M., Ravenscroft, P., Rahman, M., 1998. Arsenic poisoning of Bangladesh groundwater. Nature 395, 338-338.

Nickson, R.T., McArthur, J.M., Ravenscroft, P., Burgess, W.G., Ahmed, K.M., 2000. Mechanism of arsenic release to groundwater, Bangladesh and West Bengal. Applied Geochemistry 15, 403-413.

Norrman, J., Sparrenbom, C.J., Berg, M., Nhan, D.D., Nhan, P.Q., Rosqvist, H., Jacks, G., Sigvardsson, E., Baric, D., Moreskog, J., Harms-Ringdahl, P., Van Hoan, N., 2008. Arsenic mobilisation in a new well field for drinking water production along the Red River, Nam Du, Hanoi. Applied Geochemistry 23, 3127-3142.

Opar, A., Pfaff, A., Seddidue, A.A., Ahmed, K.M., Graziano, J.H., van Geen, A., 2007. Responses of 6500 households to arsenic mitigation in Araihazar, Bangladesh. Health & Place 13, 164-172.

Panaullah, G.M., Alam, T., Hossain, M.B., Loeppert, R.H., Lauren, J.G., Meisner, C.A., Ahmed, Z.U., Duxbury, J.M., 2009. Arsenic toxicity to rice (Oryza sativa L.) in Bangladesh. Plant and Soil 317, 31-39.

Polizzotto, M.L., Harvey, C.F., Li, G.C., Badruzzman, B., Ali, A., Newville, M., Sutton, S., Fendorf, S., 2006. Solid-phases and desorption processes of arsenic within Bangladesh sediments. Chemical Geology 228, 97-111.

Polizzotto, M.L., Kocar, B.D., Benner, S.G., Sampson, M., Fendorf, S., 2008. Near-surface wetland sediments as a source of arsenic release to ground water in Asia. Nature 454, 505-U505.

Radloff, K.A., 2010. Geochemical and hydrologic determinants of arsenic distribution in sedimentary aquifers in Bangladesh, Department of Earth and Environmental Engineering. Columbia University, New York, NY.

Radloff, K.A., Zheng, Y., Michael, H.A., Stute, M., Bostick, B.C., Mihajlov, I., Bounds, M., Huq, M.R., Choudhury, I., Rahman, M.W., Schlosser, P., Ahmed, K.M., van Geen, A., 2011. Arsenic migration to deep groundwater in Bangladesh influenced by adsorption and water demand. Nature Geoscience 4, 793-798.

Ravenscroft, P., Brammer, H., Richards, K.S., 2009. Arsenic pollution: a global synthesis. Wiley-Blackwell.

Ravenscroft, P., Burgess, W.G., Ahmed, K.M., Burren, M., Perrin, J., 2005. Arsenic in groundwater of the Bengal Basin, Bangladesh: Distribution, field relations, and hydrogeological setting. Hydrogeology Journal 13, 727-751.

Ravenscroft, P., McArthur, J.M., Hoque, M.A., 2013. Stable groundwater quality in deep aquifers of Southern Bangladesh: The case against sustainable abstraction. Science of the Total Environment 454, 627-638.

Roberts, L.C., Hug, S.J., Dittmar, J., Voegelin, A., Kretzschmar, R., Wehrli, B., Cirpka, O.A., Saha, G.C., Ali, M.A., Badruzzaman, A.B.M., 2010. Arsenic release from paddy soils during monsoon flooding. Nature Geoscience 3, 53-59.

Robinson, C., von Bromssen, M., Bhattacharya, P., Haller, S., Biven, A., Hossain, M., Jacks, G., Ahmed, K.M., Hasan, M.A., Thunvik, R., 2011. Dynamics of arsenic adsorption in the targeted arsenic-safe aquifers in Mat lab, south-eastern Bangladesh: Insight from experimental studies. Applied Geochemistry 26, 624-635.

Rowland, H.A.L., Polya, D.A., Lloyd, J.R., Pancost, R.D., 2006. Characterisation of organic matter in a shallow, reducing, arsenic-rich aquifer, West Bengal. Organic Geochemistry 37, 1101-1114.

Saalfield, S.L., Bostick, B.C., 2009. Changes in Iron, Sulfur, and Arsenic Speciation Associated with Bacterial Sulfate Reduction in Ferrihydrite-Rich Systems. Environmental Science & Technology 43, 8787-8793.

Sengupta, S., McArthur, J.M., Sarkar, A., Leng, M.J., Ravenscroft, P., Howarth, R.J., Banerjee, D.M., 2008. Do ponds cause arsenic-pollution of groundwater in the Bengal Basin? An answer from West Bengal. Environmental Science & Technology 42, 5156-5164.

Smith, A.H., Lingas, E.O., Rahman, M., 2000. Contamination of drinking-water by arsenic in Bangladesh: a public health emergency. Bulletin of the World Health Organization 78, 1093-1103.

Stollenwerk, K.G., Breit, G.N., Welch, A.H., Yount, J.C., Whitney, J.W., Foster, A.L., Uddin, M.N., Majumder, R.K., Ahmed, N., 2007. Arsenic attenuation by oxidized aquifer sediments in Bangladesh. Science of the Total Environment 379, 133-150.

Stute, M., Zheng, Y., Schlosser, P., Horneman, A., Dhar, R.K., Datta, S., Hoque, M.A., Seddique, A.A., Shamsudduha, M., Ahmed, K.M., van Geen, A., 2007. Hydrological control of As concentrations in Bangladesh groundwater. Water Resources Research 43.

Tufano, K.J., Fendorf, S., 2008. Confounding impacts of iron reduction on arsenic retention. Environmental Science & Technology 42, 4777-4783.

Tufano, K.J., Reyes, C., Saltikov, C.W., Fendorf, S., 2008. Reductive Processes Controlling Arsenic Retention: Revealing the Relative Importance of Iron and Arsenic Reduction. Environmental Science & Technology 42, 8283-8289.

van Geen, A., Ahmed, K.M., Seddique, A.A., Shamsudduha, M., 2003a. Community wells to mitigate the arsenic crisis in Bangladesh. Bulletin of the World Health Organization 81, 632-638.

van Geen, A., Bostick, B.C., Trang, P.T.K., Lan, V.M., Mai, N.-N., Manh, P.D., Viet, P.H., Radloff, K.A., Aziz, Z., Mey, J.L., Stahl, M.O., Harvey, C.F., Oates, P., Weinman, B., Stengel, C., Frei, F., Kipfer, R., Berg, M., 2013. Retardation of arsenic transport through a Pleistocene aquifer. Nature in press.

van Geen, A., Cheng, Z.Q., Jia, Q., Seddique, A.A., Rahman, M.W., Rahman, M.M., Ahmed, K.M., 2007. Monitoring 51 community wells in Araihazar, Bangladesh, for up to 5 years: Implications for arsenic mitigation. Journal of Environmental Science and Health Part a-Toxic/Hazardous Substances & Environmental Engineering 42, 1729-1740.

van Geen, A., Rose, J., Thoral, S., Garnier, J.M., Zheng, Y., Bottero, J.Y., 2004. Decoupling of As and Fe release to Bangladesh groundwater under reducing conditions. Part II: Evidence from sediment incubations. Geochimica Et Cosmochimica Acta 68, 3475-3486.

van Geen, A., Zheng, Y., Cheng, Z., He, Y., Dhar, R.K., Garnier, J.M., Rose, J., Seddidue, A., Hoque, M.A., Ahmed, K.M., 2006. Impact of irrigating rice paddies with groundwater containing arsenic in Bangladesh. Science of the Total Environment 367, 769-777.

van Geen, A., Zheng, Y., Goodbred, S., Horneman, A., Aziz, Z., Cheng, Z., Stute, M., Mailloux, B., Weinman, B., Hoque, M.A., Seddique, A.A., Hossain, M.S., Chowdhury, S.H., Ahmed, K.M., 2008. Flushing history as a hydrogeological control on the regional distribution of arsenic in shallow groundwater of the Bengal Basin. Environmental Science & Technology 42, 2283-2288.

van Geen, A., Zheng, Y., Stute, M., Ahmed, K.M., 2003b. Comment on "Arsenic mobility and groundwater extraction in Bangladesh" (II). Science 300, 584C-584C.

van Geen, A., Zheng, Y., Versteeg, R., Stute, M., Horneman, A., Dhar, R., Steckler, M., Gelman, A., Small, C., Ahsan, H., Graziano, J.H., Hussain, I., Ahmed, K.M., 2003c. Spatial variability of arsenic in 6000 tube wells in a 25 km(2) area of Bangladesh. Water Resources Research 39.

Wasserman, G.A., Liu, X.H., Parvez, F., Ahsan, H., Factor-Litvak, P., Kline, J., van Geen, A., Slavkovich, V., Lolacono, N.J., Levy, D., Cheng, Z.Q., Graziano, J.H., 2007. Water arsenic exposure and intellectual function in 6-year-old children in Araihazar, Bangladesh. Environmental Health Perspectives 115, 285-289.

Weinman, B., Goodbred, S.L., Zheng, Y., Aziz, Z., Steckler, M., van Geen, A., Singhvi, A.K., Nagar, Y.C., 2008. Contributions of floodplain stratigraphy and evolution to the spatial patterns of groundwater arsenic in Araihazar, Bangladesh. Geological Society of America Bulletin 120, 1567-1580.

Welch, A.H., Lico, M.S., 1998. Factors controlling As and U in shallow ground water, southern Carson Desert, Nevada. Applied Geochemistry 13, 521-539.

Winkel, L.H.E., Pham Thi Kim, T., Vi Mai, L., Stengel, C., Amini, M., Nguyen Thi, H., Pham Hung, V., Berg, M., 2011. Arsenic pollution of groundwater in Vietnam exacerbated by deep aquifer exploitation for more than a century. Proceedings of the National Academy of Sciences of the United States of America 108, 1246-1251.

Yu, W.H., Harvey, C.M., Harvey, C.F., 2003. Arsenic in groundwater in Bangladesh: A geostatistical and epidemiological framework for evaluating health effects and potential remedies. Water Resources Research 39, 17.

Zheng, Y., Stute, M., van Geen, A., Gavrieli, I., Dhar, R., Simpson, H.J., Schlosser, P., Ahmed, K.M., 2004. Redox control of arsenic mobilization in Bangladesh groundwater. Applied Geochemistry 19.

Zheng, Y., van Geen, A., Stute, M., Dhar, R., Mo, Z., Cheng, Z., Horneman, A., Gavrieli, I., Simpson, H.J., Versteeg, R., Steckler, M., Grazioli-Venier, A., Goodbred, S., Shahnewaz, M., Shamsudduha, M., Hoque, M.A., Ahmed, K.M., 2005. Geochemical and hydrogeological contrasts between shallow and deeper aquifers in two villages of Araihazar, Bangladesh: Implications for deeper aquifers as drinking water sources. Geochimica Et Cosmochimica Acta 69, 5203-5218.

Chapter 2:

Groundwater recharge and residence times in intermediate (35-120 m) and deep (>120 m) low-arsenic aquifers east of Dhaka, Bangladesh

I. MIHAJLOV[1,2*], M. STUTE[1,3], P. SCHLOSSER[1,4], B. J. MAILLOUX[3], YAN ZHENG[1,5], I. CHOUDHURY[6], K.M. AHMED[6] AND A. VAN GEEN[1]

[1]Lamont-Doherty Earth Observatory of Columbia University, Palisades, NY, USA

[2]Department of Earth and Environmental Sciences, Columbia University, New York, NY, USA

[3]Barnard College, New York, NY, USA

[4]Department of Earth and Environmental Engineering, Columbia University, New York, NY, USA

[5]Queens College, City University of New York, New York, NY, USA

[6]Department of Geology, Dhaka University, Dhaka, Bangladesh

Abstract

More than 100,000 community wells have been installed in the 150-300 m depth range throughout Bangladesh over the past decade to provide drinking water low in As (<10 μg/L), but little is known about these aquifers. Groundwater from a total of 65 wells in the 35-240 m depth range, mostly community wells and all but 3 containing ≤10 μg/L As, was sampled between 2003 and 2011 within a 25 km^2 area of Araihazar upazilla, east of the capital, Dhaka. All samples were analyzed for tritium (^3H), and a subset was analyzed for oxygen and hydrogen isotopes in water ($^{18}O/^{16}O$ and $^2H/^1H$), carbon isotope ratios ($^{14}C/^{12}C$ and $^{13}C/^{12}C$) in dissolved inorganic carbon (DIC), noble gases ($^3He/^4He$, Ne, Ar, Kr, and Xe), major cations (Na, Mg, K, and Ca), anions (Cl, Br, F, and SO_4), As, Fe, Mn, P, Si, alkalinity, DIC, and dissolved organic carbon. Only 4 of the 22 wells with depths >120 m contain detectable ^3H with concentrations of 0.1-0.2 TU, and the DIC radiocarbon ages cluster around 10 kyr. In contrast, 25 of the 43 analyzed wells with depths <120 m contain detectable ^3H concentrations larger than 0.1 TU, 8 of which are distinctly higher at 0.4-6 TU, and the DIC radiocarbon ages range from modern to 10 kyr. There was no systematic relationship in the wells with depths <120 m between the level of ^3H or ^{14}C and other groundwater properties, such as 11-29 μg/L As in 3 samples, or the amount of clay in well lithologs. The measurements indicate a linear relationship between the entire range of radiocarbon ages and the radiogenic ^4He content of the groundwater with a He release rate of 2.5×10^{-12} ccSTP g^{-1} yr^{-1}. The groundwater composition of all wells with depths >120 m and the 3 shallower 10 kyr-old samples is remarkably constant and low in EC, DIC, and Na, and high in Si relative to the chemical composition of the shallower and younger groundwater. Within this group of samples, systematic

relationships between $^{18}O/^{16}O$, $^{14}C/^{12}C$ and $^{13}C/^{12}C$ suggest changes in monsoon intensity and shifts in dominance of the vegetation between C4 and C3 plants at the onset of the Holocene. The recharge of deep (>120 m) groundwater at the onset of the Holocene ~10 kyr ago suggests either the entrapment of this groundwater by Holocene sediment or a very slow horizontal and vertical Holocene flow in the aquifer. Further exploitation of the deep aquifer will likely shorten its groundwater residence time, which may impact future As levels, but our data provide no current evidence of widespread As intrusion into the aquifers selected for community well installation.

2.1 Introduction

Arsenic is a toxic metalloid naturally occurring in the sediment that is released to the groundwater under anoxic conditions, such as those prevalent in the low-lying river and delta plain aquifers of South and Southeast Asia (e.g., Fendorf et al., 2010; Ravenscroft et al., 2009). The majority of the rural population in Bangladesh, like in other countries of the region, rely on the cheap and easily installed, shallow tubewells for their drinking water supply. However, a large proportion of the wells contain As concentrations of >10 μg/L, thus exposing tens of millions of Bangladeshis and >100 million people throughout South and SE Asia to the harmful effects of As, including multiple forms of cancer, cardiovascular disease, and diminished childhood intellectual function (Argos et al., 2010; BGS and DPHE, 2001; Ravenscroft et al., 2009; Smith et al., 2000; Wasserman et al., 2004). Exploiting the knowledge that peak As concentrations in the Bengal Basin are usually located 20-40 m below ground level (bgl), and that deeper, orange-colored sediments of Pleistocene origin usually host low levels of dissolved arsenic in groundwater (BGS and DPHE, 2001; Fendorf et al., 2010; McArthur et al., 2008; Ravenscroft et al., 2005; van Geen et al., 2003), NGOs and government agencies have installed >100,000 deep (150-300 m bgl) wells in Bangladesh alone to mitigate the As poisoning (Ahmed et al., 2006; Burgess et al., 2010; JICA and DPHE, 2010; Michael and Voss, 2008; Ravenscroft et al., 2013; van Geen et al., 2007). As this source of low-As drinking water is increasingly pumped for urban supply (Hoque et al., 2007), several studies have raised concerns about its sustainable use. The possibility of vertical leakage of high-As and organic laden shallow groundwater due to irrigation pumping was raised

by Harvey et al. (2002) and has been evaluated for deeper wells with basin-scale models under the assumption that pumping for irrigation purposes might in the coming decades switch to the currently safe aquifers at depths >150 m bgl (Burgess et al., 2010; Michael and Voss, 2008; Radloff et al., 2011).

Depth is a poor predictor for aquifers that are systematically low in As because of the large hydrogeological heterogeneity of the delta (Fendorf et al., 2010; McArthur et al., 2008; van Geen et al., 2003; Zheng et al., 2005). Previous studies have identified a transitional aquifer, referred to as "intermediate" in this study, in which As is low, but the residence times and other hydrogeochemical features sometimes resemble the shallow aquifer, and a "deep" aquifer at greater depths containing much older groundwater (Aggarwal et al., 2000; BGS and DPHE, 2001). The low-As aquifers have also been characterized by Pleistocene-age or older sediments that have been flushed of their labile As and/or organic carbon that could fuel the reductive release of As (BGS and DPHE, 2001; Ravenscroft et al., 2005). The flushing presumably occurred due to a sequence of sea level lowstands, resulting in deep river channel incisions, larger horizontal hydraulic gradients in aquifers compared to the present, and consequently faster groundwater flow during the Pleistocene (Goodbred and Kuehl, 2000b; McArthur et al., 2008).

Despite the considerable amount of concern for the status of the deep aquifer (Burgess et al., 2010; Fendorf et al., 2010; Hoque et al., 2007; McArthur et al., 2008; Michael and Voss, 2008, 2009a, b; Mukherjee et al., 2011; Radloff et al., 2011), and the reports of local well failures (Aggarwal et al., 2000; van Geen et al., 2007) or limited incursions of As and/or organic matter from Holocene aquifers (McArthur et al., 2011; Mukherjee et al., 2011), relatively little is known about the basic hydrology of the low-As

aquifers, such as their flow patterns and mean residence times. For example, some flowpaths of the pre-development baseline deep aquifer model described by Michael and Voss (2008) start from the elevated edges of the Bengal Basin, but it is unclear if these flow lines are representative. Groundwater dating, primarily by ^{14}C in dissolved inorganic carbon (DIC), has been limited in scope and has typically covered large areas with sparsely spaced data points (Aggarwal et al., 2000; BGS and DPHE, 2001; Fendorf et al., 2010). The available data indicate that low-As groundwater at depths >120 m bgl, and in certain locations at depths of only ~30 m bgl (Zheng et al., 2005), might be >10 kyr old. The only study that attempted to integrate spatial observations of groundwater ages argues that there is a westward flow from the Tripura Hills located along the eastern edge of the Bengal Basin (Hoque and Burgess, 2012). The flow pattern relies on a trend of increasing ^{14}C ages in DIC away from the eastern margin, ranging from modern to >20,000 yr BP, whereas in reality most of the data cluster around an age of 11-15 ky, 9-13 kyr, or 6-9 kyr BP, depending on the geochemical model used for the ^{14}C age corrections. None of the above studies have attempted to apply another tracer of groundwater age and little use has been made of the radiocarbon data to link changes in climate at the end of the last glaciation to changes in the stable isotopes of groundwater (^{2}H, ^{18}O) and C (^{13}C) in DIC, as routinely done in paleoclimate studies (Galy et al., 2008; Partin et al., 2007; Prins and Postma, 2000; Rashid et al., 2011; Sarkar et al., 2009).

In this study, we report DIC radiocarbon data from 38 low-As wells ranging in depth between 35-240 m bgl in a 25 km^2 area east of Dhaka, Bangladesh. Radiocarbon ages are interpreted using groundwater chemistry records, compared to a noble gas dating technique, and systematically linked to the stable isotopic signatures ($^{2}H/^{1}H$, $^{18}O/^{16}O$,

$^{13}C_{DIC}$). Field procedures and measurement techniques, litholog collection, and groundwater sampling and analyses for ^{3}H, $^{13}C/^{12}C$ and $^{14}C/^{12}C$ (in DIC and DOC), major cations, anions, Si, P, As, Mn, Fe, DIC and DOC concentrations, $^{2}H/^{1}H$, $^{18}O/^{16}O$, and noble gases are described in Section 2.2. The results of these measurements and analyses, along with the ^{14}C age correction models and the noble gas model used to calculate recharge temperature and radiogenic He, are presented in Section 2.3. The discussion of major results, including groundwater chemistry and ages/residence times at different depths, as well as the isotopic signatures of deglaciation in the deepest samples, is offered in Section 2.4. We also discuss the implications of our findings for the sustainability of deep, low-As aquifers before concluding the study in Section 2.5.

2.2 Methods

2.2.1 Sampling campaigns

The study was conducted in Araihazar upazila of Bangladesh, ~25 km east of the capital, Dhaka, in the field area described in detail by van Geen et al. (2003) where the majority of shallow wells (<30 m deep) exceed 50 μg/L As dissolved in groundwater. The current study focused on 65 low-As wells (<10 μg/L As, except three wells with 10-29 μg/L As) that were installed in the depth ranges of 35-104 m bgl (n = 43) and 122-238 m bgl (n = 22) (Figure 2.1 and Table 2.1). A subset of the studied wells (n = 20 at the intermediate depth, 35-120 m bgl, and n = 19 at depths >120 m bgl) was extensively sampled, whereas the remaining wells were only sampled for ^{3}H in 2006 and/or stable isotopes (^{18}O and ^{2}H) in 2004.

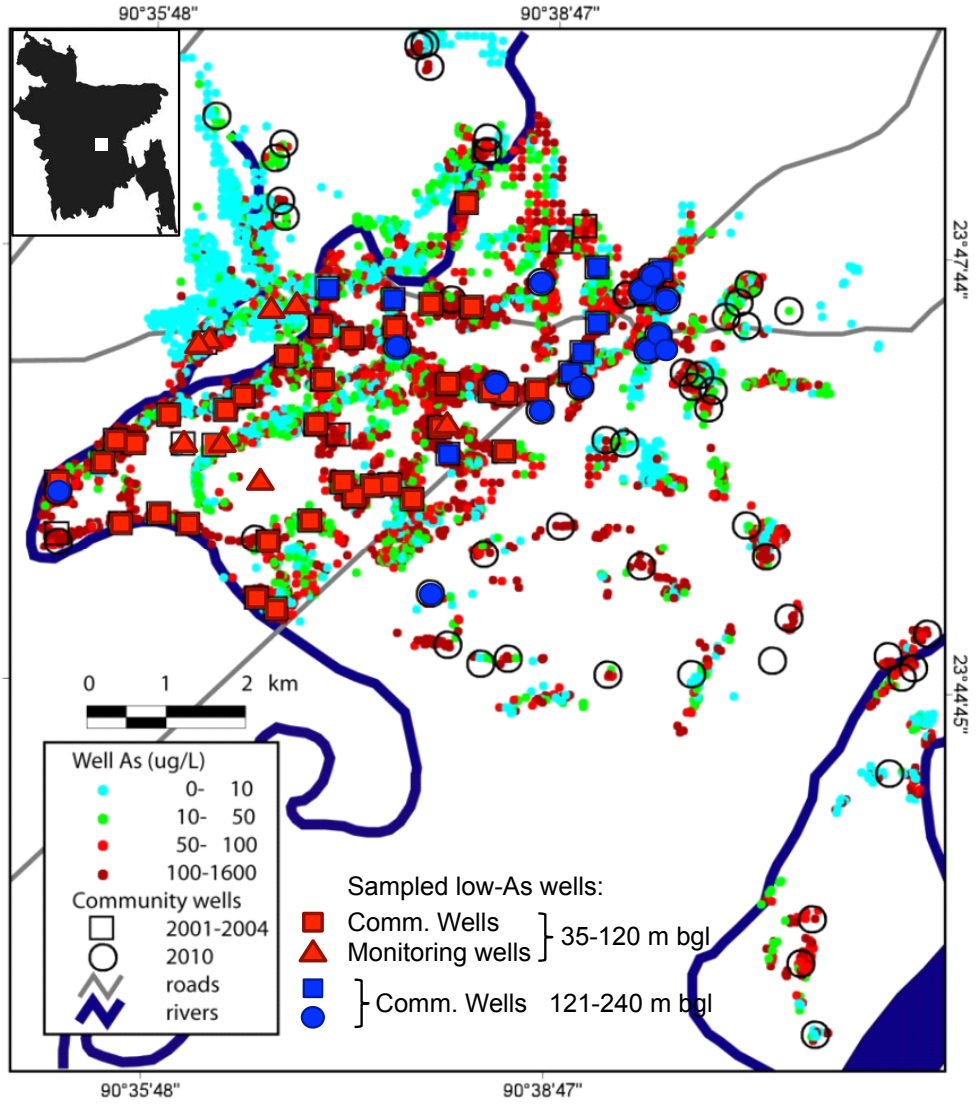

Figure 2.1. Map of the field area in Araihazar upazilla, Bangladesh, with the locations of sampled low-As wells. Community wells used for drinking are shown as large squares or circles, monitoring wells as triangles. The sampled wells are marked by solid fill: red for depths 35-120 m bgl, and blue for 121-240 m bgl. Small dots indicate shallow tubewell As concentrations in the area. The location of Araihazar within Bangladesh is indicated by the white square in the inset map.

Extensive well sampling included community wells used for drinking (17 CWs and 13 WABs) in 2010 and 2011, as well as monitoring wells M1.5 (61 m bgl, 2011), DI4 (58 m bgl, 2008), and the deepest wells from multi-level well nests A-G (36-88 m bgl, 2003). CWs were installed 35-152 m bgl by Dhaka University 2001-2004 (van Geen et al., 2007) to provide access to As-safe water in the most severely affected villages. Some CWs were sampled twice for $^{14}C_{DIC}$ (2010 and 2011) and twice or three times for ^{3}H (2006, 2010, 2011); all measured values are reported. WAB wells, installed in 2010 by the NGO Water Aid Bangladesh, are deeper (>200 m bgl) and cluster towards the eastern end of the study area. Well DI4 was used in an *in situ* study of As sorption on low-As aquifer sediments, described in Radloff et al. (2011), whereas partial results of the sampling at A-G have been featured in multiple publications (see: Zheng et al. (2005) for all data from A7, A8, and B-CW2, except stable isotopes and noble gases; Stute et al. (2007) for stable isotope data; Mailloux et al. (2013) for DIC and DOC concentrations, radiocarbon and $\delta^{13}C$ results from F5; Dhar et al. (2008) for a 2-3 year monitoring study).

2.2.2 Well purging and field measurements

Well sampling was conducted using a submersible pump producing a flow rate of 5-10 L/min (Typhoon 12-V standard pump, Groundwater Essentials), or by utilizing a hand pump when a submersible pump could not be used due to well construction (all WAB wells, except 24030). Three borehole volumes were purged out of each well before collecting samples. Electrical conductivity (EC), temperature (T), and pH were monitored by probes in a flow-through portable chamber (MP 556, YSI, Inc.) during purging with a submersible pump and stabilized before sampling. Alkalinity was also measured in the

field using standard Gran titrations (Gran, 1952b). EC and pH electrodes were calibrated on site before collecting the first sample of the day, and the flow cell was taken off the line before collecting samples to prevent cross-contamination between wells. For the wells where hand pump was used, EC and pH were measured in an overflowing bucket, which introduced a systematic error in pH (0.1-0.6 units higher) due to degasing of CO_2 from the splashing water. For these wells, pH was calculated (denoted by # in Table 2.4) from the field-measured alkalinity values and the total DIC measured at the Woods Hole NOSAMS facility. DIC samples for radiocarbon measurements were collected into glass bottles directly from the hand pump, without the splashing effect, and immediately capped.

2.2.3 Groundwater sampling and elemental analysis by ICP-MS and IC

Samples for major cations (Na, K, Mg, Ca), Si, P, S, and trace elements (As, Fe, Mn) were collected without filtration into 25 mL HDPE scintillation vials with conical polyseal caps (Wheaton, Fisher Scientific) and later acidified to 1% HCl (Optima, Fisher Scientific). Previous work demonstrated that the well screens in Bangladesh typically provide sufficient filtration without introducing artifacts associated with syringe filtration (van Geen et al., 2004) and that delayed acidification in the lab does not affect the results (van Geen et al., 2007). The samples were analyzed for Na, K, Mg, Ca, Si, P, S, As, Fe, and Mn by high-resolution inductively coupled plasma–mass spectrometry (HR ICP-MS) on a single-collector VG Axiom (Cheng et al., 2004) to a precision of ±10% or better. Accuracy of the results was checked against an internal laboratory reference standard and also found to be within <10% of the expected values. The levels of S in several samples,

when diluted 10-fold for the measurement, were near the detection limit of 0.01-0.16 mg/L (depending on the run), thus these values could not be quantified reliably and are reported with an asterisk in Table 2.4.

Samples for anion analyses were collected in parallel with cation and trace element samples, but the vials were not acidified upon collection. The concentrations of Cl, F, Br, and SO_4 were determined on a Dionex ICS-2000 ion–chromatograph (IC) with an IonPac AS18 analytical column and an AG18 guard column (Thermo Scientific) using a self-regenerating KOH eluent. A standard was run after every 8-10 samples to ensure accuracy of the measurements, and several samples were analyzed in duplicates or triplicates to confirm analytical precision (typically <5% for Cl, <10% for SO_4, and 5-15% for Br and F). The Cl result for CW15 (EC = 2.97 mS/cm) is semi-quantitative, as it exceeded the maximum standard measured.

2.2.4 Sampling and analysis of stable isotopes in water ($^{18}O/^{16}O$ and $^{2}H/^{1}H$)

Stable isotope ($\delta^{18}O$ and $\delta^{2}H$) samples were collected in 60 mL glass bottles with polyseal lined caps. Measurements of $^{18}O/^{16}O$ and $^{2}H/^{1}H$ on samples collected in 2003 (wells A-G), 2004 (several CWs), and 2008 (DI4) were performed at the Environmental Isotope Laboratory of the University of Waterloo with a precision of ±0.1‰ ($\delta^{18}O$) and ±1‰ ($\delta^{2}H$). Stable isotope measurements on samples collected in 2010 and 2011 (CWs, WABs, and M1.5) were performed on a cavity ringdown laser spectrometer at Lamont-Doherty Earth Observatory (L2130-*i* Isotopic H2O, Picarro, Santa Clara, CA) with a precision of ±0.02-0.05‰ ($\delta^{18}O$) and ±0.05-0.25‰ ($\delta^{2}H$). All values are reported as ‰ deviation from Vienna Standard Mean Ocean Water (VSMOW).

2.2.5 Sampling and analysis of ^{3}H and noble gases (He, Ne, Ar, Kr, Xe, and $^{3}He/^{4}He$)

Groundwater recharged after the onset of surface testing of nuclear devices can be detected by the presence of elevated tritium (^{3}H), a radioactive isotope of hydrogen released during the tests that peaked in the early 1960s (e.g., Weiss et al., 1979; Weiss and Roether, 1980). Samples for ^{3}H were collected in 125 mL glass bottles with polyseal caps and analyzed at Lamont-Doherty Earth Observatory's Noble Gas Laboratory using the ^{3}He ingrowth technique (Bayer et al., 1989; Clarke et al., 1976; Ludin et al., 1997). The detection limit of the ^{3}H analyses was 0.05-0.10 TU ($^{3}H/^{1}H$ ratio of 1 TU = 10^{-18}), with a precision of ±0.02-0.16 TU (Table 2.1). Noble gas samples were collected in ~1 cm outer diameter copper tubes that contain ~19 cm^{3} of groundwater. Concentrations of He, Ne, Ar, Kr, and Xe isotopes were measured by mass spectrometry (Stute et al., 1995) with typical analytical precisions of ±2% for He and $^{3}He/^{4}He$, and ±1% for Ne, Ar, Kr, and Xe. The system was calibrated with atmospheric air standards and water samples equilibrated at known temperature and pressure.

The measured concentrations of noble gases (He, Ne, As, Kr, and Xe; Table 2.3) were analyzed by a sequence of inverse numerical models to estimate the temperature of each groundwater sample at the time of recharge based on the known equilibrium solubilities of noble gases in water (Aeschbach-Hertig et al., 1999; Peeters et al., 2003). Besides fitting the equilibrium temperature, the models also account for gases in excess of the atmospheric equilibrium concentrations due to trapped bubbles (commonly referred to as "excess air"). The excess air component is either fitted without any fractionation from the atmospheric air (assuming complete dissolution of the bubbles) or

with various processes and degrees of fractionation. A constant salinity of 0 and atmospheric pressure of 1013 mbars were assumed for the model calculations. After the best fit was found for observed Ne, Ar, Xe, and Kr concentrations, the predicted He concentration was calculated according to the same model; any ^{4}He in excess of that amount was reported as "excess He" and could be considered a radiogenic input from the crustal radioactive decay processes. The output also included a χ^2 probability that the model is consistent with the data. Low χ^2 probabilities are considered a reasonable criterion to reject the models, with <1% often used and <5% being a very strong criterion to reject the run. Errors of the modeled temperature and excess He were estimated by a numerical propagation of the experimental uncertainties through the inverse procedure with data sets generated by Monte Carlo simulations.

2.2.6 Sampling and analysis of $^{14}C/^{12}C$ and $^{13}C/^{12}C$ in DIC and DOC

Samples for radiocarbon ($^{14}C/^{12}C$) and carbon stable isotopic ($^{13}C/^{12}C$) measurements on dissolved inorganic carbon (DIC) and dissolved organic carbon (DOC) were collected in 125 mL or larger glass bottles with polyseal caps and fixed with 0.1 mL of saturated mercuric chloride. All carbon isotopic measurements were performed at National Ocean Science Accelerator Mass-Spectrometer (NOSAMS) facility at the Woods Hole Oceanographic Institution following standard protocols (Elder et al., 1997). Ratios of $^{13}C/^{12}C$ are reported as $\delta^{13}C_{VPDB}$ in ‰ deviations from the Vienna Pee Dee Belemnite standard, with a typical error of ±0.1‰. Radiocarbon data ($^{14}C_{DIC}$ and $^{14}C_{DOC}$) are reported as fraction modern (FM), "modern" being defined as 95% of the AD 1950 radiocarbon concentration of NBS (National Bureau of Standards) Oxalic Acid I

normalized to $\delta^{13}C_{VPDB}$ of -19‰ (Olsson, 1970), and FM values were further normalized for C isotopic fractionation to a value of $\delta^{13}C_{VPDB}$ = -25‰. Errors in FM measurements are shown in Table 2.2. Concentrations of DIC and DOC were also reported by NOSAMS for the samples collected in 2010 and 2011 (±2% precision), including some CWs and most WAB wells; for the remaining samples, DIC was calculated from alkalinity and pH values measured in the field (in a flow cell). Comparison of the DIC concentrations calculated from the field data with those reported by NOSAMS indicated that the values were typically in agreement within <10%.

2.2.7 Lithologs

Drill cuttings were collected at 2-5 ft (0.6-1.5 m) intervals from wells ≤152 m deep (all except WAB community wells) and were used to calculate the total clay+silt thickness above the well screen (Table 2.1). The thicknesses of all clay and silt layers encountered in the litholog were added, except for the surficial clay/soil that tops the shallow aquifer, as this layer does not play a role in separating the high-As shallow aquifers from the low-As intermediate aquifers. Lithologs for the wells <90 m deep (all intermediate-depth wells that were extensively sampled fall into this category) are more reliable for the presence/absence of clay layers because the boreholes were drilled by the traditional hand-flapper method that produces compact drill cuttings (Horneman et al., 2004), unlike those collected from the mechanized pumps at depths >90 m bgl. Sand color at the depth of filter intake was noted for each well, regardless of the installation depth.

2.3 Results

2.3.1 Tritium (^{3}H), radiocarbon (^{14}C), arsenic, and lithology

With exception of three wells tapping the intermediate aquifer (<120 m bgl) containing 10-29 μg/L As, all community wells met the WHO guideline for As of 10 ug/L at the time of sampling despite many years of use (van Geen et al., 2007). Of the 65 wells sampled for ^{3}H, 8 wells had a distinctly high ^{3}H concentration of >0.3 TU, indicating a major contribution of recently recharged groundwater (Fig. 2.2a). All 8 of these wells were screened at depths ≤65 m bgl and contained <3 μg/L As, where measured. Another set of 23 wells contained low ^{3}H levels (0.10-0.27 TU) at least at one sampling time point, 21 of which had detectable ^{3}H at the 95% confidence level (0 TU was not within the range of 2σ, twice the analytical error). Most (17) of the 21 wells containing low-level, detectable ^{3}H clustered in the intermediate aquifer, whereas only 4 such samples were found in the deep aquifer (>120 m bgl) and none at depth >150 m bgl. The presence of detectable ^{3}H in upper parts of the deep aquifer (120-150 m bgl) suggests some vertical contribution of recent recharge, but the proportion of such contribution is at most 3-10%, using 2-3 TU as a 100% benchmark (any recharge since 1980, undiluted by older groundwater, would now contain ~2-3 TU). Results from the wells sampled twice or thrice between 2006-2011 (Table 2.1) showed that over this time period ^{3}H concentrations remained low in wells that initially had low ^{3}H concentrations, whereas the wells with initially elevated ^{3}H showed more variable concentrations during the same time span.

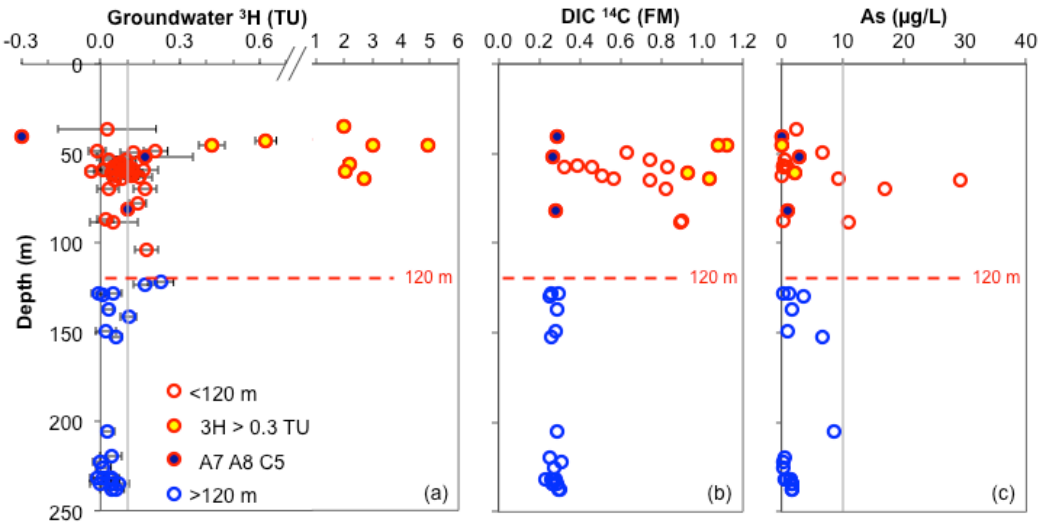

Figure 2.2. Vertical profiles of groundwater (a) ^{3}H with analytical error, (b) ^{14}C in DIC, and (c) As. Only one value per well is shown; where multiple measurements were performed, the latest non-negative value is shown for ^{3}H, and the value from 2010 is shown for ^{14}C. The data in this figure, and hereafter, are shown as open red circles for groundwater from intermediate depth (<120 m bgl), open blue circles for deep groundwater (>120 m bgl), and blue-fill red circles for the intermediate depth samples A7, A8, and C5 with consistent deep groundwater properties. Yellow fill in the red circles denotes intermediate aquifer groundwater (<120 m bgl) with particularly elevated ^{3}H concentration (>0.3 TU). The grey line in (a) indicates 0.1 TU, the concentration above which all ^{3}H samples (except two with a large analytical error) are conclusively detectable, whereas the grey line in (c) denotes the current World Health Organization limit of 10 µg/L As in safe drinking water.

Radiocarbon concentrations in dissolved inorganic carbon (DIC) ranged from 0.26-1.12 FM in groundwater from intermediate depth <120 m bgl (Fig. 2.2b and Table 2.2). Below 120 m depth, a uniform radiocarbon signature of 0.25-0.31 FM was observed

in deep aquifer DIC. Within the intermediate aquifer, 3 of the lowest $^{14}C_{DIC}$ values fell within the range of those observed in deep aquifer groundwater (A7, A8, and C5, labeled by blue fill in Fig. 2.2 and in other figures, where necessary). These samples came from a shallow outcrop of the confined Pleistocene aquifer in the northwest of our study area (van Geen et al., 2003) and carried a consistent deep groundwater signature across a range of parameters. On the other end of the spectrum, samples from 4 wells with the highest $^{14}C_{DIC}$ (0.93-1.12 FM) also had ^{3}H >2 TU (Fig. 2.3), confirming that groundwater recharged since the nuclear weapon testing began in the late 1940s reached these intermediate-depth wells, carrying so-called 'bomb' ^{14}C and ^{3}H with it. The remaining intermediate aquifer samples (below ~0.9 FM $^{14}C_{DIC}$) contained lower ^{3}H (<0.3 TU) and their ^{14}C values might be a result of groundwater aging, as well as a number of geochemical, hydrological, and biological processes.

Radiocarbon in dissolved organic carbon (DOC) was only measured in 5 samples from the intermediate aquifer from ~60-90 m bgl (Table 2.2). In two of the samples, ^{14}C of DIC and DOC was nearly identical, whereas in the remaining three, ^{14}C was 0.1-0.2 FM lower in DOC than in DIC.

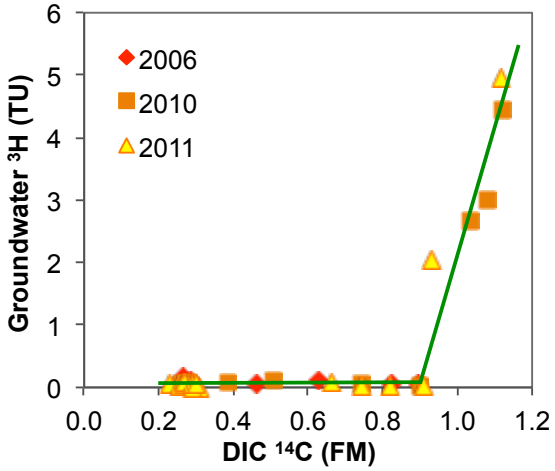

Figure 2.3. Empirical relationship between groundwater ^{3}H and ^{14}C in DIC. All available samples from the intermediate aquifer (<120 m bgl) with concurrently measured groundwater ^{3}H and ^{14}C in DIC were plotted to determine the initial $^{14}C_{DIC}$ = 0.90 FM, used to correct for the vadose zone processes before the recharge closed off from the atmosphere in C_1 and C_2 ^{14}C age calculations.

2.3.2 Radiocarbon dating

^{14}C age corrections

Three radiocarbon ages were determined for each sample (Fig. 2.4 and Table 2.2). The ^{14}C half-life of 5730 yr was used to generate the first radiocarbon age – the uncorrected ^{14}C age ("UC ^{14}C age"). This age assumes the initial ^{14}C concentration of DIC or DOC at recharge to be 1 FM and assumes a closed system evolution of DIC without any carbon reservoir corrections:

$$UC\ ^{14}C\ age\ (yr\ BP) = \frac{5730\ yr}{ln2} * ln\left(\frac{1}{FM\ ^{14}C}\right) \quad (1)$$

This approach might be appropriate for organic material (e.g. DOC or particulate OC), but the initial $^{14}C_{DIC}$ is rarely 1 FM, as total DIC is formed by the dissolution of soil CO_2 and resident soil carbonates in an open system before the system closes off from the contact with vadose zone carbon sources (Fontes and Garnier, 1979). Whereas the soil CO_2 is a product of oxidation of plant remains, the ^{14}C activity of which is often close to that of atmospheric CO_2, soil carbonates usually have a lower ^{14}C activity. One way to estimate the initial ^{14}C activity of DIC is to empirically relate $^{14}C_{DIC}$ to observed ^{3}H concentrations (Fig. 2.3), following Verhagen et al. (1974). This approach yielded an estimate of initial $^{14}C_{DIC}$ of 0.90 FM for our data set, close to the value of 0.87 FM used

by Hoque and Burgess (2012) in their Bengal Basin ^{14}C work and also close to the fixed value of 0.85 FM applied in the "Vogel" model (Vogel, 1967; Vogel and Ehhalt, 1963). Therefore, the second radiocarbon age, or the "C_1 ^{14}C age", is corrected for the initial $^{14}C_{DIC}$ formed under open system conditions, but not for any subsequent dissolution of carbonates along the flowpath:

$$C_1\ ^{14}C\ \ age\ (yr\ BP) = \frac{5730\ yr}{ln2} * ln\left(\frac{0.90}{FM}\right) \quad (2)$$

Finally, the third approach was to build upon the C_1 ^{14}C age and estimate the maximum possible contribution of carbonate dissolution along the flowpath to the total DIC and its ^{14}C signature, after the system was closed with respect to gas exchange in the vadose zone. This was achieved by using a simple isotopic mixing model based on the $\delta^{13}C$ of two end members: the initial DIC and carbonate minerals (e.g., Hoque and Burgess, 2012). In order to make this the maximum possible correction for carbonate dissolution (thus, the minimum calculated age), the value used for the initial $\delta^{13}C_{DIC}$ was -25‰, in accordance with the value used by Harvey et al. (2002) and Hoque and Burgess (2012), and appropriate for the dominance of ^{13}C-depleted C3 plants (Sarkar et al., 2009). Similarly, to make this a minimum age, the carbonate minerals in the mixture were assumed to be of marine origin ($\delta^{13}C$ = 0‰) and free of radiocarbon. Thus, the third radiocarbon age – C_2 ^{14}C age – includes a correction for mixing of different carbon pools, similar to that of Ingerson and Pearson (1964), but with the added correction for initial $^{14}C_{DIC}$ of 0.90 FM:

$$C_2\ ^{14}C\ \ age\ (yr\ BP) = \frac{5730\ yr}{ln2} * ln\left(\frac{0.90}{FM} * \frac{\delta^{13}C_{DIC}}{-25‰}\right) \quad (3)$$

None of the above ^{14}C age corrections accounted for isotopic fractionation effects during the isotopic exchange reactions of C species ($CO_{2(g)}$ to $CO_3^{2-}{}_{(aq)}$ equilibrium), which can have some impact on the final ^{13}C contents (Fontes and Garnier, 1979). The above models also did not take into account the mineralization of groundwater DOC subsequent to the initial recharge, and the impact it might have had on the budget of DIC radiocarbon. Lastly, none of the ^{14}C ages were calibrated to calendar years, as doing so would not be meaningful for dating of groundwater $^{14}C_{DIC}$ that is subject to as many uncertainties as presented above. It is important to note that the model without any corrections (UC age), and to a lesser extent the simple open system model (C1 age) without added carbonate input (dissolution, exchange), are not considered representative of most hydrological systems (Fontes and Garnier, 1979).

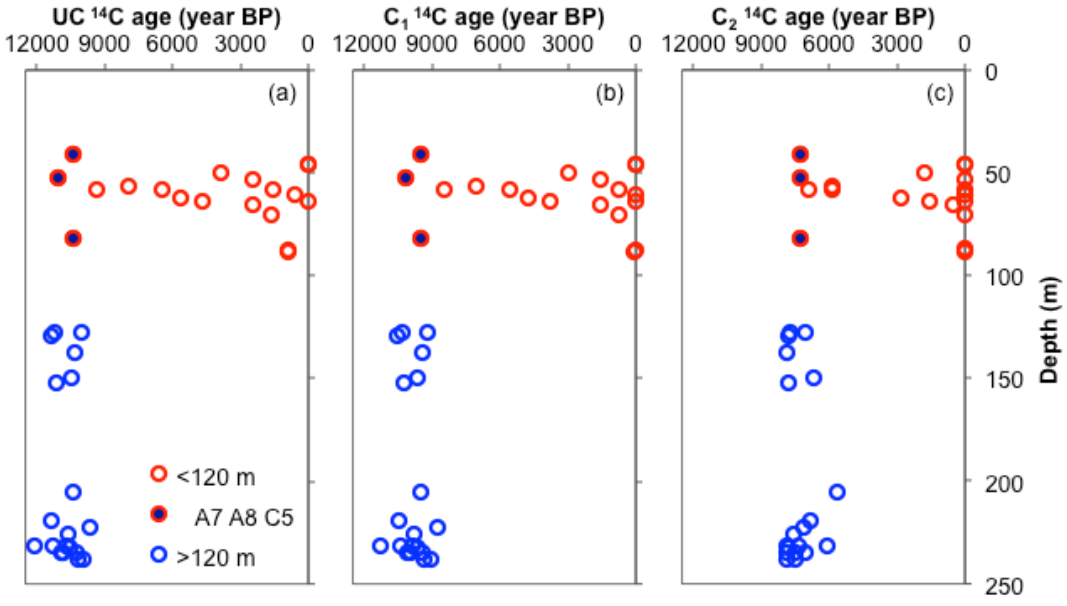

Figure 2.4. Calculated ^{14}C ages in DIC. (a) "UC", or uncorrected, ^{14}C age was calculated directly from the measured ^{14}C values without any correction. (b) C_1 ^{14}C age is a simple open system model that corrects for the initial $^{14}C_{DIC}$ at recharge of 0.90 FM,

while the C_2 ^{14}C age (c) contains an additional correction for the maximum contribution of radiocarbon-dead carbonate dissolution along the flowpath, based on a $^{13}C_{DIC}$ mixing model ($\delta^{13}C$ = -25‰ in initial DIC and 0‰ in admixing carbonate). The blue fill in red circles indicates the intermediate depth samples (<120 m bgl) with consistent deep groundwater properties.

Calculated DIC ^{14}C ages

The simplest, uncorrected (UC) ^{14}C age dated deep aquifer groundwater to a range of 9,670-12,120 ^{14}C yr before present (BP), with the average of 10,700 ^{14}C yr BP (Fig. 2.4 and Table 2.2). The intermediate aquifer groundwater UC ^{14}C ages spread along a range from modern to ~10-11 kyr in samples A7, A8, and C5 that resembled the deep aquifer. The correction for initial ^{14}C content of DIC, based on the relationship between ^{3}H and ^{14}C, resulted in shifting the range of deep aquifer ages (C_1 ^{14}C age) by ~900 years towards younger ages (8,790-11,250 ^{14}C yr BP), with the average of 9,830 ^{14}C yr BP (Table 2.2 and Fig. 2.4). The subsequent correction for dissolution of carbonates based on a simple isotopic mixing model (C_2 ^{14}C age), designed to provide an estimate of the maximum possible effect of the dissolution of radiocarbon-free carbonates along the flowpath, resulted in a more dramatic shift of the groundwater age range in deep aquifer to 5,660-7,890 ^{14}C yr BP (average 7,310 ^{14}C yr BP). The corrections from UC to C_1 and C_2 ^{14}C age had a similar effect on intermediate aquifer groundwater ages, thus shrinking their span and shifting dates towards the “modern” category with each correction.

2.3.3 Noble gas temperatures and radiogenic He

The model that best fit the data (Table 2.3) considered the equilibrium temperature, the amount of excess air, and the fractionation of excess air as variables in the simulation ("Taf-1" model), and the fractionation of excess air was thought to result from a partial equilibrium dissolution of the trapped air bubbles in a closed system [the "CE" model, (Aeschbach-Hertig et al., 1999; Peeters et al., 2003)]. Some of the model results were rejected (Table 2.3) based on a low model probability and/or a high error in model temperature estimate (>1.5 ºC error). At least some of the samples for which the model failed to converge suffered from degassing while sampling, as indicated by Ne concentrations below solubility equilibrium with the soil air ($<1.7\times10^{-7}$ ccSTP g^{-1}). Among the converged samples, model probabilities were well above the strict 5% threshold, except for CW42 with 3.4%, which was still a reasonable fit (>1 %) and had the lowest model temperature error of the entire data set, thus the fit for this sample was not rejected.

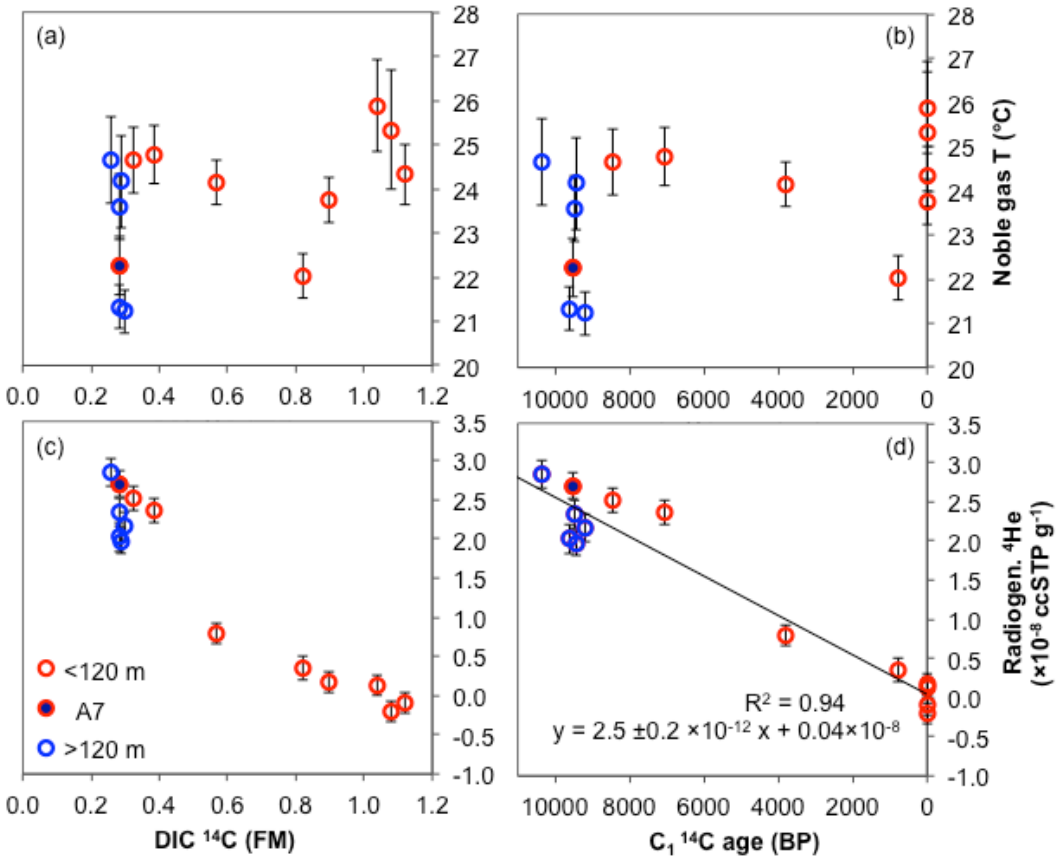

Figure 2.5. Noble gas temperatures and radiogenic ("excess") He plotted against (a and c) ^{14}C measured in DIC, and (b and d) corrected C_1 ^{14}C ages. Noble gas temperature (a and b), corresponding to a temperature at the time of recharge, and radiogenic He (c and d) were both estimated by model Taf-1 that fit the noble gas data. The errors indicated by vertical error bars combine the analytical error with model fit uncertainty. Only one sample per well is shown; where multiple noble gas measurements were made, those with the best model fit are displayed. The trend linking the radiogenic He to C_1 ^{14}C ages was calculated for combined intermediate and deep groundwater samples. The blue-fill red circle indicates an intermediate depth sample (<120 m bgl) with consistent deep groundwater properties.

Current groundwater temperatures in the intermediate aquifer cluster around an average of 26.2 °C (Table 2.4), while the average temperature in deep groundwater is slightly higher at 26.9 °C, due to the geothermal gradient. Temperatures of groundwater at the time of recharge (Table 2.3), however, were calculated by the noble gas method and are also known as the noble gas temperatures (NGTs). They are plotted only for those samples where the model converged and accurately described the observed noble gas concentrations (Fig. 2.5ab). In the intermediate aquifer, NGTs varied between 22 and 26 °C, with the average and standard deviation of 24.1±1.3 °C. Six of the nine converging samples clustered between 24 and 26 °C, close to the current average temperature of the intermediate groundwater. The rather shallow sample (A7) that exhibited the signature of deep aquifer tracers and chemistry also had a low NGT of 22.3 °C. Noble gas temperatures from the deep aquifer were slightly lower than in the intermediate aquifer, ranging between from 21 to 25 °C, with the average and standard deviation of 23.0±1.6 °C. Although the two lowest NGTs from the deep aquifer are below any observed in the intermediate aquifer, the amount of scatter in samples from both aquifers precluded any definitive conclusion of recharge temperature differences. Furthermore, NGTs plotted against C_1 ^{14}C age (Fig. 2.5b) did not have a statistically significant trend ($p = 0.19$), confirming the lack of temporal trend in recharge temperatures. There was, likewise, no significant trend between NGTs and the sample depth (not shown).

The excess He, also estimated by the NG model, stands for the He released *in situ* by the radioactive decay processes in the sediment through which groundwater flowed, hence it can also be named “radiogenic He”. It can be proportional to the age or residence time of groundwater if the aquifer matrix and release rates of He from the sediment are

fairly homogeneous and constant along the flowpaths, little degasing loss occurs, and no confounding effects of crustal He degassing occur (Torgersen and Clarke, 1985). Samples in which $^{14}C_{DIC}$ ranged from modern to ~0.25 FM showed an increasing radiogenic He contribution from ~0 to ~3×10^{-8} ccSTP g^{-1}, with the highest levels present in the deep aquifer samples and in the intermediate aquifer groundwater with low $^{14}C_{DIC}$ (Fig. 2.5c). The relationship between the radiogenic He and the C_1 ^{14}C age (Fig. 2.5d) is linear, with the empirical He accumulation rate of $^4He = 2.5\pm0.2 \times10^{-12}$ ccSTP g^{-1} yr^{-1} * ^{14}C age (yr) + 0.04×10^{-8} ccSTP g^{-1} ($R^2 = 0.94$, $p = 2\times10^{-8}$, both the intermediate and deep samples were used in regression). The $^3He/^4He$ ratio in samples that contain a high contribution of radiogenic He (up to ~35% of the measured He) ranges between 0.9-1.1×10^{-6} (Table 2.3), falling below that of the remaining samples. It is also below the $^3He/^4He$ ratio in solubility equilibrium with atmospheric air (1.36×10^{-6}) because ^3He is depleted in the radiogenic (crustal terrigenic) He that has a $^3He/^4He$ ratio of ~2×10^{-8}.

2.3.4 Chemical composition of groundwater

The greater variability of ^3H and ^{14}C in the intermediate aquifer compared to the deeper aquifer was matched by a greater scatter in the intermediate groundwater physicochemical characteristics, such as pH, electrical conductivity (EC), alkalinity, DIC, Na, and Si concentrations (Fig. 2.6 and Table 2.4). In contrast, deep aquifer groundwater carried a much more uniform signature of these parameters. In particular, deep groundwater and the three intermediate-depth samples with deep ^3H and ^{14}C signatures clustered around low values of pH (mostly 6.5-6.8), low EC (0.3-1 mS/cm), low alkalinity (1.7-3.0 mEq/L), low DIC (3-4.8 mM), low Na (<50 mg/L) and high levels of

Si (mostly 55-70 mg/L). The concentrations of DOC in the intermediate aquifer (0.05-0.25 mM) were 1-2 orders of magnitude lower than those of DIC (4.8-10.5 mM).

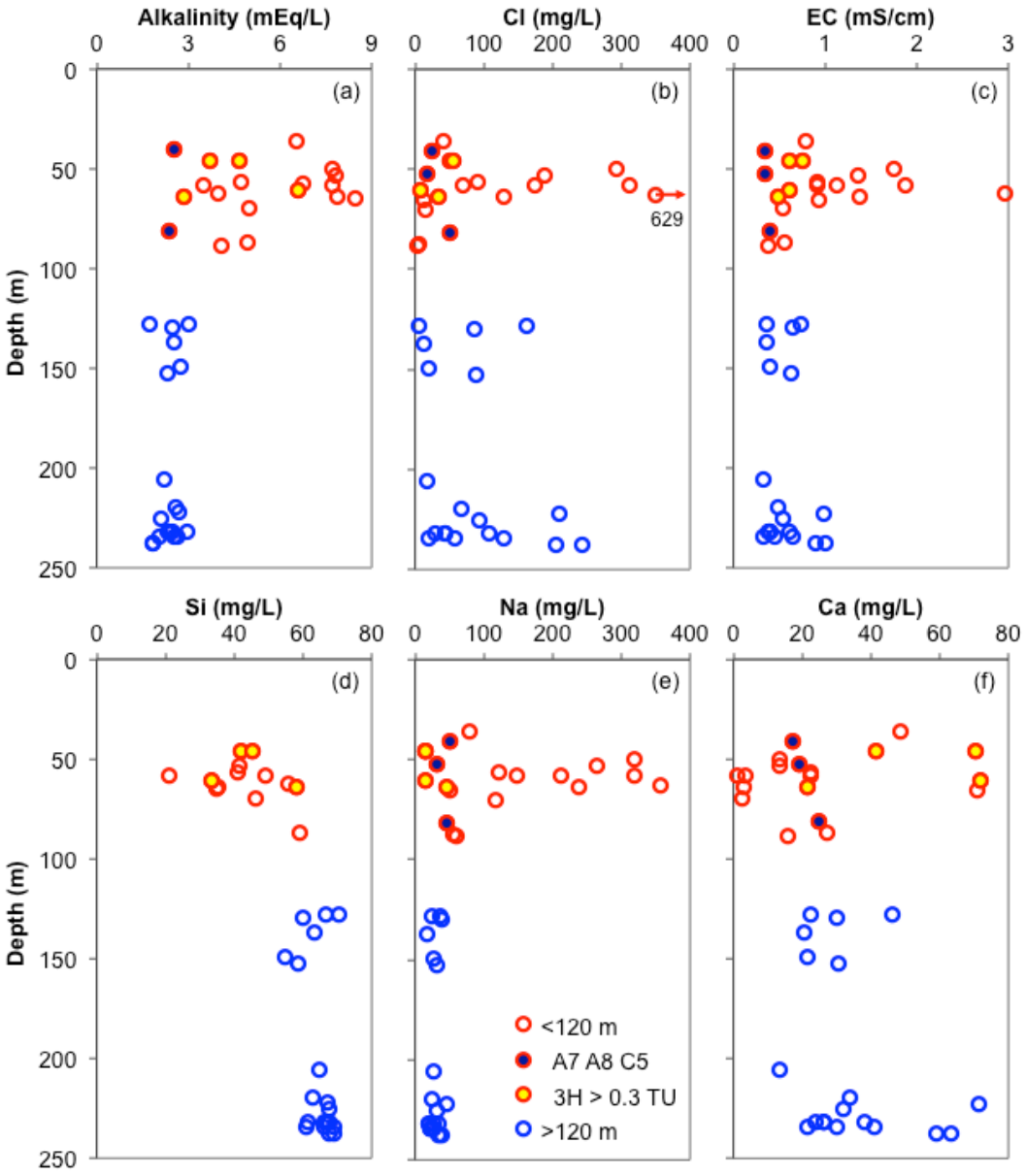

Figure 2.6. Vertical profiles of groundwater (a) alkalinity, (b) chloride, (c) electrical conductivity, (d) silicon, (e) sodium, and (f) calcium. The blue and yellow fill in red circles denote the intermediate depth samples (<120 m bgl) with consistent deep groundwater properties (blue fill) or with ^{3}H >0.3 TU (yellow fill).

The concentrations of Ca (1-83 mg/L), Mg (1-35 mg/L) and K (1-4 mg/L) ranged similarly in both aquifers (Fig. 2.6 and Table 2.4). This was the case also for Cl (4-311 mg/L) and SO_4 (0.3-17 mg/L), with a slightly higher range of values observed in the intermediate aquifer (Fig. 2.13a in Appendix and Table 2.4). Bromide concentrations were below detection in some samples, and remained ≤0.7 mg/L where detectable (Fig. 2.13b). Fluoride concentrations were <0.4 mg/L in all deep aquifer samples (except one, where it was ~0.5 mg/L, Table 2.4). A wider range of F concentrations (up to 1 mg/L F) was observed in the intermediate aquifer, with two samples in the 2-3 mg/L range. Only one of these high-F wells (CW18) was a drinking water source. One high-EC sample (CW15) had a particularly high level of Cl (629 mg/L), Br (2.2 mg/L), and SO_4 (24 mg/L).

The concentrations of SO_4 measured by ion chromatography corresponded well to those of S measured on ICP-MS (R^2 = 1.00). The slope of their relationship was 2.8, or 7% lower than the expected 3.0 based on their mass ratio. As no samples had the characteristic smell of sulfides at the time of collection, this was most likely an inter-calibration issue and all S was in the form of sulfate.

Iron and manganese were highly variable in both aquifers, with concentrations of up to 4 mg/L Fe (mostly <2 mg/L; one sample had ~10 mg/L) and up to 1,400 µg/L Mn (Table 2.4). P was generally low (<0.6 mg/L P), except for one sample at 4.7 mg/L (Table 2.4).

2.3.5 ^{13}C record

Carbon stable isotope values ($\delta^{13}C$) in DIC ranged between -15 and -22‰ in both the intermediate and deep aquifer (Table 2.2, Figs. 2.7d and 2.9, and Figs. 2.11 and 2.14 in Appendix). The observed $\delta^{13}C_{DIC}$ values fall between those expected if DIC was produced solely by the oxidation of bulk organic carbon from C3 (-28‰) and C4 plants (-13‰) in the Bengal Basin (Sarkar et al., 2009). In deep aquifer groundwater, $\delta^{13}C_{DIC}$ was correlated with alkalinity ($R^2 = 0.36$, $p = 0.006$), the heavier (more positive) values of $\delta^{13}C$ being observed at a higher alkalinity, which would be expected from the dissolution of marine or pedogenic carbonates, if there were any in the sediment.

The relationship between $\delta^{13}C_{DIC}$ and $^{14}C_{DIC}$ was different in deep and intermediate aquifers (Fig. 2.7d). Deep groundwater samples exhibited a strong ($R^2 = 0.61$) and significant ($p = 8\times10^{-5}$) trend towards more depleted (negative) $\delta^{13}C$ values as ^{14}C in DIC increased (Fig. 2.9), and the three intermediate-depth samples with characteristics of deep groundwater fit well within the trend. In the intermediate aquifer, however, the correlation between DIC $\delta^{13}C$ and ^{14}C showed an opposite trend (Fig. 2.7d): heavier (more positive) $\delta^{13}C_{DIC}$ was observed in samples with higher $^{14}C_{DIC}$, but the trend was less well defined, and significant only if the three samples with characteristics similar to those of the deep aquifer samples were excluded from the regression ($p = 0.006$).

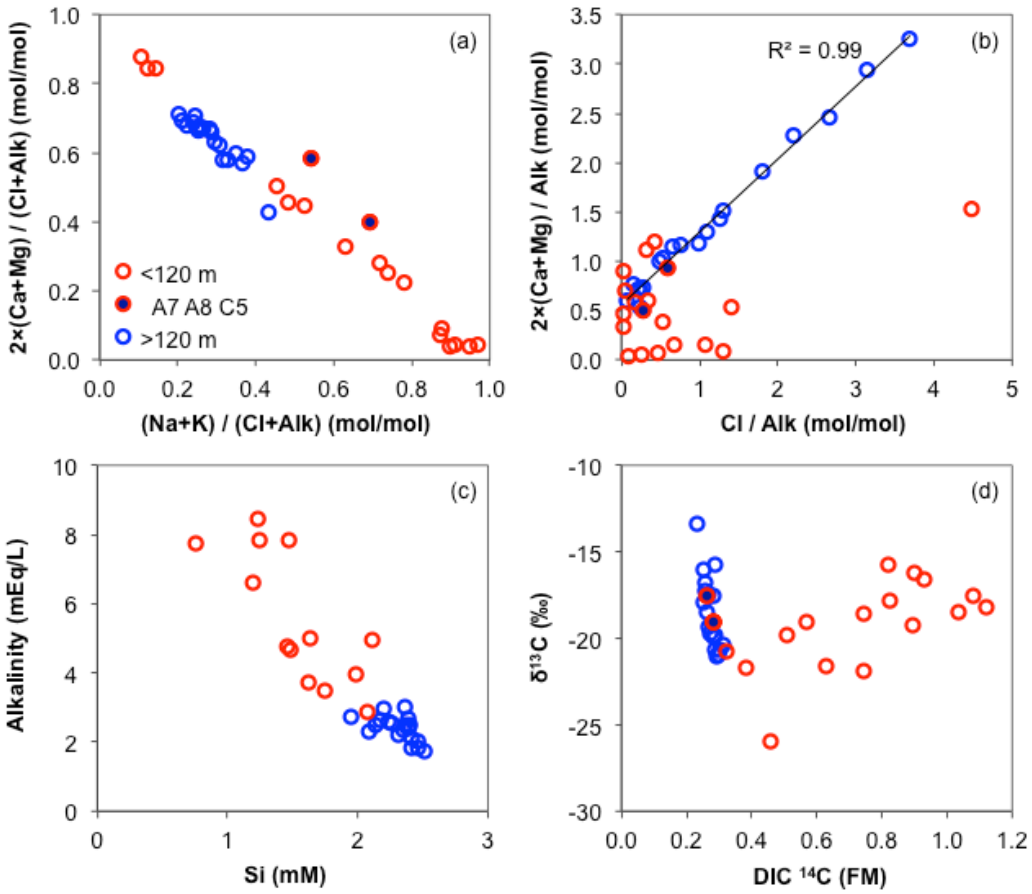

Figure 2.7. Geochemical properties of intermediate and deep groundwater. (a-c) Equivalent molar ratios and correlations between major cations (Ca, Mg, Na, and K), major anions (Cl and HCO_3, approximated by alkalinity), and dissolved Si in groundwater. (d) The relationship between $\delta^{13}C$ and ^{14}C in groundwater DIC. The blue fill in red circles denotes the intermediate depth samples (<120 m bgl) with consistent deep groundwater properties.

2.3.6 Groundwater stable isotopes ($^{2}H/^{1}H$, $^{18}O/^{16}O$)

Most stable isotope values ($\delta^{2}H$ and $\delta^{18}O$) fall on or near the global meteoric water line (GMWL: $\delta^{2}H = 8* \delta^{18}O + 10‰$), but fall to the right of this line as a result of evaporation and kinetic isotope fractionation (Fig. 2.8a). Virtually all deep aquifer

samples fall on the GMWL, indicating recharge by precipitation, and cluster around $\delta^{18}O$ values between -5 and -6‰ and $\delta^{2}H$ values between -30 and -40‰. The average isotope composition of modern precipitation in the area (Stute et al., 2007) is similar to that observed in the deep aquifer samples (Fig. 2.8a). Intermediate aquifer samples, on the other hand, span a larger range of stable isotope values, and nearly half of them are marked by a signature of slight or heavy evaporation before recharge, as judged by their distance from the GMWL (marked by pink and red fill, respectively, Fig. 2.8).

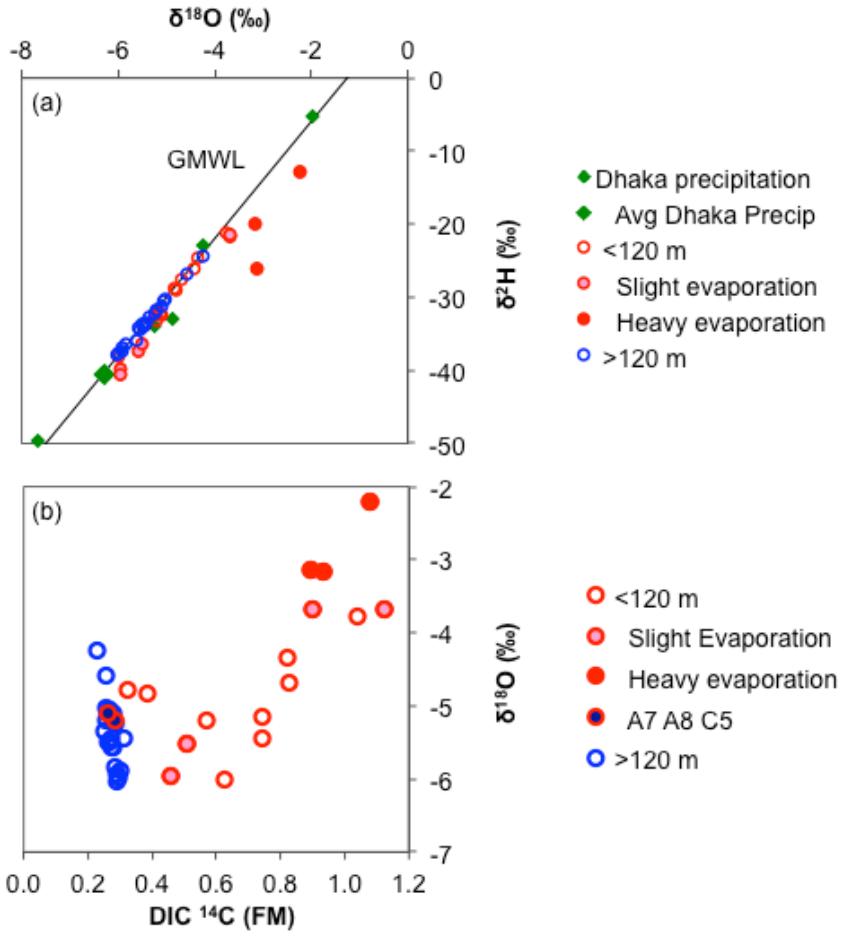

Figure 2.8. (a) Water stable isotopic ($\delta^{2}H$ and $\delta^{18}O$) composition of groundwater and (b) the relationship of $\delta^{18}O$ with ^{14}C in DIC. (a) Dhaka precipitation, including its

average (Stute et al., 2007), and the global meteoric water line (GMWL) by Craig (1961) are shown in the background. (b) A similar pattern was observed for δ^2H (not shown). The pink or red fill of the red circles indicates intermediate depth samples (<120 m bgl, a and b) with a slight or heavy evaporative signature, respectively, as judged by the distance from the GMWL. The blue fill in red circles (b) denotes the intermediate depth samples with consistent deep groundwater properties.

A striking aspect of the stable isotopic data from deep groundwater is the strong correlation of both δ^2H and $\delta^{18}O$ with $\delta^{13}C_{DIC}$ ($R^2 = 0.81$ for both isotopes, δ^2H shown in Fig. 2.11d in Appendix). Thus, as is the case of $\delta^{13}C_{DIC}$, when $\delta^{18}O$ or δ^2H in deep groundwater are plotted versus $^{14}C_{DIC}$ values (Figs. 2.8b and 2.9; δ^2H not shown as it follows an identical pattern), a remarkable trend towards more depleted (negative) $\delta^{18}O$ and δ^2H values emerges at higher ^{14}C concentrations ($R^2 = 0.57$ for $\delta^{18}O$, 0.60 for δ^2H) and this relationship is highly significant ($p = 0.0002$ for $\delta^{18}O$, 0.0001 for δ^2H). The intermediate samples (A7 and C5) with properties close to those of the deep samples also fit within the deep aquifer trend. The remaining intermediate aquifer samples suggest a less sharply defined trend toward heavier stable isotopes with higher ^{14}C concentrations, although this pattern is affected in part by the evaporated nature of the most recently recharged samples with the highest ^{14}C content. The correlation of the intermediate aquifer stable isotopes with $\delta^{13}C_{DIC}$ is also less defined than in the deep aquifer ($R^2 =$ 0.44 for δ^2H, 0.35 for $\delta^{18}O$).

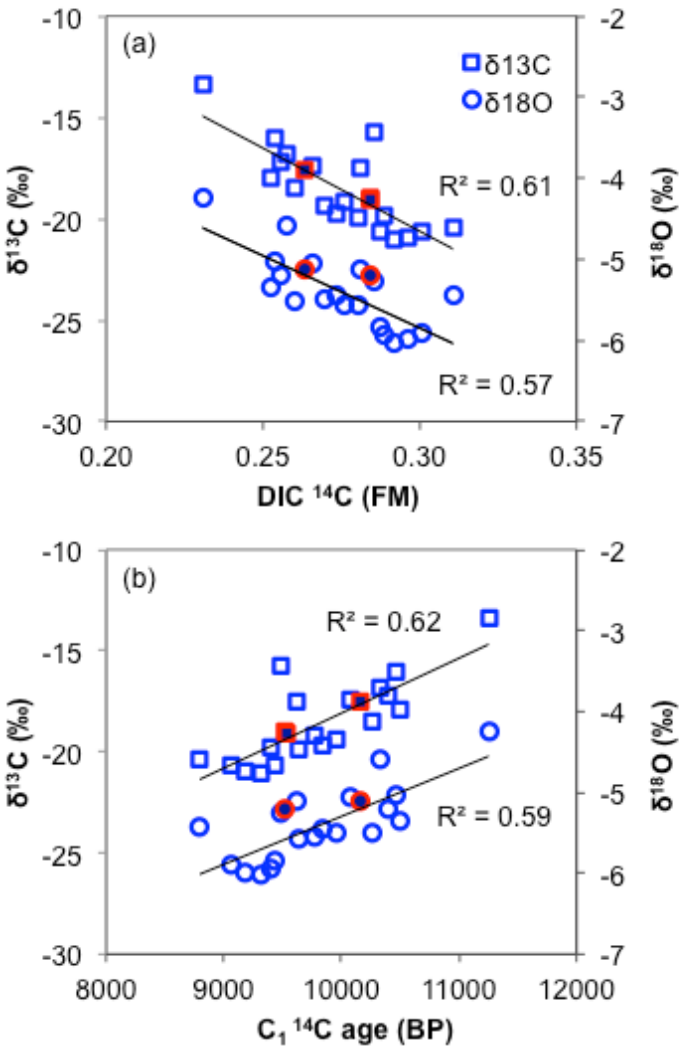

Figure 2.9. A zoom-in on the consistent correlations between $\delta^{13}C_{DIC}$ and $\delta^{18}O$ with (a) $^{14}C_{DIC}$ and (b) C_1 ^{14}C age in the deep groundwater (>120 m bgl). The deep-like groundwater samples from the intermediate aquifer (<120 m bgl) are indicated by blue-fill red circles for comparison. The trendlines and R^2 values were calculated using deep samples only.

2.4 Discussion

2.4.1 Groundwater recharge and chemistry in the intermediate-depth low-As aquifer

Based on our data from Araihazar upazilla, the low-As aquifers were defined as "intermediate" (<120 m bgl) or "deep" (>120 m bgl). The intermediate aquifer designates the low-As aquifer extending beneath the shallow aquifer depth of peaking As concentrations (van Geen et al., 2003) to the depth of ~120 m bgl. There are practically no wells between 100 m and 120 m bgl, but the lower boundary of the aquifer was picked based on the fact that 120 m was the maximum extent of the sea level difference between the Last Glacial Maximum during the Pleistocene and the Holocene (Fairbanks, 1989). A highly variable groundwater chemistry and ^{14}C ages of groundwater DIC ranging from modern to ~10 kyr are observed in this depth range (Figs. 2.2, 2.4, and 2.6). Parts of the intermediate aquifer have been recharged recently from shallow groundwater, as evidenced by multiple wells with large contributions of bomb ^{3}H and $^{14}C_{DIC}$. Much of this recent recharge, as well as some of the older intermediate aquifer groundwater, comes from a pool of surface water characterized by evaporative enrichment of stable isotopes (Fig. 2.8a), such as stagnant ponds or rice fields that can hold flood water for months at a time (Stute et al., 2007).

The levels of ^{3}H and $^{14}C_{DIC}$ in groundwater also provide a measure of vertical flow, not necessarily local, connecting the intermediate and shallow aquifers. Whether the clay units are continuous and provide confinement is of a great importance, but difficult to ascertain, hence we relate the ^{3}H and $^{14}C_{DIC}$ concentrations to the thickness of

clay in well lithologs, a simple parameter that presumably reflects the extent of vertical confinement of the aquifer. However, the amount of clay in well lithologs does not correlate very well with the observed ^{3}H and $^{14}C_{DIC}$ levels in groundwater, especially among the wells that have ≤20 m of clay above the intake screen (Fig. 2.10). Although 7 intermediate aquifer wells with <20 m of clay have elevated ^{3}H and/or ^{14}C concentrations, most samples (24 out of 31) contain low ^{3}H (<0.3 TU). Where clay above the well screen is thicker than the threshold 20 m, the proportion of high-^{3}H samples is lower (7 out of 8 samples have <0.3 TU), suggesting a local impediment to vertical flow, but 4 of the 8 samples still contain detectable ^{3}H (0.1-0.2 TU) and thus receive some recent recharge from the surface. Radiocarbon concentration shows a slight negative correlation, although insignificant ($p = 0.171$), with the thickness of clay layers in well lithologs. Only when the samples containing ^{3}H levels >0.3 TU are excluded (yellow fill in Fig. 2.10), removing the effect of a very rapid penetration of bomb ^{14}C, is the negative correlation between the $^{14}C_{DIC}$ and the clay thickness slightly more robust (trendline in Fig. 2.10b), but still not statistically significant ($p = 0.075$).

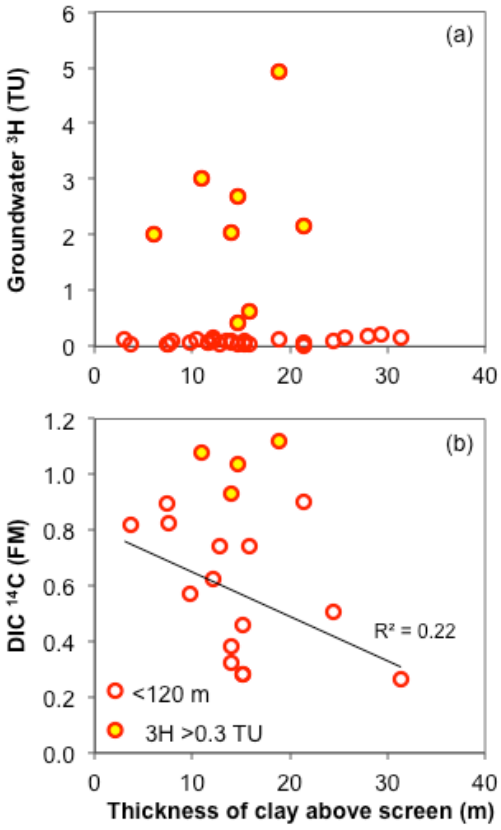

Figure 2.10. Relationship between intermediate-depth groundwater (a) ^{3}H, and (b) ^{14}C and the total thickness of clay in well lithologs. Only one value per well is shown, as described in Fig. 2.2. Yellow fill in the red circles denotes intermediate aquifer groundwater (<120 m bgl) with ^{3}H >0.3 TU – these samples were excluded from the ^{14}C trendline with clay thickness shown in (b).

The above observations are consistent with the hypothesis that recent recharge is fed into the aquifer by lateral flow and that the flow in the aquifer is mostly horizontal (Aziz et al., 2008). Temporal trends in ^{3}H concentrations of a high-^{3}H well with 18.9 m of clay above the well screen, CW27, also argue that the changes in the observed ^{3}H levels are due to horizontal flow coupled to the recharge of groundwater variable in time and/or space: 6.15 TU were observed in September 2006, which would have decayed to

5.10 TU by January 2010; instead, a ^{3}H concentration of 4.44 TU was observed at the latter time, which then rose again to 4.94 TU in January 2011. The observed vertical communication of the intermediate aquifer with the surface and shallow groundwater may occur in the areas where clay layers are thin or missing (McArthur et al., 2010) and could be driven by local pumping that increases downward and lateral hydraulic gradients.

Arsenic does not appear to have penetrated into the recently recharged waters of the intermediate aquifer because it was low in the wells with the highest ^{3}H and ^{14}C concentrations (Fig. 2.2). This could have resulted from the sorption of As to the aquifer sands and the retardation of its transport (Radloff et al., 2011; Stollenwerk et al., 2007). Alternatively, the areas with a rapid vertical recharge between the aquifers might preferentially coincide with those where the shallow aquifer is well flushed by rapid recharge, and thus contains less As (Aziz et al., 2008; Stute et al., 2007; van Geen et al., 2008). The data also suggest that the wells tapping grey sands might have a slightly higher content of dissolved As than those installed in the orange sand, as the three intermediate-depth wells containing 11-29 μg/L As were installed in the greyish sand. This feature does not appear related to recent recharge from the surface because ^{3}H is undetectable in two of the wells, whereas ^{3}H was detectable in one of the wells in 2006 (0.27 TU), but fell below detection in 2011 when 29 μg/L As was measured.

Although most of the intermediate aquifer wells tap orange sand, presumably of Pleistocene origin, there is a lack of systematic patterns in the intermediate groundwater chemistry (Figs. 2.6 and 2.7, and Fig. 2.11 in Appendix). This may not be surprising as the intermediate aquifer shows evidence of recharge with shallow groundwater and

evaporated surface water, while it also contains groundwater from the other end of the age and chemistry spectrum: notably, samples from wells A7, A8, and C5 (and to some extent CW29 and CW31 also) have the deep aquifer signature of low ^{14}C, high radiogenic He, low Na and low alkalinity (Figs. 2.4, 2.5, and 2.6). Wells A7, A8, and C5 in the NW corner of the study area tap the orange sand located close to the southern edge of the uneroded Pleistocene uplands, known as the Madhupur Terrace (Goodbred and Kuehl, 2000b). The protection of this part of the aquifer afforded by the interfluvial Madhupur paleosol might explain the Pleistocene signature of the groundwater found there (McArthur et al., 2008), and the thickest clay of all the lithologs was also found at well C5. Thus, the intermediate aquifer contains groundwaters with a range of ages and origins, matched by an equivalently large range of alkalinity, Cl, EC, Si, Na, Ca, and Mg values (Figs. 2.6 and 2.7).

The cations in intermediate aquifer groundwater vary widely between the alkaline (Na+K) and alkaline earth (Ca+Mg) dominance, whereas bicarbonate dominates among the anions with a Cl/alkalinity molar ratio typically <1 (Fig. 2.7ab). The alkalinity is used as a measure of HCO_3^- concentrations, given that the pH of our samples strongly favors bicarbonate over carbonate in equilibrium. The molar balance between alkalinity and Si (representing H_4SiO_4) can be as high as 8:1 in favor of alkalinity (Fig. 2.7c). Despite such a dominant bicarbonate contribution to groundwater chemistry, no significant correlations are found between alkalinity, ^{13}C in DIC, Ca and Mg in the intermediate aquifer (Fig. 2.11 in Appendix), thus if the dissolution of carbonates contributed to the intermediate groundwater chemistry at all, its imprint is not clearly visible.

No other particularly clear process dominates the intermediate aquifer groundwater chemistry. One high-EC sample (CW15) exhibited the evidence of mixing with remnant seawater due to its high concentrations of Cl, Br, and SO_4, and a seawater Na/Cl ratio. Most other intermediate aquifer samples have a Na/Cl ratio above that of the seawater (Fig. 2.13a in Appendix), indicating an additional input of Na ions beyond that of sea salt. The ratios of Cl/Br in both aquifers (Fig. 2.13b) are close to that of SW, indicating that both anions are ultimately sourced from the ocean, by atmospheric aerosol input or a slight mixing with remnant seawater from past coastline transgressions, and that the aquifers are largely unpolluted by wastewater (Ravenscroft et al, 2013). The three samples with the highest Cl/Br ratio (yellow fill) have an additional source of Cl and also excess SO_4 compared to the marine salt SO_4/Cl ratio, indicating mixing with surface-derived wastewater (McArthur et al., 2012). In line with the surface water penetration, these three samples from the intermediate aquifer also have the highest measured ^3H concentrations.

If we do not consider the high-EC sample (CW15) and the 5 low-$^{14}C_{DIC}$ samples (A7, A8, C5, CW29, and CW31), Na and alkalinity increase in tandem in the intermediate aquifer, as ^{14}C and ^{13}C in DIC decrease (Fig. 2.7d and Fig. 2.12 in Appendix). This observation might be related to the mineralization of old, early Holocene organic matter depleted in ^{13}C and ^{14}C (Sarkar et al., 2009), as most intermediate groundwater was recharged <10,000 years BP and thus interacted with the organic-rich Holocene sediment rapidly stored in the basin between 11-6,000 ^{14}C yr BP (Goodbred and Kuehl, 2000a; Sarkar et al., 2009). The consumption of organic matter could have produced CO_2 that subsequently weathered the sediment silicates, and helped accumulate

cations and alkalinity as weathering products under the low hydraulic gradients of the Holocene. Such a process can help explain the high EC in some of the intermediate aquifer groundwaters, but the mineralization of old OM would also bias $^{14}C_{DIC}$ ages towards older dates.

Dissolved organic carbon generally has the same or slightly older ^{14}C age than DIC (Table 2.2). A similar pattern was observed at depths >15 m bgl by Mailloux et al. (2013) who also showed that younger DOC advected from the surface is preferentially metabolized by microbes and incorporated into their DNA. Since the observed DOC concentrations are ~2 orders of magnitude lower than DIC conc. in the intermediate aquifer (Table 2.4), most DOC has likely already been converted to DIC and such a scenario could have shifted some $^{14}C_{DIC}$ ages in the intermediate aquifer towards younger dates. Given the complexity of recharge pathways and groundwater chemistry in the intermediate aquifer, therefore, it is hard to select the ^{14}C age model that would be the most appropriate for intermediate-depth groundwater.

2.4.2 Chemistry, ^{14}C ages, and the residence time of deep groundwater

Groundwater chemistry in the deep aquifer (>120 m bgl) is much more uniform than in the intermediate: the low EC, alkalinity and Na, coupled to the high Si, and a Na/Cl ratio below that of the seawater, are characteristic of the deep groundwater (Fig. 2.6 and Fig. 2.13a in Appendix). Ca and Mg are the dominant cations at 57-69 % of cation equivalence units (Fig. 2.7a), however their concentrations are not correlated with an increasing alkalinity or a more positive ^{13}C in DIC, which would be expected from marine carbonate dissolution; Ca and Mg concentrations are, in fact, negatively

correlated with alkalinity ($p = 0.036$ for Ca, Fig. 2.11 in Appendix; $R^2 = 0.35$ and $p = 0.008$ for Mg) and with $^{13}C_{DIC}$ ($p = 0.011$ for Ca; $R^2 = 0.38$ and $p = 0.005$ for Mg). The sum of Ca and Mg is well correlated instead with Cl ($R^2 = 0.99$, Fig. 2.7b), the dominant anion in ~1/2 of the deep samples (when Cl/Alk molar ratio >1), and appears unrelated to the carbonate dissolution processes (Stallard, 1980). In addition, the ratio of Ca+Mg (in equivalence units) to bicarbonate ions (approximated by alkalinity) varies between 0.5-3.2 (Fig. 2.7b), whereas it would have been ~1 if there had been a large contribution of carbonate dissolution.

Indeed, no quantifiable amount of carbonates was found in either Holocene (B. J. Mailloux and M. Stute, personal communication, 2012) or the orange, Pleistocene sand (this work, Chapter 3) in our field area, and the Pleistocene sands are also typically low in Ca content (McArthur et al., 2008; van Geen et al., 2013; this work, Chapter 3), presumably due to the more efficient aquifer flushing under the higher hydraulic gradients of the Pleistocene sea level lowstand (BGS and DPHE, 2001). The Ca+Mg cation dominance in deep groundwater (Fig. 2.7a) might instead be related to the low Na levels and the low Na/Cl ratio through a cation exchange mechanism that depletes Na and enriches Ca and Mg in groundwater during salinization of an aquifer previously well-flushed by freshwater (Ravenscroft and McArthur, 2004). Such a replacement of sedimentary Ca and Mg by Na could have occurred at the onset of the Holocene due to the rapid sea-level rise causing a minor saltwater intrusion, limited in extent because deep groundwater stable isotope and Cl concentrations are not exceptionally enriched.

The relatively low pH, EC, and alkalinity (Table 2.4 and Fig. 2.6ac), as well as the Si:Alk ratio of ~1 (Fig. 2.7c) suggested the predominance of silicate weathering in

this aquifer, as did the weak, but significant, correlation of Ca and Mg with Si ($R^2 = 0.24$, $p = 0.032$ for Ca; $R^2 = 0.23$, $p = 0.037$ for Mg). Calculations in Visual MINTEQ 3.0 (http://www2.lwr.kth.se/English/OurSoftware/vminteq/) using the typical deep aquifer groundwater composition revealed that SiO_2-containing minerals such as quartz, chalcedony, and cristobalite are saturated or near-saturation in deep aquifer (Saturation Index ~0 to 1.5) due to the accumulated Si in groundwater. The same calculations also found the deep groundwater to be well below saturation (SI < -0.5) for most carbonates, except siderite ($FeCO_3$) and rhodochrosite ($MnCO_3$). Siderite has been suggested as a possible source of groundwater DIC in the Basin (Hoque and Burgess, 2012), but it is equally plausible that bicarbonate controls Fe(II) concentrations by precipitation of siderite (Dowling et al., 2002; Nickson et al., 2000), as Fe concentrations are rather low at alkalinity >3 mEq/L in our data set. Analogously, rhodochrosite precipitation might be controlling Mn concentrations, as alkalinity and Mn in the deep aquifer are negatively correlated ($R^2 = 0.72$, $p = 4\times10^{-6}$).

The correlation of more positive $^{13}C_{DIC}$ with lower $^{14}C_{DIC}$ (Figs. 2.7d and 2.9) and higher alkalinity is suggestive of carbonate dissolution contributing older, ^{13}C-enriched DIC to the groundwater. However, when a third dimension is added to the plot (Fig. 2.14 in Appendix), it is obvious that the high alkalinity samples are dispersed throughout the trend and not focused at the more positive ^{13}C values, while Ca is at its highest at the most depleted ^{13}C, thus providing no clear evidence, once again, of carbonate dissolution contribution. Since the aquifer is dominated by silicate weathering, which adds no radiocarbon-free DIC to the system, ^{13}C correction for the DIC ^{14}C age, as in the C_2 age, is likely not required. The observed variations in ^{13}C signature of DIC can instead be

explained by a change in dominant vegetation type caused by the climate changes at the onset of the Holocene (discussed in Section 2.4.3), which would require no ^{13}C correction. The most appropriate ^{14}C age to use for the deep groundwater, therefore, is the simple open system model (C_1 ^{14}C age) that was empirically corrected for the initial ^{14}C activity of the DIC (0.9 FM) and dated the deep groundwater to ~9-11,000 years BP (Table 2.2 and Fig. 2.4b).

The influence of dissolved and particulate organic matter (DOC and POC) mineralization on the observed $^{14}C_{DIC}$ *after* groundwater of the deep aquifer was recharged and the system closed off from the vadose zone C inputs was not accounted for, but most likely was minimal. The consumption of old radiocarbon in DOC and POC from the Pleistocene (and older) sediments, coupled to reductive processes such as Fe, Mn, and SO_4 reduction or methanogenesis, could have produced ^{14}C-depleted DIC and shifted the ^{14}C ages towards older dates, introducing uncertainty in our estimates. However, the deep aquifer sediments were likely flushed of most of their reactive DOC during the sea level lowstand periods, often used to explain their low-As status and the orange color of the sands (BGS and DPHE, 2001), so it is unlikely that a large amount of old DOC was mineralized to DIC within the aquifer. In case of methanogenesis, documented in highly reducing environment of Bangladeshi aquifers (Harvey et al., 2002), the produced methane is highly depleted in ^{13}C (-70 to -90‰) regardless of whether it is generated by CO_2 reduction or the fermentation of organic C, thus resulting in a highly enriched ^{13}C signature (-15 to +5‰) of the remaining groundwater DIC (Aravena et al., 1995; Harvey et al., 2002). Virtually all of our samples (except one higher and another lower outlier) contain $^{13}C_{DIC}$ concentrations between -16 and -22‰,

thus methanogenetic processing of old DOC played a limited role in the generation of observed DIC. Assuming that the initial $\delta^{13}C$ of both DIC and DOC was -25‰, and the final DIC $\delta^{13}C$ of -16‰ was a result of methanogenesis adding residual DIC enriched by the process to $\delta^{13}C$ of 15‰, the maximum contribution of old, ^{14}C-free DOC to the resident DIC could have been ~¼ to ⅕ of the total DIC. Likewise, younger DOC from the surface is unlikely to have been metabolized in this aquifer, since there is no evidence that a substantial amount of younger groundwater from the organic matter-rich Holocene aquifer penetrates to this depth and transport of reactive DOC has been shown to be a slow process (Mailloux et al., 2013).

Since the wells analyzed in this study are all clustered in one small area of 25 km^2, it is useful to place the observed groundwater ages in a regional context provided by other studies that reported ^{14}C measurements in DIC. Except for very few samples, some of which might be impacted by shallow groundwater leaks or seawater mixing (Aggarwal et al., 2000; BGS and DPHE, 2001), most ^{14}C ages of the groundwater from wells with depths >120 m, calculated in a way analogous to our C_1 ^{14}C age, are ~9,500 yr BP and similar to those found in our study, but some older samples also exist with ages as high as >20,000 yr BP (Aggarwal et al., 2000; BGS and DPHE, 2001; Hoque and Burgess, 2012). Another method of estimating ^{14}C ages by assuming a closed system evolution of groundwater with respect to gas exchange with the atmosphere (no dissolution of soil carbonates within the vadose zone), and correcting for the dissolution of radiocarbon-free carbonate along the flowpath by using the sample pH, placed the upper limit on ^{14}C ages in the Basin at depths >120 m bgl to a similar value of 10 kyr or higher (Fendorf et al., 2010).

The linear relationship between C_1 ^{14}C age and the radiogenic He greatly increased the confidence in the progression of ^{14}C ages of groundwater DIC (Fig. 2.5cd), including also the intermediate aquifer, even if the noble gas data did not constrain the absolute ^{14}C age. The slope of the ^{14}C age-radiogenic He relationship, 2.5±0.2 $\times 10^{-12}$ ccSTP g^{-1}_{GW} yr^{-1} for both aquifers combined, represents the accumulation rate of He in groundwater due to the radioactive decay of U and Th from the surrounding sediment. To evaluate this result, the median value of He accumulation rate in groundwater was calculated (Craig and Lupton, 1976; Torgersen, 1980) based on the U and Th concentrations found in the contemporary river sediment from the Ganges, the Brahmaputra and the Chittagong area rivers (Chabaux et al., 2012; Chowdhury et al., 1999; Granet et al., 2010; Granet et al., 2007; Molla et al., 1997), as well as for the average U and Th contents of the upper crust (Torgersen, 1989). Assuming an aquifer porosity of 0.3, a sediment density of 2.75 g/cm^3, and a He release factor (lambda) of 1 (Torgersen and Clarke, 1985) i.e. the produced He in the grain is assumed to be in diffusive equilibrium with the surrounding groundwater, the calculated He release rates are 4.9×10^{-12} and 4.1×10^{-12} ccSTP g^{-1} yr^{-1}, respectively, for the Bengal Basin sediment and the average upper crust, which is similar (within a factor of 2) to the rate determined from our data.

Our data suggest that the noble gas technique possibly can be applied to even older groundwater, such as that found at >200 m bgl in southern parts of Bangladesh with ^{14}C ages of >20,000 yr BP (Aggarwal et al., 2000; Hoque and Burgess, 2012), provided that it is not affected by He diffusing upward from deep, thermogenic natural gas deposits (Dowling et al., 2003). Dowling et al. (2003) reported radiogenic He values based on He

and Ne measurements, and estimated ages of groundwater from ~100-240 m depth to be several hundred to >1000 years using an assumed radiogenic He accumulation rate 8-fold higher than in our study. However, if their radiogenic He values are plotted versus the $^{14}C_{DIC}$ data reported for the same set of wells by Aggarwal et al. (2000), and the samples affected by He emanating from deep natural gas deposits are excluded, they yield a correlation between the radiogenic He values and ^{14}C ages similar to that reported in our study, thus the hypothesized He release rate of Dowling et al. (2003) might have been overestimated.

2.4.3 Chemical/isotopic signatures of deglaciation in deep aquifer groundwater

Stable isotopes of water (δ^2H and $\delta^{18}O$) in the deep aquifer indicate that the aquifer was recharged by precipitation subject to little or no evaporation, suggesting that the groundwater recharge/vertical flow may have been faster at the time of transition between the Late Pleistocene and the Early Holocene. This observation argues for the existence of higher gradients at the onset of the Holocene and also suggests that many near-surface clay layers may have been eroded away by incised rivers, thus preventing the surface geology from holding as many ponds of water as today.

Moreover, the progressively lighter (more depleted) δ^2H (by ~13‰) and $\delta^{18}O$ (by ~1.5-2‰) from 11 to 9,000 ^{14}C yr BP suggest that the summer monsoon intensified over this time period: the larger amounts of precipitation when summer monsoon cyclones hit the continent would bring more isotopically depleted rains (Dansgaard, 1964). Another effect of the stronger monsoon might have been longer cyclone pathways, which would equivalently produce a more isotopically depleted rain, as seen in a modern study in the

province of Meghalaya, NE India (Breitenbach et al., 2010). The Bay of Bengal seawater was also getting more diluted at the onset of Holocene by the fresh water from global glacial melt and the stronger river flows in the Ganges-Brahmaputra-Meghna delta (due to both the mountain ice caps melting and the stronger monsoon feedback), so the starting rain produced over the Bay of Bengal must have also been slightly more depleted. The rates of evapotranspiration might have also been affected by the changing temperature and moisture patterns, as well as the vegetation cover, however they did not leave an imprint on the observed $\delta^{18}O$ and $\delta^{2}H$ signatures of groundwater because the deep aquifer was recharged with mostly unevaporated rainwater.

More depleted $\delta^{18}O$ signatures ca. 12-8 kyr BP have been related to a more intense and wetter SE Asian summer monsoon in a number of studies performed on foraminifera record (1-2‰ negative excursions) from the ocean floor of the Arabian Sea or the Bay of Bengal, as well as on cave stalactites (up to 3‰ negative excursions) from China and Borneo (Partin et al., 2007; Prins and Postma, 2000; Rashid et al., 2011). To our knowledge, this is the first time such a record from groundwater in tropical Asia is systematically discussed. A similar pattern towards a ~2‰ lighter $\delta^{18}O$ is noted ca. 12-10 kyr BP for the uncorrected ^{14}C ages by Hoque and Burgess (2012), but the authors conclude that a ^{13}C correction is necessary to account for the effects of carbonate dissolution on ^{14}C ages, upon which the pattern is no longer visible. In another deep aquifer study reporting the stable isotope data, Mukherjee et al. (2007) has no ^{14}C data and finds that the shallow and deep groundwater stable isotope signatures are similar, including the partial recharge by evaporatively enriched meteoric water. Only the IAEA report by Aggarwal et al. (2000) relates a few data points with low DIC radiocarbon

concentration, and presumably old groundwater, to a more positive stable isotope signature, but it does not explicitly discuss a paleoclimatic pattern in the data.

The strongest correlation observed of the deep groundwater ^{13}C signature in DIC is that with the stable isotopes of water (Fig. 2.11d in Appendix) and, like with $\delta^{18}O$ and $\delta^{2}H$, the values of $^{13}C_{DIC}$ are progressively more depleted (by ~8‰) between 11 and 9,000 ^{14}C yr BP (Fig. 2.9). A likely reason for the observed trend, rather than the effect of carbonate dissolution already discounted by the groundwater chemistry, is a fairly rapid shift in vegetation cover from C4 to C3 plants as the summer South Asian monsoon intensified at the onset of Holocene and resulted in a wetter climate in the area. Climatic changes can also explain why $\delta^{13}C$ in DIC and stable isotopes of the water molecule (^{2}H and ^{18}O) vary in tandem in our data, as all three isotopes trend towards more depleted values under a wetter climate, and this is the first report, to our knowledge, of a climate signal in ^{13}C of groundwater DIC from South Asia.

Other studies from the region have also indicated a switch in ^{13}C signature over a similar time period: $\delta^{13}C$ in bulk sediment organics of marine cores from the Bay of Bengal affected by continental OC inputs got depleted by ~2‰ from 14-8 ^{14}C kyr BP and this was matched by a 2‰ decrease in foraminifera shell ^{18}O (Galy et al., 2008). On land, excursions of $\delta^{13}C$ in sedimentary organic C similar in magnitude to the ones observed in Araihazar deep aquifer groundwater were reported to occur between the Last Glacial Maximum paleosol, deposited during a dry climate, and the ~8 kyr old sediment of the wetter, early Holocene (Sarkar et al., 2009), as well as in the bulk OC of clays in our recent study of a Late Pleistocene intermediate aquifer (this work, Chapter 3). In the above studies, ^{13}C shifts in sedimentary OC or IC have been attributed to the changes in

vegetation cover related to the deglaciation: weaker summer monsoon and drier climate at the LGM were more suited for the C4-type grassy vegetation with an enriched (more positive) $\delta^{13}C$ signature. Upon the monsoon intensification, a shift towards C3-type bushes, forests, and mangroves has been called upon to explain the more negative $\delta^{13}C$ values. As the Holocene progressed, a slow return to slightly drier climate conditions and vegetation adapted to aridity was observed by Sarkar et al. (2009), and the trend is also noticeable in our data from intermediate-depth groundwater. Excluding the three intermediate-depth samples with deep groundwater characteristics, $\delta^{13}C$ increases in tandem with increasing FM of ^{14}C in DIC of the intermediate-depth groundwater, the trend being notably less defined and more gradual over the course of the Holocene in comparison to the rapid depletion of stable isotopes in the deep samples between 11 and 9,000 ^{14}C yr BP. Such a contrast argues for a rapid climate change with a leap in monsoon intensity at the onset of the Holocene, followed by a more gradually increasing aridity since then.

Another potential indicator of climate change during the last deglaciation, the temperature of recharge from the noble gas models, did not yield a conclusive result. The data do suggest a lower average noble gas T in deep groundwater and the oldest intermediate aquifer sample (A7) compared to the remaining intermediate-depth groundwater, however the NGT data do not display a significant correlation to either the different groundwater ages (Fig. 2.5ab) or the sample depths (not shown). Despite the reports of a ~3 ºC lower sea surface T during the LGM in the Bay of Bengal, based on the Mg/Ca thermometer coupled to foraminifera ^{18}O (Rashid et al., 2011) or on the long-chain alkenone unsaturation index (Sarma et al., 2006), which would certainly translate

into larger T variations on land due to its lower heat capacity, we did not observe a strong temporal trend in the noble gas T data.

An error in the estimates of NGTs could have been introduced by our assumption that the altitude of recharge was at sea level, i.e. that the atmospheric pressure was 1 atm. If groundwater from >120 m depth had been recharged from highlands at the basin edges, the noble gas temperatures could have been overestimated by using the pressure of 1 atm in the model. However, the nearest highlands are the Tripura Hills, approximately 100 km east of our field site, and virtually all of the hilly area within a 100-150 km distance lies at elevations of <200 m above sea level (ASL). If recharge occurred at 200 m ASL, the NGTs could be overestimated by 0.8-0.9 ºC, as determined from additional runs of the model, but this effect is practically compensated by the lower temperature at the higher elevation (tropospheric lapse rate). Thus the error introduced by the uncertainty of the recharge area elevation is minimal. It is more likely, instead, that the lower annual average T signal was lost by a pattern of rapid recharge occurring in a season when T was higher than the annual average, such as the summer monsoon season. The extremes in T also could have been larger between the seasons in a drier climate, thus if the recharge had occurred over a warm season, the annually lower air T signal could have been lost.

2.4.4 Implications for the sustainability of deep low-As aquifers

Based on the likely timing of deep groundwater recharge in Araihazar ~10,000 years ago at the transition from the Pleistocene to Holocene, three recharge scenarios are plausible.

Under the first scenario, Pleistocene groundwater was trapped in the deep aquifer >120 m bgl as the sea level rose at the onset of the Holocene (12-8 kyr BP), the strength of the summer monsoon intensified (Prins and Postma, 2000), and the young, Holocene sediment rapidly accumulated (11-6 kyr BP) (Goodbred and Kuehl, 2000a; Sarkar et al., 2009), reducing the horizontal flow gradients to a minimum. In this case, effectively minimal recharge occurred since the onset of Holocene, therefore the flow regime would radically change with increased pumping from the aquifer.

Under the second scenario, groundwater flowed slowly from the basin edge, somewhat akin to the conceptual flow model of Michael and Voss (2009b) and Hoque and Burgess (2012). Assuming the nearest basin edge to be in the Tripura Hills, ~100 km due east, a constant advective velocity of ~10 m/yr would satisfy the observed groundwater ^{14}C age of ~10,000 years. Furthermore, assuming a porosity of 0.3 and a representative horizontal hydraulic conductivity of 5×10^{-4} m/s from the basin-scale hydrological models of Michael and Voss (2008), the calculated horizontal hydraulic gradient in the deep aquifer would be 2×10^{-4} or 0.2 m km^{-1}. This hydraulic gradient falls in the mid-range between the gradients estimated by BGS and DPHE (2001) to be 1 m km^{-1} in the north, and 0.01 m km^{-1} in the south of Bangladesh. The horizontal gradients induced by active pumping are likely to be larger and significantly alter the flow regime, especially in places where a cone of depression developed, such as around Dhaka (Hoque et al., 2007).

The third scenario would be a slow vertical recharge from the shallow aquifer. A simple case of the uniform and constant vertical recharge would require an estimated advective velocity of ~2 cm/yr for the groundwater to reach a depth of 200 m bgl in

10,000 years. Assuming a porosity of 0.3, the recharge rate (Darcy velocity) would be 0.6 cm/yr, a reasonable value of vertical recharge (<1% of total precipitation) in a region that receives ~2 m/yr of precipitation (Harvey et al., 2006), and falling within the range of vertical leakage rates estimated for Araihazar by Zheng et al. (2005). This recharge rate would certainly be exceeded by the deep pumping (0.2-0.6 m/yr) for industrial and/or agricultural purposes in the densely pumped areas (Harvey et al., 2002; Michael and Voss, 2008; Zheng et al., 2005).

The second and the third scenario provide upper limits for the amount of horizontal and vertical flow to the deep aquifer during Mid-to-Late Holocene, and approach the first scenario of the trapped Late Pleistocene-Early Holocene groundwater under non-steady-state conditions. If groundwater found at depth >120 m bgl had recharged along much steeper horizontal and vertical gradients at the onset of the Holocene, the subsequent recharge rates during Mid-to-Late Holocene would have been much lower, allowing little flow to the aquifer until the recent deep pumping might have induced higher gradients and recharge rates again.

Whichever scenario might be correct, the pre-development residence time of deep groundwater is ~10 kyr in Araihazar and enough vertical anisotropy existed to maintain the pronounced stratification between the intermediate and the deep aquifer in Araihazar, and elsewhere in the Basin (Hoque and Burgess, 2012; Michael and Voss, 2009b). The increasing downward vertical hydraulic differences, currently as large as 5.6 m between the shallow and the intermediate aquifer near well C5 (Fig. 2.15 in Appendix), indicate a growing potential for more rapid recharge of the deeper aquifers that might shorten the residence time of deep groundwater. The question is whether this recharge will be mainly

vertical, putting the system at risk of contamination by shallow groundwater, or whether the lateral recharge from major rivers and/or mountain ranges might also play a role. If the growing, localized cones of depression (Hoque et al., 2007) are far from or poorly connected to the lateral sources of recharge, a significant amount of vertical leakage of groundwater from the shallow aquifer that contains high As and high DOC concentrations seems inevitable. On the other hand, if recharge from the basin edges to deeper parts of the aquifer occurs at present time, faster recharge from the highlands might be able to offset some of the pumping withdrawals and protect the aquifer to a certain degree from vertical intrusion of shallow groundwater. If the deep aquifer receives enhanced recharge from the major rivers flowing through the basin, the effect such a scenario would have on its As status will depend on the type of sediment through which the river water flows on its way to the deep aquifer (Berg et al., 2008).

These results along with other recent studies have raised concerns about the sustainability of the deep aquifer over the long term, especially if the irrigation pumping were to switch to the deep aquifer (Burgess et al., 2010; Michael and Voss, 2008; Mukherjee et al., 2011; Radloff et al., 2011). At the same time, our data from Araihazar upazilla show that although recharge with shallow groundwater was found in the intermediate-depth aquifer, no widespread intrusion of As has occurred at any depth of the low-As aquifers in this region. This finding is in agreement with the recent study by Ravenscroft et al. (2013) that also offered a new point of view on the ethical questions surrounding the long-term preservation of the low-As aquifers: pumping of the deep aquifer for both the drinking water and irrigation might simply be the best solution at the moment. The benefits of limiting the As exposure via drinking water and preserving crop

yields adversely affected by As accumulated in soils might outweigh in the present the harm of contaminating the deep aquifer in the future, at which point other ways to provide low-As drinking water might be found.

2.5 Conclusions

Our study of ^{3}H, DIC radiocarbon ages, groundwater chemistry (major cations, anions, Si, P, As, Mn, Fe, DIC and DOC concentrations), and stable isotopes ($^{2}H/^{1}H$, $^{18}O/^{16}O$, $^{13}C_{DIC}$) in groundwater from low-As wells spanning the depth range of 35-240 m bgl in a 25 km^2 area of Bangladesh showed that two distinct depth zones exist in the low-As aquifers. At depths <120 m bgl, the presence of recent recharge with evaporated surface water was detected by bomb-^{3}H and ^{14}C, the groundwater chemistry was quite variable, and radiocarbon ages in DIC ranged from modern to ~10 kyr. The presence of high ^{3}H and ^{14}C was not correlated with the presence or absence of clay in the well lithologs, nor did these samples bear evidence of As intrusion from the shallow zone.

The deep aquifer >120 m bgl contained groundwater of uniform ^{14}C ages clustered ~10 kyr BP, water stable isotopes indicated recharge with unevaporated rain water, and a uniform chemical signature of low Na, low DIC and high Si was observed. The radiocarbon ages in this study were cross-checked by another dating technique provided by the noble gas data (He, Ne, Ar, Kr, and Xe), from which the accumulation of radiogenic ^{4}He was calculated and shown to range linearly between zero in modern ^{14}C samples to 3×10^{-8} ccSTP g^{-1} in the ~10 kyr samples from both the intermediate and deep aquifers. Given that, according to several hydrological scenarios, the deep aquifer at a central location in the Bengal Basin was last substantially recharged ~10 kyr ago, concerns about its sustainable usage arise as the flowpaths and residence time of deep groundwater are likely to be significantly shortened with growing exploitation of the aquifer.

The systematic relationships between the deep groundwater $^{13}C/^{12}C$, $^{2}H/^{1}H$, $^{18}O/^{16}O$, and radiocarbon suggested changes in monsoon intensity and shifts in the dominance between C4 and C3 vegetation at the onset of the Holocene. These findings are consistent with the estimated deep groundwater ^{14}C age of ~10 kyr and provide the first report of a paleoclimate record contained within the Bengal Basin groundwater.

Acknowledgements

I would like to thank to our field assistant, Shahidullah Shahud, for his tireless help in opening up the community wells that we sampled and helping fix them again for use. Linda Baker worked hard to ensure we got the best quality noble gas data, together with Ronny Friedrich who was also expedient with the stable isotope analysis. Ronny and Bob Newton were responsible for ^{3}H data acquisition and always there to answer my questions. This paper also benefited from insightful comments of Benjamín C. Bostick, Peter S. K. Knappett, and Holly Michael.

2.6 References

Aeschbach-Hertig, W., Peeters, F., Beyerle, U., Kipfer, R., 1999. Interpretation of dissolved atmospheric noble gases in natural waters. Water Resources Research 35, 2779-2792.

Aggarwal, P.K., Basu, A.R., Poreda, R.J., Kulkarni, K.M., Froehlich, K., Tarafdar, S.A., Ali, M., Ahmed, N., Hussain, A., Rahman, M., Ahmed, S.R., 2000. Isotope hydrology of groundwater in Bangladesh: Implications for characterization and mitigation of arsenic in groundwater, IAEA-TC Project (BGD/8/016). International Atomic Energy Agency.

Ahmed, M.F., Ahuja, S., Alauddin, M., Hug, S.J., Lloyd, J.R., Pfaff, A., Pichler, T., Saltikov, C., Stute, M., van Geen, A., 2006. Epidemiology - Ensuring safe drinking water in Bangladesh. Science 314, 1687-1688.

Argos, M., Kalra, T., Rathouz, P.J., Chen, Y., Pierce, B., Parvez, F., Islam, T., Ahmed, A., Rakibuz-Zaman, M., Hasan, R., Sarwar, G., Slavkovich, V., van Geen, A., Graziano, J., Ahsan, H., 2010. Arsenic exposure from drinking water, and all-cause and chronic-disease mortalities in Bangladesh (HEALS): a prospective cohort study. Lancet 376, 252-258.

Aziz, Z., van Geen, A., Stute, M., Versteeg, R., Horneman, A., Zheng, Y., Goodbred, S., Steckler, M., Weinman, B., Gavrieli, I., Hoque, M.A., Shamsudduha, M., Ahmed, K.M., 2008. Impact of local recharge on arsenic concentrations in shallow aquifers inferred from the electromagnetic conductivity of soils in Araihazar, Bangladesh. Water Resources Research 44.

Bayer, R., Schlosser, P., Boenisch, G., Rupp, H., Zaucker, F., Zimmek, G., 1989. Performance and blank components of a mass spectrometric system for routine measurement of helium isotopes and tritium by the 3He ingrowth method. Sitzungsberichte (5) der Heidelberger Akademie der Wissenschaften, Mathematisch-naturwissenschaftliche Klasse, Jahrgang, Heidelberg, Germany.

Berg, M., Trang, P.T.K., Stengel, C., Buschmann, J., Viet, P.H., Van Dan, N., Giger, W., Stueben, D., 2008. Hydrological and sedimentary controls leading to arsenic contamination of groundwater in the Hanoi area, Vietnam: The impact of iron-arsenic ratios, peat, river bank deposits, and excessive groundwater abstraction. Chemical Geology 249, 91-112.

BGS and DPHE, 2001. Arsenic contamination of groundwater in Bangladesh, in: Kinniburgh, D.G., Smedley, P.L. (Eds.), BGS Technical Report WC/00/19. British Geological Survey, Keyworth, UK.

Breitenbach, S.F.M., Adkins, J.F., Meyer, H., Marwan, N., Kumar, K.K., Haug, G.H., 2010. Strong influence of water vapor source dynamics on stable isotopes in

precipitation observed in Southern Meghalaya, NE India. Earth and Planetary Science Letters 292, 212-220.

Burgess, W.G., Hoque, M.A., Michael, H.A., Voss, C.I., Breit, G.N., Ahmed, K.M., 2010. Vulnerability of deep groundwater in the Bengal Aquifer System to contamination by arsenic. Nature Geoscience 3, 83-87.

Chabaux, F., Blaes, E., Granet, M., Roupert, R.D., Stille, P., 2012. Determination of transfer time for sediments in alluvial plains using U-238-U-234-Th-230 disequilibria: The case of the Ganges river system. C. R. Geosci. 344, 688-703.

Cheng, Z., Zheng, Y., Mortlock, R., van Geen, A., 2004. Rapid multi-element analysis of groundwater by high-resolution inductively coupled plasma mass spectrometry. Analytical and Bioanalytical Chemistry 379.

Chowdhury, M.I., Alam, M.N., Hazari, S.K.S., 1999. Distribution of radionuclides in the river sediments and coastal soils of Chittagong, Bangladesh and evaluation of the radiation hazard. Appl. Radiat. Isot. 51, 747-755.

Clarke, W.B., Jenkins, W.J., Top, Z., 1976. Determination of tritium by mass-spectrometric measurement of He-3. International Journal of Applied Radiation and Isotopes 27, 515-522.

Craig, H., 1961. Isotopic variations in meteoric waters. Science 133, 1702-1703.

Craig, H., Lupton, J.E., 1976. Primordial neon, helium, and hydrogen in oceanic basalts. Earth and Planetary Science Letters 31, 369-385.

Dansgaard, W., 1964. Stable isotopes in precipitation. Tellus 16, 436-468.

Dhar, R.K., Zheng, Y., Stute, M., van Geen, A., Cheng, Z., Shanewaz, M., Shamsudduha, M., Hoque, M.A., Rahman, M.W., Ahmed, K.M., 2008. Temporal variability of groundwater chemistry in shallow and deep aquifers of Araihazar, Bangladesh. Journal of Contaminant Hydrology 99, 97-111.

Dowling, C.B., Poreda, R.J., Basu, A.R., 2003. The groundwater geochemistry of the Bengal Basin: Weathering, chemsorption, and trace metal flux to the oceans. Geochimica Et Cosmochimica Acta 67, 2117-2136.

Dowling, C.B., Poreda, R.J., Basu, A.R., Peters, S.L., Aggarwal, P.K., 2002. Geochemical study of arsenic release mechanisms in the Bengal Basin groundwater. Water Resources Research 38.

Elder, K.L., McNichol, A.P., Gagnon, A.R., 1997. Evaluating reproducibility of seawater, inorganic and organic carbon 14C results at the National Ocean Sciences AMS

Facility (NOSAMS), Proceedings of the 16th International Radiocarbon Conference. Radiocarbon 40, pp. 223-230.

Fairbanks, R.G., 1989. A 17,000-year glacio-esutatic sea-level record: influence of glacial melting rates on the Younger Drias event and deep-ocean circulation. Nature 342, 637-642.

Fendorf, S., Michael, H.A., van Geen, A., 2010. Spatial and Temporal Variations of Groundwater Arsenic in South and Southeast Asia. Science 328, 1123-1127.

Fontes, J.C., Garnier, J.M., 1979. Determination of the initial C-14 activity of the total dissolved carbon - review of the existing models and a new approach. Water Resources Research 15, 399-413.

Galy, V., Francois, L., France-Lanord, C., Faure, P., Kudrass, H., Palhol, F., Singh, S.K., 2008. C4 plants decline in the Himalayan basin since the Last Glacial Maximum. Quat. Sci. Rev. 27, 1396-1409.

Goodbred, S.L., Kuehl, S.A., 2000a. Enormous Ganges-Brahmaputra sediment discharge during strengthened early Holocene monsoon. Geology 28, 1083-1086.

Goodbred, S.L., Kuehl, S.A., 2000b. The significance of large sediment supply, active tectonism, and eustasy on margin sequence development: Late Quaternary stratigraphy and evolution of the Ganges-Brahmaputra delta. Sedimentary Geology 133, 227-248.

Gran, G., 1952. Determination of the equivalence point in potentiometric titrations. 2. Analyst 77, 661-671.

Granet, M., Chabaux, F., Stille, P., Dosseto, A., France-Lanord, C., Blaes, E., 2010. U-series disequilibria in suspended river sediments and implication for sediment transfer time in alluvial plains: The case of the Himalayan rivers. Geochimica Et Cosmochimica Acta 74, 2851-2865.

Granet, M., Chabaux, F., Stille, P., France-Lanord, C., Pelt, E., 2007. Time-scales of sedimentary transfer and weathering processes from U-series nuclides: Clues from the Himalayan rivers. Earth and Planetary Science Letters 261, 389-406.

Harvey, C.F., Swartz, C.H., Badruzzaman, A.B.M., Keon-Blute, N., Yu, W., Ali, M.A., Jay, J., Beckie, R., Niedan, V., Brabander, D., Oates, P.M., Ashfaque, K.N., Islam, S., Hemond, H.F., Ahmed, M.F., 2002. Arsenic mobility and groundwater extraction in Bangladesh. Science 298, 1602-1606.

Hoque, M.A., Burgess, W.G., 2012. C-14 dating of deep groundwater in the Bengal Aquifer System, Bangladesh: Implications for aquifer anisotropy, recharge sources and sustainability. Journal of Hydrology 444, 209-220.

Hoque, M.A., Hoque, M.M., Ahmed, K.M., 2007. Declining groundwater level and aquifer dewatering in Dhaka metropolitan area, Bangladesh: causes and quantification. Hydrogeology Journal 15, 1523-1534.

Horneman, A., van Geen, A., Kent, D.V., Mathe, P.E., Zheng, Y., Dhar, R.K., O'Connell, S., Hoque, M.A., Aziz, Z., Shamsudduha, M., Seddique, A.A., Ahmed, K.M., 2004. Decoupling of As and Fe release to Bangladesh groundwater under reducing conditions. Part 1: Evidence from sediment profiles. Geochimica Et Cosmochimica Acta 68, 3459-3473.

Ingerson, E., Pearson, F.J.J., 1964. Estimation of age and rate of motion of groundwater by the 14C-method, Recent Researches in the Fields of Hydrosphere, Atmosphere and Nuclear Geochemistry, Maruzen, Tokyo, pp. 263-283.

JICA and DPHE, 2010. Report on Situation Analysis of Arsenic Mitigation, 2009. Dept. of Public Health Engineering, Bangladesh and Japan International Cooperation Agency, Local Government Division, Government of Bangladesh, DPHE, JICA.

Ludin, A.R., Weppernig, R., Boenisch, G., Schlosser, P., 1997. Mass spectrometric measurement of helium isotopes and tritium, internal report. Lamont-Doherty Earth Observatory, Palisades, New York.

Mailloux, B.J., Trembath-Reichert, E., Cheung, J., Watson, M., Stute, M., Freyer, G.A., Ferguson, A.S., Ahmed, K.M., Alam, M.J., Buchholz, B.A., Thomas, J., Layton, A.C., Zheng, Y., Bostick, B.C., van Geen, A., 2013. Advection of surface-derived organic carbon fuels microbial reduction in Bangladesh groundwater. Proceedings of the National Academy of Sciences of the United States of America 110, 5331-5335.

McArthur, J.M., Banerjee, D.M., Sengupta, S., Ravenscroft, P., Klump, S., Sarkar, A., Disch, B., Kipfer, R., 2010. Migration of As, and H-3/(3) He ages, in groundwater from West Bengal: Implications for monitoring. Water Research 44, 4171-4185.

McArthur, J.M., Nath, B., Banerjee, D.M., Purohit, R., Grassineau, N., 2011. Palaeosol Control on Groundwater Flow and Pollutant Distribution: The Example of Arsenic. Environmental Science & Technology 45, 1376-1383.

McArthur, J.M., Ravenscroft, P., Banerjee, D.M., Milsom, J., Hudson-Edwards, K.A., Sengupta, S., Bristow, C., Sarkar, A., Tonkin, S., Purohit, R., 2008. How paleosols influence groundwater flow and arsenic pollution: A model from the Bengal Basin and its worldwide implication. Water Resources Research 44.

McArthur, J.M., Sikdar, P.K., Hoque, M.A., Ghosal, U., 2012. Waste-water impacts on groundwater: Cl/Br ratios and implications for arsenic pollution of groundwater in the Bengal Basin and Red River Basin, Vietnam. Science of the Total Environment 437, 390-402.

Michael, H.A., Voss, C.I., 2008. Evaluation of the sustainability of deep groundwater as an arsenic-safe resource in the Bengal Basin. Proceedings of the National Academy of Sciences of the United States of America 105, 8531-8536.

Michael, H.A., Voss, C.I., 2009a. Controls on groundwater flow in the Bengal Basin of India and Bangladesh: regional modeling analysis. Hydrogeology Journal 17, 1561-1577.

Michael, H.A., Voss, C.I., 2009b. Estimation of regional-scale groundwater flow properties in the Bengal Basin of India and Bangladesh. Hydrogeology Journal 17, 1329-1346.

Molla, N.I., Hossain, S.M., Basunia, S., Miah, R.U., Rahman, M., Sikder, D.H., Chowdhury, M.I., 1997. Elemental analysis in bed sediment samples of Karnafuli estuarine zone in the Bay of Bengal by instrumental neutron activation analysis. J. Radioanal. Nucl. Chem. 216, 213-215.

Mukherjee, A., Fryar, A.E., Rowe, H.D., 2007. Regional-scale stable isotopic signatures of recharge and deep groundwater in the arsenic affected areas of West Bengal, India. Journal of Hydrology 334, 151-161.

Mukherjee, A., Fryar, A.E., Scanlon, B.R., Bhattacharya, P., Bhattacharya, A., 2011. Elevated arsenic in deeper groundwater of the western Bengal basin, India: Extent and controls from regional to local scale. Applied Geochemistry 26, 600-613.

Nickson, R.T., McArthur, J.M., Ravenscroft, P., Burgess, W.G., Ahmed, K.M., 2000. Mechanism of arsenic release to groundwater, Bangladesh and West Bengal. Applied Geochemistry 15, 403-413.

Olsson, I.U., 1970. The use of Oxalic acid as a Standard, in: Olsson, I.U. (Ed.), Radiocarbon Variations and Absolute Chronology, Nobel Symposium, 12th Proc. John Wiley & Sons, New York, p. 17.

Partin, J.W., Cobb, K.M., Adkins, J.F., Clark, B., Fernandez, D.P., 2007. Millennial-scale trends in west Pacific warm pool hydrology since the Last Glacial Maximum. Nature 449, 452-U453.

Peeters, F., Beyerle, U., Aeschbach-Hertig, W., Holocher, J., Brennwald, M.S., Kipfer, R., 2003. Improving noble gas based paleoclimate reconstruction and groundwater dating using Ne-20/Ne-22 ratios. Geochimica Et Cosmochimica Acta 67, 587-600.

Prins, M.A., Postma, G., 2000. Effects of climate, sea level, and tectonics unraveled for last deglaciation turbidite records of the Arabian Sea. Geology 28, 375-378.

Radloff, K.A., Zheng, Y., Michael, H.A., Stute, M., Bostick, B.C., Mihajlov, I., Bounds, M., Huq, M.R., Choudhury, I., Rahman, M.W., Schlosser, P., Ahmed, K.M., van Geen, A., 2011. Arsenic migration to deep groundwater in Bangladesh influenced by adsorption and water demand. Nature Geoscience 4, 793-798.

Rashid, H., England, E., Thompson, L., Polyak, L., 2011. Late Glacial to Holocene Indian Summer Monsoon Variability Based upon Sediment Records Taken from the Bay of Bengal. Terr. Atmos. Ocean. Sci. 22, 215-228.

Ravenscroft, P., Brammer, H., Richards, K.S., 2009. Arsenic pollution: a global synthesis. Wiley-Blackwell.

Ravenscroft, P., Burgess, W.G., Ahmed, K.M., Burren, M., Perrin, J., 2005. Arsenic in groundwater of the Bengal Basin, Bangladesh: Distribution, field relations, and hydrogeological setting. Hydrogeology Journal 13, 727-751.

Ravenscroft, P., McArthur, J.M., 2004. Mechanism of regional enrichment of groundwater by boron: the examples of Bangladesh and Michigan, USA. Applied Geochemistry 19, 1413-1430.

Ravenscroft, P., McArthur, J.M., Hoque, M.A., 2013. Stable groundwater quality in deep aquifers of Southern Bangladesh: The case against sustainable abstraction. Science of the Total Environment 454, 627-638.

Sarkar, A., Sengupta, S., McArthur, J.M., Ravenscroft, P., Bera, M.K., Bhushan, R., Samanta, A., Agrawal, S., 2009. Evolution of Ganges-Brahmaputra western delta plain: clues from sedimentology and carbon isotopes. Quat. Sci. Rev. 28, 2564-2581.

Sarma, N.S., Pasha, S.G., Krishna, M.S.R., Shirodkar, P.V., Yadava, M.G., Rao, K.M., 2006. Long-chain alkenone unsaturation index as sea surface temperature proxy in southwest Bay of Bengal. Curr. Sci. 91, 82-86.

Smith, A.H., Lingas, E.O., Rahman, M., 2000. Contamination of drinking-water by arsenic in Bangladesh: a public health emergency. Bulletin of the World Health Organization 78, 1093-1103.

Stallard, R.F., 1980. Major element geochemistry of the Amazon River system, PhD thesis, Woods Hole Oceanographic Institution. Massachusetts Institute of Technology.

Stollenwerk, K.G., Breit, G.N., Welch, A.H., Yount, J.C., Whitney, J.W., Foster, A.L., Uddin, M.N., Majumder, R.K., Ahmed, N., 2007. Arsenic attenuation by oxidized aquifer sediments in Bangladesh. Science of the Total Environment 379, 133-150.

Stute, M., Clark, J.F., Schlosser, P., Broecker, W.S., Bonani, G., 1995. A 30,000 yr Continental Paleotemperature Record Derived from Noble Gases Dissolved in

Groundwater from the San Juan Basin, New Mexico. Quaternary Research 43, 209-220.

Stute, M., Zheng, Y., Schlosser, P., Horneman, A., Dhar, R.K., Datta, S., Hoque, M.A., Seddique, A.A., Shamsudduha, M., Ahmed, K.M., van Geen, A., 2007. Hydrological control of As concentrations in Bangladesh groundwater. Water Resources Research 43.

Torgersen, T., 1980. Controls on pore-fluid concentration of the He-4 and Rn-222 and the calculation of He-4/Rn-222 ages. J. Geochem. Explor. 13, 57-75.

Torgersen, T., 1989. Terrestrial helium degassing fluxes and the atmospheric helium budget: Implications with respect to the degassing processes of continental crust. Chemical Geology 79, 1-14.

Torgersen, T., Clarke, W.B., 1985. Helium accumulation in groundwater, I: An evaluation of sources and the continental flux of crustal He-4 in the Great Artesian Basin, Australia. Geochimica Et Cosmochimica Acta 49, 1211-1218.

van Geen, A., Bostick, B.C., Trang, P.T.K., Lan, V.M., Mai, N.-N., Manh, P.D., Viet, P.H., Radloff, K.A., Aziz, Z., Mey, J.L., Stahl, M.O., Harvey, C.F., Oates, P., Weinman, B., Stengel, C., Frei, F., Kipfer, R., Berg, M., 2013. Retardation of arsenic transport through a Pleistocene aquifer. Nature in press.

van Geen, A., Cheng, Z.Q., Jia, Q., Seddique, A.A., Rahman, M.W., Rahman, M.M., Ahmed, K.M., 2007. Monitoring 51 community wells in Araihazar, Bangladesh, for up to 5 years: Implications for arsenic mitigation. Journal of Environmental Science and Health Part a-Toxic/Hazardous Substances & Environmental Engineering 42, 1729-1740.

van Geen, A., Zheng, Y., Goodbred, S., Horneman, A., Aziz, Z., Cheng, Z., Stute, M., Mailloux, B., Weinman, B., Hoque, M.A., Seddique, A.A., Hossain, M.S., Chowdhury, S.H., Ahmed, K.M., 2008. Flushing history as a hydrogeological control on the regional distribution of arsenic in shallow groundwater of the Bengal Basin. Environmental Science & Technology 42, 2283-2288.

van Geen, A., Zheng, Y., Versteeg, R., Stute, M., Horneman, A., Dhar, R., Steckler, M., Gelman, A., Small, C., Ahsan, H., Graziano, J.H., Hussain, I., Ahmed, K.M., 2003. Spatial variability of arsenic in 6000 tube wells in a 25 km(2) area of Bangladesh. Water Resources Research 39.

Verhagen, B.T., Mazor, E., Sellscho.Jp, 1974. Radiocarbon and tritium evidence for direct rain recharge to ground waters in northern Kalahari. Nature 249, 643-644.

Vogel, J.C., 1967. Investigation of groundwater flow with radiocarbon, Isotopes in Hydrology. International Atomic Energy Agency, Vienna, pp. 355-368.

Vogel, J.C., Ehhalt, D., 1963. The use of carbon isotopes in groundwater studies, Radioisotopes in Hydrology. International Atomic Energy Agency, Vienna, pp. 383-395.

Wasserman, G.A., Liu, X.H., Parvez, F., Ahsan, H., Factor-Litvak, P., van Geen, A., Slavkovich, V., Lolacono, N.J., Cheng, Z.Q., Hussain, L., Momotaj, H., Graziano, J.H., 2004. Water arsenic exposure and children's intellectual function in Araihazar, Bangladesh. Environmental Health Perspectives 112, 1329-1333.

Weiss, W., Bullacher, J., Roether, W., 1979. Evidence of pulsed discharges of tritium from nuclear energy installations in Central Europe precipitation, Behaviour of Tritium in the Environment. IAEA-SM-232118, pp. 17-30.

Weiss, W., Roether, W., 1980. The rates of tritium input to the world oceans. Earth and Planetary Science Letters 49, 435-446.

Zheng, Y., Stute, M., van Geen, A., Gavrieli, I., Dhar, R., Simpson, H.J., Schlosser, P., Ahmed, K.M., 2004. Redox control of arsenic mobilization in Bangladesh groundwater. Applied Geochemistry 19.

Zheng, Y., van Geen, A., Stute, M., Dhar, R., Mo, Z., Cheng, Z., Horneman, A., Gavrieli, I., Simpson, H.J., Versteeg, R., Steckler, M., Grazioli-Venier, A., Goodbred, S., Shahnewaz, M., Shamsudduha, M., Hoque, M.A., Ahmed, K.M., 2005. Geochemical and hydrogeological contrasts between shallow and deeper aquifers in two villages of Araihazar, Bangladesh: Implications for deeper aquifers as drinking water sources. Geochimica Et Cosmochimica Acta 69, 5203-5218.

2.7 Appendix

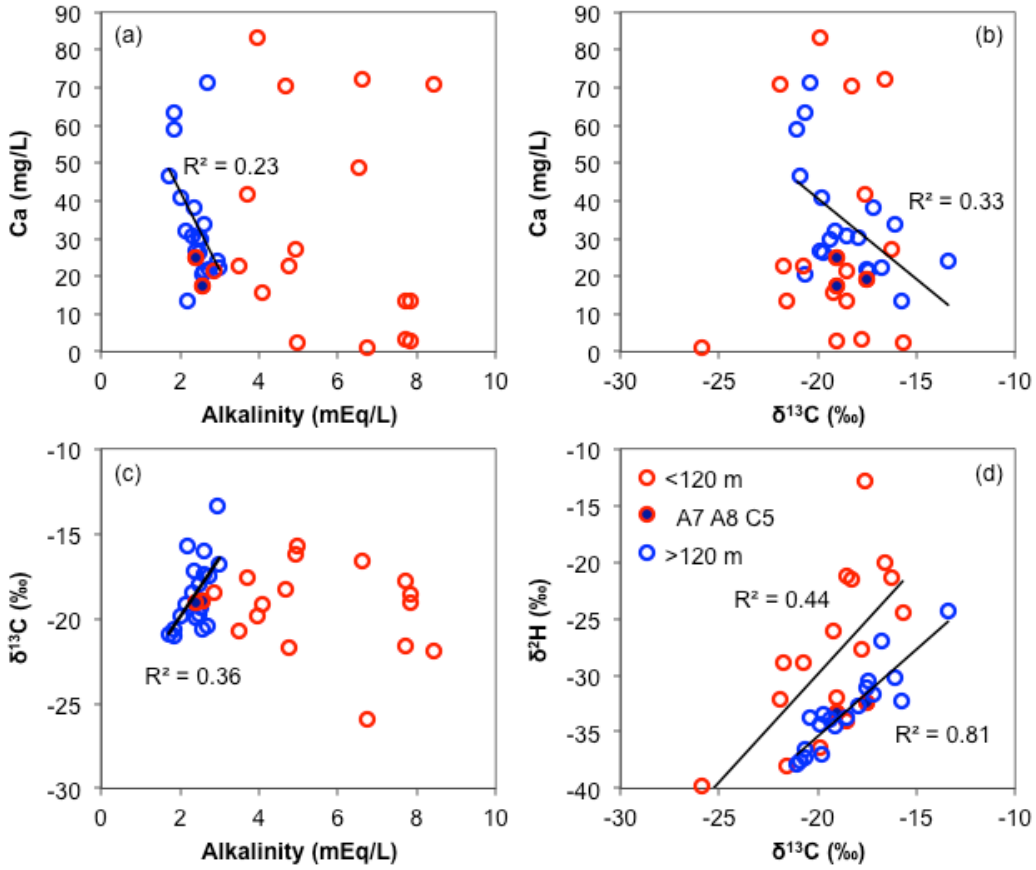

Figure 2.11. Trends and correlations between Ca, alkalinity, $\delta^{13}C_{DIC}$ and $\delta^{2}H$. The trendlines and R^2 values are shown for the deep aquifer (>120 m bgl) only, except in the $\delta^{2}H$ vs. $\delta^{13}C_{DIC}$ graph, where the intermediate aquifer samples also had a significant correlation.

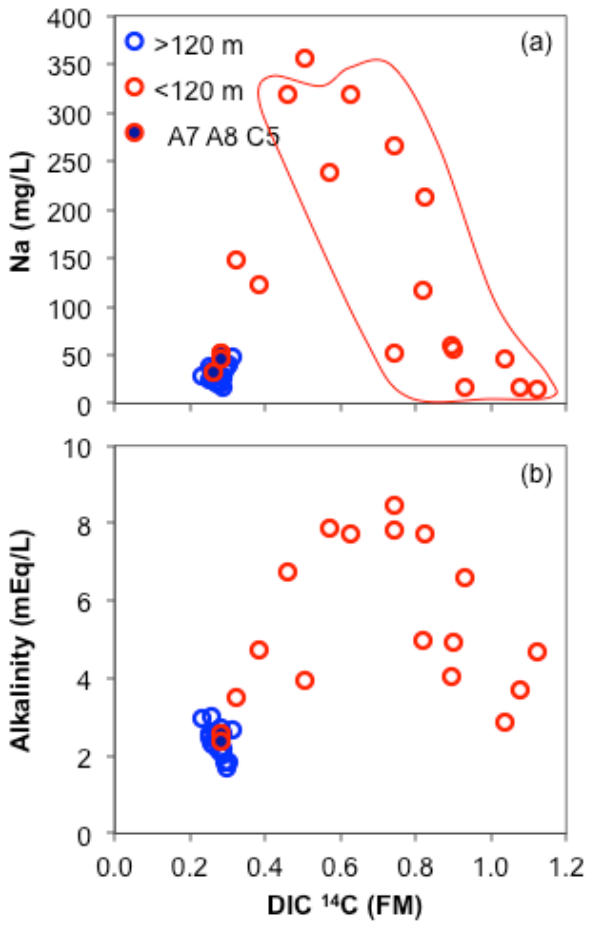

Figure 2.12. The relationship of (a) Na and (b) alkalinity with ^{14}C measured in DIC. When the low-^{14}C samples and the high salinity sample are excluded from the intermediate aquifer group (outside the red oval), Na and alkalinity are seen to increase with decreasing ^{14}C in DIC.

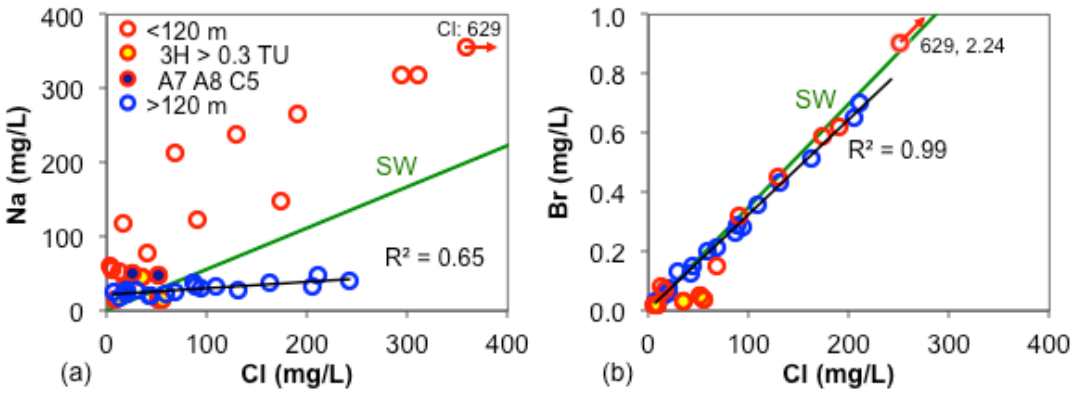

Figure 2.13. The correlations of (a) sodium and (b) bromide to chloride. Green lines indicate the trend with seawater Na/Cl and Br/Cl ratios. Black lines are the trendlines for deep aquifer groundwater (>120 m bgl) only. The high Cl sample in (a) actually falls on the seawater line.

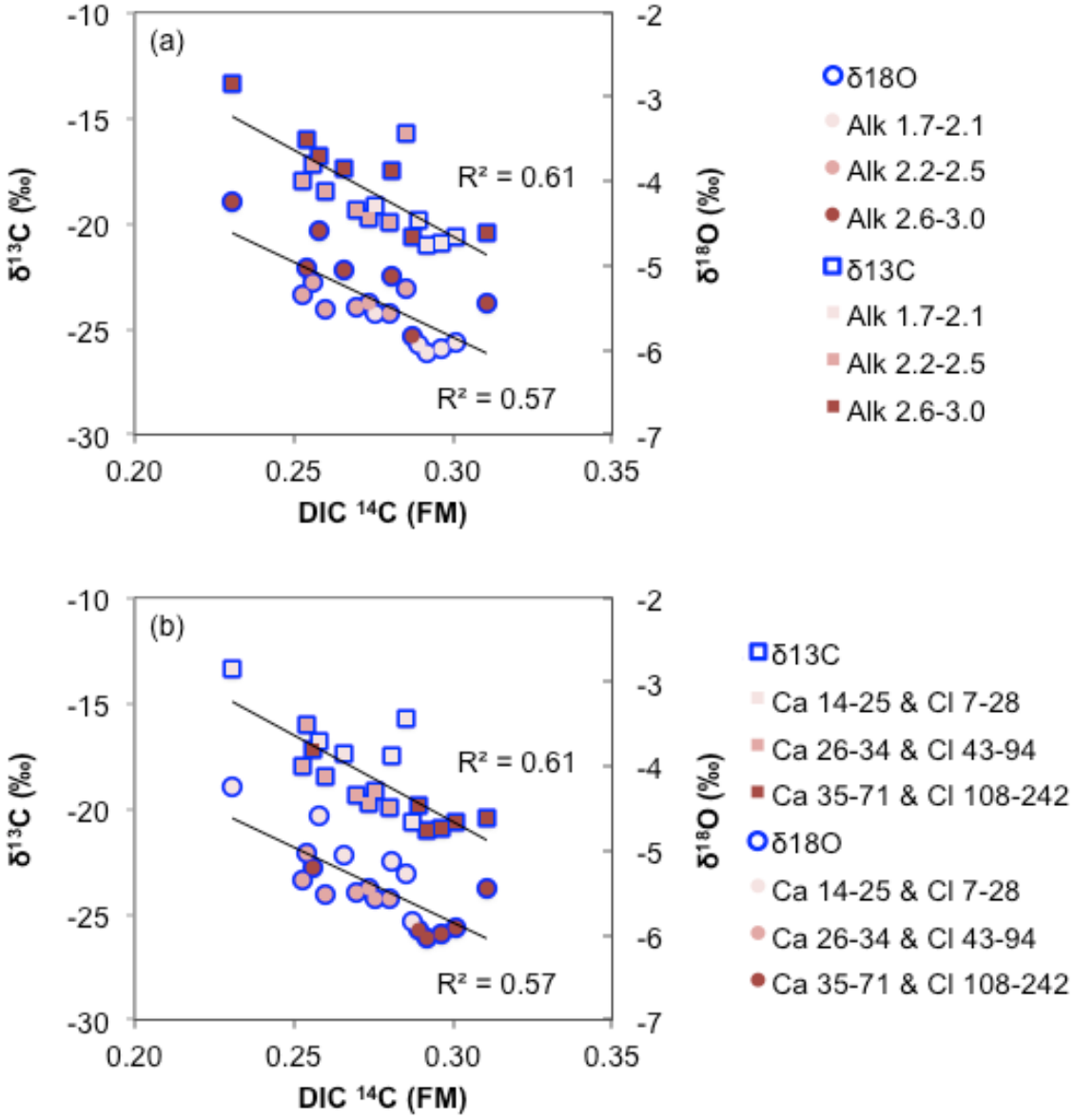

Figure 2.14. Plots of the deep groundwater (>120 m bgl) $\delta^{13}C_{DIC}$ and $\delta^{18}O$ against $^{14}C_{DIC}$, as in Fig. 2.9a, but with an added third dimension of (a) alkalinity, or (b) Ca and Cl concentrations. The units of alkalinity concentrations shown in the legend are mEq/L, and those of the Ca and Cl concentrations are mg/L. Three concentration ranges of alkalinity, or Ca and Cl, were selected based on the spread in the data.

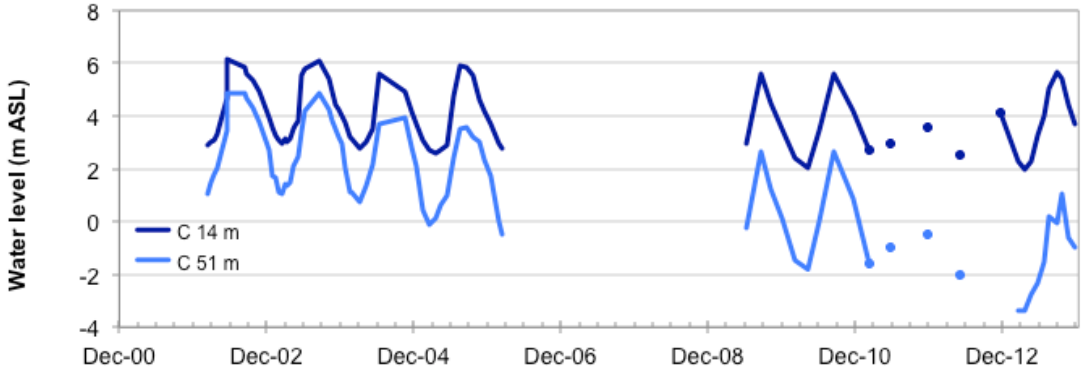

Figure 2.15. Hydrographs of a shallow well (14 m bgl) and an intermediate well (C5 in this study, 51 m bgl) at the location of multi-level nest C. Hydraulic head data since 2001 indicate a steady rise in water level difference between the shallowest and the deepest well at this site, corresponding to an increasing downward vertical hydraulic gradient.

Table 2.1. Well names, depths, and locations, along with lithological information, ^{3}H and groundwater stable isotope (^{18}O and ^{2}H) concentrations

Well ID	Depth (m)	Lat (°N)	Long (°E)	Cumm. Clay[#] (m)	Sand color	2006 ^{3}H (TU)	± σ (TU)	2010 ^{3}H (TU)	± σ (TU)	2011 ^{3}H (TU)	± σ (TU)	$\delta^{2}H$ (‰)	± σ (‰)	$\delta^{18}O$ (‰)	± σ (‰)
CW28	34.7	23.76845	90.62760	6.1	Orange	2.01	0.04								
E5	36.1	23.78999	90.61588	14.6	Orange	0.03*	0.18					-26.18	1	-4.43	0.1
A7	40.7	23.78534	90.60322	15.2	Orange	-0.30*	n/a					-33.28	1	-5.20	0.1
CW39	42.7	23.76458	90.59310	15.8	Orange	0.63	0.04					-37.41	1	-5.60	0.1
CW27	45.7	23.76813	90.62888	18.9	Orange	6.15	0.13	4.44	0.08	4.94	0.10	-21.56	0.04	-3.68	0.02
CW23	45.7	23.78743	90.61733	11.0	Orange	3.36	0.07	3.01	0.06			-12.83	0.08	-2.22	0.02
CW9	45.7	23.78614	90.62142	14.6	Orange	0.42	0.05								
CW24	48.8	23.78139	90.61780	29.3	Orange	0.21	0.05								
CW37	48.8	23.76285	90.61137	18.3	Orange	-0.01	0.03								
G5	49.8	23.77376	90.60069	12.2	Orange	0.12*	0.05					-38.06	1	-6.01	0.1
C5	52.2	23.78955	90.61113	31.4	Orange	0.17*	0.18					-32.44	1	-5.11	0.1
CW14	53.3	23.76468	90.60143	12.8	Orange	0.06	0.03			0.03	0.03	-34.02	0.05	-5.45	0.02
CW16	53.3	23.76574	90.59781	13.4	Orange	0.10	0.04								
CW8	55.5	23.77374	90.59457	11.6	Orange	0.08	0.03								
CW11	56.1	23.77347	90.64032	21.3	Brownish-grey	2.17	0.16								
CW29	56.4	23.76932	90.62417	14.0	Orange	0.15	0.03	0.07	0.03			-28.89	0.06	-4.82	0.02
F5	57.9	23.77364	90.60453	15.2	Orange	0.05*	0.05					-39.78	1	-5.95	0.1
CW31	57.9	23.76812	90.62185	14.0	Yellowish-grey	0.10	0.03	-0.03	0.02			-28.95	0.01	-4.78	0.00
DI4	57.9	23.77100	90.60941	7.6	Orange	0.05^	0.02					-27.65	1	-4.68	0.1
CW6	58.5	23.78060	90.64434	7.9	Orange	0.10	0.03								
CW20	58.5	23.77768	90.60592	3.0	Orange	0.12	0.03								
CW35	59.1	23.80112	90.63520	21.3	Orange	0.08	0.02								
CW32	59.4	23.76968	90.62048	25.6	Orange	0.16	0.05								
CW50	59.4	23.77364	90.60453	no data	Orange	0.01	0.04								
CW3	59.7	23.78013	90.64050	3.7	Orange	-0.03	0.03								
M1.5	60.5	23.77612	90.63238	14.0	Orange					2.04	0.06	-20.05	0.09	-3.16	0.01
CW10	61.0	23.79000	90.63612	12.2	Orange	0.11	0.03								
CW21	61.0	23.77928	90.60805	10.4	Orange	0.12	0.04								
CW30	61.0	23.76525	90.61650	21.3	Orange	0.04	0.04								
CW15	62.5	23.75635	90.61013	24.4	Orange	0.08	0.04	0.11	0.05	-0.01	0.03	-36.34	0.09	-5.51	0.03
CW13	62.8	23.75499	90.61245	11.6	Orange	0.06	0.03					-32.51	1	-5.21	0.1
CW19	62.8	23.77703	90.59895	18.9	Orange	0.12	0.02								
CW17	63.4	23.77158	90.59070	12.2	Orange	0.15	0.05					-40.51	1	-5.95	0.1
CW18	64.0	23.77413	90.59233	9.8	Orange	0.06	0.02	-0.02	0.03	0.08	0.04	-31.95	0.04	-5.20	0.03
CW22	64.0	23.78395	90.61327	14.6	Orange			2.67	0.06			-21.27	0.03	-3.77	0.02
CW4	65.2	23.78108	90.63325	15.8	Brownish-grey	0.01	0.03	0.05	0.02			-32.13	0.05	-5.15	0.01
CW25	70.1	23.77623	90.61705	3.7	Yellowish-grey	0.27	0.04			0.03	0.04	-24.52	0.11	-4.35	0.03
CW33	70.1	23.78758	90.62680	no data	Orange	0.17	0.04								
CW38	78.0	23.76919	90.58512	no data	Orange	0.14	0.03								
A8	81.5	23.78534	90.60322	15.2	Orange	0.10*	n/a								
CW12	87.2	23.77612	90.63238	21.3	Grey			0.02	0.03	0.02	0.03	-21.35	0.04	-3.67	0.03
B CW2	88.5	23.78036	90.63856	7.3	Grey	0.05	0.09					-26.11	1	-3.13	0.1
CW34	103.6	23.79025	90.63115	28.0	Orange	0.17	0.04								
CW41	121.9	23.79158	90.65763	31.7	Orange	0.23	0.05					-35.95	1	-5.62	0.1
CW7	123.1	23.78822	90.65173	23.2	Orange	0.17	0.04								
CW46	128.0	23.79188	90.61815	12.2	Orange			-0.01	0.03			-26.95	0.03	-4.58	0.02
CW42	128.0	23.79463	90.65992	18.3	Orange					0.05	0.03	-37.60	0.08	-5.99	0.02
CW45	129.5	23.78267	90.64853	12.2	Orange	0.10	0.03	0.01	0.02			-32.75	0.24	-5.35	0.05
CW47	137.2	23.79475	90.65147	18.3	Orange	-0.06	0.04	0.03	0.02			-36.47	0.13	-5.85	0.01
CW5	141.4	23.77305	90.63365	2.4	Orange	0.11	0.03								
CW36	149.4	23.79062	90.62635	6.7	Orange			0.09	0.03	0.02	0.04	-31.17	0.07	-5.11	0.02
CW44	152.4	23.78500	90.64982	21.3	Orange			0.06	0.02			-33.76	0.12	-5.50	0.02
WAB24030	205.4	23.75098	90.63160	no data	Orange			0.03	0.03			-32.26	0.04	-5.26	0.03
WAB24529	219.5	23.78147	90.63872	no data	Orange					0.04	0.04	-30.26	0.00	-5.02	0.00
WAB24509	222.5	23.76812	90.58532	no data	Orange					0.00	0.03	-33.70	0.01	-5.43	0.01
WAB24522	225.6	23.79296	90.64467	no data	Orange					0.01	0.03	-34.51	0.08	-5.56	0.02
WAB24531	231.6	23.77832	90.64477	no data	Whitish-gray					0.04	0.03	-24.34	0.05	-4.25	0.01
WAB24501	231.6	23.78110	90.64968	no data	Orange					0.01	0.04	-31.75	0.02	-5.20	0.00
WAB24527	231.6	23.78598	90.65933	no data	Orange					-0.01	0.03	-33.49	0.06	-5.44	0.00
WAB24538	232.3	23.78538	90.65800	no data	Whitish-grey					0.04	0.03	-34.29	0.09	-5.57	0.01
WAB24511	234.7	23.78545	90.62695	no data	Orange					0.04	0.03	-30.58	0.05	-5.06	0.02
WAB24504	234.7	23.79211	90.65718	no data	Orange					0.00	0.04	-36.97	0.07	-5.93	0.02
WAB24528	234.7	23.78707	90.65923	no data	Whitish-grey					0.07	0.04	-33.87	0.01	-5.49	0.00
WAB24513	237.7	23.79385	90.65831	no data	Whitish-grey					0.04	0.04	-37.80	0.03	-6.02	0.01
WAB24502	237.7	23.79117	90.66017	no data	Whitish-grey					0.06	0.03	-37.29	0.03	-5.90	0.01

[#] Cummulative thickness of silt and clay layers above well filter, excluding the top soil

* Sampled for ^{3}H in 2003

^ Sampled for ^{3}H in 2008

n/a = not available

Table 2.2. Radiocarbon and ^{13}C data, with calculated ^{14}C ages[#]

Well ID	Depth (m)	Phase	FM ^{14}C*	± σ (FM)	$\delta^{13}C$	UC ^{14}C age	C_1 ^{14}C age	C_2 ^{14}C age	$\Delta^{14}C$	Accession #
A7	40.7	DIC	0.2843	n/a	-19.0	10,400	9,530	7,260	-721.0	
CW27 (2010)	45.7	DIC	1.1216	0.0040	-18.3	Modern^	Modern	Modern	113.5	OS-80269
CW27 (2011)	〃	DIC	1.1165	0.0036	-18.3	Modern	Modern	Modern	108.3	OS-87014
CW23	45.7	DIC	1.0792	0.0029	-17.6	Modern	Modern	Modern	71.4	OS-80003
G5	49.8	DIC	0.6266	n/a	-21.6	3,860	2,990	1,790	-369.5	
C5	52.3	DIC	0.2631	n/a	-17.6	11,040	10,170	7,250	-735.2	
CW14	53.3	DIC	0.7419	0.0024	-18.6	2,470	1,600	Modern	-263.5	OS-87015
CW29	56.4	DIC	0.3841	0.0022	-21.7	7,910	7,040	5,880	-618.7	OS-80000
F5	57.9	DIC	0.4600	0.0020	-25.9	6,430	5,560	5,860	-542.5	OS-41275
F5	〃	DOC	0.5010	0.0030	n/a	5,710	-	-	-502.0	
CW31	57.9	DIC	0.3238	0.0014	-20.8	9,320	8,450	6,910	-678.6	OS-80004
DI4	57.9	DIC	0.8259	0.0031	-17.8	1,580	710	Modern	-179.9	OS-68866
M1.5	60.5	DIC	0.9312	0.0030	-16.6	590	Modern	Modern	-75.6	OS-90066
M1.5	〃	DOC	0.8259	0.0021	-24.9	1,580	-	-	-180.3	OS-101857
CW15 (2010)	62.5	DIC	0.5064	0.0017	-19.9	5,620	4,750	2,850	-497.3	OS-80002
CW15 (2011)	〃	DIC	0.5027	0.0028	-19.8	5,690	4,810	2,880	-501.0	OS-87016
CW18 (2010)	64.0	DIC	0.5692	0.0023	-19.0	4,660	3,790	1,540	-434.9	OS-79994
CW18 (2011)	〃	DIC	0.6628	0.0025	-18.4	3,400	2,530	Modern	-342.1	OS-87124
CW18 (2010)	〃	DOC	0.4436	0.0020	-26.5	6,720	-	-	-559.6	OS-80285
CW22	64.0	DIC	1.0374	0.0030	-18.5	Modern	Modern	Modern	29.9	OS-79996
CW4	65.2	DIC	0.7429	0.0023	-21.9	2,460	1,590	490	-262.4	OS-79992
CW4	〃	DOC	0.7521	0.0041	-24.3	2,360	-	-	-253.3	OS-80290
CW25	70.1	DIC	0.8199	0.0025	-15.7	1,640	770	Modern	-186.1	OS-87122
A8	81.5	DIC	0.2842	n/a	-19.1	10,400	9,530	7,290	-721.0	
CW12 (2010)	87.2	DIC	0.8992	0.0029	-16.3	880	Modern	Modern	-107.3	OS-80268
CW12 (2011)	〃	DIC	0.9096	0.0029	-16.3	780	Modern	Modern	-97.0	OS-87013
CW12 (2011)	〃	DOC	0.7373	0.0022	n/a	2,520	-	-	-268.1	OS-86918
B CW2	88.5	DIC	0.8940	n/a	-19.2	930	60	Modern	-100.4	
CW46	128.0	DIC	0.2578	0.0013	-16.8	11,210	10,340	7,050	-744.1	OS-79995
CW42	128.0	DIC	0.2965	0.0017	-20.9	10,050	9,180	7,710	-705.7	OS-87052
CW45	129.5	DIC	0.2526	0.0016	-18.0	11,370	10,500	7,760	-749.2	OS-79998
CW47	137.2	DIC	0.2872	0.0012	-20.7	10,310	9,440	7,870	-714.9	OS-79855
CW36 (2010)	149.4	DIC	0.2809	0.0013	-17.5	10,500	9,630	6,680	-721.2	OS-79997
CW36 (2011)	〃	DIC	0.2636	0.0014	-17.8	11,020	10,150	7,320	-738.4	OS-87123
CW44	152.4	DIC	0.2600	0.0012	-18.5	11,140	10,260	7,780	-741.9	OS-79856
WAB24030	205.4	DIC	0.2856	0.0016	-15.7	10,360	9,490	5,660	-716.4	OS-79999
WAB24529	219.5	DIC	0.2540	0.0018	-16.1	11,330	10,460	6,800	-747.8	OS-87239
WAB24509	222.5	DIC	0.3106	0.0022	-20.4	9,670	8,790	7,120	-691.7	OS-87236
WAB24522	225.6	DIC	0.2757	0.0017	-19.2	10,650	9,780	7,580	-726.4	OS-87248
WAB24531	231.7	DIC	0.2307	0.0013	-13.4	12,120	11,250	6,100	-771.0	OS-87238
WAB24501	231.7	DIC	0.2558	0.0014	-17.2	11,270	10,400	7,320	-746.1	OS-87252
WAB24527	231.7	DIC	0.2737	0.0018	-19.7	10,710	9,840	7,870	-728.3	OS-87240
WAB24538	232.3	DIC	0.2804	0.0020	-19.9	10,510	9,640	7,760	-721.6	OS-87245
WAB24511	234.7	DIC	0.2660	0.0013	-17.4	10,950	10,080	7,090	-736.0	OS-87237
WAB24504	234.7	DIC	0.2889	0.0014	-19.8	10,260	9,390	7,470	-713.2	OS-87254
WAB24528	234.7	DIC	0.2698	0.0015	-19.4	10,830	9,960	7,850	-732.2	OS-87246
WAB24513	237.7	DIC	0.2916	0.0018	-21.1	10,190	9,320	7,890	-710.5	OS-87258
WAB24502	237.7	DIC	0.3007	0.0017	-20.6	9,930	9,060	7,470	-701.5	OS-87253

[#] ^{14}C ages were calculated as described in section 2.3.2. C_1 and C_2 ages are not applicable to DOC

* FM stands for fraction modern radiocarbon n/a = not available

^ Age is reported as "Modern" when FM≥1 or the age correction resulted in a negative age

Table 2.3. Noble gas concentrations and the resulting model recharge temperature and He surplus*

Well ID	Depth (m)	He ccSTP g^{-1}_{GW}	Ne ccSTP g^{-1}_{GW}	Ar ccSTP g^{-1}_{GW}	Kr ccSTP g^{-1}_{GW}	Xe ccSTP g^{-1}_{GW}	$^3He/^4He$	Model prob. (%)^	Model T (°C)	err Model T (°C)	He surplus[$] ccSTP g^{-1}_{GW}	err He surp. ccSTP g^{-1}_{GW}
E5	36.2	4.00E-08	1.29E-07	2.40E-04	5.51E-08	7.73E-09	1.27E-06	0				
A7	40.7	7.96E-08	2.12E-07	3.22E-04	6.92E-08	9.17E-09	9.09E-07	98.4	22.26	0.65	2.71E-08	1.72E-09
CW27 (2010)	45.7	5.46E-08	2.20E-07	3.17E-04	6.65E-08	8.29E-09	2.75E-06	54.9	31.95	3.44	-1.55E-09	1.51E-09
CW27 (2011, 1)	45.7	5.54E-08	2.25E-07	3.20E-04	6.76E-08	8.75E-09	3.07E-06	73.4	24.33	0.68	-9.22E-10	1.31E-09
CW27 (2011, 2)	45.7	5.46E-08	2.24E-07	3.20E-04	6.77E-08	8.73E-09	3.18E-06	59.7	24.40	0.71	-1.47E-09	1.29E-09
CW23	45.7	5.60E-08	2.33E-07	3.35E-04	7.09E-08	8.92E-09	1.54E-06	16.0	25.34	1.34	-2.04E-09	1.28E-09
G5	49.8	5.35E-08	1.47E-07	2.42E-04	5.41E-08	7.32E-09	1.03E-06	0				
CW14	53.3	5.19E-08	1.74E-07	2.65E-04	5.94E-08	8.06E-09	1.25E-06	0				
CW29	56.4	7.25E-08	1.96E-07	2.97E-04	6.40E-08	8.41E-09	9.31E-07	78.2	24.77	0.66	2.37E-08	1.58E-09
CW31	57.9	7.40E-08	1.96E-07	3.00E-04	6.42E-08	8.49E-09	9.05E-07	70.0	24.65	0.75	2.51E-08	1.59E-09
CW15 (2010)	62.5	5.01E-08	1.03E-07	1.64E-04	3.78E-08	5.56E-09	8.15E-07	0				
CW15 (2011, 1)	62.5	4.71E-08	9.88E-08	1.63E-04	3.72E-08	5.48E-09	8.76E-07	0				
CW15 (2011, 2)	62.5	4.77E-08	9.73E-08	1.59E-04	3.73E-08	5.52E-09	8.38E-07	0				
CW18 (2010)	64.0	5.49E-08	1.72E-07	2.80E-04	6.07E-08	8.00E-09	1.07E-06	0.1				
CW18 (2011)	64.0	5.28E-08	1.82E-07	2.88E-04	6.32E-08	8.45E-09	0	82.1	24.15	0.50	7.98E-09	1.35E-09
CW22	64.0	5.71E-08	2.22E-07	3.21E-04	6.71E-08	8.58E-09	1.69E-06	82.1	25.88	1.04	1.33E-09	1.30E-09
CW4	65.2	4.77E-08	1.84E-07	2.93E-04	6.41E-08	8.21E-09	1.15E-06	1.7	25.51	7.87	1.58E-09	1.72E-09
CW25	70.1	5.68E-08	2.13E-07	3.17E-04	6.78E-08	9.15E-09	1.51E-06	36.0	22.03	0.50	3.48E-09	1.46E-09
CW12 (2010)	87.2	5.16E-08	2.09E-07	3.06E-04	6.54E-08	8.22E-09	1.09E-06	20.0	30.92	2.74	-1.47E-09	1.38E-09
CW12 (2011, 1)	87.2	5.32E-08	2.05E-07	3.03E-04	6.53E-08	8.64E-09	1.27E-06	95.1	23.74	0.52	1.76E-09	1.38E-09
CW12 (2011, 2)	87.2	5.34E-08	2.09E-07	3.05E-04	6.54E-08	8.74E-09	1.42E-06	48.9	23.55	0.51	1.02E-09	1.42E-09
CW46	128.0	8.45E-08	2.24E-07	3.26E-04	6.94E-08	8.83E-09	8.77E-07	18.7	24.66	0.98	2.85E-08	1.80E-09
CW42	128.0	7.40E-08	2.12E-07	3.17E-04	6.81E-08	9.39E-09	1.09E-06	3.4	21.22	0.48	2.17E-08	1.78E-09
CW45	129.5	8.02E-08	2.26E-07	3.27E-04	6.97E-08	8.73E-09	9.42E-07	25.2	31.42	2.56	2.28E-08	1.87E-09
CW47	137.2	7.34E-08	2.16E-07	3.23E-04	6.87E-08	8.90E-09	1.02E-06	75.0	24.16	1.04	1.97E-08	1.58E-09
CW36 (2010)	149.4	7.84E-08	2.26E-07	3.28E-04	7.02E-08	8.71E-09	9.70E-07	8.9	30.83	2.88	2.12E-08	1.86E-09
CW36 (2011)	149.4	7.69E-08	2.27E-07	3.25E-04	6.95E-08	9.42E-09	1.04E-06	13.7	21.32	0.49	2.02E-08	1.86E-09
CW44	152.4	8.05E-08	2.26E-07	3.21E-05	6.90E-08	8.62E-09	8.91E-07	0				
WAB24030	205.4	8.03E-08	2.28E-07	3.28E-04	7.02E-08	8.97E-09	9.52E-07	15.0	23.59	0.74	2.34E-08	1.74E-09

Grey shading indicates samples that were not used for plots and discussion due to: low model probability and/or model T error >1.5 °C

* The model used is described in section 2.3.3.

^ The probability that model is consistent with the data (>1% is minimum, >5% is a strong criterion)

[$] He surplus is equivalent to radiogenic He

Table 2.4. Groundwater chemistry and physicochemical parameters

Well ID	Depth (m)	EC (mS/cm)	Temp. (°C)	pH	Alkalinity (mEq/L)	DIC (mM)	DOC (mM)	Na (mg/L)	Mg (mg/L)	K (mg/L)	Ca (mg/L)	Si (mg/L)	P (mg/L)	Mn (µg/L)	Fe (mg/L)	As (µg/L)	S (mg/L)	Cl (mg/L)	SO_4 (mg/L)	Br (mg/L)	F (mg/L)
E5	36.2	0.79	26.1	6.61	6.55	10.28^	0.15	78	17	2.9	49	-	0.16	288	3.5	2.4	0.1*	41	-	-	-
A7	40.7	0.35	26.1	6.23	2.55	6.05^	-	51	5	1.2	17	-	0.25	110	0.1	0.0	1.3	25	-	-	-
CW27	45.7	0.75	25.7	6.87	4.68	5.70	-	15	20	3.9	70	42	0.09	1,374	0.1	0.0	6.4	52	17.4	0.05	0.29
CW23	45.7	0.62	25.9	6.64	3.70	5.18	-	16	29	2.0	42	45	0.27	471	0.0	0.1	5.8	55	16.7	0.04	0.70
G5	49.8	1.76	26.4	6.80	7.70	10.54^	0.05	319	6	2.2	13	-	0.25	588	0.6	6.6	1.1	294	-	-	-
C5	52.3	0.34	26.2	6.37	-	-	0.06	32	9	2.2	19	-	0.11	769	9.9	2.9	0.7	18	-	-	-
CW14	53.3	1.36	26.2	7.57	7.84	8.74	-	265	6	1.1	14	41	0.48	2	0.0	0.5	0.6	190	1.1	0.62	0.70
CW29	56.4	0.92	26.1	6.87	4.75	6.15	-	123	9	1.8	23	41	0.18	302	0.0	0.4	2.0	91	5.3	0.32	0.94
F5	57.9	1.88	26.2	6.94	6.74	8.54^	0.09	319	7	1.8	1	-	0.13	487	1.6	1.0	0.5	311	-	-	-
CW31	57.9	1.13	26.1	6.58	3.49	5.13	-	149	9	1.9	23	49	0.21	297	0.1	0.3	5.7	173	15.5	0.59	0.66
DI4	57.9	0.92	27.2	7.21	7.72	8.82^	-	213	3	2.7	4	21	0.58	152	0.6	0.6	0.1*	69	n/d	0.15	1.94
M1.5	60.5	0.61	26.5	7.05	6.61	7.89	0.18	16	29	2.1	72	34	0.15	618	0.2	2.2	0.5*	8	0.5	0.02	0.48
CW15	62.5	2.97	26.1	6.22	3.96	7.83	-	356	23	2.7	83	56	0.12	123	0.3	0.1	8.6	629	23.9	2.24	0.33
CW18	64.0	1.38	26.1	7.35	7.86	8.68	0.25	239	4	3.5	3	35	0.53	415	0.4	9.4	0.1*	130	n/d	0.45	2.48
CW22	64.0	0.49	26.2	6.50	2.86	4.76	-	46	8	1.6	21	58	0.17	60	0.5	0.0	3.5	35	10.2	0.04	0.57
CW4	65.2	0.93	26.0	7.03	8.45	10.11	0.12	52	29	2.3	71	35	0.15	1,139	2.2	29.1	0.2*	13	0.2	0.08	0.72
CW25	70.1	0.55	26.0	7.30	4.98	5.63	-	117	1	0.7	2	46	4.75	73	0.0	16.9	0.3	16	0.7	0.07	0.94
A8	81.5	0.41	26.2	6.17	2.40	6.17^	-	47	12	2.0	25	-	0.31	440	0.3	1.0	1.3	51	-	-	-
CW12	87.2	0.56	26.5	6.53	4.93	7.28	0.07	55	12	2.1	27	59	0.11	392	0.1	0.4	0.1*	5	0.3	0.02	0.39
B CW2	88.5	0.37	26.2	6.94	4.07	5.15^	-	59	7	1.6	16	-	0.12	55	0.6	11.0	0.0*	4	-	-	-
CW46	128.0	0.37	26.7	6.55	3.00	4.77	-	26	9	1.7	22	66	0.21	30	0.1	1.3	0.3*	7	0.6	0.03	0.52
CW42	128.0	0.75	27.2	6.58	1.71	2.99	-	37	23	2.2	46	70	0.15	782	0.0	0.2	2.7	162	7.7	0.51	0.11
CW45	129.5	0.64	26.7	6.64	2.50	3.82	-	38	18	2.6	30	60	0.18	432	0.1	3.6	1.3*	87	3.8	0.27	0.32
CW47	137.2	0.36	26.7	6.77	2.55	3.75	-	17	11	2.3	21	64	0.24	281	0.2	1.8	0.7*	13	1.7	0.05	0.37
CW36	149.4	0.40	26.4	6.72	2.74	4.18	-	27	11	2.1	22	55	0.13	143	1.0	1.0	0.5	20	1.1	0.07	0.38
CW44	152.4	0.64	26.8	6.60	2.29	3.76	-	32	18	2.6	31	58	0.21	485	0.6	6.7	1.1*	89	3.0	0.29	0.33
WAB24030	205.4	0.32	26.5	6.34	2.20	4.48	-	26	6	1.4	14	65	0.37	244	4.1	8.7	0.3*	18	0.6	0.06	0.33
WAB24529	219.5	0.50	26.8	6.83#	2.59	3.48	-	25	16	2.0	34	63	0.09	124	1.6	0.7	0.7	69	2.0	0.22	0.13
WAB24509	222.5	0.99	26.4	6.63#	2.68	4.16	-	47	31	2.5	71	67	0.09	92	0.9	0.3	2.4	210	6.6	0.70	0.18
WAB24522	225.6	0.54	26.9	6.54#	2.12	3.54	-	31	17	2.5	32	68	0.13	338	0.1	0.4	1.5	94	4.3	0.28	0.09
WAB24531	231.7	0.39	26.7	7.11#	2.95	3.48	-	27	12	1.6	24	62	0.08	100	0.8	0.6	0.5	28	1.1	0.13	0.19
WAB24501	231.7	0.61	26.5	6.58#	2.34	3.79	-	34	20	2.4	38	66	0.07	263	0.5	0.9	1.6	108	4.0	0.36	0.11
WAB24527	231.7	0.40	27.4	6.77#	2.49	3.85	-	20	14	2.1	26	68	0.11	408	1.1	1.4	0.7	43	1.8	0.12	0.18
WAB24538	232.3	0.40	27.3	6.77#	2.39	3.32	-	20	14	2.2	27	67	0.11	352	0.9	1.4	0.6	45	1.5	0.15	0.22
WAB24511	234.7	0.34	26.7	6.71#	2.63	3.81	-	22	10	1.5	22	61	0.12	288	1.7	1.6	0.4	21	1.1	0.06	0.23
WAB24504	234.7	0.65	27.2	6.60#	2.03	3.22	-	28	22	2.7	41	69	0.12	847	0.4	1.6	1.1	130	3.1	0.43	0.16
WAB24528	234.7	0.45	26.7	6.81#	2.51	3.41	-	22	17	2.4	30	66	0.11	477	0.6	1.7	1.0	59	2.6	0.20	0.17
WAB24513	237.7	0.89	27.6	6.47#	1.83	3.29	-	34	30	3.0	59	69	0.13	686	3.3	1.8	1.7	205	5.2	0.65	0.11
WAB24502	237.7	1.00	27.8	6.58#	1.85	2.99	-	40	35	3.2	63	68	0.11	1,069	4.1	1.8	5.3	242	14.4	-	0.15

pH calculated from alkalinity and DIC concentrations (field samples suffered from degassing)

^ DIC calculated from pH and alkalinity

* S values near the detection limit of ICP-MS

n/d = not detected; " - " indicates no measurement was performed

Chapter 3:

Arsenic contamination exacerbated by clay layers in a low-arsenic aquifer in Bangladesh

IVAN MIHAJLOV[1,2], BENJAMÍN C. BOSTICK[2], MARTIN STUTE[2,3], BRIAN J. MAILLOUX[3], PETER S. K. KNAPPETT[2], MD. RAJIB H. MOZUMDER[1,2], IMTIAZ CHOUDHURY[4], KAZI MATIN AHMED[4], PETER SCHLOSSER[2,5], ALEXANDER VAN GEEN[2]

[1]Department of Earth and Environmental Sciences, Columbia University, New York, NY 10025

[2]Lamont-Doherty Earth Observatory of Columbia University, Palisades, NY 10964

[3]Barnard College, New York, NY 10025

[4]Department of Geology, University of Dhaka, Dhaka, Bangladesh

[5]Department of Earth and Environmental Engineering, Columbia University, New York, NY 10025

Abstract

Confining clay layers are widely perceived to provide protection to Pleistocene low-arsenic aquifers against intrusion of shallower high-arsenic groundwater. This notion is challenged here by showing that organic carbon drawn downwards from such a clay layer into an aquifer depressurized by pumping promotes the reduction of sedimentary iron and releases arsenic to groundwater. This finding provides an explanation for the previously documented failing of a structurally sound community well that had been installed in the same aquifer. Tritium measurements indicate that groundwater from the affected 40-50 m depth interval was recharged >60 years ago. Groundwater at 55-70 m depth in the same aquifer bypassed the clay layer and was recharged 10-50 years ago, but is still low in As and aquifer sands at that depth are orange. In this particular configuration, recharge accelerated by groundwater pumping protected a low-arsenic aquifer instead of putting it at risk. Thus, a contact with shallow aquifer via recent recharge may not necessarily adversely affect the low-As aquifers, whereas the confining clay layers may not always protect them from As contamination. The findings point to the need for re-evaluating the vulnerability of low-arsenic aquifers that are key for reducing the exposure of a large population in South and Southeast Asia.

3.1 Introduction

The majority of rural population of Bangladesh, located in the Bengal Basin of South Asia, obtains drinking water by pumping groundwater from shallow tubewells that often exceeds the limit of 10 µg/L arsenic (As), a level judged unsafe by the World Health Organization (BGS and DPHE, 2001). Chronic low-dose exposure to As, a toxic metalloid, has been linked to various cancers, skin lesions, cardio-vascular diseases, increased mortality rates, and diminished children's intellectual function (Argos et al., 2010; Smith et al., 2000; Wasserman et al., 2004; Yu et al., 2003). With intentions to reduce As poisoning, government and non-governmental organizations in Bangladesh have installed >100,000 deeper, shared (or "community") wells, typically >100-150 m below ground level (bgl) in low-As aquifers (Aggarwal et al., 2000; Ahmed et al., 2006; BGS and DPHE, 2001; JICA and DPHE, 2010; Michael and Voss, 2008; Ravenscroft et al., 2005; Ravenscroft et al., 2013). By 2006 (Ahmed et al.), 12% of the affected population had switched from a high-As shallow well to a deep community well, confirming the effectiveness of this mitigation strategy.

Although 95% of wells installed deeper than 150 m bgl have <10 µg/L As (BGS and DPHE, 2001), depth *per se* is a poorly defined boundary of deeper aquifers, as low-As aquifers can also be found in the 20-150 m bgl interval (McArthur et al., 2008; van Geen et al., 2007; Zheng et al., 2005). Deeper aquifers were typically deposited in the Pleistocene, exposed to valley incision and steep groundwater hydraulic gradients during the sea level lowstand, until the rapid valley infill during deglaciation-induced sea level rise accumulated the Holocene, shallow aquifer sequence on top of them (Allison et al.,

2003; BGS and DPHE, 2001; Goodbred and Kuehl, 2000a, b; McArthur et al., 2008; Ravenscroft et al., 2005). The Holocene aquifers host shallow groundwater with up to >1000 μg/l dissolved As, primarily released by the microbially-mediated reduction of iron(III) oxyhydroxides (FeOOH) coupled to organic matter (OM) oxidation that changes the sand color from orange to grey (BGS and DPHE, 2001; Fendorf et al., 2010; Islam et al., 2004; McArthur et al., 2004; Nickson et al., 1998; Nickson et al., 2000). The sources of OM have been a matter of contention, but generally include plant matter co-deposited with aquifer sands and clays, or dissolved OM infiltrating with groundwater recharge, possibly made more vigorous by widespread shallow irrigation and massive excavation of ponds (BGS and DPHE, 2001; Fendorf et al., 2010; Harvey et al., 2002; Klump et al., 2006; Mailloux et al., 2013; McArthur et al., 2004; Neumann et al., 2010; Polizzotto et al., 2008; Sengupta et al., 2008; van Geen et al., 2008).

The occurrence of predominantly Fe(III)-containing orange sand at depth, used by local drillers to target low-As well installation, is often a clear sign of Pleistocene, deeper aquifer sediments with previous exposure to more oxic conditions (BGS and DPHE, 2001; McArthur et al., 2008; van Geen et al., 2007; Zheng et al., 2005), but deeper aquifers can also contain grey sediment with low-As groundwater (BGS and DPHE, 2001; Burgess et al., 2010; Zheng et al., 2005). Although orange sands can immobilize As more strongly onto highly adsorbing FeOOH surfaces (McArthur et al., 2008; Radloff et al., 2011; van Geen et al., 2004; van Geen et al., 2008; Zheng et al., 2005), both grey and orange sands of low-As aquifers are characterized by low concentrations of labile (or mobilizable) As pools in the solid phase (Dhar et al., 2011; Zheng et al., 2005). This is presumably because the labile As and/or OM that could cause As release had been

flushed away from these aquifers by more vigorous river and groundwater flow regime of the Pleistocene (BGS and DPHE, 2001; McArthur et al., 2008; Ravenscroft et al., 2005).

The hydrologic and geochemical balance that maintained low dissolved As in deeper aquifers might be disturbed by future water use patterns. Water levels in the deep aquifer around Dhaka have already dropped by up to 40 m (2002) due to the pumping for municipal water supply (Hoque et al., 2007). Depressurization at depth creates a downward vertical hydraulic gradient that can draw shallow groundwater into the low-As aquifer in places where clay layers separating it from the shallow zone are leaky, thin, patchy, or missing entirely. Basin-scale hydrological models have addressed the potential threat to deep aquifer sustainability by testing various scenarios of water resource development in the future, as well as by varying and lumping, on large-scale, aquifer properties such as vertical and horizontal hydraulic conductivity, randomized clay layer distribution, and As retardation on sediments (Burgess et al., 2010; Michael and Voss, 2008, 2009a, b; Radloff et al., 2011). These studies have shown that withdrawing deep aquifer groundwater for irrigation supply, accounting for >90% of water consumption in the country (Michael and Voss, 2008), would likely contaminate deeper aquifers with shallow groundwater within <1,000 years. Shallow groundwater can transport both As and organic matter that could reduce deeper aquifer sediment, decrease its otherwise considerable As sorption capacity, and perhaps cause additional As release (Dhar et al., 2011; McArthur et al., 2008; Robinson et al., 2011; Stollenwerk et al., 2007).

Few studies have, however, thus far presented direct evidence of contamination of vulnerable low-As aquifers under flow conditions present in the field. Point failures of deep wells to produce low-As groundwater have been noted in isolated cases, attributed

to screened intervals at multiple depths or mechanical problems in individual wells, such as cracked tubewell PVC at high-As depth, both of which would allow the shallow groundwater to infiltrate (Aggarwal et al., 2000; van Geen et al., 2007). A larger-scale contamination of Pleistocene aquifers due to the inflow of high-As and organic-rich groundwater from the overlying Holocene aquifers has been convincingly demonstrated in the Red River delta of Vietnam (Winkel et al., 2011) where deep groundwater abstraction has occurred for >100 years. Mukherjee et al. (2011) reported As contamination at >100 m depth in a ~200-km transect along West Bengal that lacked major confining units, but the classic Pleistocene orange beds founds elsewhere in the Basin were absent. On a village site scale, McArthur et al. (2010; 2011; 2008) and van Geen et al. (2013) described a lateral movement of high-As reduction front along a horizontal hydraulic gradient from Holocene grey sand to Pleistocene orange sand. McArthur et al. (2010; 2011) also demonstrated a downward migration of contaminated groundwater into the underlying Pleistocene sands in paleo-channel locales lacking low-permeability clay (paleosol) capping.

The common denominator in most of these studies are the notions that (1) the presence of a thick or multiple clay layers is desirable to prevent the contamination of deeper low-As aquifers due to confinement, and (2) that the inflow of young groundwater from the shallow zone can transport the As and organics deeper and fuel further reduction and As release. However, recent studies in Vietnam have proposed explanations of dissolved As distribution that challenge the first notion of protection afforded by the clay layers. Berg et al. (2008) and Norrman et al. (2008) report As contamination of Pleistocene aquifers at several locations in the Red River delta where these deeper

aquifers are separated from the high-As shallow aquifer by clay or peat layers, across which downward hydraulic gradients exist due to groundwater abstraction at depth. While Berg et al. (2008) attributes the arrival of high As, DOC, Fe, NH3, and alkalinity to the infiltration of shallow groundwater from the shallower Holocene aquifer, they propose that the passage of groundwater through the confining unit mobilized additional As and organic matter that helped fuel reduction in the Pleistocene aquifer. The lateral extent of the clay layer and clay pore water chemistry, however, were not investigated. Erban et al. (2013) go a step further and propose that the contamination of the Pleistocene aquifer in the Mekong delta might be widespread *because* of the clay layers, dated to Pliocene and Miocene, getting compacted at depth by the increased pumping-induced subsidence, thus releasing their retained As, organic C and competing ions. This novel mechanism of As release to the low-As aquifers awaits further studies for confirmation.

In this study, we describe the geochemistry of a vulnerable low-As aquifer on the scale of ~200×200 m, centered locally around a reported community well failure for which no obvious mechanical explanation was found (van Geen et al., 2007). This aquifer, dubbed as "intermediate" for its depth of ~40-75 m bgl and its late Pleistocene sediment deposition age, lies beneath a 10-15 m thick clay layer separating it from the high-As shallow aquifer. Two community well installations in orange sands (55m depth) of the intermediate aquifer initially produced low-As groundwater, but experienced a sudden increase in dissolved As within <18 months post-installation. After the first CW12 failure, a mechanical cause such as shallow cracks or annular flow was considered, but the second failure raised the flag for non-mechanical causes. Since no cracks were detected by testing the well casing with an inflatable packer (van Geen et al.,

2007), it was suspected that As reached the community well intake by transport across the clay layer and/or As release within the low-As aquifer, warranting further study.

We show that the upper layer of the intermediate aquifer, lying directly beneath the Holocene clay unit that maintains a downward vertical hydraulic gradient of ~1m, is contaminated with As and receives little lateral inflow. The slow leakage of reactive organic matter and dissolved constituents, including Fe and As, from the pore water of the ~8,500 year old clay helps fuel reduction in the upper portion of the intermediate aquifer. On the other hand, a fairly rapid flow of recently recharged water exists in the middle-to-lower portion of the intermediate aquifer that coincides with the dissolved As minimum and less reducing conditions in both the sediment and groundwater. Thus, the observations made at this location challenge both the notion that clay layers are protective of the low-As aquifers at depth and the notion that recent recharge from the shallow aquifer necessarily promotes reduction and As contamination.

3.2 Methods

3.2.1 Site description and installation.

The study site (23.7760° N and 90.6325° E, Fig. 1), named "site M", is located in Araihazar upazila of Bangladesh, ~25 km east of the capital, Dhaka. The site is located in the vicinity of village Baylakandi / site B (Fig. 3.1b); both this region and site B, in particular, were described in detail by van Geen et al. (2003), Zheng et al. (2005), and Dhar et al. (2008). The site of detailed studies in this publication (~200×200 m, Fig. 3.1b&c) is centered on the previously failed community well 12 (CW12), reported by van Geen et al. (2007). Stratigraphic layers at site M generally include a shallow, high-As aquifer composed of grey, Holocene sands, and an older, low-As aquifer (nicknamed "intermediate" aquifer) composed of layers of grey and orange sands. A clay/silt layer of variable thickness (~10-15 m) separates the two aquifers, but pinches out at site T [near TW-5 in Horneman et al. (2004)], ~300 m S/SE of site M, identifying this location as a potential source of shallow groundwater recharge into the intermediate aquifer. The patchiness of the local clay aquitard is also seen ~750 m NE at site B, where it is manifested as two thinner (<5m) clay layers (Zheng et al., 2005).

The discontinuity of confining layers in this area is supplemented by another key observation raising concerns about the long-term status of the intermediate-depth aquifer: head difference between the shallow and the intermediate aquifer documented at site B (Fig. 3.13 in Appendix) has gradually increased since 2000 to >1 m. Such a downward gradient at the study site could induce leakage of shallow groundwater and clay pore water into the underlying low-As aquifer. Indeed, several community wells in the vicinity

installed in orange sand 35-56 m bgl deep have ^{3}H levels of 2-6 TU (2006, Table 2.1 in Ch. 2 Appendix), indicating recharge with shallow groundwater in the area (Fig. 3.1b). A survey of private tubewells installed within the equivalent depth range (45-75 m) in the area, showed that As concentrations are quite patchy in groundwater at this depth, whereas they are relatively low directly to the north, and high further south (van Geen, personal comm.). Thus, the site under investigation could be a transition zone where the intermediate-depth low-As aquifers are highly vulnerable.

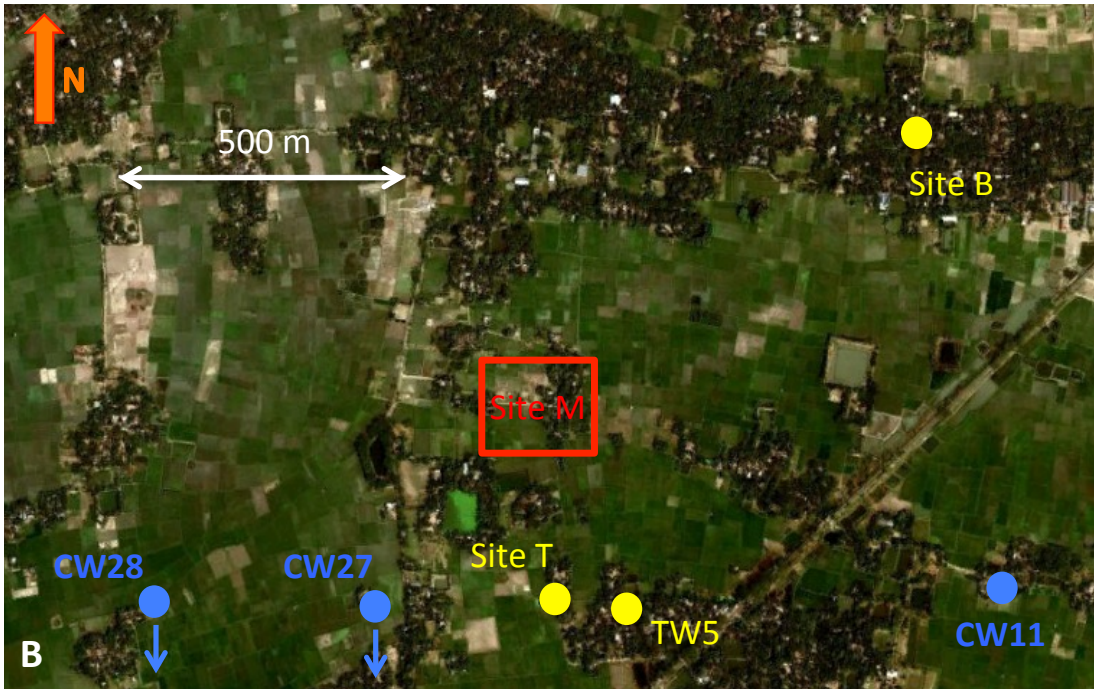

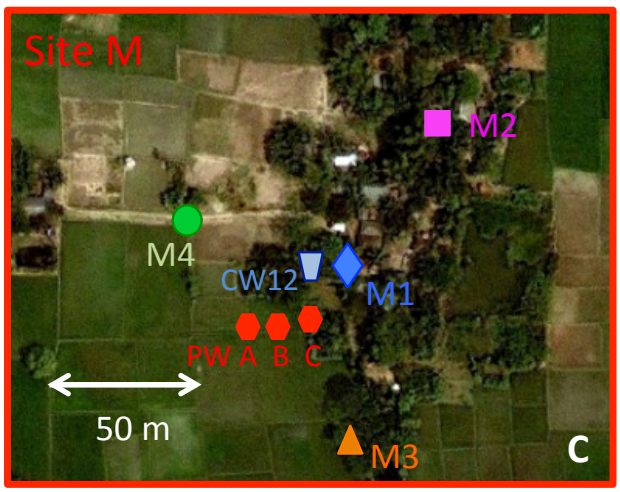

Figure 3.1. Field site within the regional context. Clockwise from bottom left: (a) Location of the field area of Araihazar within Bangladesh. (b) Greater area around the study site marked by a red rectangle. Sites of previous detailed Columbia University studies in the area [TW-5 in Horneman et al. (2004) and Site B in Zheng et al. (2005)], and site T, an auxiliary well nest in the this study, are indicated by yellow dots. Community wells in the vicinity with ^{3}H levels of 2-6 TU (2006), installed in orange sand 35-56 m bgl, are indicated by blue dots. (c) Blow-up of the field site, showing individual multi-level well nests, pumping wells, and the current on-site community well (CW12) installed at 87 m bgl. The two failed community wells were located between well nest 1 and the current CW12.

Four multi-level observation well nests were installed at site M in the winter 2010/11 (Fig. 3.1c), with 1.5 m long well screens strategically placed so as to monitor all major depth zones of the intermediate aquifer. In the shallow aquifer, observation wells either had long screens permeating the entire aquifer (nests 1 and 2), or 1.5 m long screens near the middle of the aquifer (nests 3 and 4). Pumping wells were installed in both the shallow aquifer (PW A) and intermediate aquifer (PW B), with long intake screens permeating the entire aquifer of respective wells. An additional pumping well (C) was screened in the bottom 2/3 of the intermediate aquifer, but was used as a monitoring well for pumping tests. An auxiliary well nest of four observation wells, named "Site T" (23.7731° N and 90.6326° E, Fig. 3.1b), was installed at the site of suspected "recharge window" from the shallow to intermediate aquifer, ~300m S/SE of site M. The elevations of tops of well casings relative to the reference well (shallow well at nest M1, "M1.1")

were determined visually within ±1mm by leveling with a transparent, flexible U-tube filled with boiled deionized water. All well depths reported, thus, are relative to the M1.1 top of casing. Well M1.1 was, in turn, leveled by the same method to top of casing of well BayP7 at site B, for which the absolute elevation above sea level was known (Zheng et al., 2005). Thus, measured hydraulic head elevations could be referenced to the absolute elevation.

3.2.2 Sampling and analyses of solid materials.

Sediment cuttings were collected at 0.6 m (2 ft) or 1.5 m (5 ft) intervals while drilling by the traditional "hand-flapper" or "sludger" method (Horneman et al., 2004) to install the wells. This method biases samples slightly towards the coarser fraction, especially when sand and silt are mixed. Cuttings were described by grain size (clay, silty clay, or sand) and by sediment color (gray or orange) to construct lithologs. On the day of collection, diffuse spectral reflectance between 530 and 520 nm was measured on the cuttings wrapped in Saran wrap to indicate the Fe speciation in the solid phase (Horneman et al., 2004). The cuttings were also analyzed by X-ray fluorescence (XRF) using a portable InnovX Delta instrument for total elemental concentrations of Ca, As, Fe, and Mn contained within the sediment. Samples were run without drying or grinding to powder, and the internal calibration of the instrument was checked before and after each run by NIST reference materials SRM 2709, 2710, and 2711. A subset of ~20 cuttings from representative depths at well nests 1 and 4 were additionally subjected to same-day extractions by a hot 10% (1.2M) HCl leach for 30 minutes to release Fe from amorphous Fe minerals (Horneman et al., 2004). The acid leachates were analyzed

immediately for Fe(II) and total Fe concentrations by ferrozine colorimetry (Stookey, 1970).

While drilling through clay and silt layers, various leaf fragments, pieces of wood, a piece of charcoal, and select samples of clay itself (for bulk organic carbon) were carefully preserved in zip-lock bags for ^{14}C dating and ^{13}C isotopic analysis. $^{14}C/^{12}C$ and $^{13}C/^{12}C$ analyses were performed at National Ocean Science Accelerator Mass-Spectrometer (NOSAMS) facility of Woods Hole Oceanographic Institution following standard protocols (Elder et al., 1997). Radiocarbon data were reported as fraction modern (FM) ^{14}C, with measurement errors listed in Table 1. The values of $^{13}C/^{12}C$ were calculated as deviations in per mil (‰) from the Vienna Pee Dee Belemnite standard ($\delta^{13}C_{VPDB}$), with analytical errors typically <0.1‰. Radiocarbon ages were calculated using 5568 years as half-life of ^{14}C (Stuiver and Polach, 1977) and no reservoir corrections or calibration to calendar years were made. Clay samples on which ^{14}C and ^{13}C analyses of bulk organic C were performed, as well as 17 other representative sand and clay samples from various depths at site M, were refrigerated and analyzed ~2 years later for C content in the sediment. Total C (TC) and inorganic C (IC) in the sediment were measured on the solid analysis unit of the Shimadzu carbon analyzer, and the difference between the two measurements was reported at total organic C (TOC) percentage in the sediment. Quantification limits for TC were 0.06% and 0.03% (% of total sediment) in clay and sand samples, respectively, while the respective limits of IC analyses in clay and sand were 0.02% and 0.01%.

3.2.3 Field measurements

Hydraulic head measurements

Variations in hydraulic heads relative to the top of the well casing were manually measured on a monthly basis using a Solinst Model 101 meter. Monitoring in some wells started in January 2011, but monthly readings were taken in all M wells simultaneously starting in July 2011, and all T wells starting in December 2012. The reported *annual average* water levels (Fig. 8a) include readings from December 2012 to November 2013. Submersed pressure transducers with data loggers (Levelogger, Solinst) were used to record long-term water levels and barometric pressure at 20-min intervals in select wells at M1 nest starting in February 2011 and at site T in November 2012. All water level elevations are reported in meters above sea level (m ASL; see above for elevation leveling).

Chemical measurements in the field

Groundwater was sampled in April 2011 (M nests) and January 2013 (T nest) for pH, oxidation/reduction potential (ORP), temperature and conductivity in a tight flow-through chamber (MP 556 from YSI, Inc). equipped with appropriate probes until the readings were stable. At the same time, at M nests, dissolved oxygen was measured with a CHEMet kit and alkalinity samples were obtained by Gran titration (Gran, 1952a). Dissolved inorganic carbon (DIC) values reported for site M groundwater were then calculated from the concurrently measured pH values and alkalinity. Ammonia was measured in select M nest wells using a NH_3 electrode (AmmoLyt^{Plus} 700 IQ from YSI, Inc.) in May 2012.

3.2.4 Sampling and analyses of groundwater and clay pore water chemistry

Clay pore water collection

Clay pore water samples were collected in May 2012 by squeezing clay cuttings from a borehole drilled near well nest M1. Immediately upon the clay cutting collection and the squeezing of 2-20 mL of pore water, the pore water samples were filtered through 0.45 μm syringe filters (Whatman 6753-2504) and processed for various analyses, described below, in the same way as groundwater samples.

Dissolved organic and inorganic carbon (DOC and DIC) laboratory analyses

Dissolved organic carbon (DOC) samples were collected in May 2012 at M nests, immediately filtered through the 0.45 μm syringe filters into glass vials, and acidified to 1% HCl. Some of the samples were purposefully left unacidified in tightly capped vials filled without a headspace of air, then analyzed for DOC two months later. The DOC that decayed in unacidified samples was calculated by subtracting DOC levels of unacidified samples from those of acidified samples, and expressed as % reactive DOC. DOC (from all M samples) and DIC (clay pore water only, unacidified) were measured in triplicates on a Shimadzu carbon analyzer to a precision of <5% for most samples, and the average was reported. DOC (acidified to 1% HCl final conc.) and DIC (unacidified) samples from well nest T were collected in December 2012 and their concentration analyzed at the NOSAMS facility of Woods Hole Oceanographic Institution to a precision of <2%.

Sampling and analyses of major cations, trace elements, and major anions

Groundwater samples for major and trace elemental analysis by high-resolution inductively coupled plasma-mass spectrometry (HR ICP-MS) were collected on a monthly basis from July 2011 to June or August 2012 from certain wells, for which a time-series average and standard deviation is reported; for other wells, 1-5 samples were collected over a period between April 2011-December 2012, and their time-series average is reported without standard deviations, unless >3 samples were analyzed. All samples were acidified to 1% HCl in the laboratory at least one week prior to the analyses of Na, K, Ca, Mg, P, As, Fe, Mn, Sr, and Ba using HR ICP-MS (Cheng et al., 2004) to a precision of <10% and accuracy of <10% when compared to internal laboratory reference standards. Groundwater samples for anion analysis were collected at the same time as the HR ICP-MS samples, but were not acidified, and only a subset of 1-8 samples per well were analyzed for the period of April 2011-July 2012. Anion samples were analyzed for Cl, SO_4, and F using ion chromatography, with a precision of <5% for Cl and 5-15% for SO_4 and F. The anion results are reported as averages of time-series, with time-series standard deviations reported only where >3 monthly samples were analyzed.

3.2.5 Tracer sampling and analyses (δ^2H and $\delta^{18}O$, ^{14}C and ^{13}C in DIC and DOC, ^3H, and noble gases)

Stable isotopes (δ^2H and $\delta^{18}O$) in water

Samples for stable isotope (^2H and ^{18}O) measurements were collected in 60 mL glass bottles with polyseal-lined caps in April 2011 (site M groundwater), May 2012 (site M clay pore water), and July 2012 (site T). They were analyzed on a Picarro Isotopic

Water Analyzer at Lamont-Doherty Earth Observatory with a precision of ±0.01-0.07‰ ($\delta^{18}O$) and ±0.01-0.24‰ ($\delta^{2}H$) for all samples, except T2 and T3, where analytical errors were somewhat higher (Table 2). The values were reported in per mil (‰) differences from the Vienna Standard Mean Ocean Water values (VSMOW).

Radiocarbon (^{14}C) and ^{13}C of DIC and DOC

Samples for the analysis of ^{14}C and ^{13}C were collected in 125 mL (DIC) or 250 mL (DOC) glass bottles with polyseal-lined caps in April 2011 (Site M DIC) and October 2012 (site T DIC, and sites M/T DOC). They were preserved with mercury chloride (DIC) or acid (1% HCl final concentration, DOC) to arrest potential biological processes after collection. The three clay pore water samples for ^{14}C and ^{13}C in DOC were much smaller (5-10 mL) and collected in May 2011. All radiocarbon and ^{13}C analyses were performed, and the results reported, as described above for sediment samples.

^{3}H and noble gas sampling

The atmospheric testing of nuclear weapons released ^{3}H, a radioactive isotope of H that peaked in the early 1960s, which made it possible to date groundwater recharged since the onset of tests by the $^{3}H/^{3}He$ technique (Poreda et al., 1988; Schlosser et al., 1989; Tolstikhin and Kamenski, 1969). Samples for $^{3}H/^{1}H$ measurements were collected in 125 mL glass bottles with polyseal-lined caps and analyzed at Lamont-Doherty Earth Observatory's Nobel Gas Laboratory using the ^{3}He ingrowth technique (Bayer et al., 1989; Clarke et al., 1976). The analytical precision and detection limit of the ^{3}H measurements were ±0.03-0.06 TU (Table 4) and 0.05-0.10 TU, respectively ($^{3}H/^{1}H$ ratio

of 10^{-18} corresponds to 1 TU). Samples for He and Ne isotopic measurements were collected in ~1 cm outer diameter soft copper tubes that hold ~19 cm^3 of groundwater. Concentrations of He, Ne, and $^3He/^4He$ were measured by mass spectrometry (Ludin et al., 1997) at Lamont-Doherty Earth Observatory's Noble Gas Laboratory, with typical analytical precisions of ±0.05-0.10% for He and Ne concentrations and ±0.6-0.7% for $^3He/^4He$ ratio.

3.2.6 Aquifer testing by slug tests and pumping tests

Slug tests

Hydraulic conductivities around individual well screens were estimated by slug tests. Wells were pressurized by pumping air with a bicycle pump through a custom-fitted, leak-proof well head, and the pressure monitored by a Solinst pressure transducer (barologger). Upon releasing the pressure, the temporal response of the hydraulic head was monitored at 1-sec intervals by another Solinst pressure transducer submerged in the well. The slug test was repeated 4-5 times at each well at a range of 2-3 pressure values. The hydraulic conductivity was determined by fitting the response curves as in Butler and Garnett (2000), with a typical standard deviation of the measurements of 2-4%.

Pumping tests

In order to probe the response of the intermediate aquifer to pumping and its hydraulic connectivity to the shallow aquifer, and to characterize the vertical hydraulic conductivity and/or the lateral extent of the thick clay layer, two pumping tests were performed. The first one involved pumping the entire vertical extent of the intermediate

aquifer from the fully penetrating pumping well B for the duration of ~48 hours, whereas the second test was performed by pumping from the fully penetrating pumping well A in the shallow aquifer for ~24 hours. A locally purchased irrigation pump (1.75 horsepower, 1 atm maximum lift) was powered by a generator to maintain a constant flow rate of ~200 L/min (58 m^3/d), measured by a flow meter (McMaster-Carr) connected in-line to a PVC tube carrying the pump outflow. The pump could not be used to control the flow rate directly as it had only one setting and its output was dependent on the water level elevation around the well, thus a manual shut-off valve was installed between the pump and the flow meter to initially constrict the outflow tube slightly. As the pumping-induced cone of depression spread out through the aquifer, the valve was slowly opened up to release the backpressure and maintain a nearly constant flow rate. The groundwater was channeled for disposal through a hose to a large shallow pond ~200 m SW of the site.

No precipitation events occurred during the tests, but irrigation was ongoing from at least two wells screened in the shallow aquifer within the 200 m radius around the site, with pumps turning on and off several times a day. Hydraulic heads in observation wells and pumping well C (closest intermediate aquifer well to PW B) were simultaneously monitored by pressure loggers at 2-second intervals for the first 70 min of the tests, and at 1-minute intervals for the remainder of the pumping tests and for a 24-hr recovery period post-pumping. A barometric pressure logger recorded atmospheric pressure changes on site at the same time intervals. Several pressure loggers were deployed for weeks prior to and after the pumping tests to monitor the seasonal declining hydraulic head trend and atmospheric pressure changes at 20-min intervals.

3.3 Results

3.3.1 Stratigraphic description

Stratigraphy at site M established that both the silty clay layer separating the shallow and intermediate aquifers and the layering of the geochemically stratified intermediate aquifer were laterally continuous on village-site scale of ~100×100 m, albeit with variations in depth of each layer. The five lithologs collected at site M (Fig. 3.2) demonstrated a repeated vertical sequence of clay or silt layers and sediment color, as indicated by the difference in reflectance at 530 and 520 nm (ΔR). The shallow aquifer was entirely composed of grey sands (low ΔR) extending to the depth of 25-31 m below ground level (bgl), where a few interlaced sandy and silty layers were encountered. Below the shallow aquifer, a 10-15 m thick clay layer, entirely grey in color, marked a clear boundary between the shallow and intermediate aquifers. The upper ⅓ to ½ of the thick clay layer was lighter in color and contained more silt than the darker, sticky lower section of the clay. The actual depth range of this clay layer, though present at all site M lithologs, varied significantly in such a small area; for instance, the elevation-corrected bottom depth varied between 38-45 m bgl. Underneath it, the intermediate aquifer extended to 68-77 m bgl with a top-down sequence of grey, orange, and grey sands. The upper stretch of grey sand contained a few thin clay lenses at sporadic depths and was thicker (10-15 m) than the deeper grey sand (5-10 m). The orange sand that previously hosted the failed community wells was present everywhere at ~60 m bgl, 7-12 m thick, and its exact upper and lower limits also varied. Beneath the intermediate aquifer, a continuous sticky, plastic layer of clay, found at depths varying by almost 10 m, proved

to be the lower limit of the hand-drilling method. The lithology at site T, ~300 m S/SE of site M, was strikingly different due to the absence of the thick clay confining unit at ~30-40 m bgl, thus permitting a lateral contact between the shallow aquifer at T and intermediate aquifer at M. A thinner clay unit was found at site T at 55-58 m bgl, below which the intermediate aquifer sequence was limited to only ~10 m of thickness, though it displayed a similar grey-orange-grey sand sequence.

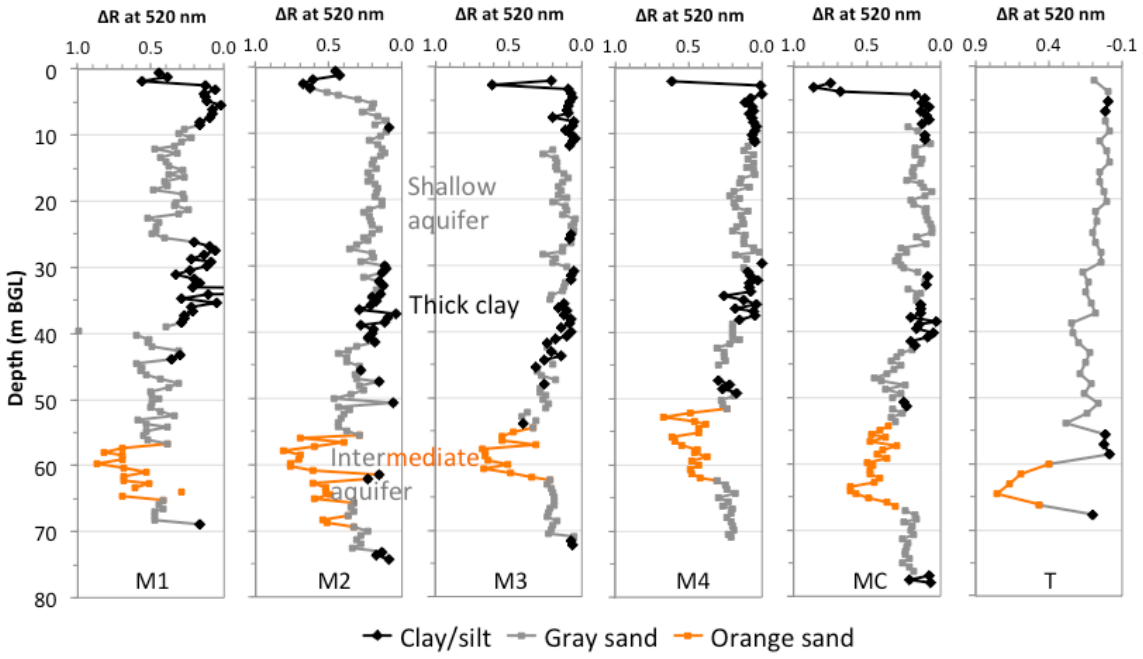

Figure 3.2. Lithologs collected at sites M and T. Cuttings recovered while drilling were used for same-day measurements of the difference in diffuse spectral reflectance (ΔR) between 530 and 520 nm, correlated with sediment color and Fe speciation. Drill cuttings that contained orange or grey sand are represented by their respective colors; all clay/silt layers were gray.

3.3.2 Sediment composition, redox status, and organic content

Elemental compositions by XRF

Having established that a layer of more oxidized, orange sand was sandwiched between two grey layers in the intermediate aquifer at site M, we investigated whether the elemental compositions of intermediate aquifer layers was uniform and different from that of the shallow aquifer. Multi-element X-ray fluorescence data (Ca, Fig. 3.3a; Mn, Fe, and K, Fig. 3.14aeg in Appendix) demonstrated a difference in total elemental composition of the sediment contained in the shallow aquifer, where total concentrations of all four elements were higher, and the intermediate aquifer where they were lower and consistent in all three layers. The total As content (0-4 mg/kg, Fig. 3.14c) was not significantly different between the two aquifers, whereas the strongest contrast found was in Ca content. The surface clay and the shallow aquifer contained ~5-10,000 mg/kg Ca, however the intermediate aquifer sedimentary Ca stayed within the 2-5,000 mg/kg range. Constant elemental composition of the intermediate aquifer suggested that it was deposited as one stratigraphic unit, as the sediment likely came from the same source, their coloring only reflecting post-depositional environmental differences (e.g. flow regime, subaerial exposure, organics supply). At site T, the total elemental concentrations followed a similar vertical distribution as at site M, except that the thick clay layer was missing and replaced by sand of a composition similar to that of the shallow aquifer (Figs. 3.3b and 3.14bdfh) and elemental compositions transitioned rather smoothly towards the intermediate aquifer at >50 m depth.

Redox status examined by acid leachates and total organic and inorganic carbon (OC and IC) content

Whereas the three distinctly colored layers of the intermediate aquifer sands were compositionally equivalent, the upper gray layer was more reduced than the orange and gray layers underneath. Acid leaches with hot 10% HCl were used to release Fe from labile and poorly crystalline Fe oxyhydroxides (FeOOH) and assess its redox status: more Fe(II) is present in grey sand, and conversely more Fe(III) in orange (Horneman et al., 2004). The percentage of Fe(II) within the acid-leachable Fe was 40-80% (mostly >50% Fe(II)/Fe) in the shallow aquifer and clay units, whereas the orange and deeper gray layer of the intermediate aquifer hosted ≤45% Fe(II)/Fe (Fig. 3.3d). Orange sand had 20-35% Fe(II)/Fe, while most values in deeper gray layer were in the range of 35-45% Fe(II)/Fe; thus, the visible color transition from orange to grey sand occurred here slightly below the usual 50% Fe(II)/Fe threshold (Horneman et al., 2004; van Geen et al., 2004). In contrast to the intermediate aquifer layers beneath it, the upper gray layer was more reduced, with 50-70% leachable Fe(II)/Fe in the top 5-10 m, directly beneath the thick clay, making the redox status there comparable to that of the shallow aquifer. This finding was surprising in light of the usual isolation that a clay layer would provide from reduction occurring in the shallow aquifers. To check for potential differences in particulate organic C content between the shallow aquifer and the three layers of the intermediate aquifer, the total organic C in sands was uniformly low everywhere (mostly <0.05 wt%, near the quantification limit, Fig. 3.3e). No inorganic C was quantifiable in the sands (<0.02 wt% in all samples).

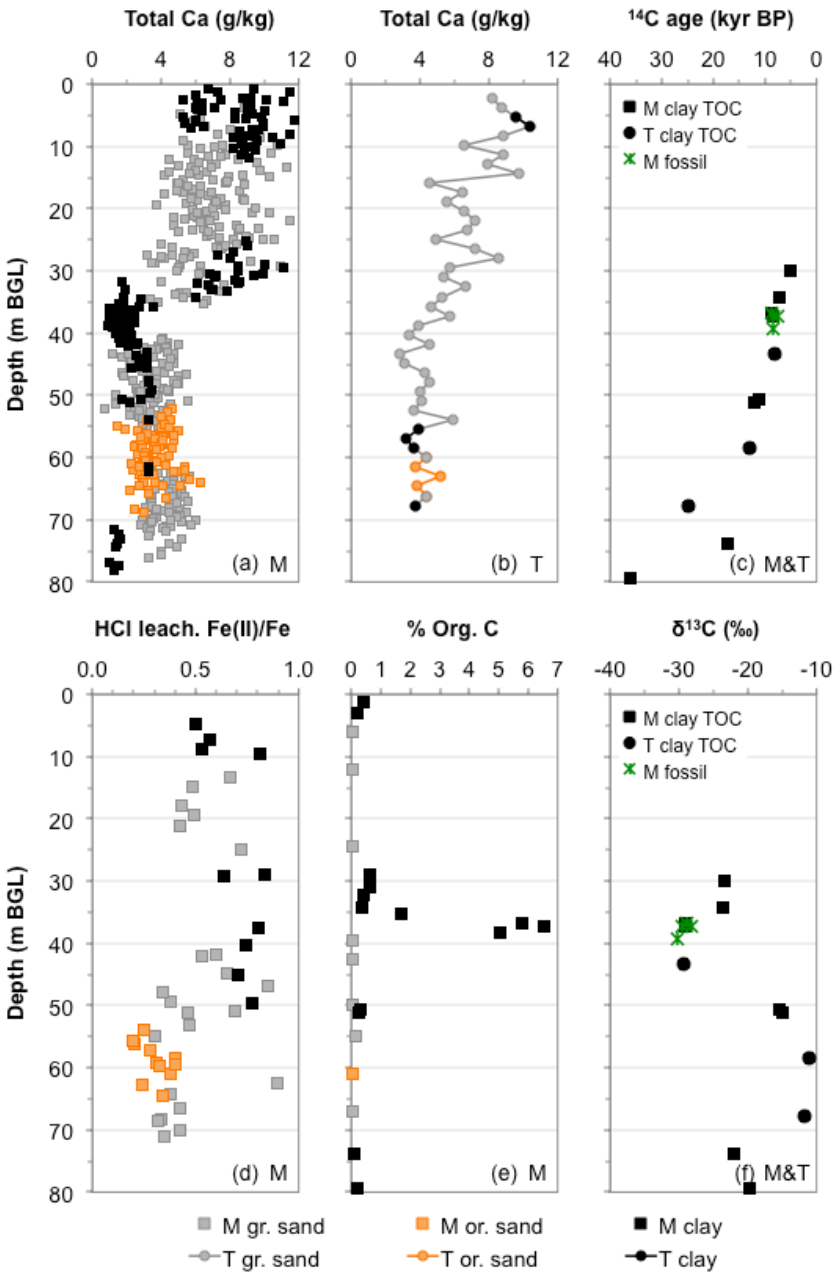

Figure 3.3. Sediment composition, Fe redox status, ^{14}C ages, and ^{13}C signature. Bulk sediment Ca concentrations measured by a portable XRF instrument at site M (a) and site T (b). Standard deviations of the XRF measurements are smaller than the symbol size. (c) ^{14}C ages of plant fossils at site M and in bulk organic matter (OM) of the clays from sites M and T. (d) The proportion of Fe(II) within the total Fe released by leachates with hot 1.2M HCl. (e) The content of bulk organic carbon as weight % of the sediment. (f) ^{13}C

signature of bulk OM in site M and T clays, and in site M plant remains. Color of the sand cuttings as in Figure 3.2.

The examination of total elemental contents of clay layers at site M indicated some differences between the upper (silty and light gray) and the lower (sticky and dark gray) sections of the thick clay layer at site M. The transition from high to low Ca content occurred within the upper half of the aquitard (Fig. 3.3a). Sediment compositions of other elements (Fe, As, Mn, and K, Fig. 3.14aceg) revealed their enrichment in all clay layers and lenses; nevertheless, they also exhibited the high-to-low transition within the thick clay layer, and remained lower and nearly constant in all deeper lenses in the intermediate aquifer. The stickier, darker clay in the lower portion of the thick clay layer was rich in organic C (1.7-6.5 wt%, Fig. 3.3e), compared to the more modest content of its upper portion (0.4-0.6 wt%) and the other dispersed clay lenses (0.1-0.4 wt%). Only one clay sample had a quantifiable amount of inorganic C (0.02 wt% in the sample with maximum OC), while all other samples were below the quantification limit of 0.01 wt% IC. The thin clays at site T did not differ much from sand in terms of composition.

3.3.3 Radiocarbon dating and ^{13}C signatures of the sediment

Another way to determine the stratigraphic relationship between different aquifers and to constrain their depositional history to Holocene or Pleistocene is to consider the sediment ages recorded by ^{14}C. Radiocarbon ages of the bulk organic C recovered from the clay layers at site M were progressively older with depth from 5.2-8.6 ka before present (BP) in the thick clay layer to 11-12 ka BP in the upper intermediate aquifer clay lenses and 17-36 ka BP in the clay beneath the intermediate aquifer (Table 3.1 and Fig.

3.3c). A rather linear rate of sedimentation is implied between 17 and 5.2 ka BP, and a similar distribution of ^{14}C ages was found in the three clay lenses at equivalent depths at site T (Fig. 3.3c also). The signature of ^{13}C in sediment organics (Fig. 3.3f) indicated a progressive shift towards heavier, more positive, values (from -22 to -15‰) going from deeper/older to shallower/younger clays found within the intermediate aquifer depth range. Above that, ^{13}C signature rapidly shifted to -28 to -30‰ at the bottom of site M thick clay layer ~40 m bgl, pointing to a significant shift in the depositional environment. Both the leaf and wood fragments, and the total (bulk) OC from this portion of the thick clay layer at site M (~37-40 m bgl) had a consistent ^{14}C age (~8.5 ka BP) and ^{13}C signature throughout the site, adding confidence to the measurements. The intermediate aquifer deposition was, therefore, constrained to Late Pleistocene (8.5-36 ka BP).

3.3.4 Groundwater and clay pore water chemistry

Trace metals and reduction products

The vertical profiles of groundwater composition at site M (Fig. 3.4; Fig. 3.15 and Table 3.2 in Appendix) revealed differences in redox chemistry between the shallow and the intermediate aquifer groundwater, as well as a steep geochemical gradient within the intermediate aquifer. Arsenic, iron, phosphorus and ammonia were elevated in the shallow aquifer (up to >300 µg/L As, 8 mg/L Fe, 1.8 mg/L P, and 1.5 mg/L NH_3), while the middle (orange) and lower (grey) reaches of the intermediate aquifer contained groundwater with rather low As (<10 µg/L), Fe, P, and NH_3, except a high-Fe sample from M4.6a, located at the lower limit of the aquifer and near the Pleistocene clay. Groundwater in the upper gray layer, however, consistently contained high levels of As,

Fe, P, and NH_3: As ranged between 15-270 µg/L, Fe and P were present at levels comparable to those of the shallow groundwater, whilst NH_3 rose up to 5 to 10-fold higher than in the shallow aquifer (up to ~10 mg/L). Dissolved Fe, As, and P were similarly elevated in the pore water of the thick clay overlying the intermediate aquifer. Another redox sensitive element, manganese, was also abundant in the shallow aquifer (600-1,300 µg/L), but followed a distinct mirror-image pattern (with respect to As, Fe, P, and NH_3) within the thick clay and the intermediate aquifer. Low Mn concentrations in thick clay pore water and in the upper, reduced part of intermediate aquifer (<100 µg/L) rose to 200-1000 µg/L deeper in the intermediate aquifer, with a peak in the orange sands. Pore water of the thin clay layers dispersed within the intermediate aquifer had low levels of Fe, As, P, and Mn, excluding them as direct sources of these constituents. At site T, shallow aquifer samples (T1-T3; Table 3.2 in Appendix) also had elevated dissolved As, Fe, and P, but As concentrations were notably lower at all depths (75 µg/L at 10 m bgl and decreasing with depth). In the thin intermediate aquifer orange sand layer, on the other hand, As and Fe were not quite as low as in the orange sand at site M.

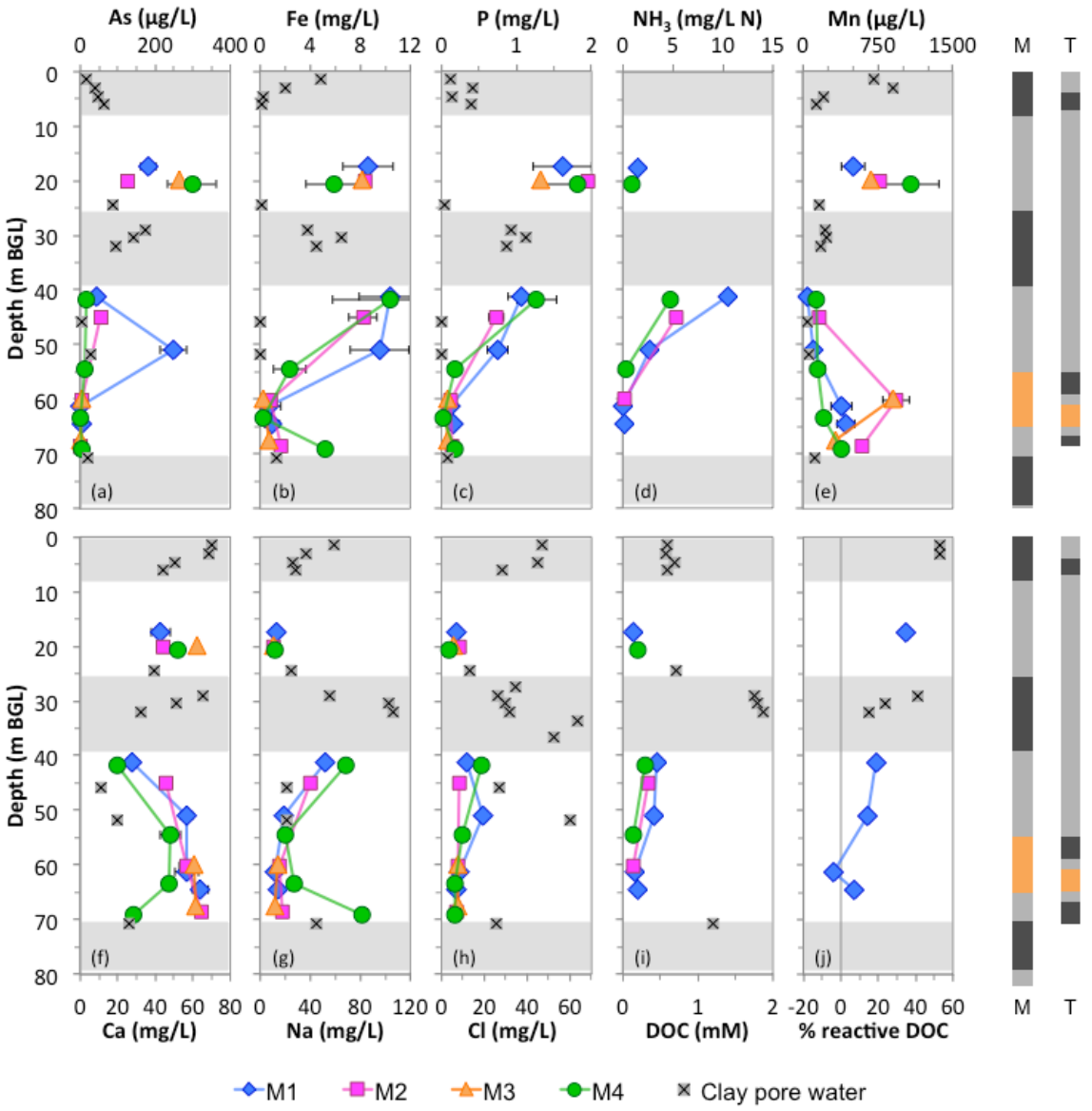

Figure 3.4. Vertical profiles of groundwater chemistry at well nests M1-4 and clay pore water squeezed from sediment cuttings recovered near well nest M1. Profiles of aqueous (a) As, (b) Fe, (c) P, (d) NH_3, (e) Mn, (f) Ca, (g) Na, and (h) Cl, (i) dissolved organic carbon (DOC), and (j) % reactive DOC in groundwater and clay pore water, where available. Averages and standard deviations of 5-12 samples (As, Fe, P, Mn, Ca, Na), or 4-8 samples (Cl), are shown where available. Otherwise, an average of 1-3 samples is shown without error bars. Note that Na and Cl error bars are smaller than the

symbol size. Profiles of NH_3, DOC, and % reactive DOC, as well as the clay pore water data in all profiles, show one-time measurements. A generic site litholog is displayed to the right of the profiles and shading indicates the extent of major clay/silt layers encountered at the site.

Dissolved carbon species

Dissolved organic carbon (DOC), the prime suspect for causing anoxia and reduction of aquifer sediment, was present at plentiful amounts within clay pore waters: 0.6-0.7 mM in surface clays and ~2 mM in the thick clay capping the intermediate aquifer at site M (Fig. 3.4i and Table 3.2 in Appendix). Groundwater from both aquifers, on the other hand, contained 0.1-0.2 mM DOC, except, notably, in the upper grey layer of the intermediate aquifer where higher DOC of 0.3-0.45 mM was found, perhaps advected from the overlying clay. To test for the reactivity of DOC, often recalcitrant if sourced from the organic matter co-deposited with sediment (Rowland et al., 2006), some DOC samples were not acidified upon collection and DOC was let to be freely consumed by microbes within the sample vials (Fig. 3.4j). DOC from the shallow aquifer groundwater and the thick clay layer pore water at site M was only slightly less reactive than the freshest DOC found in surface clays (15-40% vs. >50% reacted away, respectively). In the intermediate aquifer, 14-19% of DOC retained reactivity in samples from the upper, reduced zone below the clay, whereas only <7% of groundwater DOC found in the orange sand layer was consumed. Dissolved inorganic C (DIC) concentrations were more uniform, ranging from 4.5-6 mM in the shallow aquifer to 5-8 mM in the silty clay layer and intermediate aquifer, with somewhat higher values (7-10 mM) in the upper, more

reduced zone of the intermediate aquifer (Fig. 3.15def in Appendix). Alkalinity (4-7 mEq/L) showed little vertical variation in the intermediate aquifer, but pH in the upper grey layer was at a minimum of 6.7-6.8 units, compared to 6.8-7.1 deeper in the aquifer.

Major cations and anions

Signatures of the major cations and anions confirmed the stratification of the intermediate aquifer that was observed in the profiles of trace elements and DOC/DIC. They also supplied more evidence of the similarity between the thick clay pore water and upper intermediate aquifer groundwater at site M. Na and Cl profiles (Fig. 3.4gh and Table 3.2 in Appendix) described a similar pattern of low concentrations in the shallow aquifer and deeper intermediate aquifers (10-20 mg/L Na and 3-7 mg/L Cl), but their levels were much higher in the upper intermediate aquifer with up to 70 mg/L Na and 20 mg/L Cl. A high Na concentration was also observed in the grey sand located at the bottom of the intermediate aquifer at well nest 4 (M4.6a). Pore water from the thick Holocene clay layer at site M exhibited an abrupt down-profile transition from the low Na and Cl values at the upper boundary, similar to those in the shallow aquifer, to much higher levels in the middle of the clay layer, peaking at 2 to 4-fold higher concentrations than those immediately below the clay. At site T, Cl concentration was remarkably high (24-28 mg/L) in the shallow aquifer at depths <21 m bgl, but fell to 9.5 mg/L in the grey sand at 53 m bgl, above the thin clay layer. Below that, the sample from the thin orange sand layer at site T contained more Cl (16 mg/L) than the equivalent samples from site M.

Among the other major ions, K profiles at site M were similar to those of Na, albeit at lower absolute concentrations, while the profiles of Ca and Mg resembled each other and were roughly a mirror image of the Na and Cl profiles, including well M4.6a (Fig. 3.4f and Fig. 3.15ab in Appendix). In the upper intermediate aquifer, the minimum Ca and Mg levels were co-located with the high As, Fe, DOC and DIC, and low pH, thus making the dissolution of carbonates as a source of DIC or As in that zone unlikely. Sulfate (Fig. 3.15c) was mostly below the detection limit in the shallow aquifer and the upper grey layer of the intermediate, but detectable SO_4 levels were found (albeit <1 mg/L) in the orange and deeper grey layers of the intermediate aquifer. Clay pore waters contained much more SO_4, ranging between 3-7 mg/L in the thick clay unit between the two aquifers, thus if any SO_4 leaks into the upper intermediate aquifer, it must immediately be consumed by reduction, and can precipitate as pyrite at the clay/sand interface (McMahon and Chapelle, 1991a; McMahon et al., 1992; Szabo et al., 2006).

3.3.5 ^{14}C ages and ^{13}C profiles of dissolved organic and inorganic carbon (DOC and DIC)

The amounts of radiocarbon in DOC and DIC of the shallow aquifer at sites M and T (<21 m) were remarkably similar to those in the orange and deeper grey sands of the site M intermediate aquifer, where less reduction was observed (Fig. 3.5a and Table 3.3 in Appendix). The values ranged from 0.82-0.85 FM (1.4-1.7 ^{14}C kyr) in DOC and 0.88-1.0 FM (0-1 ^{14}C kyr) in DIC, with DIC always slightly younger than the DOC, except in well M4.6 (orange/grey sand boundary) where a DOC sample with modern radiocarbon (0.98 FM) was found. In contrast, DOC and DIC in the upper intermediate

aquifer at site M, directly underneath the thick clay layer, showed evidence of a significantly higher age (0.54-0.67 FM or 3.2-5 ^{14}C kyr), with DOC again slightly older than DIC. These ages were, nonetheless, not as high as those of OC in the overlying clay sediment (~8.5 ^{14}C kyr). In the upper portion of the thick clay at site M, DOC in the pore water was also younger (0.66-0.81 FM or 1.7-3.3 ^{14}C kyr) compared to the clay bulk OC at that horizon (3-5 ^{14}C kyr). At site T, the two deeper wells straddling the thin clay layer had DIC ^{14}C similar to that in the deeper wells at site M intermediate aquifer, but their DOC was older (0.66-0.74 FM, 2.4-3.3 ^{14}C kyr). Groundwater samples collected close to the clay layers, therefore, contained older DOC, and in the case of the reduced, upper intermediate aquifer at site M, older DIC as well.

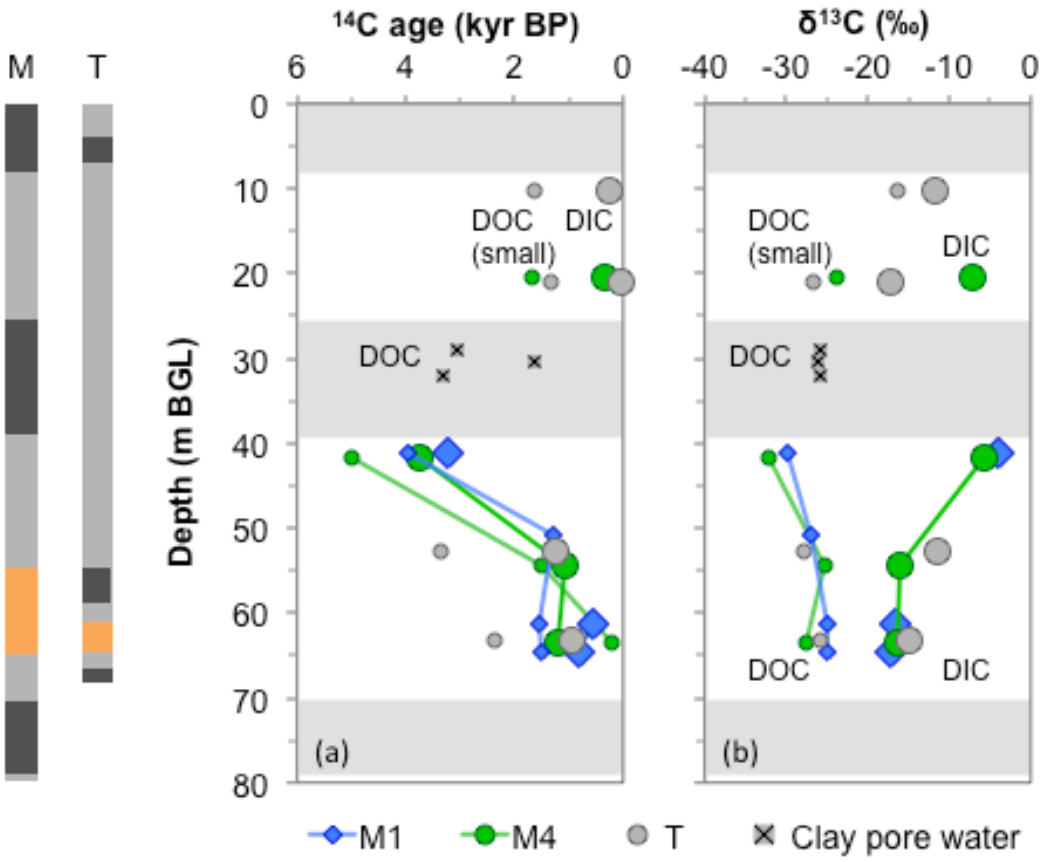

Figure 3.5. Vertical profiles of (a) radiocarbon (^{14}C) ages and (b) stable C isotopic composition ($\delta^{13}C$) in dissolved inorganic carbon (DIC) and dissolved organic carbon (DOC) from sites M and T. As in Figure 3.4, the major clay/silt layers at site M (and not at T) are indicated by the gray shading.

The C stable isotope (^{13}C) content in most DOC samples was in the range of -25 to -30‰, similar to the ^{13}C signature of the thick Holocene clay at site M (Fig. 3.5b and Table 3.3 in Appendix). An exception was the shallowest sample at T (10 m bgl) where DOC $\delta^{13}C$ was heavier (-16‰). Within the intermediate aquifer at site M, samples from the upper grey sand (beneath the clay) had a slightly more depleted (-30 to -32‰) DOC $\delta^{13}C$ signature, similar to that found in the clay organics directly above. At -15 to -17‰, DIC $\delta^{13}C$ was generally ~10-15‰ enriched (heavier) compared to the DOC ^{13}C, but the offset was much larger in the shallow and the upper intermediate aquifer of site M, where ^{13}C was ~25‰ heavier in DIC (-4 to -7‰ $\delta^{13}C$) than in DOC. The heavy carbon isotopic signature in DIC thus coincided with the zones of the strongly reduced sediment and groundwater.

3.3.6 Hydraulic head patterns and groundwater flow

The upper layer of the intermediate aquifer contained heavily reduced sediment and groundwater, older DOC and DIC, and appeared chemically similar to the overlying Holocene clay layer. At the same time, deeper layers of the aquifer bore evidence of contact with the surface (fairly young DIC and a modern DOC sample), but retained more oxic conditions, particularly in the orange sand layer. A good understanding of the

groundwater flow patterns at the site shed more light on the way the intermediate aquifer is impacted by contacts with the shallow groundwater and the clays.

Hydraulic connections and contrasts between the shallow and intermediate aquifers

Water level elevations of the two aquifers at site M (Figs. 3.6-3.8), as expected from the trend at the nearby site B (3.13 in Appendix), also followed a downward hydraulic gradient between the shallow and the intermediate aquifer. The annual average of water level readings (Dec 2012-Nov 2013, Fig. 3.8a) revealed that hydraulic heads in the shallow aquifer were more or less identical at different well nests and, on average, ~1m higher than in the intermediate aquifer. Three years of monitoring at site M (Figs. 3.6 and 3.7) also showed the tendency of the downward hydraulic gradient across the thick clay to increase. Thus, the thick clay layer separating the two aquifers has a low enough permeability to maintain the downward gradient, while at the same time the widening downward hydraulic gradient between the aquifers sets the stage for potentially increased leakage through the clay layer. At site T, where the shallow aquifer extends down to 54 m bgl, the hydraulic head only decreased slightly from the top (T1 at 10 m bgl) to the bottom (T3 at 53 m bgl) of the aquifer (Figs. 3.6 and 3.8a), thus laterally juxtaposing a higher, shallow aquifer hydraulic head (T3) to the lower heads measured in the intermediate aquifer at site M. The thin clay at site T also caused a relatively smaller drop in hydraulic head (~0.65 m) between well T3 and well T4 installed in the orange sand, allowing for a higher head at T4 compared to the intermediate aquifer at M also.

Groundwater gradients from both the shallow aquifer and the thin sliver of intermediate aquifer at site T, therefore, point towards site M.

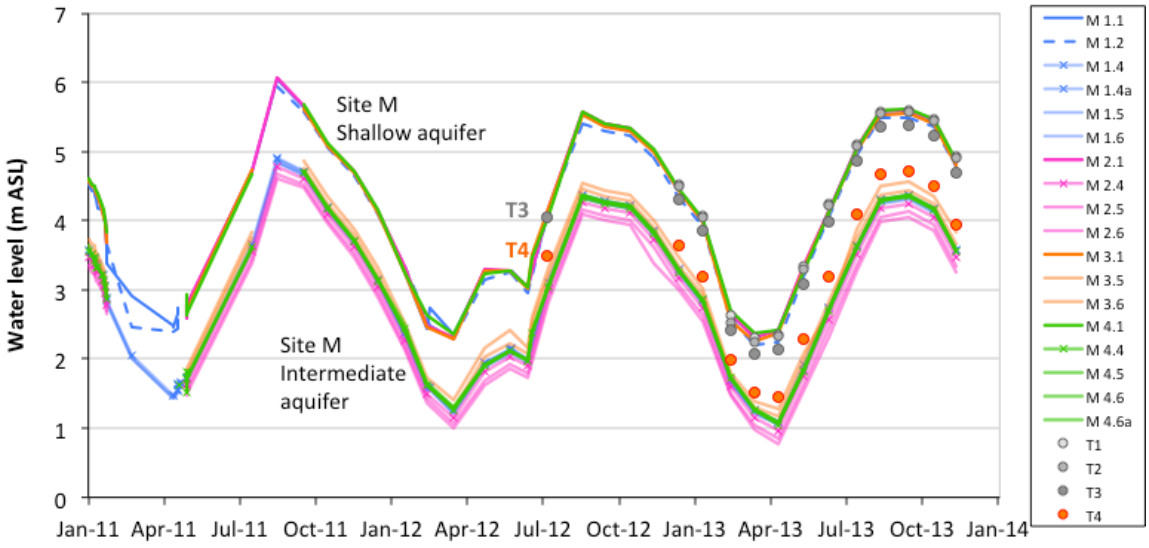

Figure 3.6. A 3-year time series of elevation-corrected manual water levels from sites M and the more recently installed site T. Each line color corresponds to a different well nest at site M. The cluster of lines at higher hydraulic heads corresponds to the shallow aquifer. Within the cluster of ~1 m lower hydraulic heads in the intermediate aquifer, heads are persistently the highest on southern end of the site (M3, orange lines), and the lowest on the northern end (M2, pink lines). Blue (M1) and green (M4) lines largely overlap in the middle. Site T hydraulic head elevations are shown as grey circles (T1-T3 in the shallow, grey aquifer) and orange circles (T4 from the thin orange layer), and are constantly higher than the heads at M.

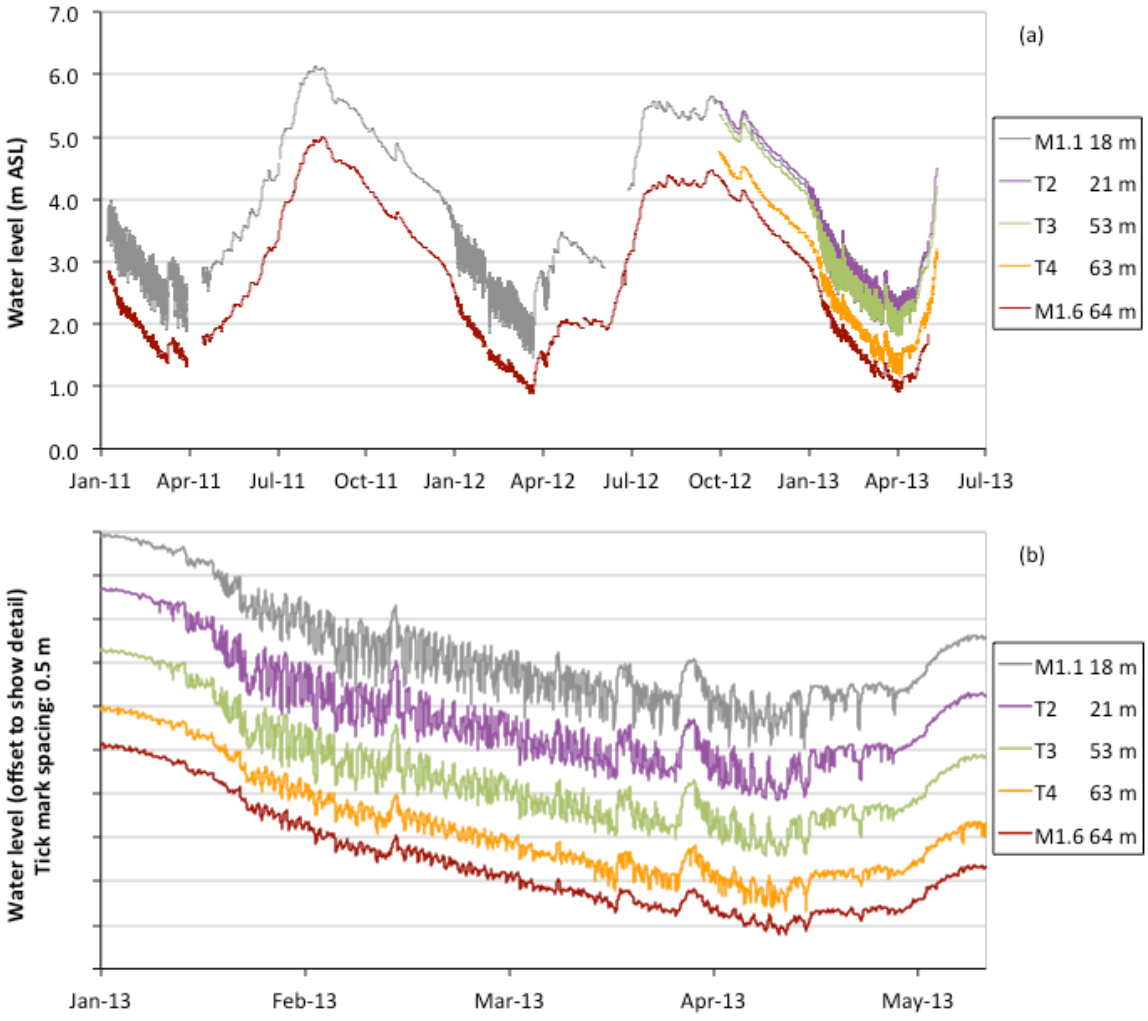

Figure 3.7. Time series of hydraulic head elevations recorded by pressure loggers at sites M and T. (a) The entire time series of elevation-corrected hydraulic heads showing similar weekly-to-seasonal patterns in M1.1 (M1 shallow well, 18 m bgl), M1.6 (M1 intermediate aquifer, 64 m bgl), T2 (shallow aquifer, 21 m bgl), T3 (shallow aquifer, 53 m bgl) and T4 (intermediate aquifer, 63 m bgl). (b) Enlarged irrigation season hydrographs, offset to clearly show daily variations in water levels. Note the progressively smaller influence of shallow pumping on the hydrographs from M1.1/T2 to M1.6.

A closer look at temporal variations in piezometers from the shallow (M1.1, T2, and T3) and intermediate (M1.6 and T4) aquifers, recorded by pressure loggers (Fig. 3.7a), revealed that the two aquifers follow identical patterns of recharge and discharge, ranging in time scale from weekly humps and dips to several months, as in seasonal recharge by monsoon (roughly May-Sep) or the rapid drop in hydraulic heads over the irrigation season (roughly Jan-Apr). During the irrigation season, shallow aquifer heads were observed to fluctuate by up to ~80 cm on a daily basis, due to the irrigation pumps turning on and off, resulting in very noisy hydrographs of M1.1, T2 and T3 (Fig. 3.7b). The intermediate aquifer also responded to the irrigation localized in the shallow aquifer between January and April, as the hydrographs were also noisier in those periods, but the daily amplitude of water level variations was much subdued at ~20 cm in well T4 below the thin clay and only ~10 cm at M1.1 tucked below the thick clay and away from its discontinuity at T. The above observations together indicate that the intermediate and shallow aquifers are connected, but clays do provide a degree of hydraulic separation by isolating deeper layers from the local irrigation pumping effects coming from the shallow aquifer.

Hydraulic gradients within the intermediate aquifer

Within the intermediate aquifer at site M, there was a greater diversity of water levels than in the shallow (Figs. 3.6 and 3.8a), but hydraulic heads generally decreased slightly with depth at each well nest, thus maintaining a gentle downward vertical hydraulic gradient. The downward vertical hydraulic gradient actually continued below the intermediate aquifer, with another ~1 m drop in hydraulic head across the Pleistocene

clay layer underlying the aquifer, measured twice in the current installation of CW12 at 87 m bgl (data not shown). Horizontally, hydraulic heads in orange and deeper grey layer of the intermediate aquifer followed a northward gradient from well nest 3 at the southern end of the site to well nest 2, ~110 m to the north, where head elevation was on average ~0.35 m lower, resulting in a horizontal hydraulic gradient of ~0.0035 across the site (also see Fig. 3.16 in Appendix). A northward horizontal gradient of similar magnitude in fact extended from site T, and was fairly constant throughout the seasons, as seen when hydraulic heads from the orange layer at site M were plotted along with those from well T3 that taps the bottom of the Holocene aquifer at site T (Fig. 3.16). If the horizontal hydraulic gradient also had an East-West component, it was not inferred due to the mostly South-North arrangement of the observation wells. Along the upper grey layer of the intermediate aquifer, the horizontal hydraulic gradient was less pronounced as head values in that layer were more uniform [Fig. 3.6 (markers with a cross) and Fig. 3.8a]. Individual monthly hydraulic head readings, taken simultaneously over a 3-year period (Fig. 3.6), showed the persistence of hydraulic head trends, similar to those of the yearly average, throughout the seasons at site M.

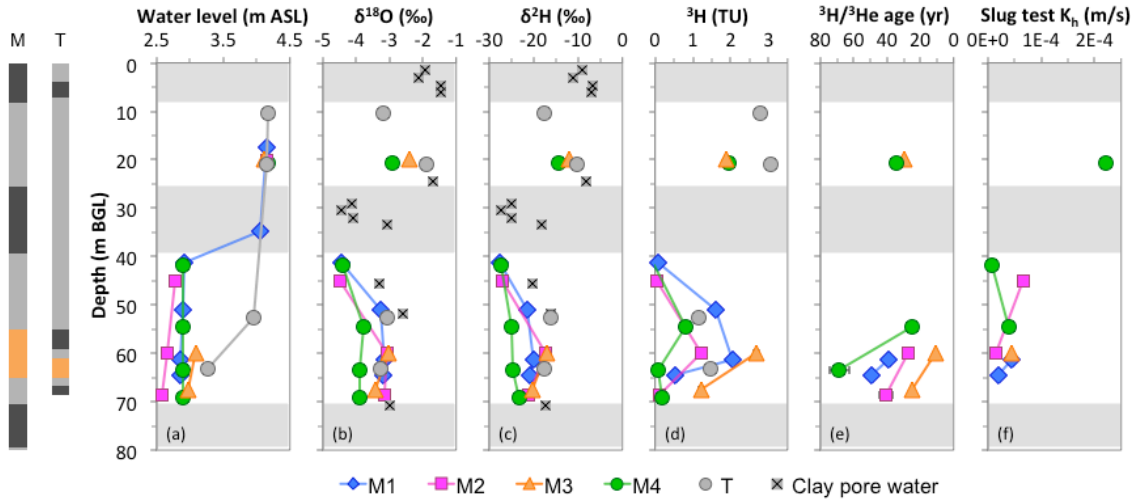

Figure 3.8. Vertical profiles of hydrology-related parameters at site M and site T (where available). (a) Annual average (December 2012-November 2013) of hydraulic heads at site M and T; (b) and (c) water stable isotopes, $\delta^{18}O$ and $\delta^{2}H$, in groundwater at sites M and T, and in site M clay pore water; (d) groundwater ^{3}H at sites M and T; (e) $^{3}H/^{3}He$ ages, corrected where necessary for radiogenic He contribution and degassing at the time of sampling; (f) estimates of horizontal hydraulic conductivity from slug tests at select wells. The lithologs and gray shading as in Figure 3.4.

3.3.7 Stable isotopic signatures of groundwater (^{2}H and ^{18}O)

Groundwater from the shallow aquifer and clay pore water from the surface and shallow aquifer clays displayed the most enriched/positive stable isotopic signature (Fig. 3.8bc; Fig. 3.17 and Table 3.3 in Appendix). The thick clay layer at site M, as well as the upper grey layer of the intermediate aquifer had, on the other hand, the most depleted stable isotopic values, albeit with some scatter. The rest of the intermediate aquifer samples at site M (from the orange and the deeper gray layers) formed a spread of $\delta^{2}H$ and $\delta^{18}O$ values in between those noted for the shallow aquifer and the upper

intermediate aquifer/thick clay (Fig. 3.17). Within this range, groundwater from well nest 3 at the southern end of site M had the most positive δ^2H and $\delta^{18}O$, whereas the most negative values were observed at well nest 4, west of the South-North transect (Fig. 3.8bc). The two deeper samples from site T (from above and below the thin clay layer at this site) plotted within the more positive end of the range of δ^2H and $\delta^{18}O$ for site M intermediate aquifer. All of the samples bore a signature of evaporation to a various extent before the groundwater was recharged because they plotted to the right of the values expected for rainwater, represented by the global meteoric water line (GMWL, Fig. 3.17 in Appendix) described by $\delta^2H = 8^* \delta^{18}O + 10‰$ (Craig, 1961).

3.3.8 ^3H tracer and $^3H/^3He$ dating of groundwater

Quite a similar vertical and horizontal distribution to that of the water stable isotopes was observed at site M for another tracer of groundwater flow, tritium (^3H; Fig. 3.8d and Table 3.4 in Appendix). Elevated levels of ^3H, a telltale sign of recharge with young groundwater, were found in the intermediate aquifer at site M, at depths of >50 m bgl, and that despite the presence of a 10-15 m thick clay layer at the site. The amount of ^3H decreased along the S-N transect at site M, while well nest 4, west of the transect, appeared isolated from the supply of the radioactive H isotope. Tritium values at each M well nest were the highest in the orange sand layer, and decreased in the grey layers at top and bottom of the aquifer, but the upper intermediate aquifer immediately beneath the thick clay layer was markedly devoid of detectable ^3H. The highest overall levels of ^3H were found in the upper part of the shallow aquifer at site T, whereas more modest amounts were observed in the two site T wells straddling the thin clay layer at depth.

The concentrations of ^{3}H and its radioactive daughter ^{3}He were used to estimate the age of the intruding young groundwater by calculating the time elapsed since recharge ($^{3}H/^{3}He$ age, Figs. 3.8e and 3.9, and Tables 3.4 and 3.5 in Appendix). In order to calculate the amount of ^{3}He contributed by the radioactive decay of ^{3}H ("tritiogenic ^{3}He" or "$^{3}He_{trit}$"), the concentrations of noble gases He (as ^{4}He) and Ne were plotted against each other to account for different pools of He (Fig. 3.18 in Appendix). The recharge temperature for all samples was assumed to be 26 °C, close to the current average shallow groundwater temperatures at the site (Table 3.2). The concentrations of He and Ne exceeded the contributions of the solubility equilibrium with the atmosphere due to excess air formation (trapped bubbles) by a large amount only in sample M3.1, and slightly in samples M4.1 and M2.5. Samples M4.1 and M2.5 also had excess He compared to the excess air curve at 26 °C, which was attributed to the production of radiogenic He. All other samples were degassed compared to the solubility equilibrium to various degrees: 3 samples had a slight deficit of Ne (<10%), while the remaining 4 samples lost up to 30% of the He and 40% of the Ne expected at equilibrium.

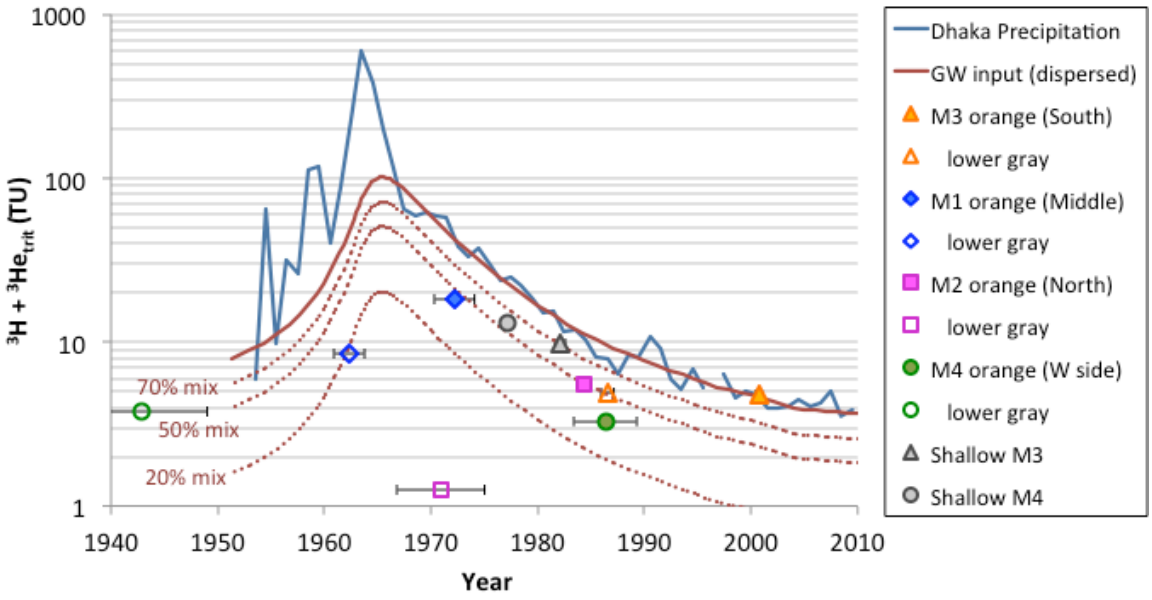

Figure 3.9. "Total ^{3}H" tracer (sum of current ^{3}H levels and estimated tritiogenic ^{3}He) plotted against the year of groundwater recharge obtained from ^{3}H/^{3}He age, and compared to the input of ^{3}H from precipitation. This approach to analyzing the ^{3}H/^{3}He ages (Ekwurzel et al., 1994) can demonstrate if a dated groundwater sample was recharged in its entirety in a given year, provided that the sample falls on the ^{3}H input curve from precipitation. If it falls below the input curve, it is a mixture of groundwater with different ages; in the case of binary mixing between ^{3}H-dead (recharged >70 yr ago) and recently recharged groundwater, the proportion of recent recharge can be estimated and is shown as percentage by the dashed lines. The estimated input of ^{3}H from Dhaka precipitation, and its dispersed signature in groundwater, were calculated as in Stute (2001) and Stute et al. (2007). Grey symbols indicate samples from the shallow aquifer, while filled and open symbols in color are from the orange sand and lower gray sand layers of the intermediate aquifer, respectively.

For the ages presented in Figs. 3.8e and 3.9, the degassing loss was assumed to have occurred at sampling, without a significant amount of fractionation between He and Ne and their isotopes. The concentrations of He were then back corrected for the degassed samples to the values they would have had (1) at solubility equilibrium, (2) with a slight excess air amount as in sample M2.5, or (3) with a larger amount of excess air as in sample M3.1. Six of the degassed samples (all except M4.5) were also assumed to have a contribution of radiogenic He similar to that of the samples M2.5 and M4.1 because they had larger deficits of Ne than He, whereas loss due to degassing would have favored larger deficits of He (Aeschbach-Hertig et al., 1999; Stute and Schlosser, 1999). The $^{3}He/^{4}He$ ratio in solubility equilibrium with the atmosphere (1.36×10^{-6}), and where necessary the ratio in the atmosphere (1.384×10^{-6}) and in the radiogenic He (crustal 2×10^{-8}), were then utilized to calculate the amount of $^{3}He_{trit}$ and the $^{3}H/^{3}He$ ages. In case of the degassed samples, the average of the three corrections for degassing was reported. The standard deviations of the three ages resulting from the back corrections (σ corr.), as well as the standard deviations in ages resulting from the analytical errors alone (σ anal.), were reported in Table 3.4 (Appendix); the larger of the two errors in individual samples was used in Figs. 3.8e and 3.9.

The calculation presented above was also carried out, as a quality control, without radiogenic He corrections in the 8 samples with probable radiogenic He contributions, assuming either (1) the three scenarios of degassing at the time of sampling, or (2) that degassing occurred at the time of recharge by exchange with atmosphere. The resulting age averages and error estimates from these additional calculations are presented in Table 3.5 (Appendix).

The apparent $^3H/^3He$ ages of site M samples in 2011 (Fig. 3.8e) ranged from 11 to 69 years. Samples from ~20 m bgl in the shallow aquifer had a constant age of roughly 30 years. In the intermediate aquifer, however, the samples collected from the orange sand layer had younger ages than those from the deeper grey sand layer, providing further evidence that the flow in the grey layer is less vigorous. The youngest age of ~11 years was found in well M3.5, screened in the orange layer at the southern edge of the site, but there was otherwise no evidence of a simple S-N flowpath along the orange sand layer at the site, as the $^3H/^3He$ age increased to ~39 years at well nest 1 (middle of the transect), but leveled off at ~25-27 years at well nests 2 (northern end of the transect) and 4 (west of the S-N transect). The above interpretation of $^3H/^3He$ ages only holds true either if the sampled groundwater was entirely recharged at one time point since the nuclear bomb testing started, or if the groundwater is a binary mix of recently recharged groundwater containing bomb-produced ^3H and older, pre-bomb groundwater. In the latter case, the $^3H/^3He$ ages only apply to the fraction of groundwater contributed by recent recharge.

The actual amount of mixing or dispersion in groundwater samples can be estimated by adding the measured ^3H to the estimated $^3He_{trit}$, their sum acting as a "stable ^3H" conservative tracer (Ekwurzel et al., 1994; Stute et al., 1997; Stute et al., 2007). The initial input of ^3H from the atmosphere by precipitation was estimated for Bangladesh, and its signal in groundwater predicted using typical rates of dispersion, by Stute (2001) and Stute et al. (2007). The comparison of $^3H+^3He_{trit}$ estimates at site M to the groundwater input curve (Fig. 3.9) showed that only the most recently recharged sample at M3.5 (orange sand at southern edge of the site) fell on the input curve, and thus was not mixed with the pre-bomb groundwater. High percentages of admixed younger

groundwater were found in the shallow groundwater (50-70%), and in the orange sand layer along the S-N transect (nests M1 and M2, ~50%). Lower contributions of recent recharge were observed in the deeper grey layer of the intermediate aquifer compared to the orange sand, and well nest 4 at both intermediate aquifer depths received less young groundwater input than the wells along the S-N transect.

3.3.9 Aquifer testing results

Slug tests

Slug testing of individual wells on site determined the horizontal hydraulic conductivity (K_h) in the vicinity of well screens to be ~1-7×10^{-5} m/s in the intermediate aquifer (Fig. 3.8f, and Table 3.3 in Appendix). No pattern in the vertical distribution of K_h was noted that could be correlated to the observed inflow of young groundwater in the middle of the aquifer. Specifically, K_h in the upper intermediate aquifer was both at a minimum value for the aquifer (well M4.4) and at a maximum (wells M1.4 and M2.4). The response to the slug test at well M1.4 was oscillatory, indicating a high horizontal conductivity, and such a response curve could not be fitted by the method used for the non-oscillating wells. In the shallow aquifer, K_h was roughly one order of magnitude higher, as the measured value at M4.1 was 2.2×10^{-4} m/s. The response curve in M1.1, the well with a long screen permeating the entire shallow aquifer, was also oscillatory.

Pumping tests

Pumping in either aquifer did not induce measureable drawdown in the other (Fig. 3.10). A temporary water level increase (reverse water level fluctuation from the

expected) was actually noted in the unpumped aquifer, noted in the literature as the Noordbergum effect (Kim and Parizek, 1997). This can be attributed to the existence of a compressible low-conductivity unit between the two aquifers: mechanical propagation of the pumping stress (deformation in the compressible, soft aquitard) is faster than the hydraulic response (drawdown) propagation in low-conductivity units (Kim and Parizek, 1997).

The observed drawdown curves in the intermediate aquifer during pumping tests were subject to corrections for barometric fluctuations and the background seasonal downward water level trend, discussed further in section 3.7.1 (Appendix). The early-time segment (initial 100 minutes) of the corrected drawdown curves was used to make estimates of the intermediate aquifer hydraulic conductivity and storativity by linear fitting of the drawdown observed over time or distance from the pumping well (see Fig. 3.21 in Appendix for examples), resulting in estimates on the order of $\sim 1\times10^{-4}$ m/s for the horizontal hydraulic conductivity and $\sim 6\times10^{-4}$ for storativity (Table 3.6 in Appendix). Because these methods assume a laterally extensive, homogeneous, confined aquifer, only early time points were used for the estimates, as the observed drawdown at later time points was significantly less than that expected from the classical Theis drawdown (Theis, 1935) of a confined aquifer (see Fig. 22 in Appendix for an example of drawdown at M1.5 with analytical fits). The drawdown might have been reduced due to a laterally uniform leakage through the confining unit such as the thick clay layer at site M. If so, the analytical solution by Hantush-Jacob for a leaky confined aquifer (Hantush and Jacob, 1954) would estimate the vertical hydraulic conductivity of the clay layer to be on the order of $\sim 1\text{-}2\times10^{-7}$ m/s (example of analytical solutions in Fig. 22). However, an

alternative explanation of the early stabilization of drawdown in the intermediate aquifer is that it is in direct contact with the shallow aquifer at some lateral distance, as observed in the vicinity of site T where the thick clay layer is absent.

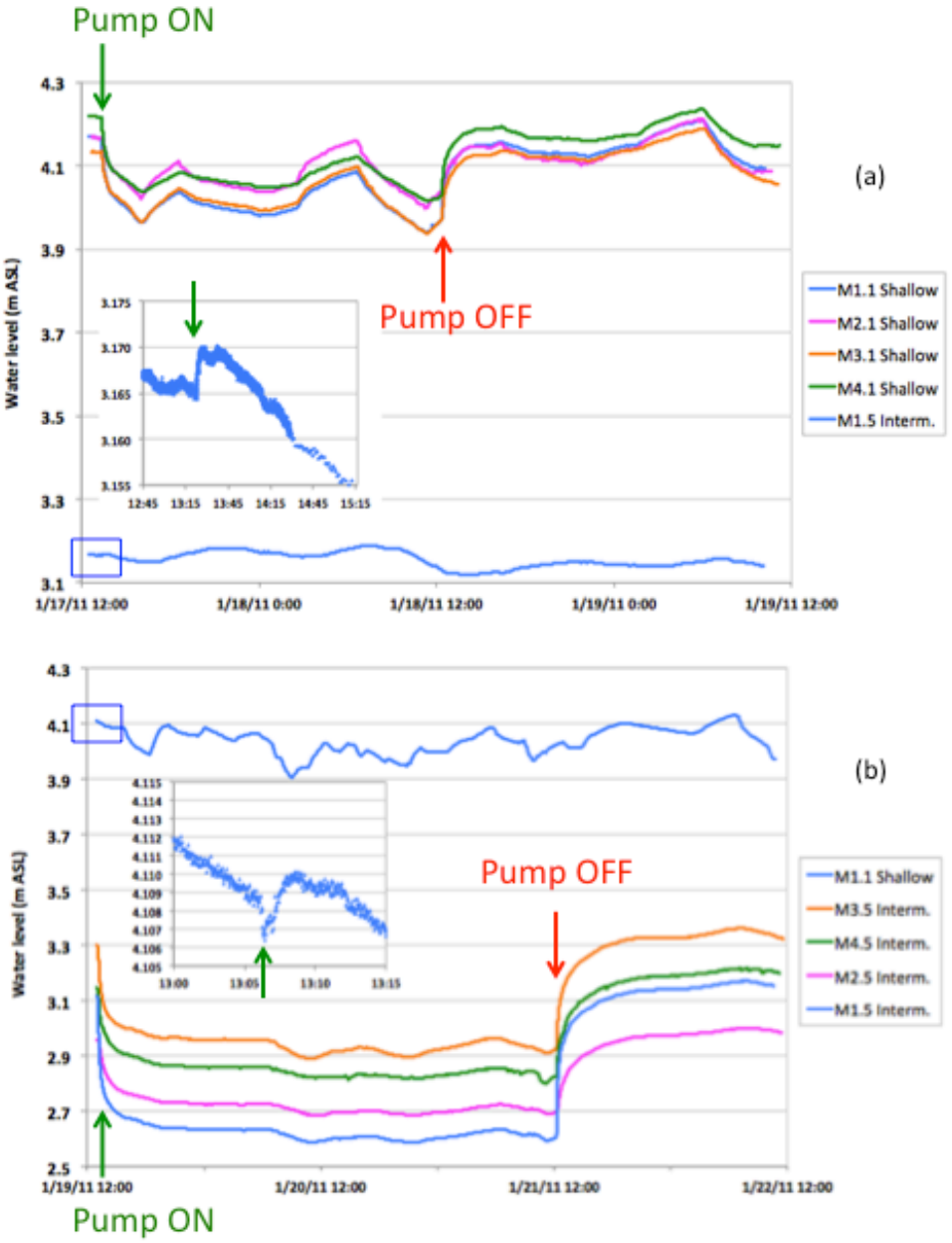

Figure 3.10. Hydraulic head response in select monitoring wells during pumping tests performed by pumping (a) from the shallow aquifer, PW A; and (b) from the intermediate aquifer, PW B. Arrows indicate the time pumps went on (green) or off

(red) in the pumped aquifer. Portions of the drawdown curves within blue squares are enlarged to demonstrate the Noordbergum effect (Kim and Parizek, 1997) – hydraulic head jump in the non-pumped aquifer – when the pump goes on in the other aquifer. Note the lack of other impacts on intermediate aquifer water levels when pumping from the shallow aquifer, and vice versa. All hydraulic heads were corrected for barometric pressure fluctuations and the seasonal water level trend.

Numerical models in MODFLOW (described in Appendix sections 3.7.2 and 3.7.3), taking into account the shallow aquifer, the clay layer, and the intermediate aquifer, showed that the high value of clay vertical conductivity (10^{-7} m/s range), causing a uniformly distributed leakage through the clay, is unrealistic because the hydraulic heads of the shallow and intermediate aquifer would equalize over time. Another conceptual approach to the model, where lower clay conductivity was set (10^{-9} m/s), but the thick clay layer was absent near site T, resulted in the shallow and intermediate aquifer water levels close to those observed both in steady state and during the pumping tests. This argues further for the lateral recharge at site M, and confirmed the K_h and S of the intermediate aquifer to be in the range of $\sim 1 \times 10^{-4}$ m/s and 6×10^{-4}, respectively.

3.4 Discussion

3.4.1 Aquifer sediment age and stratigraphic setting

The two aquifers at site M, shallow and intermediate, are made up of distinct sediments deposited at different times, as evidenced by their bulk chemistry, radiocarbon, and carbon isotopic data (Figs. 3.2 and 3.3; Fig. 3.14 and Table 3.1 in Appendix). The similarity of elemental compositions in all layers of the intermediate aquifer sands, and their depleted signature when compared to the shallow aquifer, argued that they had the same depositional history despite the variations in color and redox status. A similar trend towards lower total content of Ca, Fe, K, and Mn was observed for gray and orange Pleistocene sands in West Bengal by McArthur et al. (2008) and in Vietnam by van Geen et al. (2013), and attributed to the intense leaching of the sediment under steeper horizontal hydraulic gradients in the Pleistocene sea level lowstand. Radiocarbon data from the clay layers above, within, and below the intermediate aquifer constrained its deposition age to >8.5 ka BP and <36 ka BP, consistent with a late Pleistocene age. The age limit of 8.5 ka BP is quite robust, as the observed ^{14}C age of the overlying silty clay layer was highly consistent between the buried plant material (leaf /wood fragments) and total (bulk) organic carbon in the clay. Contrary to another report from the area (Zheng et al., 2005), sedimentary organic C measured at this depth was not affected by the addition of older C from upstream terrestrial OC pools at the time of deposition. However, radiocarbon ages of bulk sedimentary organic carbon from deeper clay lenses (~17-36 ka BP beneath the aquifer, and ~12 ka BP at ~50 m bgl in the upper gray layer) do provide an upper limit on intermediate aquifer sediment age, given the possibility that older

terrestrial OC might have affected the dating (Eglinton et al., 1997). The ^{13}C signatures of TOC samples from these clay layers, progressively enriched from -20‰ below the aquifer to -15‰ in the upper gray layer, agreed nicely nevertheless with the developing aridity during late Pleistocene, and the resulting dominance of C4 plants (e.g. grasses), observed in records elsewhere in the basin (Sarkar et al., 2009). Above the intermediate aquifer, the sudden change in ^{13}C fingerprint to -28 to -30‰ in the Holocene silty clay marked a clear signal of climatic shift.

The age of the thick clay layer (8.5 ka BP) and its bottom depth of 40-45 m bgl aligned well with the observed basin-wide onset of rapid accumulation of Holocene sediment: 40-50 m thick sequence of Holocene sediment was deposited across Bengal Basin during the second stage of rapid global sea level rise (11-7 ka BP; SL rise defined by Fairbanks (1989)). Transgression of coastlines towards the interior of the basin at ~11-9 ka BP was accompanied by monsoon intensification, resulting in stronger river flows, rapid Himalayan weathering, and massive sediment transport that peaked at ~8.5 ka BP in eastern Bengal delta and quickly filled in the space created by rising sea levels (Goodbred and Kuehl, 2000a, b; McArthur et al., 2008; Sarkar et al., 2009). At that time, peat and clay layers rich in organic matter, such as the one observed at our site (Fig. 3.3 and Table 3.1), were deposited and C3 plants adjusted to a wetter climate, mangroves in particular, dominated the vegetation, leaving behind the observed ^{13}C imprint of -25% to -30‰ (McArthur et al., 2008; Sarkar et al., 2009). The sedimentation rate between 17 and 5 ka BP was rather constant at our site, but given the ^{14}C and ^{13}C signatures that match well with the above studies, it is reasonable to consider the bottom of the thick clay layer

to be the lowest stratum of the Holocene sequence, underlain by the Pleistocene intermediate aquifer.

3.4.2 Hydrogeology at the site

The stratigraphic setting present at site M was interrupted at site T, ~300 m south of well nest M1, where the thick Holocene clay layer was absent, perhaps scoured by a small version of paleochannels like those found in the West Bengal studies (McArthur et al., 2010; McArthur et al., 2011; McArthur et al., 2008). The shallow aquifer extends deeper at site T and is laterally juxtaposed to the intermediate aquifer at M, allowing for a direct flowpath from the shallow to the intermediate aquifer without an obstruction by the clay layer. This "recharge window" of the intermediate aquifer, coupled to the increasing downward hydraulic gradient across the thick Holocene clay layer, dominated the groundwater flow patterns at site M, as conceptualized in Fig. 3.11. Presumably, there is a natural background balance achieved between the lateral flow in the intermediate aquifer, the vertical leakage through the clayey units, and the concentration of contaminants in the leakage, defining overall contaminant flux and concentrations; this balance may be altered by a local increase in pumpage from the transmissive orange sand beneath the clay layer or a regional increase in pumping from equivalent or greater depths.

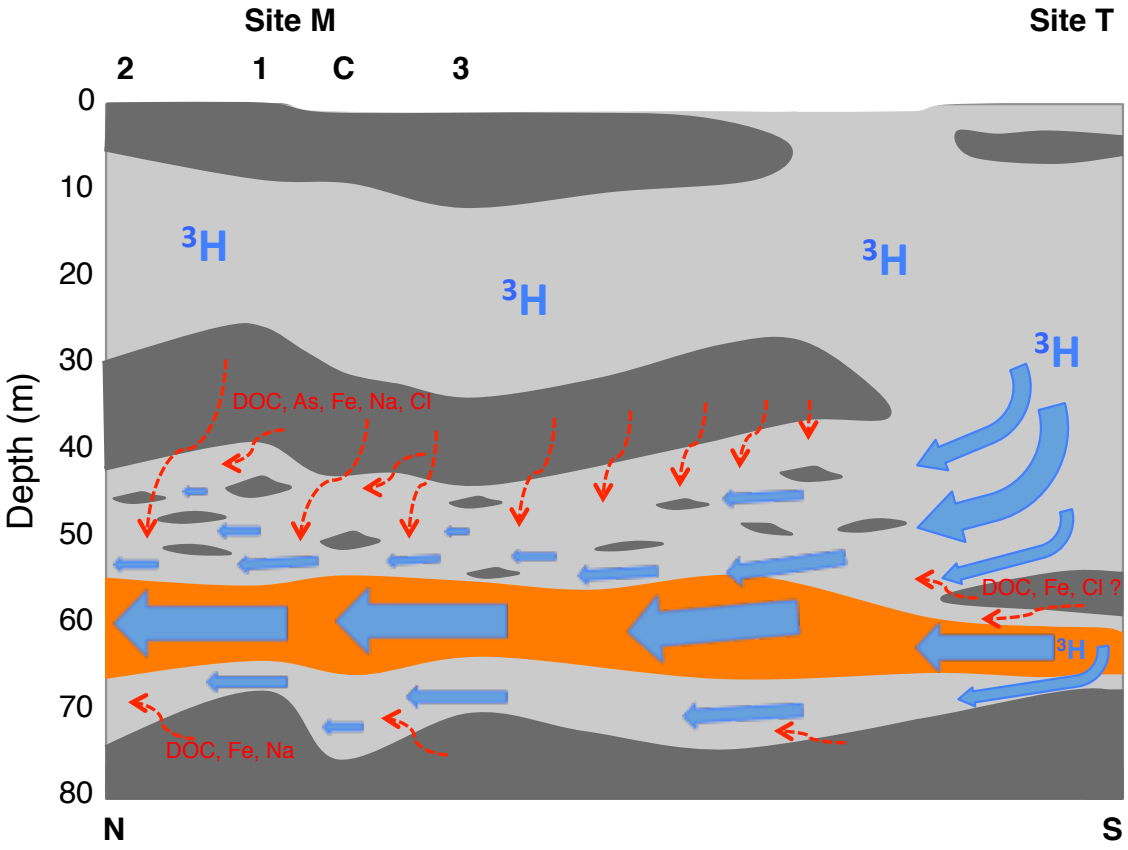

Figure 3.11. Conceptual model of flow from south to north between sites T and M. Representation of lithology beneath sites M and T is accurate; the rest is interpolated. Vertical exaggeration is ×3.5. The arrows show predominant water flow patterns and their size/length corresponds to the velocity of flow. The inflow of ^{3}H-rich groundwater from site T area is postulated, as is the leakage of DOC, Na, Cl, Fe, and As from the clay layers.

The lower and temporally declining hydraulic heads are maintained in the intermediate aquifer wherever there is a low-conductivity unit capable of sustaining a vertical hydraulic gradient, such as at site M. However, where the clay aquitard pinches

out, like at site T, the hydraulic head at 53 m bgl was high and characteristic of the shallow aquifer (Figs. 3.6, 3.7a, and 3.8a). As the distance from the recharge window and away from the clay edge increases, as across the S-N transect at site M, so does the downward vertical hydraulic gradient across the clay, and the heads in intermediate aquifer decrease. The observed constant horizontal hydraulic gradient (Fig. 3.16 in Appendix) of ~3-4×10^{-3} from the bottom of the shallow aquifer at site T to the northern end of site M, along the middle of the intermediate aquifer, provided a nice illustration of this principle and the MODLOW model with a discontinuity in the clay layer also seemed in agreement with the observations of general head patterns (Appendix 3.7.2). The flow is not necessarily aligned in the S-N direction, as the horizontal gradient is poorly constrained in the E-W direction due to the lack of monitoring wells along that axis. It is not clear as yet whether the downward hydraulic gradients from shallow to intermediate aquifers in the area are a regional feature driven by diffuse and distant pumping at greater depths, including large-scale withdrawals ~25 km west for Dhaka municipal supplies (Hoque et al., 2007), or if they occur due to local pumping from the intermediate and deep aquifers that has yet to be identified.

Another confirmation of both a degree of hydraulic separation between the shallow and intermediate aquifers provided by the clay, and of their connection at the recharge window, came from the observations made during pumping tests (Fig. 3.10) and over the long-term monitoring with pressure transducers (Fig. 3.7). Pumping from either aquifer did not induce a clear response in the other, besides the instantaneous reverse hydraulic signal called the "Noordbergum effect", indicating that the clay layer is compressible, but does provide a good amount of hydraulic barrier to flow between the

aquifers. The drawdown observed when pumping the intermediate aquifer, however, flattened out too soon for a confined aquifer (Fig. 3.22 in Appendix), and the MODFLOW model confirmed that such a feature could be explained by a connection to the shallow aquifer near site T (Figs 3.24 and 3.25 in Appendix). In terms of the long-term fluctuations recorded by pressure transducers (Fig. 3.7a), the two aquifers respond very similarly to the external forcing on a range of time scales, thus they must be connected to a degree. The daily fluctuations induced by shallow irrigation pumping, visible in dry season as noisier hydrographs (Fig. 3.7b), show a clear impact of the shallow zone pressure changes, but also illustrate that this impact is lesser in the intermediate aquifer with thicker confining clay and further away from a discontinuity in clay layer, such as at site M compared to site T.

In spite of the persistent horizontal hydraulic gradient in the intermediate aquifer, the actual groundwater flow pattern is not a simple and uniform flow from south to north, as evidenced by the variable $^{3}H/^{3}He$ ages along the S-N transect (Figs. 3.8e and 3.9). Non-uniform spatial recharge and variable length flowpaths are implied by the patchy tracer distribution. Nevertheless, the $^{3}H/^{3}He$ groundwater dating technique demonstrated that groundwater in the orange sand at southern edge of site M (M3.5) was the youngest (10.6 years) and entirely made up of recent recharge (Figs. 3.8e and 3.9). Given the distance and the horizontal hydraulic gradient between site T and M3 of 273 m and 3.2×10^{-3}, respectively, and assuming a porosity of 0.3, the hydraulic conductivity of the intermediate aquifer calculated from the $^{3}H/^{3}He$ age is 7.7×10^{-5} m/s. The true horizontal hydraulic conductivity is probably higher and the horizontal flow faster than estimated above, given that the recently recharged groundwater at site T would first need to flow

downward, which is a slower processes, before it can continue laterally towards site M. This estimate, nonetheless, falls between the lower range of conductivities estimated at individual wells by point-specific slug tests (1-7×10^{-5} m/s, Fig. 3.8f) and the higher, spatially-integrated, and more representative conductivities estimated from the pumping tests (~1×10^{-4} m/s, Table 3.6 in Appendix), also employed in the corresponding MODFLOW models (Table 3.7 in Appendix). It is plausible, therefore, that the recent recharge at site M was sourced somewhere near site T, where the highest ^{3}H levels were observed in the very shallow aquifer, but more complex flowpaths originating from various other locations cannot be excluded. The two deepest wells at site T, located within a distance of <5 m from the thin Pleistocene clay layer, were probably not directly upstream from site M in terms of the actual inflow of groundwater, judging by their relatively modest ^{3}H levels, and are likely affected by the clay layer, given also the high Cl contents, and a moderate amount of DOC in T3.

In order to establish a complete hydrologic picture of the intermediate aquifer, we must also examine the flow balance for the whole system, including the flows between the shallow and the intermediate aquifers, as well as the recharge/discharge balance for the shallow aquifer. Although the shallow groundwater mostly enters the intermediate aquifer by lateral inflow in the areas of contact between the two aquifers where the confining clay layers are absent, the overall flow from the shallow to intermediate aquifer must also have a vertical component. A spatially averaged vertical hydraulic conductivity within the zone of influence of the pumping tests, including both the clay layers and the sandy "recharge windows" where the clay is missing, was obtained by fitting the leaky aquifer Hantush-Jacob solution to the pumping test drawdown curves (Fig. 22 in

Appendix). Using a representative vertical conductivity thus obtained of 1×10^{-7} m/s, and assuming a downward hydraulic gradient of 1 m across a distance of 10 m, as encountered at the site, the calculated recharge of the intermediate aquifer from the shallow aquifer is 0.32 m/yr (Darcy velocity).

The amount of downward flow from the shallow aquifer or "leakage" calculated above is within the range of shallow aquifer recharge and discharge fluxes (~0.75 m/yr total) estimated by a detailed hydrological model in nearby Munshiganj by Harvey et al. (2006), although their model did not include any water flow from the shallow aquifer to deeper zones. The balance between precipitation and evapotranspiration at their site, which is probably similar to ours, leaves a precipitation surplus of ~0.6-0.7 m/yr that could recharge the shallow aquifer. Our site has no major streams and few ponds, so a large portion of the 0.6-0.7 m/yr surplus can be split between irrigating the fields (0.45 m/yr at the site of Harvey et al., 2006; 0.21 m/yr used in the basin models by Michael and Voss, 2008) and recharging the intermediate aquifer. Finally, our intermediate aquifer recharge rate of 0.32 m/yr is also consistent with a vertical one-dimensional back-of-the-envelope calculation of the groundwater residence time: assuming an aquifer thickness of 30 m and a porosity of 0.3, the residence time of groundwater is 28.5 yr (30 m × 0.3 / 0.32 m/yr), which compares closely to the $^{3}H/^{3}He$ ages of groundwater from the orange sand layer of the intermediate aquifer (11-39 yr, 25.5 yr average; Table 3.4).

Within the intermediate aquifer, the horizontal flow is not equally distributed in all the layers. Instead, most flow occurrs in the orange sand layer, a little less along the lower grey sand unit, and the least along the upper grey sand of the intermediate aquifer. This was implied by younger $^{3}H/^{3}He$ ages and higher percentages of recently recharged

groundwater (traced by $^{3}H+^{3}He_{trit}$, Fig. 3.9) in the orange sand than in the deeper grey, and the lack of detectable ^{3}H in the upper grey sand (Fig. 3.8d). The horizontal hydraulic gradient along the upper intermediate aquifer was also a little less pronounced (Figs. 3.6 and 3.8a). The stable isotopic signature also confirmed this flow pattern, as the intermediate aquifer samples from the orange and deeper grey layers formed a spread of values varying between the heavier $\delta^{2}H$ and $\delta^{18}O$ observed in the shallow aquifer (M and T) and the more depleted values in the intermediate aquifer's upper grey layer. The latter might reflect the stable isotopic signature of the intermediate aquifer prior to the intrusion of recent recharge because the thick Holocene clay had similarly depleted values (Fig. 3.8bc).

The reasons for less vigorous groundwater flow and less flushing of the upper intermediate aquifer, and to a lesser extent, also of the lower grey sand layer, cannot be found in a difference in the hydraulic conductivity of the grey and orange sand, as slug tests did not show such evidence (Fig. 3.8f), and the grain sizes observed while drilling were not remarkably different. Therefore, the more likely explanation of the slower flow along the upper and lower layer of the aquifer would be the effect of flow hindrance by the undulating clay layers that delimit the intermediate aquifer. Both the overlying Holocene and the underlying Pleistocene clay layers appear at quite a variable range of elevation-corrected depths even on such a small spatial scale as at site M (Figs. 3.2 and 3.11), thus the combined effect of such flow obstructions could be key to the lesser inflow of recent recharge. In addition to that, the downward gradient across the thick Holocene clay layer must allow for some groundwater leaking vertically through the clay layer, thus further dispersing the lateral inflows at this depth. The downward vertical

gradient also continues within the intermediate aquifer (this is clear from the yearly average water levels in Fig. 3.8a), which has the effect of displacing the horizontal flow lines of groundwater towards deeper parts of the aquifer. If the clay leakance component is small, the displacement, dispersion, and dilution of the lateral flow will not be great except at the clay/sand interface.

3.4.3 Impact of clay layers and recent recharge on aquifer redox status and radiocarbon ages of DIC and DOC

Based on the consistent stratigraphy at site M and the separation of Holocene and Pleistocene aquifers by a clay layer aquitard, the intermediate aquifer would be expected to contain older, low-As groundwater with a constant chemical signature different from that of the shallow aquifer. However, a lack of the thick confining layer further south at site T, the observed failures of community wells, and the variable redox status of the intermediate aquifer sediments, provided an indication that the groundwater chemistry of the aquifer might be much more complex.

The most rapidly flushed layer of the intermediate aquifer coincided with the depth of the least reducing sediment and groundwater. The orange sand has the lowest percentage of Fe(II) in the acid-leachable iron fraction (Fig. 3.3d), while groundwater in this layer contains dissolved Fe and As minima (Fig. 3.4). At the same time, Mn peaked at this depth, and there was detectable SO_4 (Fig. 3.15 in Appendix), thus the low-As orange layer of the intermediate aquifer was poised at Mn reduction, but anoxia did not go as far as Fe and SO_4 reduction. Similar correlations between the Mn peak and low As were also observed at other sites (Berg et al., 2008; McArthur et al., 2010; McArthur et

al., 2008). Groundwater composition in the deeper grey sand layer of the intermediate aquifer did not differ much from that in the orange sand, except in the deepest well of well nest 4 where high Fe and Na, as well as low Ca, typical of the upper grey layer, were observed. This "reversal" of chemistry at the bottom of the aquifer, however, occurred at the nest with the least amount of recent recharge outside of the upper grey sand zone (Figs. 3.8d and 3.9), and fairly close to the basal clay layer from which the DOC and Na could be leaching. Otherwise, like with the groundwater composition, chemical differences between the orange and the lower grey sand are minimal, as they exhibited a very slight difference in the amount of acid-leachable Fe(II)/Fe (Fig. 3.3d). The observed similarity between the labile Fe redox status of these sands indicated that they are in a delicate balance and could easily change their color, and more importantly, their sorptive capacity dependent on the Fe mineralogy.

Unlike the studies that linked increasing anoxia and As concentrations to the intrusion of shallow groundwater into the Pleistocene aquifers (Berg et al., 2008; McArthur et al., 2010; McArthur et al., 2008; van Geen et al., 2013) or the Holocene aquifers (Harvey et al., 2002; Neumann et al., 2010; Polizzotto et al., 2008), our study found that the incursion of recently recharged groundwater did not cause elevated As levels, and might in fact protect the middle of the intermediate aquifer by hydrodynamic shear, and dilution, dispersion, and diversion of the contaminated groundwater seeping from the clay layers at upper and lower limits of the aquifer. The abovementioned studies found that recent recharge exacerbated the anoxia because it contained high levels of dissolved organics coming from sources like ponds, latrines/human waste, fresh biomass, Holocene sediment OC, peat layers etc. At site M, however, there was no evidence of

increased transport or consumption of DOC along the horizontal flow lines, as DOC levels were modest in the orange sand layer (Fig. 3.4i). The shallow aquifer at site T, the possible source area of recharge, contained equally low amounts of DOC (Table 3.2 in Appendix) and only a modest As concentration at 21 m bgl of ~75 μg/L, compared to nearly 300 μg/L As at the same depth in the shallow aquifer at site M. Site T might, in fact, be one of the locations that benefit from large rates of flushing by groundwater flow, keeping the concentrations of As at bay (Berg et al., 2008; McArthur et al., 2010; Stute et al., 2007; van Geen et al., 2008). The high concentrations of SO_4 and Cl in the shallow aquifer at T (Table 3.2), coupled to very little clay capping at the surface (Fig. 3.2), lend further support to the rapid flushing and inflow of surface recharge at site T, but without causing large inputs of DOC, perhaps due to relatively few houses and ponds in the area (Fig. 3.1b).

The transport of surface-derived DOC and its arrival to the orange sand at Site M might, of course, be delayed by its adsorption to aquifer sediment (Mailloux et al., 2013), but the radiocarbon data in DOC and DIC cannot be used to prove such a scenario (Fig. 3.5a). The amounts of ^{14}C in DOC and DIC in the middle layers of the intermediate aquifer, already shown to be in contact with recharge from the surface, are not any different from the DOC and DIC ^{14}C in the shallowest wells at site T much closer to the surface (10 and 21 m bgl). Moreover, a DOC sample with an entirely modern ^{14}C signature was retrieved from well M4.6, arguing that recently recharged DOC can reach site M wells. As is the case with ^{3}H and $^{3}He_{trit}$, the observed radiocarbon signatures of DOC and DIC in the orange and deeper grey sand of the intermediate aquifer are likely mixtures of bomb-produced, modern ^{14}C transported from the surface and the older ^{14}C

from the pre-existing groundwater pool recharged before the onset of large downward hydraulic gradients and the ensuing penetration of younger groundwater. It is also possible that the younger, more reactive pool of DOC is immediately scavenged by microbial activity, leaving the more recalcitrant fraction of DOC behind and obscuring the relationship of DOC to recent recharge (Harvey et al., 2002). In support of that, ^{14}C was slightly younger in DIC than in DOC for most samples, perhaps reflecting the preference of microbial metabolism for younger OC pool or a greater subsurface mobility of DIC, or both, but the question of DOC influx to the intermediate aquifer might be settled by the studies of ^{14}C in microbial DNA, and microbial population and genetic diversity (Mailloux et al., 2013).

In the upper gray sand of the intermediate aquifer, the radiocarbon content of both DOC and DIC was remarkably lower than in the deeper parts of the aquifer. This observation could be explained either by the lack of inflow of younger, surface-derived C pools, or by the leakage of the old clay-derived DOC and DIC from the overlying early Holocene clay, or both. As this zone of the intermediate aquifer had the highest measured DOC concentrations (second only to those in the clay pore water, Fig. 3.4i), and a well-advanced anoxia with high levels of As, Fe, P, and NH_3 (Fig. 3.4abcd), contributions of DOC from the clay are likely and would help explain the local reducing environment. Microbially mediated oxidation of DOC coupled to reduction of Fe oxyhydroxides produces NH_3 and CO_2 as byproducts, explaining the NH_3 and DIC maxima at this depth (Fig. 3.4d and 3.15f). The correlation of high NH_3 to elevated As concentrations has been used as an indicator of advanced reduction of Fe oxyhydroxides (Berg et al., 2008;

Postma et al., 2007), which dissolves and rearranges Fe oxide phases and can release adsorbed As and PO_4 to groundwater (McArthur et al., 2001; Nickson et al., 2000).

In addition, ^{13}C signature of the DOC in upper intermediate aquifer (Fig. 5b) matches precisely the ^{13}C of clay TOC and organic materials (leaves etc.) retrieved from the bottom of the thick, sticky Holocene clay (Fig. 3.3f). The extremely enriched ^{13}C DIC record (shifted towards more positive values) at this depth is likely a result of methanogenesis operating amid the advanced reduction (Eh values were also quite negative, Table 3.2 in Appendix), and was matched by a similar observation in the shallow aquifer sample (M4.1). Although methane was not explicitly measured, the methanogenesis metabolism preferably consumes ^{12}C, so the DIC left behind is enriched in ^{13}C, and this process has been linked to high As in groundwater (Harvey et al., 2002). The older ^{14}C and more enriched ^{13}C in DIC of upper gray intermediate aquifer are unlikely to have been produced by carbonate dissolution, given the minimum concentration of dissolved Ca at this depth (Fig. 3.4f) and the observation that no sedimentary inorganic C could be measured (<0.01 wt%). In addition, the existence of old DOC pool that retained reactivity and could be mineralized to DIC (Fig. 3.4j), potentially oozing from the clay along with old DIC, provided a simpler explanation for the observed low radiocarbon and enriched C isotopic signatures in DIC at that depth (Aravena et al., 1995; Wassenaar et al., 1990).

Besides the similarity of trace elemental contents (high Fe, As, and P; low Mn) and isotopic signatures of C species and water molecules in the upper grey sands of the intermediate aquifer and in the pore water of thick Holocene clay, there were also other lines of evidence that indicated the contamination might be coming from the low-

permeability units. Less reactive elements, such as Na and Cl, were elevated in the clay pore water and also in the aquifer layer directly beneath it. In the deeper grey layer of well nest 4 (M4.6a), Na and Fe, but not the more mobile Cl, were also higher and might be a result of the contact with the Pleistocene clays. The evidence of seepage through the clay layer, aided by the downward gradients, was found within the clay layer itself also. There appeared to be a moving front of fresher and younger pore water in the upper part of the clay layer, as pore water Na and Cl increased with depth within the clay unit and the DOC contained a greater fraction of modern ^{14}C compared to the surrounding sediment, resulting in younger ^{14}C age by ~2-4 kyr (Figs. 3.3c, 3.4gh and 3.5a; Tables 3.1 and 3.3 in Appendix). The high Na and Cl in the mid-to-lower part of the thick clay layer could be a remainder of relic seawater (Appelo and Postma, 2005; Szabo et al., 2006), flushing of which was delayed prior to the onset of higher downward hydraulic gradients.

3.4.4 Modes of clay pore water delivery to the aquifer

The models in MODFLOW (Appendix 3.7.2-3) constrained the overall vertical conductivity of the thick clay layer to $\leq 10^{-9}$ m/s in order to explain the maintained water level difference of ~1 m between the shallow and intermediate aquifers. Assuming a clay thickness of 10 m and a porosity of 0.3, this vertical conductivity would result in a modest vertical advective velocity of ~1 cm/yr, similar to earlier estimates of Zheng et al. (2005) at nearby site B. That low amount of uniform downward leakage may not be great, but if contaminant concentrations are high and the hydraulic gradients are constant or increasing, as is the case in our field area (Fig. 3.13 in Appendix), the relative and absolute flux is still important (Chen et al., 2005). Besides the uniform vertical leakage

along the downward hydraulic gradient, there are also other ways to disperse the contents of clay pore waters. The fact that the bottom depth of the clay layer undulates considerably even within the 5 litholog locations on the scale of ~200 m (Figs. 3.2 and 3.11) means that the surface of contact between the aquifer and the aquitard is large and spread out over many different depths. The organics and As oozing from the clays can be transported across this surface along diffusive gradients at various depths, and then dispersed by horizontal flow within a large section of the upper grey layer.

Furthermore, the downward vertical gradient within the intermediate aquifer focuses downward both the clay seepage and the more rapid lateral recharge occurring beneath it in the orange sand layer. Such gradients also partly explain why the impact of the overlying, Holocene clay layer is larger on the aquifer chemistry than that of the underlying Pleistocene clay; the underlying units would likely be an important source of leakage and solutes if hydraulic gradients were upwards (Szabo et al., 1997), but the downward hydraulic gradient continues at greater depths at our site. The Pleistocene clay also has less impact compared to the Holocene clay because its pore water contains less DOC, Fe, As, P, Na, and Cl (Fig. 3.4abcgh), and lower levels of total Fe and OC are present in the sediment (Fig. 3.3e, and Fig. 3.14a in Appendix), perhaps heavily leached in a period of extensive recharge at the end of Last Glacial Maximum.

Another way to increase the delivery of clay pore waters to the aquifer includes the squeezing of the clay due to subsidence, recently linked to the widespread As contamination of the Pleistocene aquifer in the Mekong Delta (Erban et al., 2013), where the land subsidence due to deep aquifer pumping can reach up to 3 cm/yr in places. Near Dhaka, land subsidence can reach up to 1.2 cm/yr (Steckler et al., 2010), thus it could

have an impact on the availability of labile organics in local aquifers. Moreover, as the observed Noordbergum effect when turning irrigation pumps on and off (Fig. 3.10) has been linked to the rapid deformations of the low-permeability unit skeleton (Kim and Parizek, 1997), it means that the clay present on site is squeezable and might deliver a pulse of organics and/or Fe and As every time farmers irrigate in the vicinity, as they did during our pumping tests. The irrigation at our site takes place at shallow depths, but the Noordbergum effect operates when either aquifer, below or above the compressible low-conductivity unit, is pumped (Fig. 3.10). The barometric efficiency estimate of 0.1 for the intermediate aquifer (Appendix 3.7.1) also indicates a highly compressible confining unit, as 90% of the atmospheric pressure changes are transmitted to the aquifer, and additional measurement may allow for a degree of vulnerability assessment (Hussein et al., 2013). McMahon and Chapelle (1991b) showed that DOC fermentation outpaces DOC respiration in low-permeability units, resulting in the accumulation of simple organic acids in clay layers; when this DOC reaches aquifer sediments, it gets readily respired and fuels the reduction of Fe and/or SO_4, or methanogenesis (McMahon and Chapelle, 1991a; McMahon et al., 1992). In Southeast Asia, such seeping of DOC from clay/peat OM has been proposed in a Plesitocene aquifer of the Red River delta and in a shallow, Holocene aquifer in West Bengal, India (Berg et al., 2008; McArthur et al., 2004), transporting along Fe, As, and PO_4, and helping release more by reducing iron oxyhydroxides (FeOOH) present in the aquifer sands.

3.4.5 Estimates of clay pore water mixing in groundwater and redox mass balances impacting groundwater contaminants

In order to constrain the amount of reduction occurring in the upper horizon of the intermediate aquifer, which contains a maximum in Na and Cl concentrations within the intermediate aquifer, Na and Cl from all groundwater samples and from the mid-clay-layer pore water were plotted together on a binary plot (Fig. 3.12a) and the contributions of different endmembers assessed. Chloride can be used as an inert tracer because it does not participate in redox reactions, its uptake by biota is small relative to its concentrations, and it sorbs minimally to negatively charged sand and clay surfaces at circumneutral pH. The arrival of high As groundwater to a deep pumping well was, for example, traced to a peak in Cl in West Bengal (Mukherjee et al., 2011). Sodium, on the other hand, can participate in cation exchange reactions on sediment surfaces, but it sorbs much less than the divalent Ca or Mg ions, or K ion with the much smaller hydrated radius (Kielland, 1937). The average of samples in the upper intermediate aquifer fell ~1/3 of the distance along the mixing line from deeper groundwater to the clay pore water. That implied the groundwater in upper, grey layer of the intermediate aquifer contained ~1/3 clay pore water from above, and ~2/3 groundwater flowing horizontally within the aquifer. Based on that mixing ratio, additional releases of Fe, PO_4, and some As must occur when the advected DOC is coupled to dissimilatory iron reduction in order to match their concentrations within the upper intermediate aquifer.

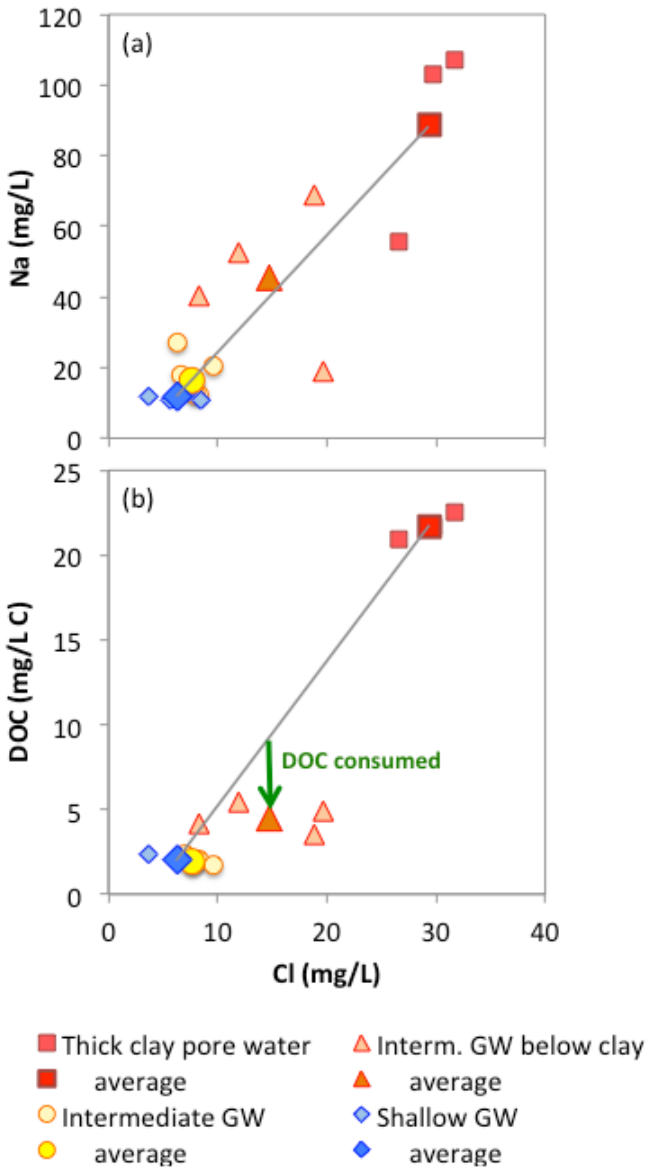

Figure 3.12. Binary mixing plots of (a) Na and (b) dissolved organic carbon (DOC) plotted against the conservative anion, Cl. Groundwater was grouped into "shallow" (shallow aquifer), "interm. below clay" (from the reduced upper grey layer of the intermediate aquifer) and "intermediate" (below the reduced zone, orange and deeper grey layer of the intermediate aquifer). Average compositions of each group of groundwater and that of the clay pore water are shown as larger and bolder-color

symbols. The grey line represents a mixing line, connecting averages of two endmember compositions: clay pore water and intermediate groundwater; groundwater composition falling along or near the line represents a mixture of the two endmembers. Shallow groundwater from site M has a similar DOC, Na, and Cl composition to the "intermediate".

The amount of DOC available for the reduction processes can also be obtained by the binary mixing plot with Cl (Fig. 3.12b). The average of upper intermediate aquifer samples (0.37 mM) fell below the mixing line because DOC was depleted relative to the expected 0.71 mM if 1/3 of the mixture came from the clay pore water. The difference (0.34 mM) suggested the amount of DOC that reacted and was consumed, per pore volume (PV), in resident reduction processes of the upper intermediate aquifer, such as Fe and SO_4 reduction and methanogenesis. Adding to that the ~15% of unconsumed DOC that retained reactivity (Fig. 3.4j) in the upper interm. aquifer, we obtain ~0.4 mM of DOC per PV available for reduction processes. Assuming a ratio of 4 moles of Fe reduced by 1 mole of DOC (Postma et al., 2007), up to 1.6 mM (or ~90 mg/L) of Fe could be released into the groundwater via reduction of sediment by 1 PV of flow, assuming 100% of the reduced Fe is released to the dissolved phase. Although much of the reduced Fe can be incorporated into rearranged Fe mineral phases instead, such as magnetite (Horneman et al., 2004; van Geen et al., 2004), or mixed-layer "green" rust , the quantity of reductants present is sufficient for the observed maximum of 10 mg/L Fe below the clay.

Dissolved arsenic observed in the upper intermediate aquifer could be a product of As release when FeOOH was reduced to the point at which little As resorption to mixed Fe phases occurs (McArthur et al., 2008). However, given a high degree of decoupling in Fe and As release from sediment (Dhar et al., 2011; Horneman et al., 2004; Tufano and Fendorf, 2008; Tufano et al., 2008; van Geen et al., 2004), and the modest concentrations (18-54 μg/L As, except a well in nest 1 with ~250 μg/L, Fig. 3.4a), it is hard to resolve whether As came from the reduction occurring in upper parts of the aquifer or was transported from the overlying clay and met by minimal sorption to reduced Fe phases in the aquifer. Another process that might exert control over As release in the upper intermediate aquifer could be SO_4 reduction: the 1-2 mg/L SO_4 (i.e. 0.01-0.02 mM, based on the mixing ratio) likely contributed by the clay pore water seepage into the upper intermediate aquifer must be reduced in that layer, as no SO_4 was detected there (Fig. 3.15c). That would require 0.02-0.04 mM DOC, assuming again that DOC can give off 4 electrons to reduce S from +6 to -2 oxidation state. Sulfate reduction, therefore, consumes a relatively small proportion of the available DOC, but could exert some control over the μM-range dissolved As concentrations by precipitating As in Fe-As-sulfides (Buschmann and Berg, 2009) or promoting Fe mineral rearrangements that favor the sequestration of As (Saalfield and Bostick, 2009).

The arrival and additional release of As and other reduction products in upper portion of the intermediate aquifer due to the large surface area contact with Holocene clays, combined with less vigorous flushing of the layer, resulted in accumulation of As in this part of the aquifer. When the failed community well was pumped, increasing vertical flow velocities and/or opening up the preferential flow paths, dissolved As could

migrate freely and relatively fast within the sandy aquifer without hindrance by additional confining layers. Such a scenario was likely responsible for the documented failures of community well 12 at our site; once the well was abandoned and the pumping had ceased, the encroaching As within deeper layers of the intermediate aquifer was resorbed to the still-orange sediment. An equivalent scenario was observed by McArthur et al. (2010) in a well installed in Pleistocene sands in direct contact (no clay separation) with high-As aquifer above: As increased while well was hand-pumped by villagers, but fell back to previous levels <1 year upon the cessation of pumping.

3.4.6 Significance and implications

This is the first time to the authors' knowledge that a low-As Pleistocene aquifer in the Bengal Basin was shown to be possibly contaminated by the seepage of organic C, As and other reduction products from a confining unit. It offers, thus, a novel perspective that the low-conductivity units can also add to the contamination owing to their pore water chemistry, as recently proposed by Erban et al. (2013) based on a large-scale survey in the Mekong delta, and therefore, their presence is not always singularly beneficial, as considered in the hydrological models of vertical transport of As by Michael and Voss (2008, 2009b). Although the confining unit in our study isolates the underlying aquifer from direct vertical incursions of the shallow groundwater and electron donors, as did the Pleistocene, orange colored paleosol in the studies by McArthur et al. (2010; 2011; 2008), the clay was dated to early Holocene at our site, and DOC accumulated in its pore water is drawn down along the increasingly downward

hydraulic gradient and squeezed by pressure pulses from large scale pumping to set off and/or exacerbate reduction in the Late Pleistocene aquifer.

Furthermore, because the reactive DOC leached from a clay layer whose bulk organic radiocarbon age precisely matched that of the buried plant material (~8.5 ka BP), the contribution of young OM coming from the surface by way of shallow irrigation and/or recharge from freshly excavated ponds (Harvey et al., 2002; Neumann et al., 2010; Polizzotto et al., 2008) could be excluded. Thus, we provided additional evidence that organic matter buried in, and co-deposited with, Holocene sediments can retain a great amount of reactivity, fueling the sediment reduction and As contamination in previously low-As aquifers. Concurrently, we showed that recent recharge from the surface does not necessarily contaminate the aquifer. The nature of organic matter and chemical composition of the infiltrating shallow groundwater will affect the result such recharge has on As release or retention (Neumann et al., 2010; Rowland et al., 2006). If it contains low amounts of reactive DOC and/or high levels of oxidants such as SO_4, like shallow groundwater at the likely location of recharge in our study does, it could help maintain the vulnerable intermediate-depth aquifer low in As.

The above findings point to the need for re-evaluating the vulnerability of low-As aquifers that reduce the exposure of population to As in drinking and cooking water. Whereas well installations in the intermediate-depth low-As aquifers (35-150 m bgl) might be cheaper to install because they usually only require the traditional “hand flapper” or “sludger” method, these aquifers may be more vulnerable to As contamination than previously presumed. The increasing usage of deep wells is only likely to further magnify the downward vertical hydraulic gradients, drawing down more

contaminants from leaky clay units and causing a more rapid recharge adjacent to patchy low-permeability layers by shallow groundwater of either beneficial or detrimental compositions (like witnessed near public supply wells in the U.S., e.g. Ayotte et al., 2011; Landon et al., 2008). Certainly, the vertical anisotropy of aggregated smaller clay and silt layers can delay the migration of contaminated groundwater (Burgess et al., 2010; Michael and Voss, 2009a, b), and so can the geochemical properties of the sediment that result in the adsorption and retardation of As plume (Burgess et al., 2010; Radloff et al., 2011; Robinson et al., 2011; Stollenwerk et al., 2007). However, as the aforementioned studies also argued, local evaluation of heads and aquifer properties especially including leakance (Hussein et al., 2013) in vulnerable areas is vital, as is the groundwater quality monitoring in areas where intermediate-depth wells are used for water supply (Dhar et al., 2008). Attention should be paid also to the potential impacts of deeper, pre-Pleistocene clay layers that might affect As in groundwater, as has been proposed by Erban et al. (2013) in the lower Mekong.

Our study provided an example of aquifer contamination with As once the aquitard protection had been breached and a portion of the pumped low-As aquifer had been reduced: the contamination of a pumped well ensued rapidly under the lower vertical anisotropy within the aquifer. That the intermediate aquifers are vulnerable to inflows of shallow groundwater potentially carrying along high DOC and As is not new. However, this study argues that care must be taken not only to also install wells deeper, but also to install them away from the confining units, in particular if they contain, like the Holocene clays do at our site, high levels of organics and dissolved reduction products.

3.5 Conclusions

The presented geochemical and hydrologic study of an intermediate-depth (40-75 m bgl) low-arsenic aquifer on a single village scale revealed that clay layers do not necessarily protect low-As aquifers from As contamination. In this particular configuration, the clay layer contributed As to the aquifer, as well as organic matter that may have enhanced reductive processes and *in situ* As release. The recharge with shallow groundwater that bypassed the clay layer, on the other hand, may actually have helped flush the aquifer, preventing the accumulation of reduction products and maintaining low-As conditions. Pumped wells, like the local community well, can fail if As contamination already exists in the aquifer and frequent pumping accelerates As migration within the aquifer toward the well screen. Thus, although the intermediate aquifers can be an important and affordable source of low-As drinking water in Bangladesh, care must be taken to install the drinking wells deep enough, away from organic-rich clay layers, and to test the wells regularly for arsenic.

Acknowledgements

This work would not have been possible without the help of our field staff members Md. Shahidullah Shahud and Md. Majibul Hosain. We must also be grateful to the villagers from site M who put up with our noisy generators and delayed the irrigation of their fields for a few days when we performed pumping tests. Ronny Friedrich helped analyze the stable isotopes and together with Bob Newton ensured a prompt analysis of ^{3}H and He data and proved to be a great resource for discussing groundwater dating. The work was inspired in its early stages by ideas brought forth by my master thesis adviser, Yan Zheng. The ideas on groundwater flow at the site and model set-up also benefited from numerous discussions with Holly Michael and Charles Harvey.

3.6 References

Aeschbach-Hertig, W., Peeters, F., Beyerle, U., Kipfer, R., 1999. Interpretation of dissolved atmospheric noble gases in natural waters. Water Resources Research 35, 2779-2792.

Aggarwal, P.K., Basu, A.R., Poreda, R.J., Kulkarni, K.M., Froehlich, K., Tarafdar, S.A., Ali, M., Ahmed, N., Hussain, A., Rahman, M., Ahmed, S.R., 2000a. Isotope hydrology of groundwater in Bangladesh: Implications for characterization and mitigation of arsenic in groundwater, IAEA-TC Project (BGD/8/016). International Atomic Energy Agency.

Ahmed, M.F., Ahuja, S., Alauddin, M., Hug, S.J., Lloyd, J.R., Pfaff, A., Pichler, T., Saltikov, C., Stute, M., van Geen, A., 2006. Epidemiology - Ensuring safe drinking water in Bangladesh. Science 314, 1687-1688.

Allison, M.A., Khan, S.R., Goodbred, S.L., Kuehl, S.A., 2003. Stratigraphic evolution of the late Holocene Ganges-Brahmaputra lower delta plain. Sedimentary Geology 155, 317-342.

Appelo, C.A.J., Postma, D., 2005. Geochemistry, groundwater and polution, 2nd ed. Taylor & Francis, Leiden, The Netherlands.

Aravena, R., Wassenaar, L.I., Plummer, L.N., 1995. Estimating C-14 groundwater ages in a methanogenic aquifer. Water Resources Research 31, 2307-2317.

Argos, M., Kalra, T., Rathouz, P.J., Chen, Y., Pierce, B., Parvez, F., Islam, T., Ahmed, A., Rakibuz-Zaman, M., Hasan, R., Sarwar, G., Slavkovich, V., van Geen, A., Graziano, J., Ahsan, H., 2010. Arsenic exposure from drinking water, and all-cause and chronic-disease mortalities in Bangladesh (HEALS): a prospective cohort study. Lancet 376, 252-258.

Ayotte, J.D., Szabo, Z., Focazio, M.J., Eberts, S.M., 2011. Effects of human-induced alteration of groundwater flow on concentrations of naturally-occurring trace elements at water-supply wells. Applied Geochemistry 26, 747-762.

Bayer, R., Schlosser, P., Boenisch, G., Rupp, H., Zaucker, F., Zimmek, G., 1989. Performance and blank components of a mass spectrometric system for routine measurement of helium isotopes and tritium by the 3He ingrowth method. Sitzungsberichte (5) der Heidelberger Akademie der Wissenschaften, Mathematisch-naturwissenschaftliche Klasse, Jahrgang, Heidelberg, Germany.

Berg, M., Trang, P.T.K., Stengel, C., Buschmann, J., Viet, P.H., Van Dan, N., Giger, W., Stueben, D., 2008. Hydrological and sedimentary controls leading to arsenic contamination of groundwater in the Hanoi area, Vietnam: The impact of iron-

arsenic ratios, peat, river bank deposits, and excessive groundwater abstraction. Chemical Geology 249, 91-112.

BGS and DPHE, 2001. Arsenic Contamination of Groundwater in Bangladesh, in: Kinniburgh, D.G., Smedley, P.L. (Eds.). British Geological Survey and Department of Public Health Engineering, BGS Technical Report WC/00/19. British Geological Survey, Keyworth, UK.

Burgess, W.G., Hoque, M.A., Michael, H.A., Voss, C.I., Breit, G.N., Ahmed, K.M., 2010. Vulnerability of deep groundwater in the Bengal Aquifer System to contamination by arsenic. Nature Geoscience 3, 83-87.

Buschmann, J., Berg, M., 2009. Impact of sulfate reduction on the scale of arsenic contamination in groundwater of the Mekong, Bengal and Red River deltas. Applied Geochemistry 24, 1278-1286.

Butler, J.J., Garnett, E.J., 2000. Simple procedures for analysis of slug tests in formations of high hydraulic conductivity using spreadsheet and scientific graphics software, Rep. OFR 2000-40. Kansas Geol. Surv., Lawrence.

Chen, X.H., Yin, Y.F., Goeke, J.W., Diffendal, R.F., 2005. Vertical movement of water in a High Plains Aquifer induced by a pumping well. Environmental Geology 47, 931-941.

Cheng, Z., Zheng, Y., Mortlock, R., van Geen, A., 2004. Rapid multi-element analysis of groundwater by high-resolution inductively coupled plasma mass spectrometry. Analytical and Bioanalytical Chemistry 379.

Clarke, W.B., Jenkins, W.J., Top, Z., 1976. Determination of tritium by mass-spectrometric measurement of He-3. International Journal of Applied Radiation and Isotopes 27, 515-522.

Craig, H., 1961. Isotopic variations in meteoric waters. Science 133, 1702-1703.

Dhar, R.K., Zheng, Y., Saltikov, C.W., Radloff, K.A., Mailloux, B.J., Ahmed, K.M., van Geen, A., 2011. Microbes Enhance Mobility of Arsenic in Pleistocene Aquifer Sand from Bangladesh. Environmental Science & Technology 45, 2648-2654.

Dhar, R.K., Zheng, Y., Stute, M., van Geen, A., Cheng, Z., Shanewaz, M., Shamsudduha, M., Hoque, M.A., Rahman, M.W., Ahmed, K.M., 2008. Temporal variability of groundwater chemistry in shallow and deep aquifers of Araihazar, Bangladesh. Journal of Contaminant Hydrology 99, 97-111.

Eglinton, T.I., BenitezNelson, B.C., Pearson, A., McNichol, A.P., Bauer, J.E., Druffel, E.R.M., 1997. Variability in radiocarbon ages of individual organic compounds from marine sediments. Science 277, 796-799.

Ekwurzel, B., Schlosser, P., Smethie, W.M., Plummer, L.N., Busenberg, E., Michel, R.L., Weppernig, R., Stute, M., 1994. Dating of shallow groundwater - comparison of the transient tracers H-3/He-3, chlorofluorocarbons, and Kr-85. Water Resources Research 30, 1693-1708.

Elder, K.L., McNichol, A.P., Gagnon, A.R., 1997. Evaluating reproducibility of seawater, inorganic and organic carbon 14C results at the National Ocean Sciences AMS Facility (NOSAMS), Proceedings of the 16th International Radiocarbon Conference. Radiocarbon 40, pp. 223-230.

Erban, L.E., Gorelick, S.M., Zebker, H.A., Fendorf, S., 2013. Release of arsenic to deep groundwater in the Mekong Delta, Vietnam, linked to pumping-induced land subsidence. Proceedings of the National Academy of Sciences of the United States of America 110, 13751-13756.

Fairbanks, R.G., 1989. A 17,000-year glacio-esutatic sea-level record: influence of glacial melting rates on the Younger Drias event and deep-ocean circulation. Nature 342, 637-642.

Fendorf, S., Michael, H.A., van Geen, A., 2010. Spatial and Temporal Variations of Groundwater Arsenic in South and Southeast Asia. Science 328, 1123-1127.

Fetter, C.W., 2001. Applied Hydrogeology, 4th ed. Prentice Hall, Upper Saddle River, NJ.

Gonthier, G.J., 2007. A Graphical Method for Estimation of Barometric Efficiency from Continuous Data - Concepts and Applications to a Site in the Piedmont, Air Force Plant 6, Marietta, Georgia. U.S. Geological Survey Scientific Investigations Report 2007-5111, Reston, Virginia.

Goodbred, S.L., Kuehl, S.A., 2000a. Enormous Ganges-Brahmaputra sediment discharge during strengthened early Holocene monsoon. Geology 28, 1083-1086.

Goodbred, S.L., Kuehl, S.A., 2000b. The significance of large sediment supply, active tectonism, and eustasy on margin sequence development: Late Quaternary stratigraphy and evolution of the Ganges-Brahmaputra delta. Sedimentary Geology 133, 227-248.

Gran, G., 1952b. Determination of the equivalence point in potentiometric titrations. 2. Analyst 77, 661-671.

Hantush, M.S., Jacob, C.E., 1954. Plane potential flow of ground-water with linear leakage. Transactions, American Geophysical Union 35, 917-936.

Harvey, C.F., Swartz, C.H., Badruzzaman, A.B.M., Keon-Blute, N., Yu, W., Ali, M.A., Jay, J., Beckie, R., Niedan, V., Brabander, D., Oates, P.M., Ashfaque, K.N., Islam, S., Hemond, H.F., Ahmed, M.F., 2002. Arsenic mobility and groundwater extraction in Bangladesh. Science 298, 1602-1606.

Hoque, M.A., Hoque, M.M., Ahmed, K.M., 2007. Declining groundwater level and aquifer dewatering in Dhaka metropolitan area, Bangladesh: causes and quantification. Hydrogeology Journal 15, 1523-1534.

Horneman, A., van Geen, A., Kent, D.V., Mathe, P.E., Zheng, Y., Dhar, R.K., O'Connell, S., Hoque, M.A., Aziz, Z., Shamsudduha, M., Seddique, A.A., Ahmed, K.M., 2004. Decoupling of As and Fe release to Bangladesh groundwater under reducing conditions. Part 1: Evidence from sediment profiles. Geochimica Et Cosmochimica Acta 68, 3459-3473.

Hussein, M.E.A., Odling, N.E., Clark, R.A., 2013. Borehole water level response to barometric pressure as an indicator of aquifer vulnerability. Water Resources Research 49.

Islam, F.S., Gault, A.G., Boothman, C., Polya, D.A., Charnock, J.M., Chatterjee, D., Lloyd, J.R., 2004. Role of metal-reducing bacteria in arsenic release from Bengal delta sediments. Nature 430, 68-71.

JICA and DPHE, 2010. Report on Situation Analysis of Arsenic Mitigation, 2009. Dept. of Public Health Engineering, Bangladesh and Japan International Cooperation Agency, Local Government Division, Government of Bangladesh, DPHE, JICA.

Kielland, J., 1937. Individual activity coefficients of ions in aqueous solutions. Journal of the American Chemical Society 59, 1675-1678.

Kim, J.M., Parizek, R.R., 1997. Numerical simulation of the Noordbergum effect resulting from groundwater pumping in a layered aquifer system. Journal of Hydrology 202, 231-243.

Klump, S., Kipfer, R., Cirpka, O.A., Harvey, C.F., Brennwald, M.S., Ashfaque, K.N., Badruzzaman, A.B.M., Hug, S.J., Imboden, D.M., 2006. Groundwater dynamics and arsenic mobilization in Bangladesh assessed using noble gases and tritium. Environmental Science & Technology 40, 243-250.

Landon, M.K., Clark, B.R., McMahon, P.B., McGuire, V.L., Turco, M.J., 2008. Hydrogeology, chemical characteristics, and transport processes in the zone of contribution of a public-supply well in York, Nebraska. U. S. Geological Survey Scientific Investigations Report 2008-5050.

Ludin, A.R., Weppernig, R., Boenisch, G., Schlosser, P., 1997. Mass spectrometric measurement of helium isotopes and tritium, internal report. Lamont-Doherty Earth Observatory, Palisades, New York.

Mailloux, B.J., Trembath-Reichert, E., Cheung, J., Watson, M., Stute, M., Freyer, G.A., Ferguson, A.S., Ahmed, K.M., Alam, M.J., Buchholz, B.A., Thomas, J., Layton, A.C., Zheng, Y., Bostick, B.C., van Geen, A., 2013. Advection of surface-derived organic carbon fuels microbial reduction in Bangladesh groundwater. Proceedings of the National Academy of Sciences of the United States of America 110, 5331-5335.

McArthur, J.M., Banerjee, D.M., Hudson-Edwards, K.A., Mishra, R., Purohit, R., Ravenscroft, P., Cronin, A., Howarth, R.J., Chatterjee, A., Talukder, T., Lowry, D., Houghton, S., Chadha, D.K., 2004. Natural organic matter in sedimentary basins and its relation to arsenic in anoxic ground water: the example of West Bengal and its worldwide implications. Applied Geochemistry 19.

McArthur, J.M., Banerjee, D.M., Sengupta, S., Ravenscroft, P., Klump, S., Sarkar, A., Disch, B., Kipfer, R., 2010. Migration of As, and H-3/(3) He ages, in groundwater from West Bengal: Implications for monitoring. Water Research 44, 4171-4185.

McArthur, J.M., Nath, B., Banerjee, D.M., Purohit, R., Grassineau, N., 2011. Palaeosol Control on Groundwater Flow and Pollutant Distribution: The Example of Arsenic. Environmental Science & Technology 45, 1376-1383.

McArthur, J.M., Ravenscroft, P., Banerjee, D.M., Milsom, J., Hudson-Edwards, K.A., Sengupta, S., Bristow, C., Sarkar, A., Tonkin, S., Purohit, R., 2008. How paleosols influence groundwater flow and arsenic pollution: A model from the Bengal Basin and its worldwide implication. Water Resources Research 44.

McArthur, J.M., Ravenscroft, P., Safiulla, S., Thirlwall, M.F., 2001. Arsenic in groundwater: Testing pollution mechanisms for sedimentary aquifers in Bangladesh. Water Resources Research 37, 109-117.

McMahon, P.B., Chapelle, F.H., 1991a. Geochemistry of dissolved inorganic carbon in a Coastal Plain aquifer. 2. Modeling carbon sources, sinks, and delta C-13 evolution. Journal of Hydrology 127, 109-135.

McMahon, P.B., Chapelle, F.H., 1991b. Microbial production of organic acids in aquitard sediments and its role in aquifer geochemistry. Nature 349, 233-235.

McMahon, P.B., Chapelle, F.H., Falls, W.F., Bradley, P.M., 1992. Role of microbial processes in linking sandstone diagenesis with organic-rich clays. Journal of Sedimentary Petrology 62, 1-10.

Michael, H.A., Voss, C.I., 2008. Evaluation of the sustainability of deep groundwater as an arsenic-safe resource in the Bengal Basin. Proceedings of the National Academy of Sciences of the United States of America 105, 8531-8536.

Michael, H.A., Voss, C.I., 2009a. Controls on groundwater flow in the Bengal Basin of India and Bangladesh: regional modeling analysis. Hydrogeology Journal 17, 1561-1577.

Michael, H.A., Voss, C.I., 2009b. Estimation of regional-scale groundwater flow properties in the Bengal Basin of India and Bangladesh. Hydrogeology Journal 17, 1329-1346.

Mukherjee, A., Fryar, A.E., Scanlon, B.R., Bhattacharya, P., Bhattacharya, A., 2011. Elevated arsenic in deeper groundwater of the western Bengal basin, India: Extent and controls from regional to local scale. Applied Geochemistry 26, 600-613.

Neumann, R.B., Ashfaque, K.N., Badruzzaman, A.B.M., Ali, M.A., Shoemaker, J.K., Harvey, C.F., 2010. Anthropogenic influences on groundwater arsenic concentrations in Bangladesh. Nature Geoscience 3, 46-52.

Nickson, R., McArthur, J., Burgess, W., Ahmed, K.M., Ravenscroft, P., Rahman, M., 1998. Arsenic poisoning of Bangladesh groundwater. Nature 395, 338-338.

Nickson, R.T., McArthur, J.M., Ravenscroft, P., Burgess, W.G., Ahmed, K.M., 2000. Mechanism of arsenic release to groundwater, Bangladesh and West Bengal. Applied Geochemistry 15, 403-413.

Norrman, J., Sparrenbom, C.J., Berg, M., Nhan, D.D., Nhan, P.Q., Rosqvist, H., Jacks, G., Sigvardsson, E., Baric, D., Moreskog, J., Harms-Ringdahl, P., Van Hoan, N., 2008. Arsenic mobilisation in a new well field for drinking water production along the Red River, Nam Du, Hanoi. Applied Geochemistry 23, 3127-3142.

Polizzotto, M.L., Kocar, B.D., Benner, S.G., Sampson, M., Fendorf, S., 2008. Near-surface wetland sediments as a source of arsenic release to ground water in Asia. Nature 454, 505-U505.

Poreda, R.J., Cerling, T.E., Salomon, D.K., 1988. Tritium and helium isotopes as hydrologic tracers in a shallow unconfined aquifer. Journal of Hydrology 103, 1-9.

Postma, D., Larsen, F., Hue, N.T.M., Duc, M.T., Viet, P.H., Nhan, P.Q., Jessen, S., 2007. Arsenic in groundwater of the Red River floodplain, Vietnam: Controlling geochemical processes and reactive transport modeling. Geochimica Et Cosmochimica Acta 71, 5054-5071.

Radloff, K.A., Zheng, Y., Michael, H.A., Stute, M., Bostick, B.C., Mihajlov, I., Bounds, M., Huq, M.R., Choudhury, I., Rahman, M.W., Schlosser, P., Ahmed, K.M., van

Geen, A., 2011. Arsenic migration to deep groundwater in Bangladesh influenced by adsorption and water demand. Nature Geoscience 4, 793-798.

Ravenscroft, P., Burgess, W.G., Ahmed, K.M., Burren, M., Perrin, J., 2005. Arsenic in groundwater of the Bengal Basin, Bangladesh: Distribution, field relations, and hydrogeological setting. Hydrogeology Journal 13, 727-751.

Ravenscroft, P., McArthur, J.M., Hoque, M.A., 2013. Stable groundwater quality in deep aquifers of Southern Bangladesh: The case against sustainable abstraction. Science of the Total Environment 454, 627-638.

Robinson, C., von Bromssen, M., Bhattacharya, P., Haller, S., Biven, A., Hossain, M., Jacks, G., Ahmed, K.M., Hasan, M.A., Thunvik, R., 2011. Dynamics of arsenic adsorption in the targeted arsenic-safe aquifers in Mat lab, south-eastern Bangladesh: Insight from experimental studies. Applied Geochemistry 26, 624-635.

Rowland, H.A.L., Polya, D.A., Lloyd, J.R., Pancost, R.D., 2006. Characterisation of organic matter in a shallow, reducing, arsenic-rich aquifer, West Bengal. Organic Geochemistry 37, 1101-1114.

Saalfield, S.L., Bostick, B.C., 2009. Changes in Iron, Sulfur, and Arsenic Speciation Associated with Bacterial Sulfate Reduction in Ferrihydrite-Rich Systems. Environmental Science & Technology 43, 8787-8793.

Sarkar, A., Sengupta, S., McArthur, J.M., Ravenscroft, P., Bera, M.K., Bhushan, R., Samanta, A., Agrawal, S., 2009. Evolution of Ganges-Brahmaputra western delta plain: clues from sedimentology and carbon isotopes. Quaternary Science Reviews 28, 2564-2581.

Schlosser, P., Stute, M., Sonntag, C., Munnich, K.O., 1989. Tritiogenic He-3 in shallow groundwater. Earth and Planetary Science Letters 94, 245-256.

Sengupta, S., McArthur, J.M., Sarkar, A., Leng, M.J., Ravenscroft, P., Howarth, R.J., Banerjee, D.M., 2008. Do ponds cause arsenic-pollution of groundwater in the Bengal Basin? An answer from West Bengal. Environmental Science & Technology 42, 5156-5164.

Smith, A.H., Lingas, E.O., Rahman, M., 2000. Contamination of drinking-water by arsenic in Bangladesh: a public health emergency. Bulletin of the World Health Organization 78, 1093-1103.

Steckler, M.S., Nooner, S.L., Akhter, S.H., Chowdhury, S.K., Bettadpur, S., Seeber, L., Kogan, M.G., 2010. Modeling Earth deformation from monsoonal flooding in Bangladesh using hydrographic, GPS, and Gravity Recovery and Climate Experiment (GRACE) data. Journal of Geophysical Research-Solid Earth 115.

Stollenwerk, K.G., Breit, G.N., Welch, A.H., Yount, J.C., Whitney, J.W., Foster, A.L., Uddin, M.N., Majumder, R.K., Ahmed, N., 2007. Arsenic attenuation by oxidized aquifer sediments in Bangladesh. Science of the Total Environment 379, 133-150.

Stookey, L.L., 1970. Ferrozine - a new spectrophotometric reagent for iron. Analytical Chemistry 42, 779-781.

Stuiver, M., Polach, H.A., 1977. Reporting of C-14 data - discussion. Radiocarbon 19.

Stute, M., 2001. 3H in precipitation in Bangladesh, in: Jacks, G.e.a. (Ed.), Groundwater Arsenic Contamination in the Bengal Delta Plain of Bangladesh, Proceedings of the KTH-Dhaka University Seminar. KTH Spec. Publ. TRITA-AMI Rep. 3084, Univ. of Dhaka, Dhaka, Bangladesh, pp. 109-117.

Stute, M., Deak, J., Revesz, K., Bohlke, J.K., Deseo, E., Weppernig, R., Schlosser, P., 1997. Tritium/He-3 dating of river infiltration: An example from the Danube in the Szigetkoz area, Hungary. Ground Water 35, 905-911.

Stute, M., Schlosser, P., 1999. Atmospheric noble gases, in: Cook, P.G., Herczeg, A.L. (Eds.), Environmental tracers in subsurface hydrology. Kluwer, Boston, pp. 349-377.

Stute, M., Zheng, Y., Schlosser, P., Horneman, A., Dhar, R.K., Datta, S., Hoque, M.A., Seddique, A.A., Shamsudduha, M., Ahmed, K.M., van Geen, A., 2007. Hydrological control of As concentrations in Bangladesh groundwater. Water Resources Research 43.

Szabo, Z., Keller, E.A., Defawe, R.M., 2006. Pore-water quality in the clay-silt confining units of the lower Miocene Kirkwood Formation and hypothetical effects on water quality of the Atlantic City 800-foot sand, northeastern Cape May County, New Jersey, 2001. U.S. Geological Survey Scientific Investigations Report 2006-5134, 26p.

Szabo, Z., Pucci, A.A., Jr., Feigenson, M.D., 1997. Sr-isotopic evidence for leakage of pore water from clay-silt confining units to the Atlantic City 800-foot sand, Atlantic City, New Jersey, in: Miller, K.G., Snyder, S.W. (Eds.), Proceedings of the Ocean Drilling Program, Scientific Results, V. 150X, pp. 343-354.

Theis, C.V., 1935. The lowering of the piezometer surface and the rate and discharge of a well using ground-water storage. Transactions, American Geophysical Union 16, 519-524.

Tolstikhin, I.N., Kamenski, I.L., 1969. Determination of ground-water ages by T-He-3 method. Geochemistry International 6, 810-811.

Tufano, K.J., Fendorf, S., 2008. Confounding impacts of iron reduction on arsenic retention. Environmental Science & Technology 42, 4777-4783.

Tufano, K.J., Reyes, C., Saltikov, C.W., Fendorf, S., 2008. Reductive Processes Controlling Arsenic Retention: Revealing the Relative Importance of Iron and Arsenic Reduction. Environmental Science & Technology 42, 8283-8289.

van Geen, A., Bostick, B.C., Trang, P.T.K., Lan, V.M., Mai, N.-N., Manh, P.D., Viet, P.H., Radloff, K.A., Aziz, Z., Mey, J.L., Stahl, M.O., Harvey, C.F., Oates, P., Weinman, B., Stengel, C., Frei, F., Kipfer, R., Berg, M., 2013. Retardation of arsenic transport through a Pleistocene aquifer. Nature in press.

van Geen, A., Cheng, Z.Q., Jia, Q., Seddique, A.A., Rahman, M.W., Rahman, M.M., Ahmed, K.M., 2007. Monitoring 51 community wells in Araihazar, Bangladesh, for up to 5 years: Implications for arsenic mitigation. Journal of Environmental Science and Health Part a-Toxic/Hazardous Substances & Environmental Engineering 42, 1729-1740.

van Geen, A., Rose, J., Thoral, S., Garnier, J.M., Zheng, Y., Bottero, J.Y., 2004. Decoupling of As and Fe release to Bangladesh groundwater under reducing conditions. Part II: Evidence from sediment incubations. Geochimica Et Cosmochimica Acta 68, 3475-3486.

van Geen, A., Zheng, Y., Goodbred, S., Horneman, A., Aziz, Z., Cheng, Z., Stute, M., Mailloux, B., Weinman, B., Hoque, M.A., Seddique, A.A., Hossain, M.S., Chowdhury, S.H., Ahmed, K.M., 2008. Flushing history as a hydrogeological control on the regional distribution of arsenic in shallow groundwater of the Bengal Basin. Environmental Science & Technology 42, 2283-2288.

van Geen, A., Zheng, Y., Versteeg, R., Stute, M., Horneman, A., Dhar, R., Steckler, M., Gelman, A., Small, C., Ahsan, H., Graziano, J.H., Hussain, I., Ahmed, K.M., 2003. Spatial variability of arsenic in 6000 tube wells in a 25 km(2) area of Bangladesh. Water Resources Research 39.

Wassenaar, L.I., Hendry, M.J., Aravena, R., Fritz, P., 1990. Organic carbon isotope geochemistry of clayey deposits and their associated porewaters, southern Alberta. Journal of Hydrology 120, 251-270.

Wasserman, G.A., Liu, X.H., Parvez, F., Ahsan, H., Factor-Litvak, P., van Geen, A., Slavkovich, V., Lolacono, N.J., Cheng, Z.Q., Hussain, L., Momotaj, H., Graziano, J.H., 2004. Water arsenic exposure and children's intellectual function in Araihazar, Bangladesh. Environmental Health Perspectives 112, 1329-1333.

Winkel, L.H.E., Pham Thi Kim, T., Vi Mai, L., Stengel, C., Amini, M., Nguyen Thi, H., Pham Hung, V., Berg, M., 2011. Arsenic pollution of groundwater in Vietnam exacerbated by deep aquifer exploitation for more than a century. Proceedings of the National Academy of Sciences of the United States of America 108, 1246-1251.

Yu, W.H., Harvey, C.M., Harvey, C.F., 2003. Arsenic in groundwater in Bangladesh: A geostatistical and epidemiological framework for evaluating health effects and potential remedies. Water Resources Research 39, 17.

Zheng, Y., van Geen, A., Stute, M., Dhar, R., Mo, Z., Cheng, Z., Horneman, A., Gavrieli, I., Simpson, H.J., Versteeg, R., Steckler, M., Grazioli-Venier, A., Goodbred, S., Shahnewaz, M., Shamsudduha, M., Hoque, M.A., Ahmed, K.M., 2005. Geochemical and hydrogeological contrasts between shallow and deeper aquifers in two villages of Araihazar, Bangladesh: Implications for deeper aquifers as drinking water sources. Geochimica Et Cosmochimica Acta 69, 5203-5218.

3.7 Appendix

3.7.1 Pumping test drawdown curve corrections

The drawdown curves in individual wells were first corrected for atmospheric pressure fluctuations recorded by air pressure transducer during the pumping tests. Three methods were used to estimate the barometric efficiency, necessary for correcting the water levels appropriately: the slope method, the Clark method, and the graphic method (Fig. 3.19). The methods are suitable for a confined aquifer with instantaneous pressure equilibration in the wellbore (no wellbore storage nor "skin" effects), and are described in a USGS report by Gonthier (2007). Pressure logger data at 20-min intervals from May-August were used for the estimates, avoiding the random daily noise from shallow irrigation pumping. The estimated barometric efficiency is 0.1, which means that 90% of the atmospheric pressure changes are not borne by the confining unit matrix. In other words, the confining clay attenuates 10% of the atmospheric pressure change and transmits 90% of it to the aquifer, indicating a highly compressible unit. In practice, the water levels reported by pressure transducers need to be corrected by $-0.9\times\Delta p_{atm}$, as the pressure transducers in an open well record the total downhole pressure, consisting of the atmospheric pressure (changed by $+1.0\times\Delta p_{atm}$) and the water level (changed by $-0.1\times\Delta p_{atm}$ because of the 10% higher or lower pressure in the atmosphere than in the confined aquifer).

After the barometric pressure changes were corrected for, a correction for the seasonal water level trend was also applied to the intermediate aquifer drawdown curves. The trend used was -4.2154 cm/day, obtained by a linear fit of pressure transducer data

from 16th-25th January 2011, excluding the times when the aquifer was pumped for our experiments (Fig. 3.20). The successful pumping test reported was performed between 19th-22nd January. The remaining features visible in the intermediate aquifer drawdown curves are likely tidal signals and/or the effects of regional pumping, and are present throughout the data set.

3.7.2 MODFLOW model set-up

A numerical, 3D flow model was setup to model hydraulic heads observed in the field during pumping tests and to assess if leakage through the thick clay layer or through the clay layer discontinuity at site T is responsible for the observed drawdown curves. GMS8.1 software (Aquaveo) was used to run MODFLOW-2000, a U.S. Geological Survey modular finite-difference groundwater flow model, version 1.19.01. The model grid was made of 15 layers, simulating three distinct formations: shallow aquifer (3 layers), thick clay (5 layers), and intermediate aquifer (7 layers). The thickness of each formation was set to the thickness observed in the litholog of well nest M1 (Fig. 3.2), as listed in Table 3.7, and referenced layer elevations in m above sea level were used, as in the field data. The model layers (4-8) corresponding to the thick clay also contained a polygon centered on site T used to simulate the discontinuity in clay layer. Total length of the grid in x and y direction was 1,800×1,800 m, with pumping well B (intermediate aquifer) occupying the middle of the grid (Figs. 3.23 and 24). The grid cell x and y dimensions ranged from 1 to 50 m, with refined grid (1×1 m) located at well nests M1-M4, as well as pumping well B. Observation wells were nested in the middle of the 1×1 m cells, in a layer corresponding to their elevation-corrected depth (Table 3.8).

Two conceptual models were examined: (1) laterally extensive, but leaky, clay layer (with a higher vertical conductivity, K_z), without a break in clay layer near site T; and (2) clay layer cells in an arbitrarily-defined polygon near site T were assigned the intermediate aquifer parameters instead in order to simulate recharge from shallow to intermediate aquifer that bypasses the clay layer. The clay vertical conductivity (K_z) outside the polygon was, in turn, lower by 2 orders of magnitude relative to the leaky clay K_z in model (1).

A steady state model with representative parameters (K_h, K_z/anisotropy, S, Table 3.7) for all layers was run to calibrate the model against the initial head distribution, as observed in the field immediately before the pumping test started (Table 3.8). The values used for the intermediate aquifer K_h and S were set to the average of time-drawdown estimates made from early-time drawdown curves (Fig. 3.21 and Table 3.6). The vertical anisotropy was assumed to be 10, resulting in $K_z = K_h / 10$. Ten-fold higher values of K_h and K_z were used for the shallow aquifer, based on the slug test results for K_h (Table 3.2) and assuming the same vertical anisotropy as in the intermediate aquifer, while the specific yield was set to that of a typical medium-to-fine sand aquifer, 0.23 (p.79, Fetter, 2001). General head boundaries (head-dependent flux boundary) were used along the model side edges, while the bottom of the model was a no-flow boundary. Initial heads for the steady-state model, including the boundaries, were set to: (a) observed hydraulic head in the shallow aquifer, ~1 m higher than in the intermediate aquifer, and (b) a gradient across the intermediate aquifer from south (higher head) to north (lower head).

After a satisfactory distribution of initial hydraulic heads was obtained, matching the field observations to <10 cm, 3D hydraulic heads from the steady state model were

transferred as starting hydraulic heads to a transient model. The transient model was run with field-observed pumping flow rates and time periods, and was checked against drawdown curves in observation wells. The time step used ranged from 5 minutes at the time when the pumping started and the water levels were changing rapidly, gradually increasing to 2 hours at later stages of pumping. A similar time step spacing pattern was applied during the recovery phase when the pumping ceased.

3.7.3 MODFLOW results

In scenario (1), simulating the laterally extensive leaky clay layer, without a lateral discontinuity, the clay vertical hydraulic conductivity (K_z) was set to a typical value of 1.6×10^{-7} m/s, estimated from the leaky confined aquifer analytical solution by Hantush-Jacob (example in Fig. 3.22). This scenario resulted in the equalization of hydraulic heads between the shallow and the intermediate aquifer in the model. In order to maintain the hydraulic head difference between the two aquifers as observed at site M, an unrealistically high horizontal gradient across the intermediate aquifer and low heads at the northern general head boundary of the model had to be imposed. This conceptual model was, thus, discarded from further consideration.

In scenario (2), simulating a discontinuity in an otherwise non-leaky clay layer, the approach was to first set the vertical hydraulic conductivity of the clay to a value that would result in a typical confined aquifer drawdown, i.e. the Theis curve. The model was, thus, first run in a transient mode to test the clay layer conductivity values. The Theis drawdown was obtained using a clay K_z of 1×10^{-9} m/s everywhere (no recharge window). This K_z value is in the regular range of clay vertical conductivities (p.85, Fetter, 2001)

and was observed by Zheng et al. (2005) at the nearby site B. Model boundaries did not affect the Theis drawdown, and the model could accurately replicate this analytical solution. Next, parameters in the polygon overlying site T, and corresponding to the model layers in the clay, were changed to match those of the intermediate aquifer, while the rest of the clay vertical conductivities were maintained at 10^{-9} m/s (as in Table 3.7). The steady-state model with these parameters was fine-tuned to produce a distribution of hydraulic heads matching the observed initial heads in the field (Table 3.8), the errors ranging from <1 to 9 cm. The general head boundaries within the intermediate aquifer ranged from 3.45 m at southern edge of the model to 1.30 m at the northern edge, which was realistic given the field-observed lateral gradients (Fig. 3.16). The plan (at mid-depth through the intermediate aquifer) and a S-N view of the modeled steady state hydraulic heads are shown in Fig. 3.23. Note the locally elevated hydraulic heads beneath the recharge window and the increasing vertical hydraulic gradient across the clay layer with lateral distance away from the discontinuity.

The initial head 3D distribution produced above was fed into the transient model of the pumping test from the intermediate aquifer using the observed flow rates and pumping duration. A plan view of the hydraulic heads at mid-depth through the intermediate aquifer at final stages of the pumping, showing the drawdown cone, is presented in Fig. 3.24. The model managed to reproduce the major features of observed drawdown curves (Fig. 3.25), including the rapid stabilization of drawdown and the lack of induced drawdown in the shallow aquifer. Upon the cessation of pumping, hydraulic heads recovered to a level higher than the initial heads, likely due to being on a rising edge of the cyclical variations also noted during the stable segment of drawdown curves

and possibly related to tidal forcing. The model suggests that the lateral inflow of groundwater from site T area is realistic and that the hydraulic conductivity and storativity estimated from analytical models are reasonable. It also provides a constraint on the vertical conductivity of the thick clay layer, likely to be ~10^{-9} m/s.

3.7.4 Appendix References

Craig, H., 1961. Isotopic variations in meteoric waters. Science 133, 1702-1703.

Fetter, C.W., 2001. Applied Hydrogeology, 4th ed. Prentice Hall, Upper Saddle River, NJ.

Gonthier, G.J., 2007. A Graphical Method for Estimation of Barometric Efficiency from Continuous Data - Concepts and Applications to a Site in the Piedmont, Air Force Plant 6, Marietta, Georgia. U.S. Geological Survey Scientific Investigations Report 2007-5111, Reston, Virginia.

Zheng, Y., van Geen, A., Stute, M., Dhar, R., Mo, Z., Cheng, Z., Horneman, A., Gavrieli, I., Simpson, H.J., Versteeg, R., Steckler, M., Grazioli-Venier, A., Goodbred, S., Shahnewaz, M., Shamsudduha, M., Hoque, M.A., Ahmed, K.M., 2005. Geochemical and hydrogeological contrasts between shallow and deeper aquifers in two villages of Araihazar, Bangladesh: Implications for deeper aquifers as drinking water sources. Geochimica Et Cosmochimica Acta 69, 5203-5218.

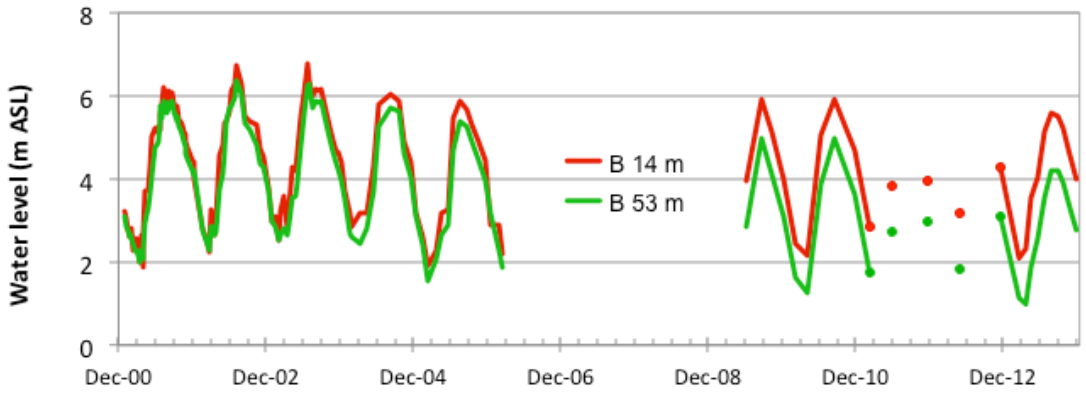

Figure 3.13. Long-term hydrographs from the nearby site B. Hydrographs collected at site B (Zheng et al., 2005) since 2000 demonstrate a growing water level contrast between the shallow (14 m bgl) and the intermediate (53 m bgl) aquifer, separated by two thin (<5 m) clay layers.

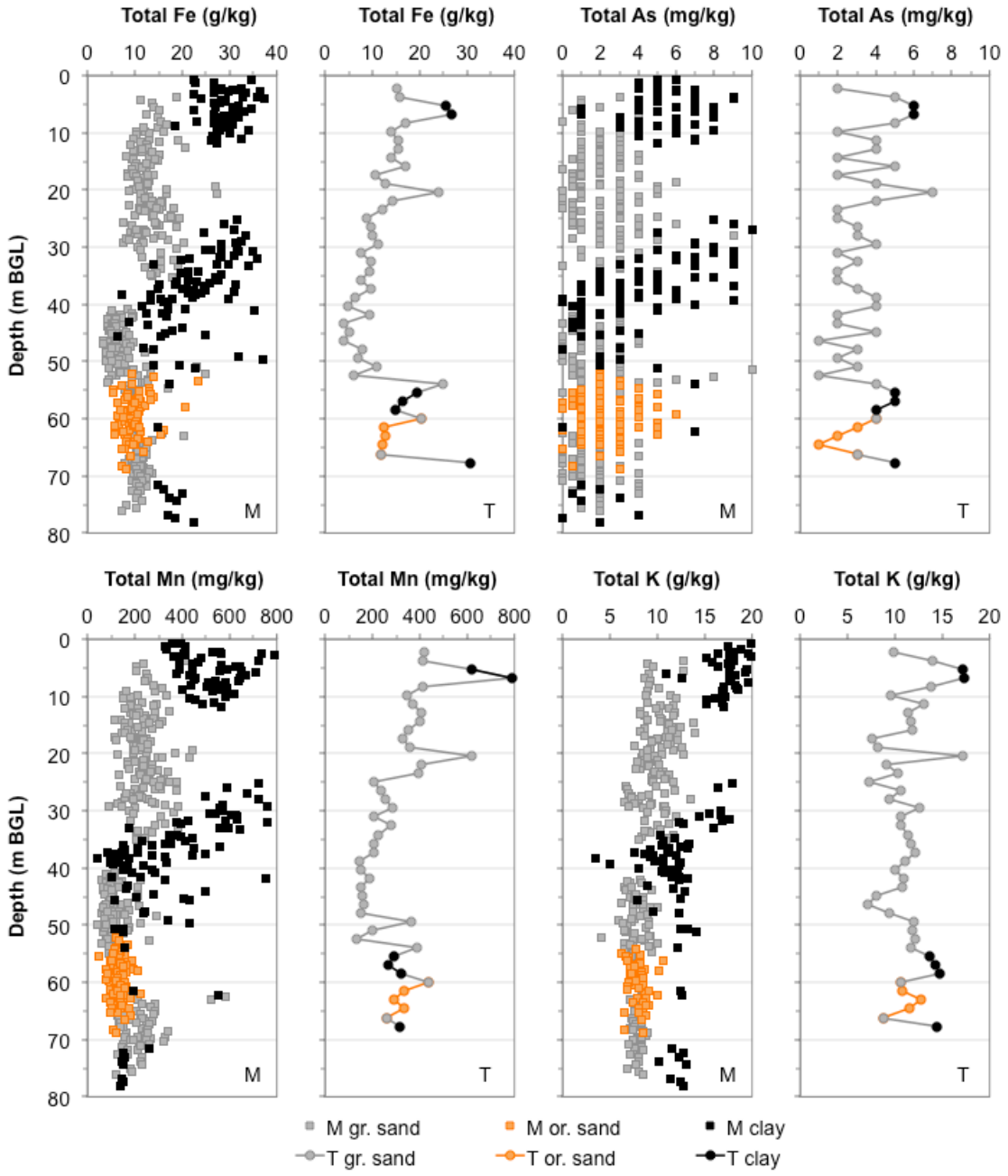

Figure 3.14. Additional vertical profiles of bulk sediment composition. Bulk sediment concentrations of Fe, As, Mn, and K in the sediment from sites M and T measured by a portable XRF instrument. Standard deviations of the XRF measurements are mostly smaller than the symbol size, except those of As that were ±1 ppm.

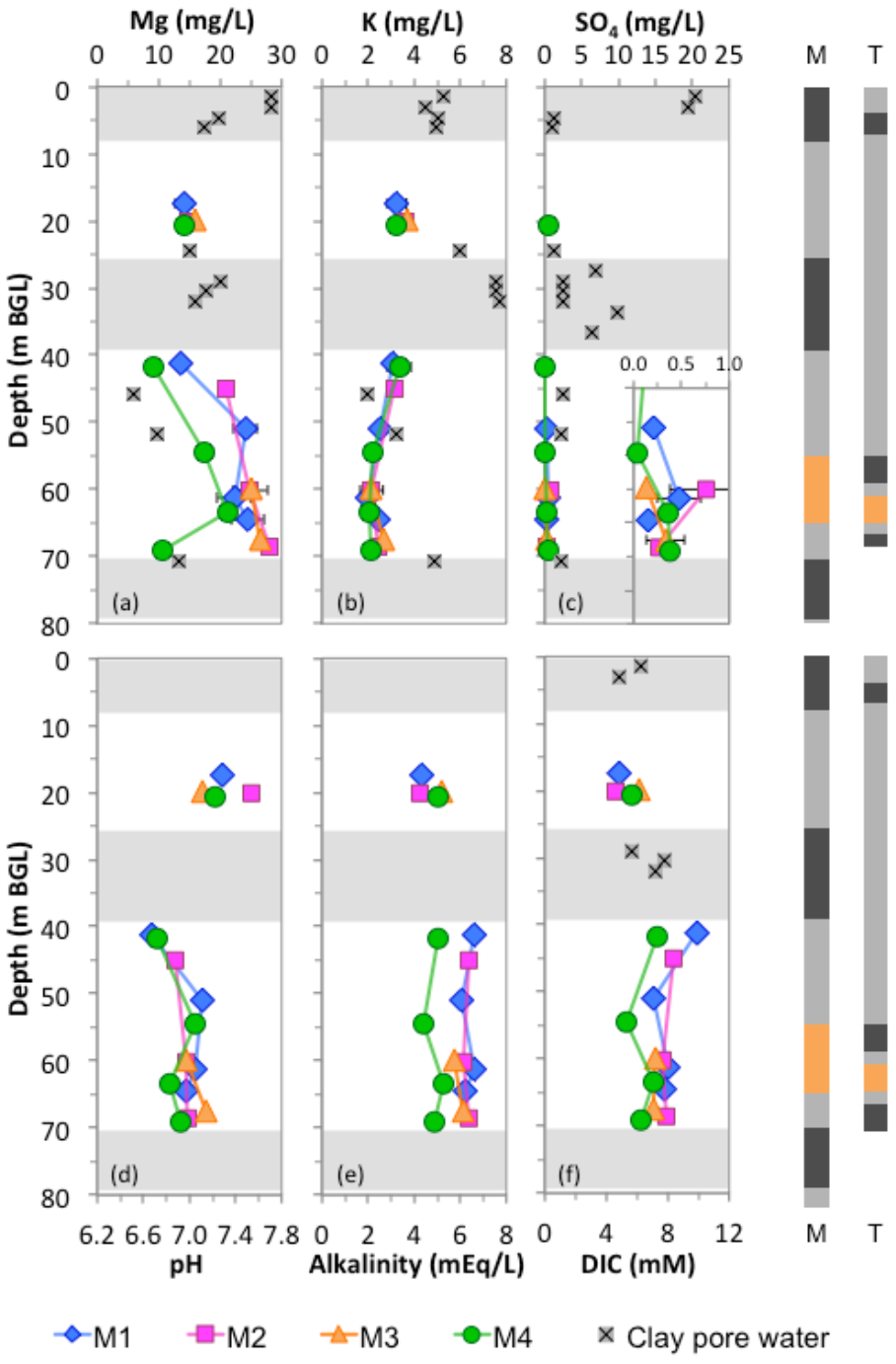

Figure 3.15. Additional vertical profiles of groundwater chemistry at well nests M1-4 and clay pore water squeezed from sediment cuttings recovered near well nest M1. Profiles of aqueous (a) Mg, (b) K, and (c) SO_4, (d) pH, (e) alkalinity, and (f) dissolved inorganic carbon (DOC). Averages and standard deviations of 5-12 samples (Mg and K),

or 4-8 samples (SO_4), are shown where available. Otherwise, an average of 1-3 samples is shown without error bars. Single time-point measurements of pH, alkalinity, and DIC are shown. A generic site litholog is displayed to the right of the profiles and the shading indicates the extent of major clay/silt layers encountered at the site.

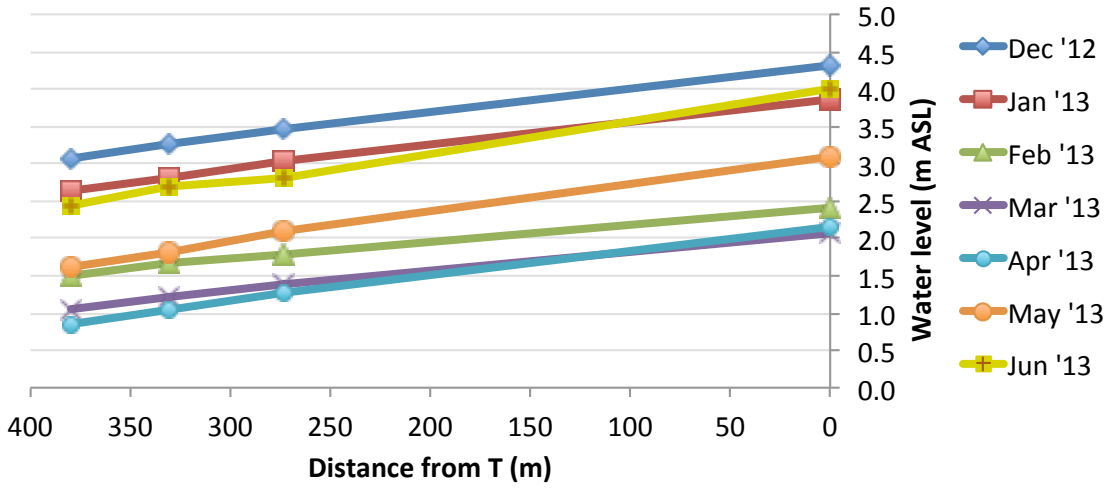

Figure 3.16. Nearly constant northward horizontal hydraulic gradient from site T to site M from December to June. Hydraulic heads plotted are from the bottom of the shallow aquifer at site T (T3, 52 m bgl) and from wells tapping the orange sand layer in the intermediate aquifer at site M, along the south-to-north transect: M3.5 (60 m bgl), M1.5 (61 m bgl), and M2.5 (60 m bgl). The horizontal gradient is on average ~3-4×10^{-3} (3-4 m/km).

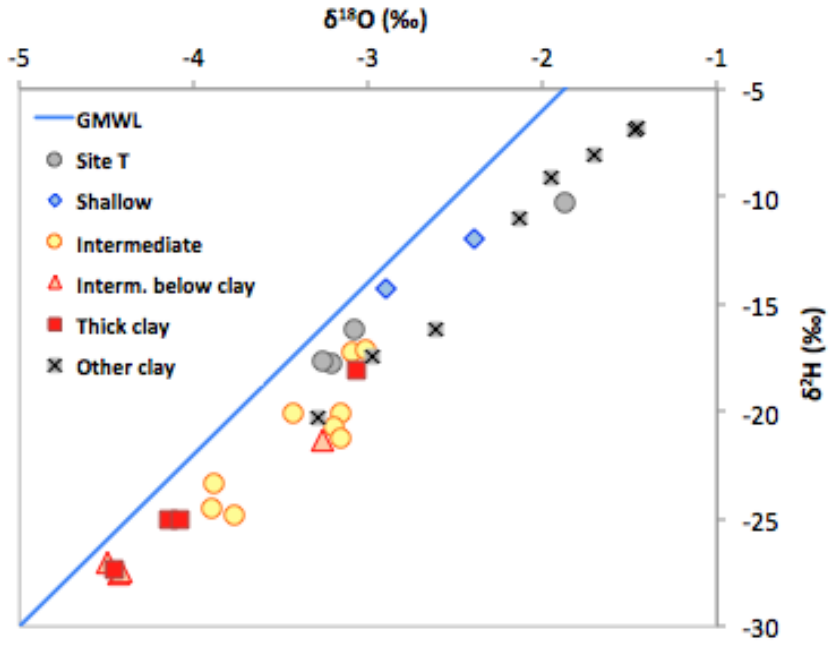

Figure 3.17. Stable isotopic composition ($\delta^{18}O$ and $\delta^{2}H$) of various types of groundwater and clay pore water from sites M and T, plotted along the Global Meteoric Water Line (GMWL). Note the similarity in stable isotope signatures from the thick clay layer at site M and the upper grey sand of the intermediate aquifer. Site T and shallow aquifer groundwater at site M are also closely aligned. The GMWL from Craig (1961).

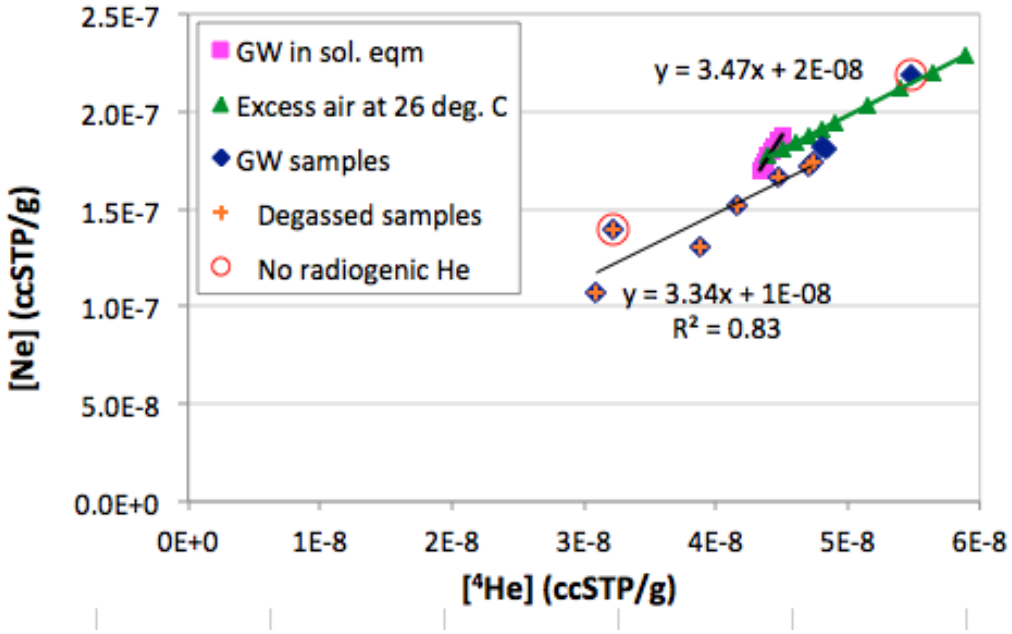

Figure 3.18. A plot of Ne vs. He (as ^{4}He) concentrations in site M groundwater showing the effects of degassing and radiogenic He contributions. Expected concentrations of Ne and He in solubility equilibrium with the atmosphere at a temperature range of 18-32 °C (pink symbols), and those with excess air at 26 °C (additional dissolution of bubbles with atmospheric concentrations, green line) are shown to aid the interpretation of observed groundwater concentrations. Most samples, except the two marked by circles, contain radiogenic He due to the excess of He relative to Ne. The majority of samples (marked by crosses) are also degassed, as their Ne concentrations are lower than that expected in the solubility equilibrium with atmosphere at 26 °C.

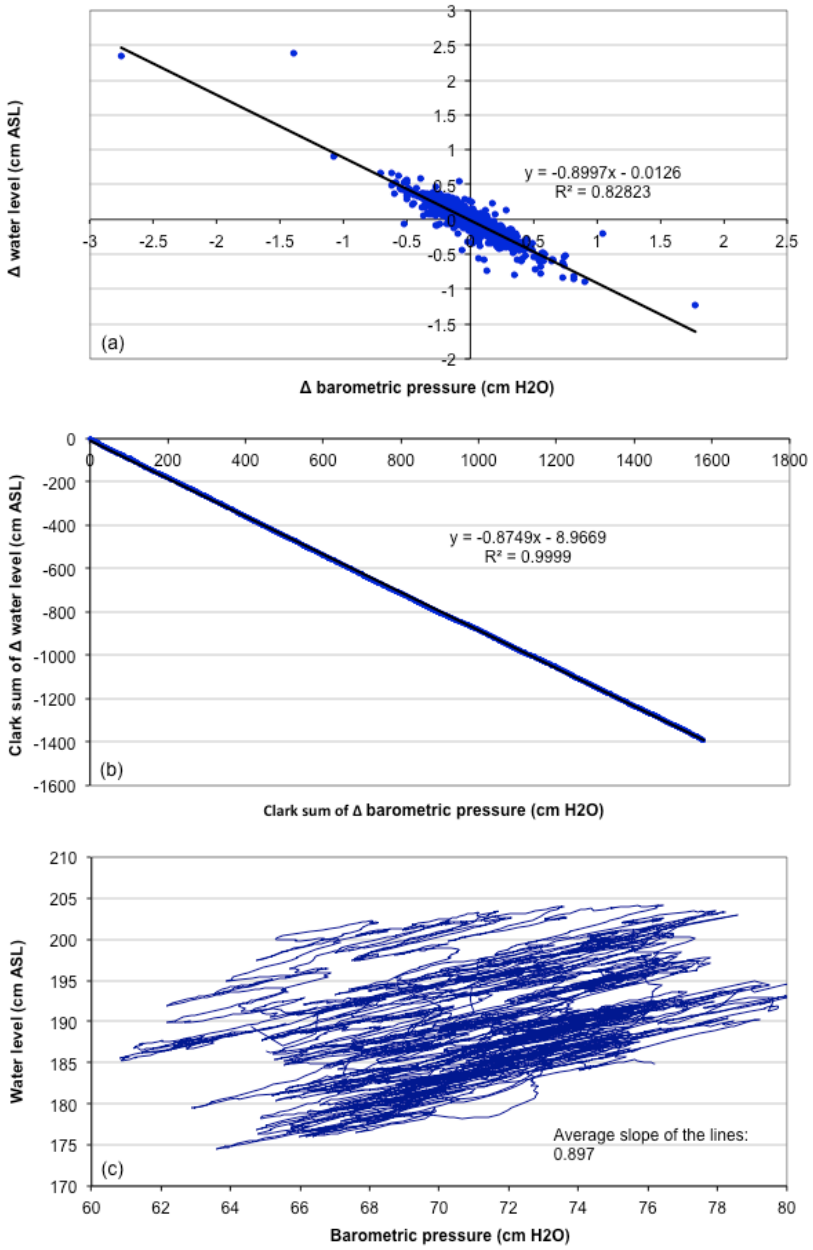

Figure 3.19. Graphs used to determine the barometric efficiency of the intermediate aquifer by (a) the slope method, (b) the Clark method, and (c) the graphic method. The methods are described in a USGS report by Gonthier (2007). The estimated barometric efficiency is 0.1, which means that the confining clay attenuates 10% of the atmospheric pressure change and transmits 90% of it to the aquifer, indicating a highly compressible unit.

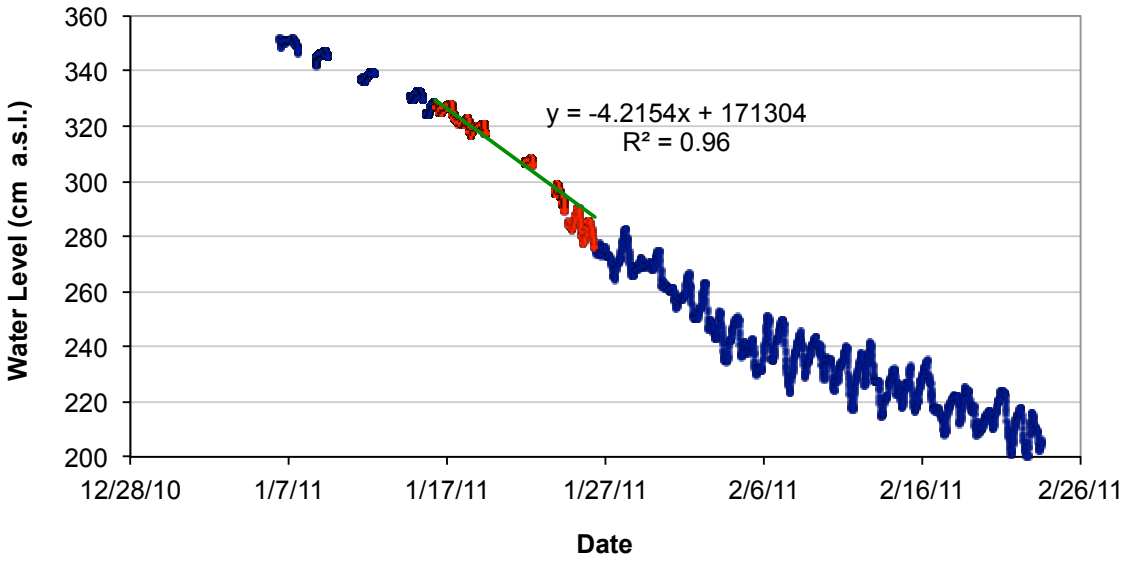

Figure 3.20. Declining seasonal water trend in the intermediate aquifer at the time of pumping tests. A linear fit (green line) of the pressure logger data from January 16-25 (shown in red) were used for the estimated seasonal trend of -4.2154 cm/day during the pumping test from intermediate aquifer performed January 19-22. The gaps in water level data occur at the times of pumping tests, which were not taken into account for the season trend estimate.

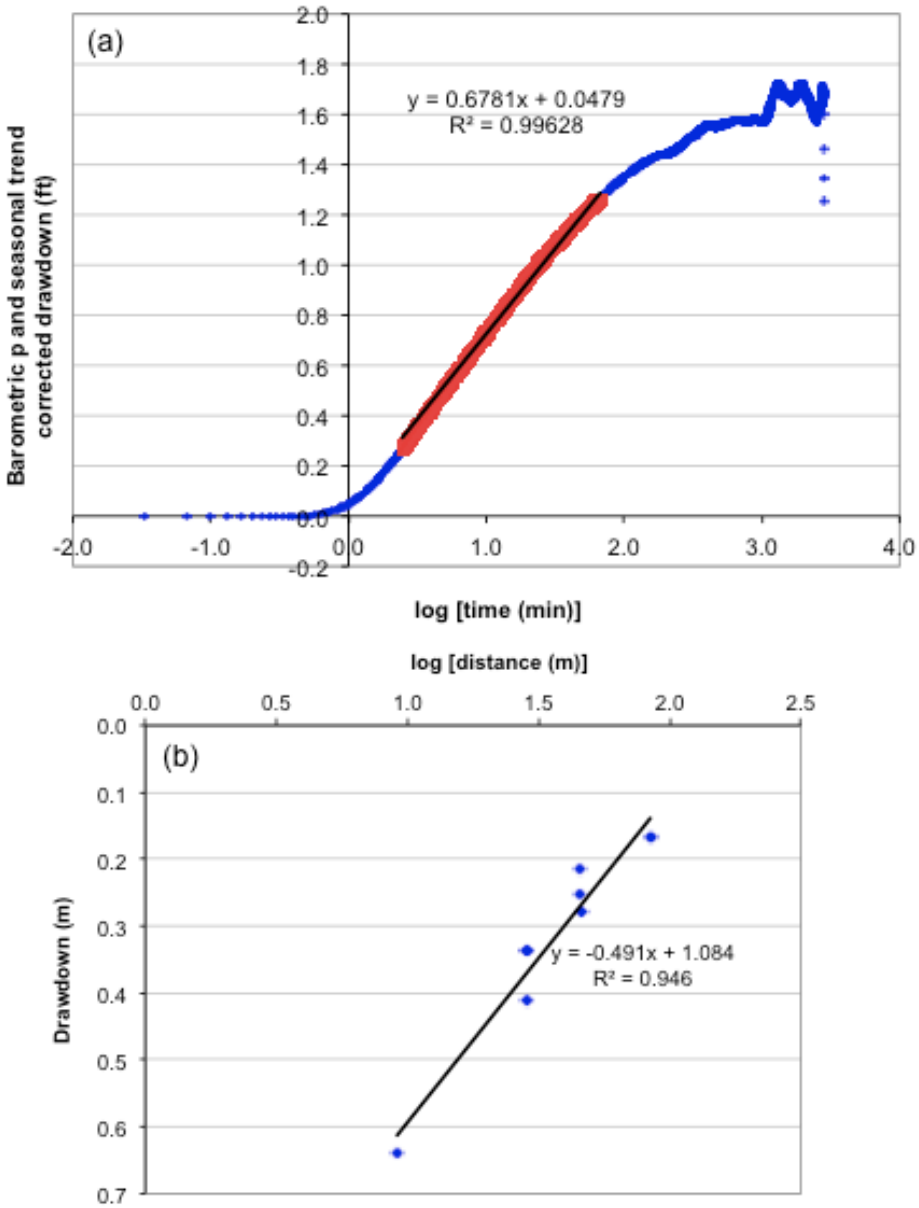

Figure 3.21. Examples of the methods used to determine hydraulic conductivity and storativity of the intermediate aquifer at early time points of the pumping test. (a) Time drawdown at well M1.5 in the intermediate aquifer with the data (red) used for the linear fit. (b) Distance drawdown method showing measured drawdown across different wells at t = 100 min of the pumping test. The values from different observation wells are reported in Table 3.6.

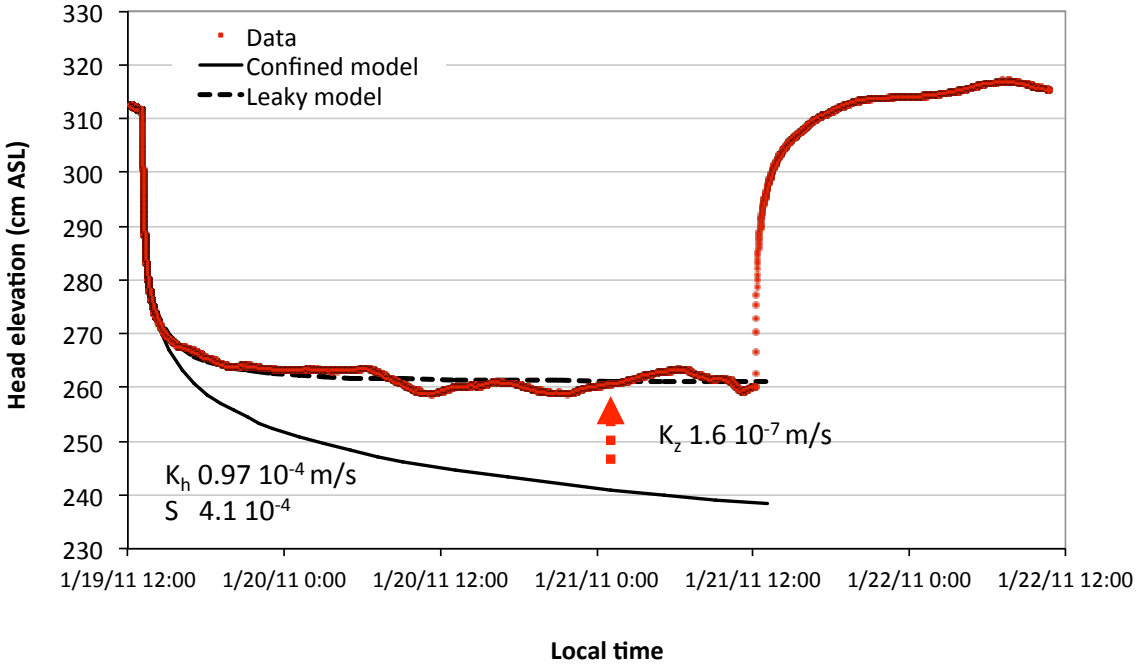

Figure 3.22. Example of analytical models for the confined aquifer (Theis solution) and leaky confined aquifer (Hantush-Jacob solution) used to fit the observed drawdown in M1.5 tapping the intermediate aquifer when pumping from the same aquifer. All hydraulic heads were corrected for barometric pressure fluctuations and the seasonal water level trend. The indicated values of horizontal hydraulic conductivity (K_h) and storativity (S) of the intermediate aquifer were obtained by linear fits of early time drawdown data (as in Figure 3.20a). The value for vertical hydraulic conductivity in the thick clay (K_z) was visually estimated from the plot. Instead of a leaky confining unit, an alternative explanation for the reduced drawdown, relative to that expected in a confined aquifer, would be a discontinuity in the clay layer at some lateral distance away.


Head : 1/21/2011 12:10:00 PM
4.08
3.83
3.58
3.33
3.08
2.83
2.58
2.33
2.08
1.83
1.58
1.33
Site B
Site T
Image © 201 DigitalGlobe

(a)

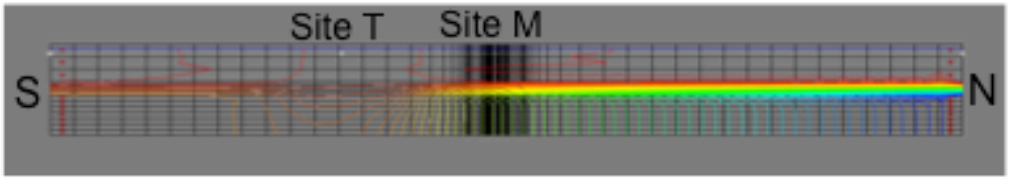
Site T
Site M
S
N

(b)

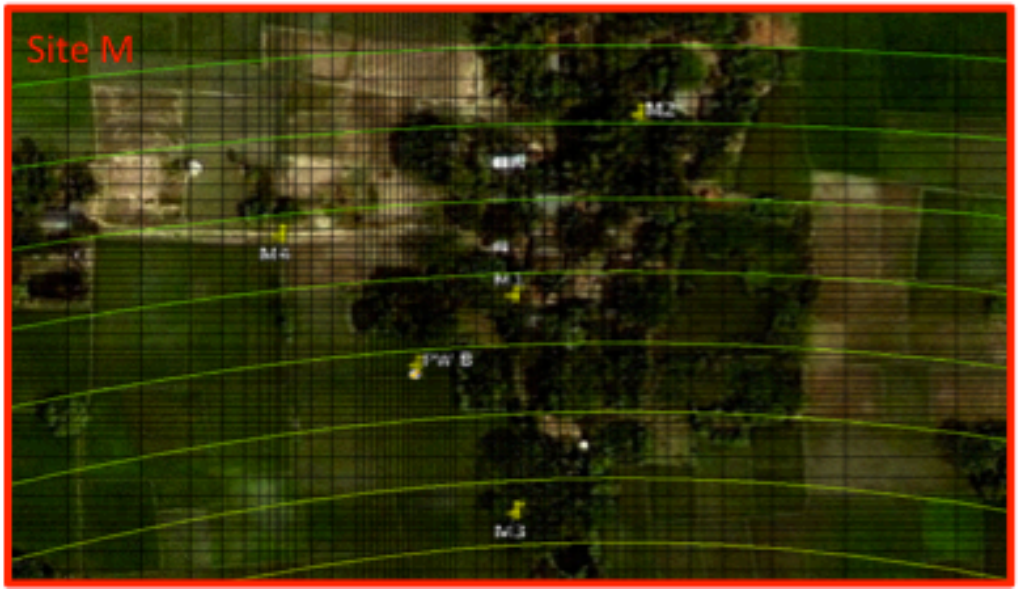
Site M

(c)

Figure 3.23. Steady state (initial) hydraulic heads in the MODFLOW model. (a) Plan view of the modeled area and the grid. Site M is located at the center of the refined grid, while site T is in the middle of the recharge polygon shown in white. Hydraulic heads contours are shown for layer 13, mid-depth through the intermediate aquifer. Vertical hydraulic conductivity in the clay is set to a low value ($K_z = 10^{-9}$ m/s) everywhere except in the white polygon, where K_z equals that of the intermediate aquifer (1.2×10^{-5} m/s). Note the elevated heads near the recharge polygon. (b) South-North transect through the middle of the model, showing the vertical distribution of hydraulic heads. Note the increasing vertical hydraulic gradient across the clay with distance from the discontinuity. (c) Plan view of the initial heads at site M, zoomed in from (a).

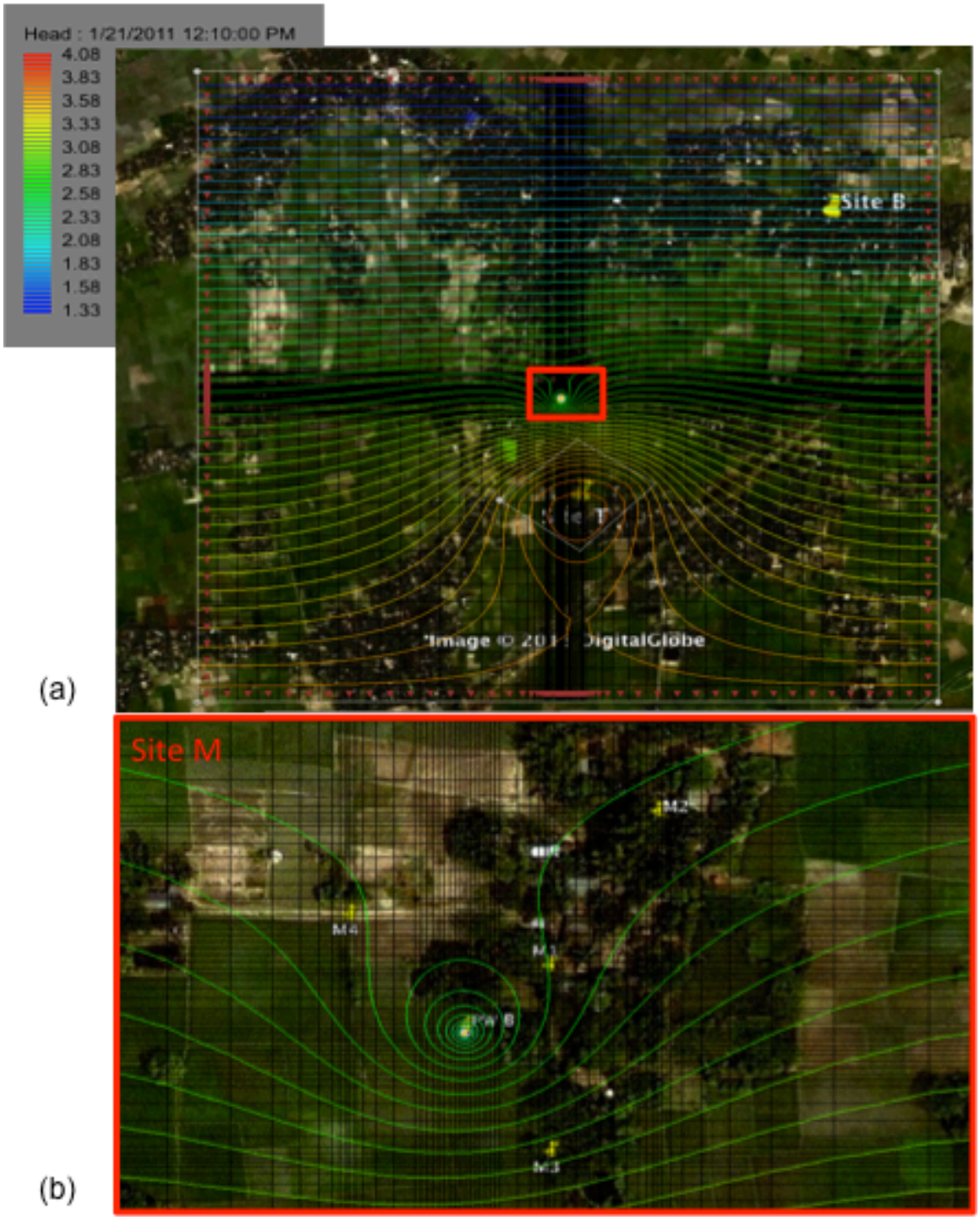

Figure 3.24. MODFLOW modeled hydraulic heads in the intermediate aquifer during the pumping test. Plan view of (a) the entire grid and (b) the site M area after ~47 hr of pumping, just before the pump was turned off for the recovery phase. All model parameters and hydraulic heads shown as in Figure 3.22.

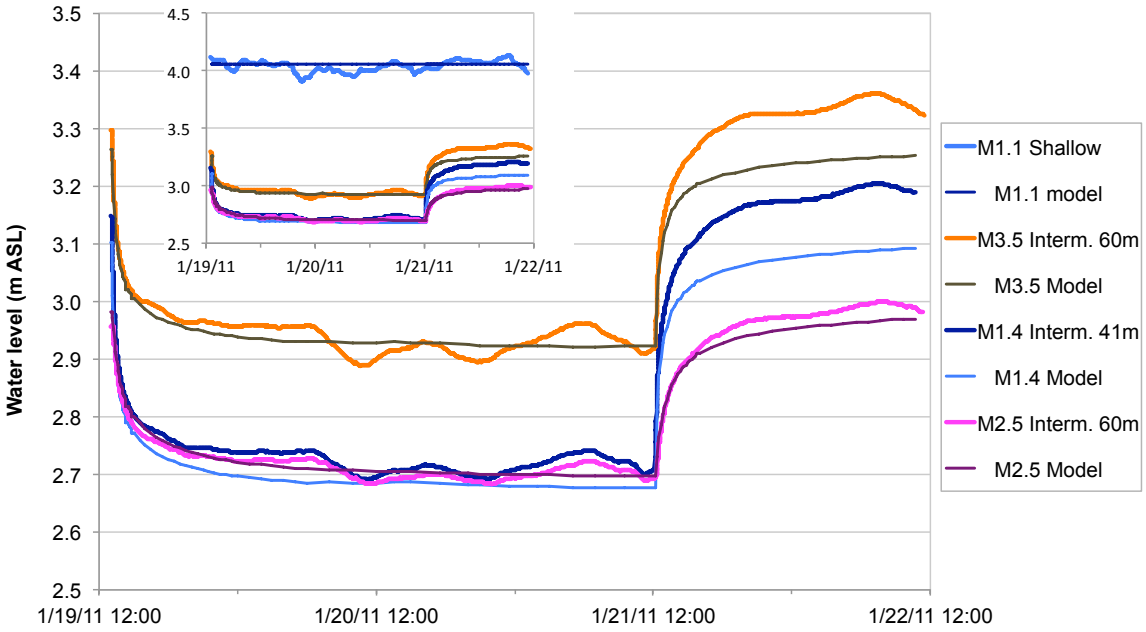

Figure 3.25. MODFLOW model fits (thin lines) of the observed drawdown in select monitoring wells across site M. The inset shows hydraulic heads in the shallow aquifer (M1). Major features are reproduced, except the water level recovery upon the cessation of pumping to hydraulic heads above their initial values. This feature is related to the semi-diurnal cycles not subtracted from the background, also visible during the stable segment of the drawdown curves, and likely related to the tidal forcing.

Table 3.1. Radiocarbon dating and ^{13}C analysis of the sediment samples.

Well nest	Depth (m)	C phase	% OC[a]	^{14}C FM[b] ± σ	^{14}C age (ka BP)	$\delta^{13}C$ (‰PDB)	NOSAMS #[c]
2	29.9	clay TOC[d]	0.61	0.5244 ± 0.0027	5.18 ± 0.04	-23.36	OS-103433
2	34.1	clay TOC	0.41	0.4120 ± 0.0034	7.12 ± 0.07	-23.68	OS-103479
4	36.9	leaves	-	0.3384 ± 0.0015	8.70 ± 0.04	-28.92	OS-91989
4	36.9	clay TOC	5.78	0.3399 ± 0.0018	8.67 ± 0.04	-29.01	OS-91887
1	37.2	charcoal	-	0.3897 ± 0.0018	7.57 ± 0.04	-28.29	OS-91885
2	37.2	wood	-	0.3506 ± 0.0022	8.42 ± 0.05	-29.59	OS-91886
2	37.2	clay TOC	6.53	0.3483 ± 0.0015	8.47 ± 0.04	-29.03	OS-91888
3	39.3	leaves	-	0.3443 ± 0.0015	8.57 ± 0.04	-30.25	OS-91942
2	50.6	clay TOC	0.32	0.2474 ± 0.0014	11.20 ± 0.05	-15.44	OS-92087
C	51.2	clay TOC	0.27	0.2243 ± 0.0013	12.00 ± 0.05	-14.94	OS-91944
2	73.8	clay TOC	0.10	0.1176 ± 0.0009	17.20 ± 0.07	-21.91	OS-92782
C	79.2	clay TOC	0.19	0.0110 ± 0.0022	36.20 ± 1.60	-19.80	OS-91949
T	43.3	clay TOC	n/a	0.3605 ± 0.0017	8.20 ± 0.04	-29.31	OS-98335
T	58.5	clay TOC	n/a	0.1963 ± 0.0016	13.10 ± 0.07	-10.98	OS-98597
T	67.7	clay TOC	n/a	0.0456 ± 0.0016	24.80 ± 0.28	-11.70	OS-98598

[a] % OC Is organic carbon as a percentage of total sediment mass (clay TOC samples only)

[b] FM is "fraction modern". ^{14}C FM of 1 indicates ^{14}C age of 0

[c] NOSAMS # is the tracking number at the National Ocean Science Accelerator Mass-Spectrometer facility

[d] TOC stands for "total organic carbon" i.e. bulk sedimentary OC

n/a = not analyzed

Table 3.2. (part I): Groundwater and pore water chemical and physical parameters

Well	Depth (m)	Na (mg/L)	± σ	Mg (mg/L)	± σ	Si (mg/L)	± σ	P (mg/L)	± σ	K (mg/L)	± σ	Ca (mg/L)	± σ	Mn (µg/L)	± σ	Fe (mg/L)	± σ	As (µg/L)	± σ	Sr (µg/L)	± σ	Ba (µg/L)	± σ	Cl (mg/L)	± σ	F (mg/L)	± σ	SO_4 (mg/L)	± σ
M1.1	17.5	13	2	14	1	32	3	1.6	0.4	3.2	0.4	43	5	503	116	8.6	2.1	182	20	72	6	88	16	7.3	1.2	0.17	0.04	n/d	n/d
M1.4	41.1	52	2	14	0	43	3	1.1	0.2	3.1	0.1	28	2	41	8	10.4	2.4	45	10	92	5	149	16	12.0	0.7	0.25	0.04	n/d	n/d
M1.4a	50.9	19	2	24	2	31	2	0.7	0.1	2.6	0.2	57	3	108	30	9.6	2.3	248	37	161	4	184	13	19.7	1.5	0.29	0.04	0.20	-
M1.5	61.3	12	2	22	3	38	4	0.1	0.1	2.0	0.3	57	6	391	104	0.8	0.9	2	3	151	6	129	8	8.3	1.0	0.41	0.04	0.47	0.23
M1.6	64.5	14	1	24	3	37	4	0.2	0.1	2.4	0.3	64	4	434	90	1.0	0.6	5	1	179	14	162	22	7.0	0.6	0.44	0.05	0.16	-
M2.1	20.1	11	-	15	-	34	-	2.0	-	3.6	-	44	-	768	-	8.4	-	127	-	69	-	97	-	8.4	-	0.17	-	n/d	n/d
M2.4	44.9	40	2	21	1	42	3	0.7	0.1	3.1	0.1	46	1	170	39	8.2	1.1	54	7	149	6	185	13	8.3	0.4	0.24	0.02	n/d	n/d
M2.5	60.1	16	1	25	3	46	4	0.1	0.0	2.1	0.5	57	4	935	132	0.8	0.5	3	4	162	6	154	15	7.8	0.7	0.30	0.04	0.76	0.38
M2.6	68.6	18	-	28	-	35	-	0.1	-	2.4	-	65	-	597	-	1.6	-	2	-	176	-	143	-	6.7	-	0.32	-	0.27	-
M3.1	19.9	11	-	16	-	24	-	1.3	-	3.7	-	62	-	681	-	8.1	-	266	-	94	-	113	-	5.7	-	0.19	-	n/d	n/d
M3.5	59.8	14	-	25	-	34	-	0.1	-	2.2	-	61	-	900	-	0.3	-	3	-	n/a	n/a	35	-	7.9	-	0.40	-	0.13	-
M3.6	67.4	12	-	26	-	35	-	0.1	-	2.6	-	62	-	333	-	0.7	-	2	-	168	-	93	-	8.0	-	0.45	0.03	0.34	0.20
M4.1	20.6	12	1	14	1	28	3	1.8	0.5	3.2	0.2	52	4	1087	276	5.9	2.2	298	66	89	13	69	15	3.6	0.8	0.27	0.02	0.44	-
M4.4	41.8	69	4	9	1	41	7	1.3	0.3	3.4	0.5	20	1	129	54	10.4	4.7	18	3	59	2	140	24	18.8	1.4	0.28	0.07	0.12	-
M4.5	54.5	20	4	17	1	40	5	0.2	0.1	2.2	0.1	48	6	152	76	2.3	1.3	11	2	126	8	182	13	9.7	1.3	0.30	0.04	0.04	-
M4.6	63.5	27	-	21	-	43	-	0.0	-	2.0	-	48	-	203	-	0.3	-	2	-	n/a	n/a	97	-	6.3	-	0.35	-	0.36	-
M4.6a	69.2	82	-	11	-	51	-	0.2	-	2.1	-	29	-	389	-	5.2	-	5	-	60	-	60	-	6.4	0.3	0.29	0.07	0.39	-
M1 CLAY	1.5	59		28		37		0.1		5.2		70		718		4.9		16		94		228		47.3		0.18		20.36	
M1 CLAY	3.0	36		28		36		0.4		4.5		68		897		2.0		42		88		139		87.2		0.26		19.52	
M1 CLAY	4.6	27		20		42		0.1		5.1		50		213		0.2		47		81		126		44.7		0.20		1.17	
M1 CLAY	6.1	29		17		41		0.4		4.9		44		133		0.2		64		81		113		28.5		0.22		0.90	
M1 CLAY	24.4	25		15		39		0.0		6.0		39		169		0.1		88		74		111		13.0		0.13		1.30	
M1 CLAY	27.4	n/a		n/a		n/a		n/a		n/a		n/a		n/a		n/a		n/a		n/a		n/a		34.7		0.21		7.00	
M1 CLAY	29.0	56		20		60		0.9		7.6		66		226		3.8		175		126		173		26.6		0.18		2.43	
M1 CLAY	30.5	103		18		70		1.1		7.6		51		241		6.5		141		107		145		29.8		0.19		2.35	
M1 CLAY	32.0	107		16		63		0.9		7.7		32		186		4.5		95		80		137		31.7		0.18		2.54	
M1 CLAY	33.5	n/a		n/a		n/a		n/a		n/a		n/a		n/a		n/a		n/a		n/a		n/a		63.2		0.19		9.95	
M1 CLAY	36.6	n/a		n/a		n/a		n/a		n/a		n/a		n/a		n/a		n/a		n/a		n/a		52.8		0.27		6.46	
M1 CLAY	45.7	21		6		18		n/d		2.0		11		48		0.0		3		33		67		27.2		0.24		2.43	
M1 CLAY	51.8	21		10		16		n/d		3.2		20		62		0.1		27		57		95		59.8		0.25		2.31	
M1 CLAY	70.7	45		13		45		0.1		4.8		26		119		1.4		21		81		162		25.8		0.22		2.14	
T1	9.8	20		16		29		2.6		5.2		58		230		9.6		75		105		117		24.3		0.19		3.09	
T2	20.6	25		19		29		0.9		3.1		47		1269		12.2		27		71		117		27.7		0.10		23.46	
T3	52.2	22		26		26		0.9		3.5		40		173		3.2		6		102		57		9.5		0.55		0.24	
T4	63.1	15		29		27		0.2		2.4		41		1362		1.7		9		93		34		16.4		0.36		n/d	

" - " means std. deviation was not calculated because only 1-3 monthyl samples were averaged

n/a = not analyzed

n/d = not detected

Table 3.2. (part II): Groundwater and pore water chemical and physical parameters; also slug test results.

Well	Depth (m)	NH_3 (mg/L N)	Alk. (mEq/L)	DIC (mM)^	DOC (mM)*	% reactive DOC	Cond. (mS/cm)	pH	eH	Temp. (C)	$\delta^{18}O$ (‰)	± σ	$\delta^{2}H$ (‰)	± σ	Slug test K_h (m/s)
M1.1	17.5	1.45	4.3	4.8	0.15	35.1	0.459	7.29	-163.5	n/a	n/a	n/a	n/a	n/a	Oscill.[&]
M1.4	41.1	10.43	6.6	9.9	0.45	18.7	0.655	6.68	-122.9	26.34	-4.43	0.02	-27.54	0.03	Oscill.
M1.4a	50.9	2.62	6.0	7.1	0.41	14.0	0.679	7.11	-171.3	26.37	-3.26	0.04	-21.32	0.08	n/a
M1.5	61.3	0.08	6.6	8.0	0.17	-3.5	0.612	7.05	-54.6	26.52	-3.16	0.01	-20.05	0.09	4.53E-5
M1.6	64.5	0.22	6.2	7.8	0.20	6.8	0.634	6.97	-69.6	26.63	-3.20	0.04	-20.73	0.02	2.00E-5
M2.1	20.1	n/a	4.3	4.6	n/a	n/a	0.425	7.54	-165.9	n/a	n/a	n/a	n/a	n/a	n/a
M2.4	44.9	5.38	6.4	8.4	0.35	n/a	0.668	6.87	-112.0	26.30	-4.49	0.02	-27.04	0.10	6.56E-5
M2.5	60.1	0.21	6.1	7.6	0.15	n/a	0.607	6.97	-32.8	26.39	-3.09	0.02	-17.20	0.07	1.49E-5
M2.6	68.6	n/a	6.4	7.9	n/a	n/a	0.635	6.98	-66.8	26.50	-3.15	0.03	-21.23	0.02	n/a
M3.1	19.9	n/a	5.2	6.1	n/a	n/a	0.564	7.12	-160.6	26.20	-2.39	0.02	-12.02	0.07	n/a
M3.5	59.8	n/a	5.7	7.1	n/a	n/a	0.572	6.97	-67.8	26.16	-3.02	0.02	-17.15	0.02	4.36E-5
M3.6	67.4	n/a	6.1	7.1	n/a	n/a	0.611	7.15	-78.0	26.18	-3.44	0.01	-20.13	0.05	n/a
M4.1	20.6	0.92	5.0	5.7	0.20	n/a	0.514	7.22	-168.2	26.46	-2.90	0.01	-14.25	0.04	22.0 E-5
M4.4	41.8	4.7	5.1	7.3	0.30	n/a	0.604	6.72	-90.0	26.69	-4.41	0.01	-27.45	0.06	0.71E-5
M4.5	54.5	0.33	4.4	5.3	0.14	n/a	0.472	7.05	-82.0	26.43	-3.77	0.04	-24.86	0.10	3.87E-5
M4.6	63.5	n/a	5.3	7.1	n/a	n/a	0.538	6.83	-50.3	26.56	-3.90	0.03	-24.55	0.01	n/a
M4.6a	69.2	n/a	4.9	6.2	n/a	n/a	0.501	6.92	-68.0	26.65	-3.89	0.04	-23.32	0.09	n/a
M1 CLAY	1.5			6.3	0.60	52.9					-1.95	0.03	-9.17	0.13	
M1 CLAY	3.0			4.8	0.57	52.8					-2.14	0.03	-10.98	0.02	
M1 CLAY	4.6			n/a	0.69	n/a					-1.46	0.06	-6.82	0.24	
M1 CLAY	6.1			n/a	0.60	n/a					-1.47	0.04	-6.91	0.23	
M1 CLAY	24.4			n/a	0.72	n/a					-1.71	0.02	-8.12	0.08	
M1 CLAY	27.4			n/a	n/a	n/a					n/a	n/a	n/a	n/a	
M1 CLAY	29.0			5.7	1.75	41.1					-4.15	0.06	-25.01	0.19	
M1 CLAY	30.5			7.7	1.80	24.1					-4.45	0.05	-27.35	0.20	
M1 CLAY	32.0			7.2	1.88	14.8					-4.08	0.02	-25.07	0.23	
M1 CLAY	33.5			n/a	n/a	n/a					-3.06	0.01	-18.12	0.07	
M1 CLAY	36.6			n/a	n/a	n/a					n/a	n/a	n/a	n/a	
M1 CLAY	45.7			n/a	n/a	n/a					-3.29	0.01	-20.27	0.14	
M1 CLAY	51.8			n/a	n/a	n/a					-2.61	0.02	-16.20	0.06	
M1 CLAY	70.7			n/a	1.21	n/a					-2.97	0.07	-17.40	0.09	
T1	9.8			5.3	0.20		0.481	7.58	-88.5	25.73	-3.21	0.02	-17.75	0.12	
T2	20.6			6.2	0.22		0.535	7.71	-117.9	25.81	-1.88	0.14	-10.27	1.08	
T3	52.2			6.7	0.33		0.554	7.82	-99.9	25.85	-3.08	0.07	-16.21	0.80	
T4	63.1			5.4	0.11		0.495	7.73	-43.8	25.90	-3.26	0.01	-17.63	0.04	

^DIC values for site M nests 1-4 were calculated from pH and alkalinity measured simultaneously in the field.
DIC in M1 clay pore water was measured on the Shimadzu carbon analyzer. DIC at site T was measured by NOSAMS
*DOC values were measured on the Shimadzu carbon analyzer, except at site T (measured by NOSAMS)
[&]Oscillating water level during slug test
n/a = not analyzed

Table 3.3. Radiocarbon dating and ^{13}C analysis of dissolved inorganic and organic carbon (DIC and DOC) in groundwater

Well	Depth (m)	DIC ^{14}C Fm[a]	± σ	DIC ^{14}C age (yr)	± σ	DIC $\delta^{13}C$ (‰)	NOSAMS #[b]	DOC ^{14}C FM	± σ	DOC ^{14}C age (yr)	± σ	DOC $\delta^{13}C$ (‰)	NOSAMS #
M4.1	20.6	0.9607	0.0034	320	30	-7.1	OS-89968	0.8114	0.0030	1680	30	-23.9	OS-102042
M1 CLAY	29.0	n/a	n/a	n/a	n/a	n/a	n/a	0.6821	0.0027	3070	30	-25.8	OS-101625
M1 CLAY	30.5	n/a	n/a	n/a	n/a	n/a	n/a	0.8147	0.0024	1650	25	-26.0	OS-101626
M1 CLAY	32.0	n/a	n/a	n/a	n/a	n/a	n/a	0.6629	0.0018	3300	20	-25.7	OS-102082
M1.4	41.1	0.6705	0.0025	3210	30	-4.0	OS-90067	0.6110	0.0032	3960	40	-29.7	OS-101494
M4.4	41.8	0.6278	0.0022	3740	25	-5.7	OS-89969	0.5369	0.0023	4990	35	-32.2	OS-102041
M1.4a	50.9	n/a	n/a	n/a	n/a	n/a	n/a	0.8521	0.0021	1280	20	-26.8	OS-101813
M4.5	54.5	0.8774	0.0027	1050	25	-16.1	OS-90175	0.8289	0.0019	1510	20	-25.3	OS-102065
M1.5	61.3	0.9312	0.0030	570	25	-16.6	OS-90066	0.8259	0.0021	1540	20	-24.9	OS-101857
M4.6	63.5	0.8592	0.0028	1220	25	-16.2	OS-90173	0.9748	0.0027	205	20	-27.6	OS-102111
M1.6	64.5	0.9018	0.0034	830	30	-17.1	OS-90176	0.8304	0.0027	1490	25	-25.0	OS-101682
T1	9.8	0.9682	0.0023	260	20	-11.9	OS-100759	0.8163	0.0025	1630	25	-16.4	OS-102154
T2	20.6	0.9967	0.0024	25	20	-17.1	OS-100760	0.8451	0.0029	1350	25	-26.8	OS-102130
T3	52.2	0.8549	0.0023	1260	20	-11.3	OS-100762	0.6589	0.0028	3350	35	-28.0	OS-102233
T4	63.1	0.8909	0.0029	930	25	-14.8	OS-100764	0.7432	0.0023	2380	25	-25.9	OS-102414

[a] FM is "fraction modern". ^{14}C FM of 1 indicates ^{14}C age of 0

[b] NOSAMS # is the tracking number at the National Ocean Science Accelerator Mass-Spectrometer facility

n/a = not analyzed

Table 3.4. $^3H/^3He$ dating parameters and ages calculated using radiogenic He correction (except where noted)

Well ID	Depth	^3H	± 1σ	^4He	Ne	δ^3He ^	$^3H + {}^3He$	$^3H/^3He$ age*	± 1σ corr.*	± 1σ anal.[&]
	m	TU	TU	$x10^{-8}$ ccSTP g^{-1}	$x10^{-8}$ ccSTP g^{-1}	%	TU	years	years	years
M1.1	17.5	n/a	n/a	n/a	n/a	n/a	n/a	n/a	n/a	n/a
M1.4	41.1	0.09	0.03	n/a	n/a	n/a	n/a	n/a	n/a	n/a
M1.4a	50.9	1.61	0.05	n/a	n/a	n/a	n/a	n/a	n/a	n/a
M1.5	61.3	2.04	0.06	4.47	16.64	50.1	18.2	39.2	1.9	0.4
M1.6	64.5	0.54	0.03	4.73	17.40	20.1	8.4	49.1	1.4	1.0
M2.1	20.1	n/a	n/a	n/a	n/a	n/a	n/a	n/a	n/a	n/a
M2.4	44.9	0.06	0.03	n/a	n/a	n/a	n/a	n/a	n/a	n/a
M2.5	60.1	1.22	0.05	4.84	18.03	7.2	5.5	27.0	-	0.6
M2.6	68.6	0.13	0.03	4.70	17.20	-3.5	1.3	40.5	1.8	4.2
M3.1[$]	19.9	1.89	0.06	5.47	21.92	24.3	9.7	29.3	-	0.4
M3.5	59.8	2.68	0.06	3.10	10.75	0.2	4.8	10.6	0.0	0.3
M3.6	67.4	1.21	0.05	3.89	13.06	0.7	4.9	24.9	0.1	0.6
M4.1	20.6	1.94	0.05	4.81	18.17	34.4	13.1	34.2	-	0.4
M4.4	41.8	-0.01	0.03	n/a	n/a	n/a	n/a	n/a	n/a	n/a
M4.5[$]	54.5	0.81	0.04	3.21	13.91	8.5	3.3	25.0	3.0	0.6
M4.6	63.5	0.08	0.03	4.15	15.22	5.6	3.7	68.6	1.2	6.2
M4.6a	69.2	0.18	0.03	n/a	n/a	n/a	n/a	n/a	n/a	n/a

^δ^3He is a % difference from the atmospheric $^3He/^4He$ ratio

*The $^3H/^3He$ age is a mean of three ages calculated from degassing corrections, and 1σ corr. is the standard deviation of the mean. Samples M2.5, M3.1, and M4.1 were not degassed (-)

[&]Standard error propagated from the analytical measurements alone, excluding degassing corrections

[$]Samples M3.1 and M4.5 were not corrected for radiogenic He contribution to the $^3He/^4He$ ratio

n/a = not analyzed

Table 3.5. $^{3}H/^{3}He$ ages and errors calculated without radiogenic He corrections, assuming degassing occurred either at time of sampling (with a range of corrections) or at time of recharge

Well ID	Depth m	$^{3}H/^{3}He$ age* years	± 1σ corr.* years	$^{3}H/^{3}He$ age ^ years	± 1σ anal.[&] years
M1.1	17.5	n/a	n/a	n/a	n/a
M1.4	41.1	n/a	n/a	n/a	n/a
M1.4a	50.9	n/a	n/a	n/a	n/a
M1.5	61.3	37.4	2.1	35.2	0.5
M1.6	64.5	44.9	1.8	42.5	1.0
M2.1	20.1	n/a	n/a	n/a	n/a
M2.4	44.9	n/a	n/a	n/a	n/a
M2.5	60.1	19.3	-	19.3	0.8
M2.6	68.6	ND	ND	ND	ND
M3.1	19.9	29.3	-	29.3	0.5
M3.5	59.8	2.8	0.1	0.2	0.6
M3.6	67.4	7.3	0.4	2.2	1.1
M4.1	20.6	32.0	-	32.0	0.5
M4.4	41.8	n/a	n/a	n/a	n/a
M4.5	54.5	25.0	3.0	18.9	0.9
M4.6	63.5	57.5	2.3	50.5	6.1
M4.6a	69.2	n/a	n/a	n/a	n/a

*The $^{3}H/^{3}He$ age is a mean of three ages calculated from degassing corrections, and 1σ corr. is the standard deviation of the mean. Samples M2.5, M3.1, and M4.1 were not degassed (-)

^ The $^{3}H/^{3}He$ age calculated by assuming degassing at time of recharge

[&]Standard error propagated from the analytical measurements alone, excluding degassing corrections

ND = not determinable because of a low measured $^{3}H/^{3}He$ ratio

n/a = not analyzed

Table 3.6. Estimates of hydraulic conductivity and storativity based on early-time drawdown methods for a confined aquifer

Estimate type	Well	Kh (m/s)	S
Time drawdown	C	0.98E-04	3.1E-04
	1.3	1.1E-04	7.7E-04
	1.4	1.1E-04	7.8E-04
	1.5	0.97E-04	4.1E-04
	2.3	1.4E-04	5.9E-04
	2.5	1.3E-04	5.8E-04
	3.5	1.2E-04	5.0E-04
	4.4	1.0E-04	9.4E-04
	4.5	1.5E-04	7.1E-04
	Average	1.2E-04	6.2E-04
	St. Dev.	0.2E-04	2.0E-04
Distance drawdown	n/a	0.82E-04	13E-04

Table 3.7. MODFLOW model parameters

Formation	Total thickness (m)	# model layers	K_h m/s	K_z m/s	Vertical ^ anisotropy	Storativity	Specific yield
Shallow aquifer	29.3	3	1.2E-03	1.2E-04	10	-	0.23
Thick clay	10.7	5	1.0E-08	1.0E-09	10	0.00012	-
Recharge window*	10.7	5	1.2E-04	1.2E-05	10	0.00062	-
Interm. aquifer	30.5	7	1.2E-04	1.2E-05	10	0.00062	-

^ Vertical anisotropy is equal to K_z/K_h, so it is listed here as a redundant parameter
K_h is the horizontal, K_z the vertical hydraulic conductivity
* Recharge window is a sub-section of the clay layer, but all parameters were set to those of the interm. Aquifer

Table 3.8. Initial heads computed by the steady state model simulating the clay discontinuity

Well	Model layer	Observed head (m)	Computed head (m)	Δ (Comp-Obs) head (m)
M1.1	2	4.112	4.057	-0.055
M1.4	9	3.149	3.103	-0.046
M1.5	13	3.115	3.102	-0.013
M1.6	14	3.110	3.102	-0.008
M2.5	13	2.957	2.981	0.024
M3.5	13	3.298	3.263	-0.035
M4.4	9	3.123	3.050	-0.073
M4.5	12	3.145	3.050	-0.095
M4.6	14	3.130	3.050	-0.080
M2.4	9	3.065	2.980	-0.085
M2.6	15	2.914	2.984	0.070
M3.6	15	3.219	3.265	0.046

Chapter 4:

Arsenic transport through columns of brown low-arsenic aquifer sand eluted in the field with shallow groundwater

IVAN MIHAJLOV[1,2], MARTIN STUTE[2,3], BENJAMÍN C. BOSTICK[2], YAN ZHENG[2,4], IMTIAZ CHOUDHURY[5], MD. REZAUL HUQ[5], SHAHIDULLAH SHAHUD[5], KAZI MATIN AHMED[5], ALEXANDER VAN GEEN[2]

[1]Department of Earth and Environmental Sciences, Columbia University, New York, NY 10025

[2]Lamont-Doherty Earth Observatory of Columbia University, Palisades, NY 10964

[3]Barnard College, New York, NY 10025

[4]Queens College, City University of New York, Flushing, NY 11367

[5]Department of Geology, University of Dhaka, Dhaka, Bangladesh

Abstract

Deep low-As aquifers in the Bengal Basin are often associated with brown Pleistocene sands and threatened by pumping-induced leakage of shallower contaminated groundwater. In order to assess this risk, cores of freshly collected brown sands were eluted for up to 15 days in the field under anoxic conditions with groundwater elevated in As, Mn, Fe, and HCO_3 pumped directly from a shallow well. Retardation factors of 20-40 for As relative to groundwater flow were calculated for flow rates of 5-60 pore volumes/day using a simple 1-dimensional flow model calibrated with Br. Sediment extractions and flushing with low-As groundwater in the field remobilized 53-89% of the adsorbed As, which is consistent with the underlying assumption of largely reversible exchange. Towards the end of the lowest flow rate experiments, solid phase Fe(III) at the front end of the columns became reduced, and combined with the reduction of unexpectedly high SO_4 in the input water, further lowered As mobility. The findings confirm the recent field observations across a range of spatial and temporal scales that brown sands have the capacity to delay As contamination of the deeper aquifers that, in Bangladesh alone, are already tapped by thousands of community wells.

4.1 Introduction

Tens of millions of people are exposed to harmful As levels via drinking groundwater with >10 μg/L As from tubewells tapping shallow, grey-colored sand aquifers in Bangladesh and throughout Southeast Asia (BGS and DPHE, 2001; Ravenscroft et al., 2009). Chronic exposure to As can have various adverse health effects, such as skin lesions, cancers of the bladder, pancreas, lungs and liver, cardiovascular disease, and the impediment of childhood intellectual development (Argos et al., 2010; Wasserman et al., 2007; Yu et al., 2003). The installation of over 100,000 community (shared) wells in Bangladesh alone, tapping aquifers below the shallow, high-As zone, starting at >30 m below ground level (bgl), and often deeper than 150 m bgl, has been an increasingly popular and effective way of providing safe drinking water in rural areas (Ahmed et al., 2006; Burgess et al., 2010; JICA and DPHE, 2010; van Geen et al., 2007). Although these aquifers can be composed of both grey and brown sands, the brown sands coated primarily by Fe(III) oxides invariably host low-As groundwater and their deposition predates the rise in sea level that started about 15,000 years ago (BGS and DPHE, 2001; Burgess et al., 2010; Zheng et al., 2005).

It has been pointed out that increased pumping from the deeper, Pleistocene aquifers for urban supply or irrigation could induce leakage of shallow groundwater around discontinuous confining units, carrying with it high As and organic matter concentrations to the depths where groundwater is typically uncontaminated (Harvey et al., 2002; Michael and Voss, 2008). The 40-m drop in groundwater level due to massive pumping recorded between 1984 and 2002 in the low-As Dupi Tila formation below

Dhaka (Hoque et al., 2007), the contamination with As of a Pleistocene aquifer beneath Hanoi in Vietnam (Winkel et al., 2011), and the purported contamination of an unconfined section of a >150 m deep aquifer in West Bengal (Mukherjee et al., 2011) are indeed all sources of concern. At a more local scale, especially in areas where groundwater levels in the deep aquifer are below groundwater in the shallow aquifer (Zheng et al., 2005), cracked casings and flow along the annulus could also contaminate aquifers and groundwater pumped from deep wells (van Geen et al., 2007).

Predictions of deeper aquifer sustainability, based on hydrological flow models of the Bengal Basin with various theoretical distributions of low-conductivity units (Michael and Voss, 2008, 2009a, b), demonstrated that the aquifer would likely remain As-safe (<10 μg/L in groundwater) for centuries, provided that the irrigation pumping remained constrained to the shallow aquifer. However, the diminishing yields and rising As concentrations in cultivated crops might justify the switch of irrigation to deep groundwater (Panaullah et al., 2009; Ravenscroft et al., 2013). At the same time, several recent field studies have indicated a degree of As adsorption in brown aquifer sands that could significantly delay contamination even if shallow groundwater were to reach a Pleistocene low-As aquifer (McArthur et al., 2010; McArthur et al., 2008; Radloff et al., 2011; van Geen et al., 2013). Hydrological models coupled to a transport model to include the possibility of As adsorption on aquifer sediment resulted in more optimistic predictions of deep aquifer sustainability (Radloff et al., 2011). On the one hand, brown sands can reduce As mobility by adsorption, but on the other As can also be mobilized from brown sands in the presence of infiltrating microbes and/or organic molecules from shallow groundwater due to reduction of sedimentary As(V) and/or Fe oxyhydroxides

(Dhar et al., 2011; Robinson et al., 2011). Therefore, the adsorption and other reactions of As on brown sand clearly require careful characterization to ensure realistic predictions can be made for the deeper aquifer sustainability.

On the one hand, field-based, *in situ* studies probably provide the most realistic assessment of As adsorption on the Pleistocene brown sands. One such study, performed in the Red River delta of Vietnam at a location where shallow Pleistocene brown sands are located laterally down-gradient from the reduced grey aquifer (van Geen et al., 2013), estimated As retardation factors based on an interpolated history of pumping and the observed groundwater ages at a reduction front moving down the Pleistocene aquifer. A similarly convenient site in the Bengal Basin with a lateral migration of As into the Pleistocene formation has been identified in West Bengal, India (McArthur et al., 2010; McArthur et al., 2008), and yielded comparable As retardation estimates, however like in Vietnam, these studies have their limitations because the history of groundwater flow over longer time scales was not fully constrained. Another *in situ* study of As sorption on brown sediment used the push/pull technique to artificially accelerate the process (Radloff et al., 2011), but the interpretation of results was complicated by discontinuous pumping, necessitated models with multivariate parameters to represent pore-scale processes, and was only possible at early time points before significant dispersion of the injected inert tracer occurred.

Laboratory studies, on the other hand, although at times easier to interpret, introduce artifacts such as the sediments disturbed by long-term storage and experimental handling, and utilize artificial groundwater (Dhar et al., 2011; Robinson et al., 2011; Stollenwerk et al., 2007). Moreover, laboratory methods like batch reactor experiments

(Dhar et al., 2011; Stollenwerk et al., 2007) do not faithfully reproduce the water-to-sediment ratio and pore scale processes. Other laboratory methods, such as column experiments, suffer from their own limitations, as they are unable to reproduce the complex dispersion patterns in aquifers (e.g. Harvey and Gorelick, 2000), and they might miss the precipitation and exchange reactions that can happen under variable ionic strength and pH conditions. The column experiments, nevertheless, provide a flow-through system that allows simple, one-dimensional modeling of As retardation properties. However, the only column study to date with the natural low-As sediment from Bangladesh (Robinson et al., 2011) used stored, repacked shallow brown sand eluted with artificial groundwater and did not provide direct estimates of As retardation.

In this study, we use column experiments to study As adsorption onto brown, low-As sand from Bangladesh in a well-controlled, one-dimensional flow system that attempts to bridge the gap between the field and laboratory studies. In order to approximate the *in situ* conditions to the greatest extent possible, the columns are made from freshly collected sediment cores fitted without repacking or disturbing the sand, and maintained under anoxic conditions at all times. Shallow, *in situ* groundwater with high levels of As, Mn, SO_4, Fe and HCO_3, and moderate levels of PO_4 and Si, is used to elute the columns until a nearly complete breakthrough of As occurs and the breakthrough curves are employed to extract As retardation parameters. Since the adsorption under column flow conditions can be kinetically limited (Darland and Inskeep, 1997; Zhang and Selim, 2006), the columns are run at various pore velocities to investigate their effect on As breakthrough, and As sorption is additionally assessed by batch equilibrium and kinetics experiments set up with deep, low-As groundwater spiked by As(III), the

predominant species of As in the shallow groundwater. The reversibility of As sorption is also evaluated by flushing the As-laden columns with low-As groundwater and/or by sediment extractions. This approach resulted in conservative and straightforward estimates of As retardation by sorption to the natural aquifer brown sands under rigorous conditions resembling those encountered in the field. Moreover, the column experiments also allowed us to directly observe redox transformations on the solid phase and their relationship to As retention on the sediment.

4.2 Methods

4.2.1 Sediment collection and column preparation

Sediment cores 30 cm long and 1.8 cm in diameter were recovered at 30-60 cm (1-2 ft) intervals from approximately 12 to 20 m (38 to 66 ft) depth from two duplicate boreholes located in the village of Purinda, Araihazar upazilla (23.8541º N, 90.6354º E). At this location, orange sand of ~medium grain size is present at a depth only 30 ft (~9 m) below ground level, beneath the layers of grey clay (0-15 ft bgl) and orange clay (15-30 ft bgl, litholog shown in Fig. 4.1b). The boreholes were spaced ~1m from each other and drilled by the traditional sludger method (Horneman et al., 2004) to a specified depth at which a manual push soil corer (AMS 424.45) was employed to recover a core. Upon retrieval, the top several centimeters of the cores were discarded to ensure only undisturbed material was utilized, and then the cores were refrigerated in nitrogen-flushed airtight Mylar bags with oxygen adsorbents (Sorbent Systems). Within 24 hours upon collection, the cores were used to prepare columns for sorption experiments (Table 4.2 lists exact lengths, depths, PV size in mL), or to combine sediment from defined depth ranges and preserve it as above for batch sorption experiments. Intact cores were cut into 11 shorter segments, selected for being well-compacted, and fit with custom-made column plugs to prepare ~10 cm long columns of sand. A small amount of glass wool (1-2 mm final thickness) was inserted between the sand and the plugs to prevent mobilization of clay-size particles. The inflow end of each column was the top end of the core in its natural orientation.

4.2.2 Column experimental set-up and sampling

Column experiments were performed to simulate natural transport of As from the shallow aquifer through the deeper, orange sediments. Ten of the columns prepared as indicated above were flushed with natural, high-As groundwater (594 µg/L As, ~99% of which is As(III), Table 4.3) from 12 m depth at a site approximately 8.3 km SW of the coring location (shallow aquifer in Dari village, 23.78534º N and 90.60322º E), described in detail by Zheng et al. (2005). High-As groundwater was brought up to the surface by a submersible pump (Typhoon, Proactive) at a flow rate of ~5 L/min through a thick, braided hose, then channeled into each column through separate pieces of Tygon tubing of various inner diameters to regulate the flow rate (Fig. 4.1a). A peristaltic pump (Minipuls 3, Gilson) maintained column flow from the bottom up at ~5, ~15-18, or ~60 pore volumes per day (linear velocities of 0.5, 15-18, and 60 m/day, respectively). A larger fraction of the submersible pump flow was used to overflow a carboy in which the columns were bathing throughout the experiment in order to assure they remained under anoxic conditions. Dissolved oxygen (DO) tests conducted on two of the columns with a 0-40 ppb DO kit (Chemetrics) showed that no O_2 was present in the effluent.

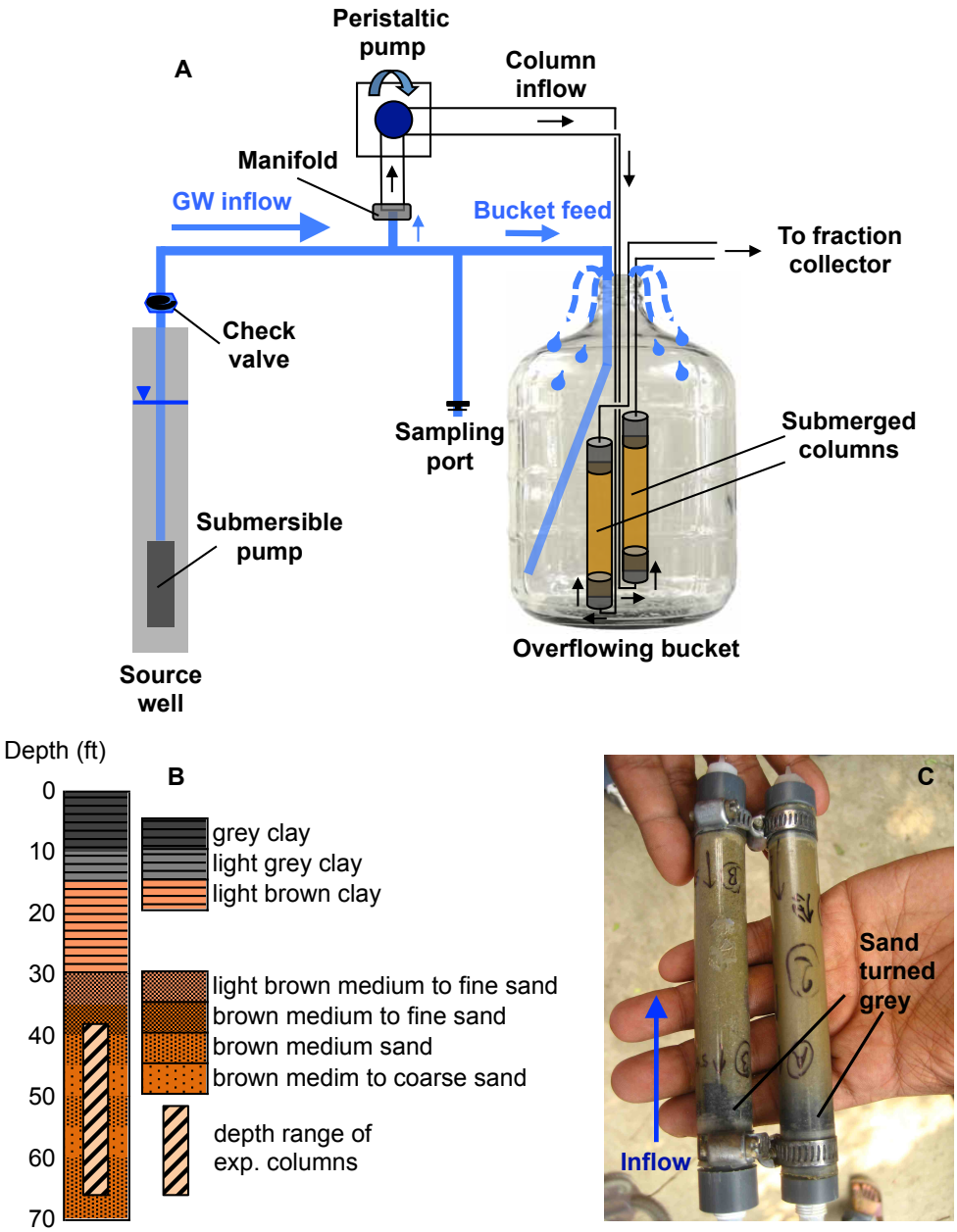

Figure 4.1. Column experiments in the field. (a) Column experimental set-up in the field; only two columns are shown in order to keep the schematic clear. (b) Litholog of the site where column cores were retrieved. (c) The two low-pore velocity (5 PV/day) columns with a visible sediment color change at the column inflow.

Eight of the columns were terminated after ~70, ~120 or ~150 PV were eluted, listed in the order of increasing pore velocities. As for the remaining two columns (from 38ft and 42ft, ~18 PV/day), the supply of inflowing well water was switched after 120-125 PV to a low-As well (<1 μg/L As, Table 4.3) from 44 m depth at the same site. After ~13 hours of low-As groundwater inflow, an unplanned interruption of flow occurred for ~22 hours, upon which the flow was reestablished for the remainder of the flushing experiment.

Fluid fractions of 6-12 mL size (~0.75-1.5 PV) were collected 2, 3, or 6-8 times per day (in order of increasing pore velocity), while the mass of eluent between the samples was monitored for flow rate and PV calculations. The first sample from each column was filtered through 0.45 μm syringe filters (Whatman 6753-2504) to collect any fine particles mobilized by the initiation of column flow. Column samples for As speciation were spiked with 1.25 mM EDTA (final concentration) prior to the collection of the sample in order to prevent Fe precipitation and Fe-As reactions in the tube (Bednar et al., 2002). These samples were passed through As speciation cartridges (Metalsoft Center, Highland Park, NJ) immediately upon collection to split As(III) from As(V) (Meng et al., 2001); prior testing in our laboratory confirmed no interference of the 1.25 mM EDTA with As species separation. Column fractions were acidified with trace analysis grade HCl (Optima, Fisher Scientific) to 1% acid (final). Occasional samples (1 in every 3-5) were left unacidified for anion analysis on an ion chromatograph.

The influent high- or low-As groundwater was sampled daily through a sampling port attached to the submersible pump hose. Dissolved O_2 was also tested daily with a 0-40 ppb kit (Chemetrics). Temperature, conductivity, pH and ORP (oxidation-reduction

potential) were monitored by probes in a flow cell (MP 556 from YSI, Inc.) Alkalinity titrations (Gran, 1952a) were performed on the well water, as well as several column samples, immediately upon collection. All parameters measured in groundwater from the source wells were reported as the average of daily samples (Table 4.3). When experiments were completed, all columns were stored refrigerated in N_2-flushed airtight Mylar bags with oxygen adsorbents.

4.2.3 Bromide (Br) tracer tests in columns

Two of the columns assembled in the field (from 42 and 66 ft bgl) were used in later laboratory testing of column porosity and longitudinal dispersivity using the breakthrough of a mostly inert (non-sorbing) bromide anion. The columns were preconditioned for ~3-4 PV at a pore velocity of 35-37 PV/day using an artificial groundwater solution without detectable bromide, upon which Br was added to the inflowing solution at 170 mg/L final concentration and the breakthrough was observed. After ~2 PV of complete Br breakthrough, the inflow was switched to a Br-free solution, and flushing of Br from the column was observed. Pore volumes were calculated based on the volume of effluent that flowed between the entry of Br (or Br-free solution) into the column and the point at which ½ of the maximum Br concentration was reached at both the rising and the falling flanks of the breakthrough curves. Porosity of the sediment within the column was then estimated from the calculated pore volumes and the total volume of the columns (Table 4.2). Only the rising portion of the Br breakthrough was used for longitudinal dispersivity estimates by the advection-dispersion model.

4.2.4 Batch adsorption experiments

The adsorption of As was also assessed in small batch reactors using the initial sediment from column experiment cores at a few select depth ranges, preserved as described above for 12 days post-collection. Approximately 5 g of the sediment was placed in 12 mL amber glass vials under N_2 atmosphere in a glove bag (Sigma-Aldrich), and ~11.5 mL of low-As groundwater (Table 4.3) was added to the brim of each vial. The groundwater was collected on the same day in 150 mL glass serum bottles by filling them inside an overflowing bucket and crimp sealing with gas impermeable blue butyl rubber septa (Bellco). The batch vials were then spiked with As(III) to a final concentration of 996 μg/L in the dissolved phase for the batch kinetic ("BK") experiments, or to a range of concentrations (217-57,700 μg/L As final) in separate vials for the batch isotherm ("BI") experiments. Arsenite from a reagent grade $NaAsO_2$ salt (Sigma-Aldrich) was used for spikes, as virtually all As was in the form of As(III) in the shallow groundwater used in column experiments. The vials were then crimped with grey butyl rubber septa (Wheaton) and left shaking at a room temperature of ~25 °C. The supernatants were collected and filtered through 0.45 μm syringe filters (Whatman 6753-2504) at a range of time points from 2.7 h to 32 d for the kinetic (BK) experiment, or at the end of the 32-day period for the isotherm (BI) experiment, with each vial providing a single point for the measurement of the dissolved phase As. Batch isotherms were constructed by plotting the concentration of As sorbed on the sediment, Q [M/M], against the concentration of As measured in the dissolved phase, C [M/L^3], after 32 days of equilibration. The values of Q were calculated the mass difference between the initial spiked concentration of As in

the dissolved phase and that measured at the end of the experiment (C), and normalizing it to the sediment mass in batch reactors.

4.2.5 Sediment analyses

Upon the completion of flow experiments, some of the columns were sectioned (inlet, middle, and outlet) and the sediment was collected for immediate extractions by 1M phosphate in the field and/or preserved refrigerated in N_2-flushed airtight Mylar bags with oxygen adsorbents for sequential extractions by MilliQ ultrapure water (18 MΩ), 1M phosphate, and 1.2N hot HCl ~3 months later in the laboratory. Initial sediment, collected from the same core as its corresponding column and not subjected to column experiments, was used in extractions for comparison to the column-flushed sediment. A weighted average of the extractions performed on column sections was used to report the total amount of As extracted from each column. The percent amount of As removed by extractions was in turn expressed relative to the amount of total As adsorbed or desorbed from the sediment during column experiments, calculated by integrating the difference between the influent and effluent As concentrations for all samples during the loading or the flushing stage.

Extractions with the ultrapure (MilliQ) water were performed by adding ~12 mL of N_2-flushed ultrapure water to ~1 g of sediment in amber glass vials, filled to the brim and crimp-shut with a grey rubber stopper inside an aerobic chamber, followed by shaking for ~1 month at the room temperature. Water extractions were designed to assess the amount of As, Fe, and Mn that could be released back to the dissolved phase by simply changing their background concentrations and allowing ample time to reach

equilibrium. Following that, or starting with 1 g of fresh sediment in case of the non-sequential extractions in the field, extractions with N_2-purged 1M NaH_2PO_4 solution for 24 h at room temperature (Jung and Zheng, 2006; Keon et al., 2001; van Geen et al., 2008) were performed. The final extraction in the sequential scheme was carried out with hot (80 °C) 1.2N HCl for 30 min (Horneman et al., 2004; van Geen et al., 2004). Sediments were washed twice between sequential extractions by centrifuging with ultrapure water. All extracts were collected through the 0.45 μm syringe filters.

Select samples of the initial and post-column sediment were neatly packed in Saran wrap immediately upon the completion of column experiments and the diffuse spectral reflectance between 530 and 520 nm (or 550 and 500 nm) was measured to indicate the speciation of Fe in solid phase (Horneman et al., 2004). Finally, grain size analysis was performed on sediment from depth ranges representative of the column experiments by separating the core sediment on sieves of various diameters (2,500, 500, 150, and 63 μm). The sieve-separated size fraction of <63 μm was subsequently analyzed for grain sizes ranging from 70 to 0.8 μm (dimension of maximum length, L) by a Coulter counter. Surface area of the sediment was estimated by combining all of the size fractions and assuming that sediment within a size fraction was shaped either as spheres with a diameter equal to the fraction's average L, or square platelets with sides equal to the size fraction's average L and a thickness of d = 1/20 × average L.

4.2.6 Analysis of groundwater samples and sediment extracts

The analysis of Na, Ca, Mg, K, Si, S, P, As, Fe, and Mn in source well and column effluent groundwater, as well as in batch experiment supernatants and sediment

extracts (As) was performed on samples acidified in the laboratory to 1% HCl (Optima, Fisher) using high-resolution inductively coupled plasma-mass spectrometry (HR ICP-MS) as outlined in Cheng et al. (2004). The analyses were performed to a precision of <10% and an accuracy of 10% or better when compared to internal laboratory reference standards. The analysis of Cl in source well and column effluent groundwater was performed to a precision of <5% on a DX-120 ion-chromatograph (Dionex, Thermo Scientific) using a $Na_2CO_3/NaHCO_3$ eluent.

4.3 Results

4.3.1 Arsenic adsorption in field columns

The shallow, reducing groundwater used to elute the columns (Table 4.3) contained high concentrations of dissolved elements related to sediment reduction, including As (594 μg/L), Fe (2.2 mg/L), and Mn (6.4 mg/L), accompanied by an unusually high level of SO_4 in anoxic groundwater (26 mg/L S). With no detectable dissolved oxygen, this groundwater also had a moderate PO_4 level (0.4 mg/L P), high alkalinity (7.6 mM) and a pH of 6.7. Arsenic is efficiently scavenged from the inflowing groundwater in column experiments, with initial breakthrough to >10 μg/L As only occurring after 10 PV in the columns from 50-66 ft depth and after 20 PV in those from 38-42 ft depth (Fig. 4.2). Similarly, the breakthrough of As to ½ of the influent concentration occurs earlier, at 17-23 PV, in the cores from 50-66 ft depth, but is delayed to 33-46 PV in the cores from 38-42 ft. Arsenic speciation in the column effluent (data not shown) indicates that most As samples are >90% As(III), with some samples in the 80-90% range, arguing that little oxidation of the dissolved phase As occurs in the columns.

Whereas a nearly complete breakthrough was observed by PV 50-80 (day 3-4) in the medium pore velocity columns (15-18 PV/d), dissolved As in most of these columns remained below the input concentration, and declined gently in the final stages of breakthrough until they were disconnected on day 7. The two fast flowing columns (60 PV/d) exhibited a transient decline in As levels, followed by a complete breakthrough (Fig. 4.2a) until they were terminated on day 3. However, in the two low pore velocity

columns (5 PV/d), As levels in the effluent started decreasing after 35-45 PV were eluted by days 7-9, and continued so until the experiment ended on day 15 (Figs. 4.2 and 4.3).

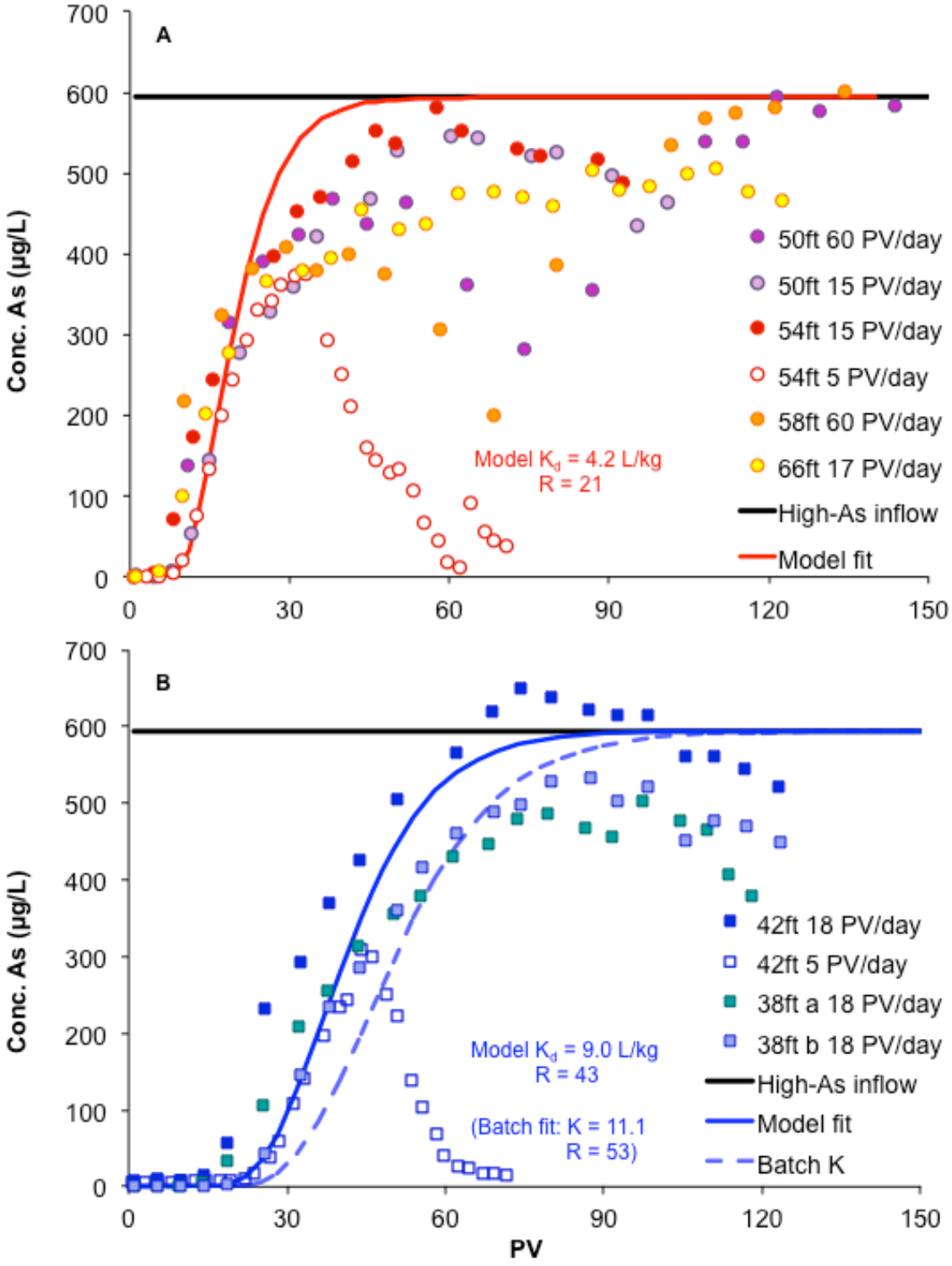

Figure 4.2. Breakthrough curves of As at various pore velocities in columns with sediment from depth ranges of (a) 50-66 ft, and (b) 38-42 ft. The model (after van Genuchten, 1982) accounted for retardation and longitudinal dispersion. The longitudinal dispersivities were set to those observed in the Br breakthrough: (a) 0.7 cm and (b) 0.5 cm (Appendix section 4.7.1), and no kinetic effects were incorporated in the model. The values of sorption constant used by models (K_d) and the resulting retardation factor (R), are indicated on the panels. Sorption constants ($K \approx K_d$) extracted from the high-As range Langmuir fits of batch sorption isotherms are similar for the 50-66 ft sediment (a), and slightly higher in the 38-42 sand (b), the model fit with this K indicated by a dashed line.

The breakthrough of As in columns containing sediment from matching depths varies surprisingly little with pore velocities ranging 12-fold from ~5 to ~60 PV/d (Fig. 4.2). The BTCs of As can be modeled by a 1-dimensional advection-dispersion model, calibrated for dispersion against a bromide tracer, and described in detail in section 4.7.1 (Appendix). The model does not take adsorption kinetics into account, but instead uses a retardation factor (R) related to the equilibrium partitioning coefficient of As between the solid and the dissolved phase (K_d) by the following equation:

$$R = 1 + \frac{K_d \rho}{\theta} \qquad \text{(eq. 1)}$$

where θ is the porosity (0.33) and ρ is the bulk sediment density (1.54 g/cm^3), calculated from the dry sediment density and θ. The dry sediment density of 2.29 g/cm^3 was estimated, in turn, from the wet sediment density (1.87 g/cm^3) of saturated columns weighed in the field and θ. The longitudinal dispersivities estimated from Br BTCs (Fig. 4.8 and Table 4.2) for the two depth ranges of column sediments were deployed in the

model. The equilibrium sorption advection-dispersion model provides rather good visual fits of the observed As BTCs in columns from 50-66 and 38-42 ft depth using K_d values of 4.2 and 9 L/kg, respectively, which is translated by eq. (1) to retardation factors of 21 and 43 (Fig. 4.2).

4.3.2 Chemical changes observed in the column experiments

The BTCs of other constituents monitored in the column effluent (Fig. 4.9 in Appendix), indicated that the breakthrough of cations occurred by PV 20, regardless of the column sediment depth, with Ca and K exchanging on the sediment for Mg, and rather constant Na concentrations. The anions, Cl and SO_4 (shown as S), achieved immediate breakthrough, as expected from their negative charges and little affinity for site-specific adsorption. Alkalinity was only measured in a few column effluent samples (data not shown) and matched that of the source well. Manganese broke through completely, with more retardation in the sediment from 38-42 ft depth, similar to As BTCs. Most Fe, and a large proportion of PO_4 (shown as P), was removed from the dissolved phase by column sediments. Only one column from the 50-66 ft depth range and two others from the 38-42 ft range exhibited a breakthrough of dissolved Fe, while PO_4 was consistently higher in the effluent from 38-42 ft columns, in line with more As retention at that depth range.

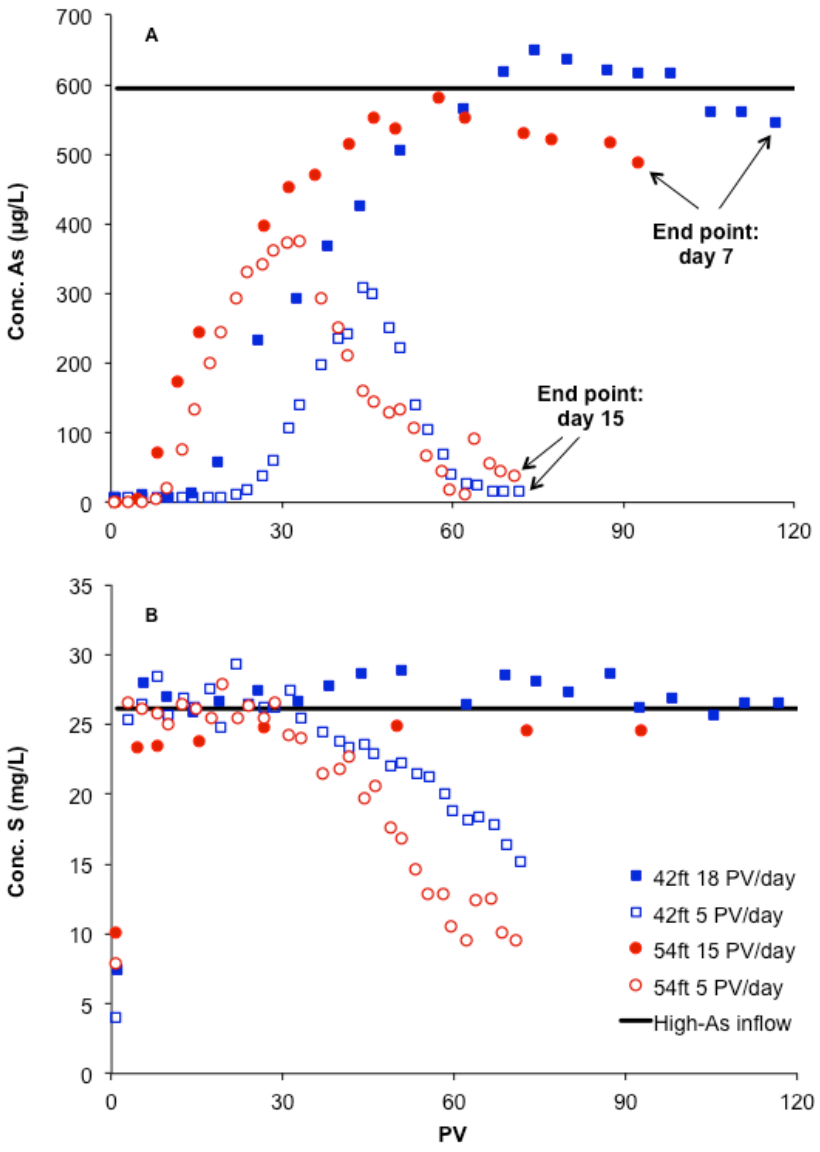

Figure 4.3. The breakthrough of (a) As and (b) S from 5 PV/day columns. As and SO_4 concentrations decreased after 35-45 PV (7-9 days) of flow in the low pore velocity columns and continued to decline until the end of experiments on day 15. The columns with sediment from corresponding depths, but performed at 15-18 PV/day and terminated on day 7, are also shown for comparison.

Most notably, SO_4 was found to decrease after 30 PV, concomitantly with the decline in As levels, only in the two low pore velocity columns (Fig. 4.3). In addition, these two columns had the most complete Mn breakthrough, releasing additional Mn above the influent concentrations, and they were among the three columns with measurable Fe in the effluent (Fig. 4.9, part III), indicating more reducing conditions in the slow-flowing columns. In agreement with more reduction occurring in these columns, sand at the tip of their inlet changed color to dark grey (Fig. 4.1c). The color change was quantified in the 54 ft low-velocity column by the reduction in diffuse spectral reflectance (ΔR) to <40% of the intial ΔR (Fig. 4.10 in Appendix), indicating that the speciation of labile Fe phases switched from Fe(III) to Fe(II) predominance (Horneman et al., 2004). In the remaining sections of this column, and all of the of medium-velocity column sections, the final ΔR ranged between 80-100% of the initial ΔR, thus remaining in the ΔR range of orange sand, with the inlet sections consistently displaying a slightly lower ΔR and, thus, more reduced Fe mineralogy.

4.3.3 Column flushing experiment with low-As groundwater

Switching the inflow of two 18 PV/d columns to a source well with low As (<1 µg/L, Table 4.3), after 4.7 and 7.6 ppm (µg/g) As were loaded onto the sediment over the 125 and 120 PV of high-As groundwater flow, flushed out 72 and 52% of the loaded As, respectively, before the experiments were terminated at PV~270 (Figure 4.4 and Table 4.1). The initial switch to a low-As source well did not result in a smooth transition towards lower dissolved As in the effluent. Instead, due to an accidental ~1 day flow interruption, As was additionally adsorbed from the stagnant dissolved phase onto the

column sediment and effluent emerged with <100 µg/L As upon the reestablishment of flow, clearly demonstrating the amount of kinetic disequilibrium in the columns under flow conditions. Following that, As was slowly desorbed from the sediment, reaching a peak in the effluent at PV~180, with a tendency towards continued desorption beyond the end point of the experiment, as the final concentrations lingered in the 60-80 µg/L range.

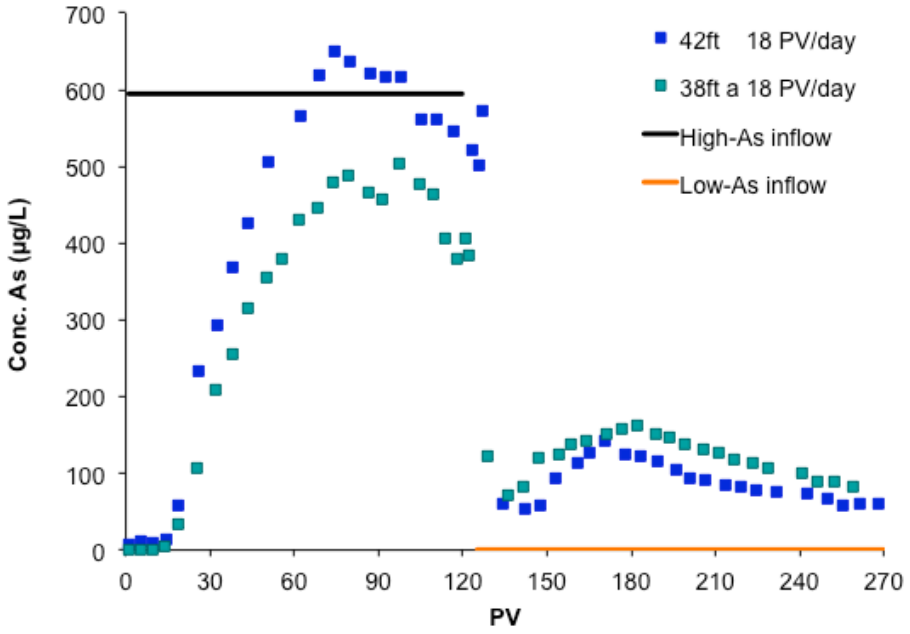

Figure 4.4. Reversibility of As sorption in the field. The inflow of the two medium-velocity columns was switched to a low-As well after 120 PV (38ft a) and 125 PV (42 ft) had been eluted over a period of 7 days. Shortly afterwards, an unplanned break in flow of ~1 day demonstrated the disequilibrium of As sorption, as As concentrations in both effluents abruptly fell to <100 µg/L. Arsenic was desorbed with continued flushing by the low-As groundwater.

4.3.4 Batch experiments

Batch isotherms, reflecting the equilibrium partitioning of As between the dissolved and solid phase, indicate that the strongest adsorption occurs on the brown sand from 40-44 ft bgl, followed by that from 46-48 ft and 60-64 ft bgl, while the weakest adsorbent is the sediment from 52-56 ft bgl (Fig. 4.5). To quantify the partitioning in each sediment sample, Langmuir isotherms were fit to the data, using the following equation, modified from Weber et al. (1991) and Limousin et al. (2007):

$$K = \frac{Q}{C(1 - \frac{Q}{Q_{max}})} \qquad \text{(eq. 2)}$$

where Q_{max} is the maximum sorption capacity [M/M, usually µg/g or mg/kg] of the sediment, and K [L^3/M, usually L/kg] is the sorption constant that includes both the affinity of As for the solid phase and the plateau solid concentration (Q_{max}). When Q << Q_{max}, K ≈ Q/C, which is nearly identical to the linear equilibrium partitioning coefficient used in the column models, K_d, and has the same units.

The values of K were calculated using least squares fits of the linearized version of equation (2):

$$\frac{1}{Q} = \frac{1}{Q_{max}} + \frac{1}{K}\frac{1}{C} \qquad \text{(eq. 3)}$$

At a high range of As concentrations, the isotherms were fit ($R^2 \geq 0.96$) using the three highest data points for each sediment depth, resulting in K values of 11.1, 7.6, 6.7, and 4.2 L/kg and Q_{max} of 93, 82, 68, and 69 µg/g for the sediment from 40-44, 46-48, 60-64, and 52-56 ft bgl, respectively. At the lower range of adsorbed (<5 µg/g) and dissolved (<300 µg/L) As concentrations, similar to the concentrations encountered in the field column experiments, better visual fits are obtained by adjusting the K to 3-fold higher

values, resulting in a range from 12.7 L/kg in the 52-56 ft sediment to 33.3 L/kg in the 40-44 ft sand batch experiment (Fig. 4.5 inset). However, as shown by the column models (Fig. 4.2), column As BTCs are fit better by the K_d values close to the K's estimated from the high-range As concentrations in batch isotherms: the K of 4.2 L/kg from the batch experiment with 52-56 ft sediment provides a good fit for the 50-66 ft cores, while using the K of 11.1 L/kg from the 40-44 ft batch results in a slightly overestimated (but still close) fit of As retardation observed in 38-42 ft cores (Fig. 4.2b).

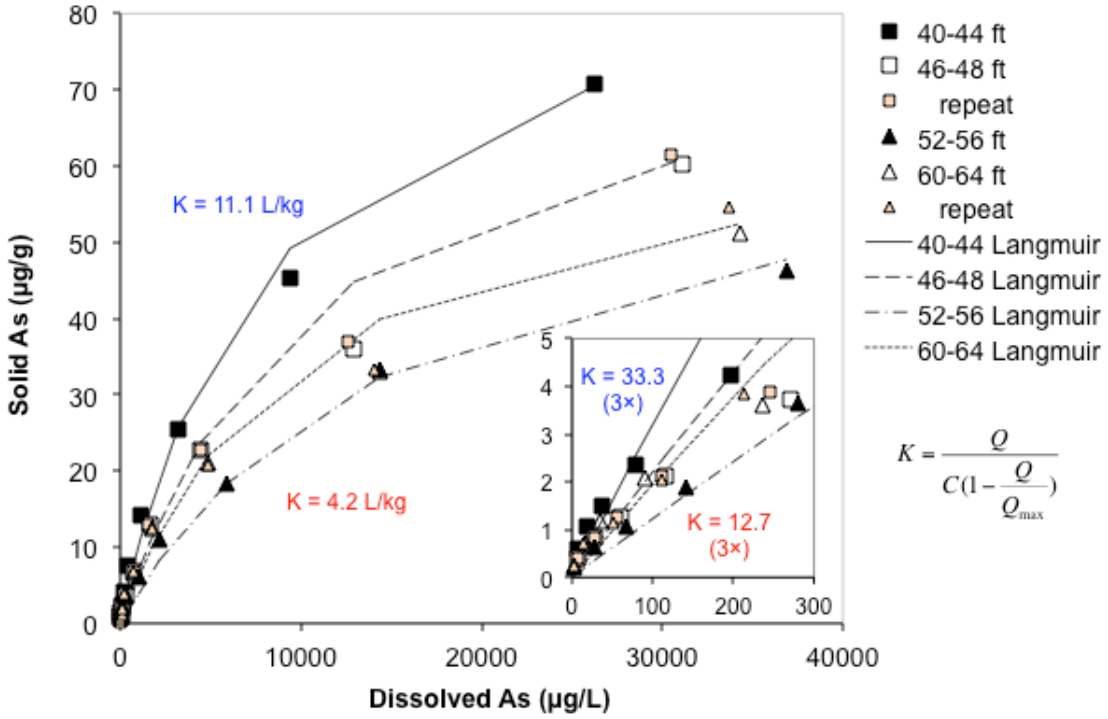

Figure 4.5. Langmuir isotherms for the column sediments across different depths. Each point represents a separate batch reactor to which sediment and low-As groundwater were added, followed by a spike of As(III). Two of the depth intervals were repeated to check for reproducibility. The range of equilibrium constants (K) used are shown. Higher (3-fold) K values were necessary to fit the data at a lower As concentration range shown in inset (same units as the main graph).

Batch kinetics experiments (Fig. 4.6) indicate a gradation of As sorption affinities among the sands from different depths similar to that observed in the column and batch isotherm experiments. The time point at which As concentration is <½ of the initial value of 996 µg/L ranges from <6 hr in the reactors containing 40-44 ft sand to >30 hr in those with the sand from 52-56 ft bgl. Likewise, the final dissolved concentrations after 32 days of incubation ranges from 102 to 186 µg/L As in the batch reactors containing 40-44 ft and 52-56 ft sands, respectively. In the batch experiments overall, dissolved As concentrations fall rather quickly initially, for instance by 15-30% within the first ~3 hr, and by ~50% within the first ~½ day. Subsequently, the rate of adsorption progressively slows toward 5 days, at which point 65-85% of the initial As is adsorbed (150-360 µg/L As remained in the dissolved phase), and only a small fraction can be further adsorbed by day 32.

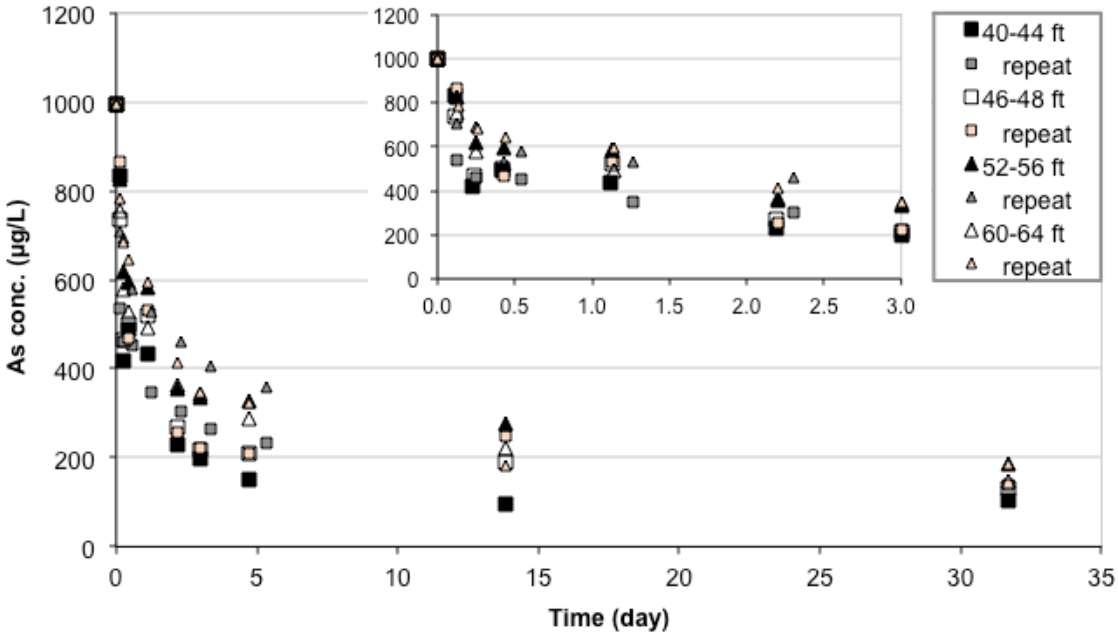

Figure 4.6. Batch kinetic experiment. Each point represents a separate batch reactor to which sediment and low-As groundwater were added, followed by a 996 µg/L spike of

As(III). All depth intervals were repeated to check for reproducibility. Data for the first 3 days are shown in the inset (same units as the main graph).

4.3.5 Sediment characteristics and extractable As

The initial sediment used in column and batch experiments contained <0.7 ppm PO_4-extractable As (Fig. 4.7), typical of the less reducing sediment hosting <10 μg/L dissolved As (van Geen et al., 2008; Zheng et al., 2005), and had the diffuse spectral reflectance derivative at 520 nm of ~1.25, typical of the brown, Pleistocene-age sands (Horneman et al., 2004; Zheng et al., 2005). The Pleistocene age of these sediments might further be inferred from their location under a brown clay layer, reminiscent of the uneroded interfluves topped by paleosol, described by McArthur at al. (2008).

Sediment extractions in the field demonstrated that ~60-70% of the 5-7 ppm total As adsorbed from the shallow groundwater (Table 4.1) can be desorbed by 1M PO_4 extractions, targeting the exchangeable, strongly adsorbed fraction of As (Keon et al., 2001). Later in the lab, sequential MilliQ water and PO_4 extractions combined together desorbed ~45-65% of the adsorbed As. PO_4 extractions on the same column sediment (66 ft, 17 PV/d) did not differ much whether performed immediately in the field or 3 months later in the lab (Fig. 4.7). Only a small additional amount of As, mostly <0.5 ppm/column section and ~7% of total As retained by columns, was mobilized by extractions with hot 1.2N HCl extractions that target As, Mn, or Fe associated with carbonates, Mn oxides, poorly crystalline Fe oxyhydroxides (Keon et al., 2001) and perhaps some more crystalline phases, such as goethite or hematite, due to the heating step (Horneman et al., 2004; van Geen et al., 2004). Overall, 53-72% of As loaded on column sediment was

removed by the sequential extractions with ultrapure water, PO_4, and hot 1.2N HCl (Table 4.1). In the column where 52% of the total As was already flushed out with low-As groundwater, sequential extractions released an additional 37% As. Relatively the least As, only 53% of the total adsorbed by the column sediment, was recovered by sequential extractions from the low pore velocity column.

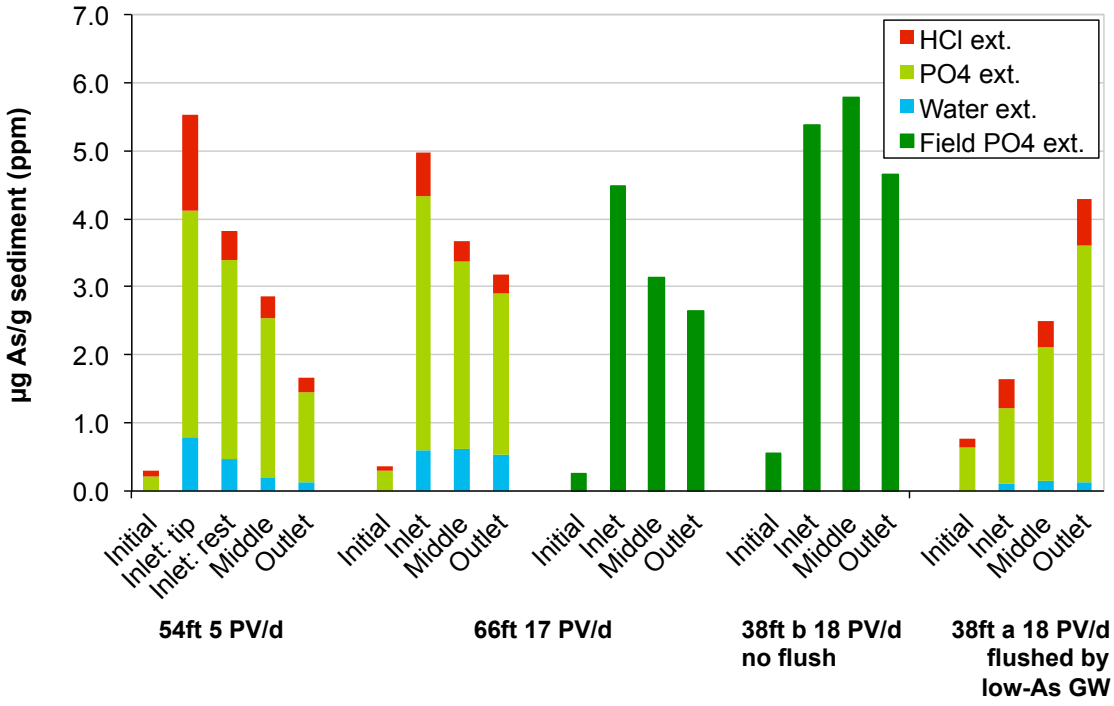

Figure 4.7. Sediment extraction results. Sequential extractions in the laboratory using MilliQ ultrapure water, 1M phosphate, and 1.2M HCl, and phosphate extractions performed immediately in the field (non-sequential). Note that the 66ft 17 PV/day column appears twice, i.e. in both the sequential and the non-sequential extractions.

Within the individual column sections, most As was retained at the inflow end of the column, except in the column flushed by low-As groundwater where As was remobilized towards the outflow end (Figure 4.7). Extractions with the ultrapure water

desorbed relatively little As (<0.8 ppm/column section), especially if the column had already been flushed with low-As groundwater, demonstrating that As is not easily desorbed even after 1 month of equilibration with As-free water. The more aggressive PO_4 extractions desorbed the largest amount of As, up to ~5.5 ppm, from individual column sections. The low pore velocity column exhibited the greatest amount of As zoning between the inflow and outflow sections of the column. The largest amount of HCl-extractable As, both absolute (>1 ppm) and relative to the PO_4-ext. As in other sections, was recovered from the inflow tip of this column, coincident with the location where sediment turned visibly dark grey in color.

4.4 Discussion

4.4.1 Adsorption of As by natural, brown sand from Bangladesh

Column experiments conducted in the field using freshly cored sediment without repacking, maintained under anoxic conditions, and eluted directly with high-As shallow groundwater, allowed for a 1-dimensional, linear flow under controlled conditions that generated a series of As breakthrough curves (BTC). Early As BTCs, before they are significantly affected by reactions other than sorption, can be fit by a simple model incorporating equilibrium sorption of As and dispersion estimated from bromide BTCs (Fig. 4.2). The transport of As is retarded by approximately 21-43 times relative to the movement of groundwater, which translates to a linear As partitioning coefficient (K_d) between the sediment and the dissolved phase of 4.2-9 L/kg. Our estimate falls within the middle-to-low range of the K_d values of 1.7-28.7 L/kg reported by recent field and laboratory studies performed on brown, Pleistocene aquifers and aquifer materials from Bangladesh, India or Vietnam (Dhar et al., 2011; McArthur et al., 2010; McArthur et al., 2008; Radloff et al., 2011; Stollenwerk et al., 2007; van Geen et al., 2013). Conversely, K_d values estimated here fall slightly above the K_d range of 1-6 L/kg found in the grey, more reduced aquifer or riverbank sediment from across the Bengal Basin (BGS and DPHE, 2001; Harvey et al., 2002; Jung et al., 2012; Radloff et al., 2011; van Geen et al., 2008), indicating a higher affinity of brown sands for As sorption.

4.4.2 Kinetic limitations of the sorption estimates

Kinetic limitations of the experiments might have resulted in an underestimated K_d and retardation factor of As in the present study due to a relatively fast linear flow in the columns (0.5-6 m/d) compared to the natural conditions of vertical (in cm's/yr) or even horizontal (in m's/yr) flow in the natural Bengal Basin aquifers (BGS and DPHE, 2001; Harvey et al., 2002; Michael and Voss, 2008; Stute et al., 2007; van Geen et al., 2008; Zheng et al., 2005). The lack of large variations between As BTCs from depth-matched columns performed at different pore velocities (Fig. 4.2) could erroneously be attributed to a lack of major kinetic effect on the sorption observed in flowing columns. The batch kinetic experiment (Fig. 4.6), however, indicated that As sorption is indeed subject to kinetic limitations because it took place over a period of multiple days in the batch reactors, whereas the longest residence time in the low velocity columns was only ~5 hr. Arguing further for the kinetic limitations of sorption in the columns, batch isotherms performed at the range of solid and dissolved concentrations present in the columns produced three-fold higher K's (Fig. 4.5) than those used to fit the observed As BTCs in column models (Fig. 4.2). This observation suggests that As could be adsorbed on column sediments to a larger extent if allowed more time to react. That exactly occurred when column flow was interrupted for ~1 day and dissolved As levels declined abruptly, confirming the sorption disequilibrium within columns (Fig. 4.4), also noted in other studies with flow interruptions (Zhang and Selim, 2006).

A puzzle remains as to why the ~12-fold changes in pore velocity did not result in larger differences between As BTC, as would be expected from the batch kinetic experiment. At least a part of the answer might lie in the limited comparisons that can be

drawn between the batch and the column experiments, even if the range of initial As concentrations used in some batch experiments, both kinetic and the low-range isotherm, is similar to As levels in the column inflow. Batch reactors have a different water-to-sediment ratio from the columns, producing a physical difference in the pore-scale processes. Moreover, the chemical composition of the background solution and the concentration gradients of As and other sorbates are distinct within the two setups. On the one hand, batch reactions were performed in low-As groundwater, with As added in a single spike; the As concentration gradient thus established between the solution and the grain surface sites was initially sharp, but quickly leveled off after the initial fast adsorption. On the other hand, the columns were continuously flushed with shallow, high-As groundwater, replenishing and maintaining high As concentrations in the solution, but also supplying an entirely different background solution with its own ionic strength and competing sorbate concentrations. These fundamental differences between the column and batch experiments highlight the advantages of column experiments as more representative of the "real world", but they also make comparisons between these two types of experiments more difficult.

However, the lack of kinetic effects in the columns might nevertheless offer additional insights into the mechanisms of As adsorption. Batch kinetic experiments in this and other studies (Radloff et al., 2011; Raven et al., 1998; Zhang and Selim, 2005, 2006) often conceptualize the pore-scale As sorption process as a two-step reaction, consisting of a rapid initial step followed by a slow approach to equilibrium. The fast and slow sites might be chemically different, due to varying site specificities and binding energies, or the slow sites might be physically limited by diffusion processes near the

grain surface, within grains, or aggregates (Harvey and Gorelick, 2000; Wood et al., 1990). It is plausible that the fast sites, occasionally included in column models (Zhang and Selim, 2005, 2006), reach equilibrium almost instantaneously at a lower K_d than that of the overall sediment. This would explain both the observed lack of sensitivity of As BTCs to the pore velocities explored and the lower column model K_d when compared to batch isotherm experiments performed in the same As concentration range. As for the slow sorption sites, the water residence time in columns may not allow enough time for these sites to impact the BTCs significantly, except near breakthrough where it is obvious that some additional As adsorption occurs, preventing the complete breakthrough in most columns.

Another plausible explanation for the lack of As BTC sensitivity to changes in pore velocity might also be that the sorption kinetics of slow sites, limited by diffusion processes, actually speed up at higher pore water velocities, as noted by Darland and Inskeep (1997). In their study, As adsorption rate constants were considered sensitive to the mixing environment in the columns, and were thus adjusted to higher values to be able to fit As BTCs at higher column flow velocities. Other studies also required an increase in sorption rate constants in response to switching from stationary batch reactors to columns (Zhang and Selim, 2006) or to *in situ* push/pull experiments (Radloff et al., 2011).

4.4.3 Reductive transformations in the sediment

The coexistence of elevated As and SO_4 is not common in Southeast Asian reduced groundwater (Burnol and Charlet, 2010; Buschmann and Berg, 2009), but could

occur in the areas of mixing, located near streams and/or close to the water table depth, as in our shallow source well. The inflow of high-SO_4 groundwater can stimulate the growth of sulfate reducing bacteria that take part in Fe redox cycling and could enhance the retention of As in our column experiments (Saalfield and Bostick, 2009; Tufano and Fendorf, 2008), potentially resulting in overestimated As retardation parameters. Indeed, in the low pore velocity columns (5 PV/day), the reductive dissolution of Fe and Mn oxides, as well as SO_4 reduction, were suggested by the presence of Fe(II) in the effluent, additional Mn relative to the influent concentrations (Fig. 4.9 in Appendix) at later stages of the breakthrough, and the concurrent decline of effluent SO_4 and As levels after 35-45 PV had been eluted by day 7-9 (Fig. 4.3). However, as the influence of sulfate and Fe reduction was mostly constrained to the later stages of breakthrough in the slow flowing columns, the observed As BTCs controlled by sorption reactions are not brought into question in the columns performed at higher pore velocities or before the onset of reduction in the low-velocity columns.

Longer water residence time and the longer experimental timescale of the low pore velocity columns could allow rate-limited microbial processes to take advantage of the high sulfate and probably higher organic matter content in shallow groundwater (Harvey et al., 2002; Islam et al., 2004; McArthur et al., 2004). The reduction of Fe oxyhydroxides and SO_4 resulted in the formation of a dark grey phase at the inlet of the low-velocity columns (Fig. 4.1c), quantified by a decrease in diffuse spectral reflectance (ΔR, Fig. 4.10 in Appendix). The dramatic decrease in dissolved As concentrations starting on day 7-9 of the slow flowing columns (Fig. 4.3) was likely related to these changes in Fe mineralogy, allowing for the resorption, or perhaps precipitation, of As

until the experiment was terminated on day 15. This additional adsorption/retention of As is also supported by the high amount of As extracted from the inlet tip of the low-velocity column compared to the downstream column sections (Fig. 4.7), and by the higher partitioning of As into the hot HCl-extractable phase at the inlet tip, indicating an association with Fe phases that are more crystalline and are binding the As somewhat stronger than by the simple adsorption. Gently declining trends in As concentrations (Fig. 4.2), and a small decrease in ΔR of the sediment near column inlets (Fig. 4.10) suggested that enhanced reduction perhaps occurred towards the end of the medium-velocity column experiments also, but the reaction did not develop fully before these columns were disconnected on day 7.

The mineral phase formed at the inlet of the slow columns is likely a mixed Fe(II)/Fe(III) mineral, such as magnetite, which has recently been shown to retain As(III) or As(V) within solid phase under column flow conditions dominated by Fe and/or SO_4 reduction (Saalfield and Bostick, 2009; Tufano and Fendorf, 2008). Arsenic could have been adsorbed onto the newly formed magnetite surface, or co-precipitated into the magnetite mineral lattice. Alternatively, a "green rust" could have formed, incorporating carbonate or SO_4 ions from the high-alkalinity and high-SO_4 inflow into the mixed Fe(II)/Fe(III) phase resulting from Fe and SO_4 reduction, but opposing reports exist as to the effectiveness of As retention on such a phase (Jonsson and Sherman, 2008; Kocar et al., 2010). It is unlikely that reduced sulfur phases, such as Fe and As sulfide, directly coprecipitated As on column sand, as sulfide is often involved in Fe redox cycling and enhances its mineralogical transformations, but is rarely found to be a major phase associated with Fe or As deposition under similar field or model conditions (Burnol and

Charlet, 2010; Kocar et al., 2010; Saalfield and Bostick, 2009). Under sulfate-reducing conditions, the sulfide mineral sink cannot be completely ruled out, as small amounts of sulfides could have formed, but would not be detectable by our analysis. The exact phase formed on natural sediment under the inflow of high-SO_4, -Fe, and -As shallow groundwater warrant future study to examine its structure and the potential to retain As more strongly, or perhaps release it with continued reduction. It would also be of interest to examine whether the presence of SO_4 reduction is necessary to limit the mobility of As similar to what was observed in the low-velocity columns.

4.4.4 Reversibility of As sorption on column sediments and variability with depth

The sorption of arsenic on column sediments was generally reversible, in particular in the high and medium velocity column experiments, as demonstrated by a large percentage of As remobilized by the flushing experiment with low-As groundwater (Fig. 4.4) and the sediment extractions (Fig. 4.7 and Table 4.1). Nevertheless, a significant amount of As (11-29% total As) retained from the shallow groundwater was not desorbed by the aggressive PO_4 extractions that target the readily mobilizable fraction of As (Keon et al., 2001) and might even overestimate it (Dhar et al., 2011), nor was it released by the sequential extractions that include a hot HCl leach, targeting amorphous and perhaps even more crystalline Fe phases (van Geen et al., 2004). The poorest recovery of retained As (53% by sequential extractions) was observed in the low-velocity column due to the non-reversible incorporation of As into rearranged Fe phases after the onset of SO_4 reduction in these columns on day 7-9. The medium velocity columns, however, were disconnected on day 7 before many of the significant biogeochemical

changes and mineral rearrangements could affect As retention by reversible sorption reactions.

Leaching of the columns with on-site low-As groundwater performed well at desorption, comparable in extent to PO_4 extractions, and might have recovered most loaded As if given more time (Fig. 4.4). The effectiveness of flushing with natural low-As groundwater might have been enhanced by the changes in pH, counter cations, and ionic strength when the source well was switched (Table 4.3), all of which are known factors that generally affect sorption (Harter and Naidu, 2001). The doubling of dissolved Si content, which could decrease As adsorption to the Pleistocene sediment (Stollenwerk et al., 2007), might have also been partly responsible for the observed mobilization.

There is significant variability in the equilibrium partitioning, sorption extent and kinetics, and the column breakthrough of As for a single location with visually similar sediment over a depth range of <30 ft (Figs. 4.2, 4.5, and 4.6). The sediment from 52-56 ft depth consistently exhibited the lowest estimated K values and the slowest adsorption kinetics, while the opposite was true of the 40-44 ft depth range, and As column BTCs could also be grouped within sediment depth groups. The shallower brown sand appeared somewhat finer grained (Fig. 4.1c); in addition, the surface area estimates resulting from grain size analysis down to 0.8 μm (Table 4.4 and Fig. 4.11 in Appendix) showed that the sand from 40 ft bgl has the highest amount of fine particles and the greatest surface area. However, the second largest surface area is on the sand from 52-56 ft bgl, coincident with the poorest As adsorption parameters, so the grain size argument does not provide a full explanation of the variability.

The initial amount of PO_4-extractable As was larger on shallower sediment, which might confirm its greater affinity for As adsorption, but fails to explain the preferential adsorption mechanism. A part of the answer might lie in the BTCs of Fe and Mn (Fig. 4.9 in Appendix): poorer Fe retention in the 38-42 ft columns perhaps indicates a slightly more reducing Fe mineralogy, which could result in the formation of magnetite that retains As more strongly by surface complex formation or structural incorporation (Kocar et al., 2010; Saalfield and Bostick, 2009; Tufano and Fendorf, 2008). Arsenite adsorption could also be enhanced in the presence of higher Fe(II) sorbed concentrations (Dixit and Hering, 2006). Furthermore, the similar initial retardation of Mn transport to that of As at equivalent depth ranges indicates that a difference in sediment Fe mineralogy might affect both the As and Mn sorption, but there is no clear explanation of these variations, barring further mineralogical or spectroscopic evidence. The oxidation of As(III) by Mn oxides, invoked to explain the strong retention of As by the Pleistocene brown sediment (Stollenwerk et al., 2007) is unlikely to have played a role in these experiments, as no evidence of As(III) oxidation to As(V) was found.

4.4.5 Other reactions occurring in the columns

The breakthrough of Ca appeared to be controlled by cation exchange with Mg and K within the initial ~20 PV of the experiments, upon which it was achieved in all columns regardless of sediment depth (Fig. 4.9 in Appendix). The saturation of Ca sorption sites and its complete breakthrough have been related to the release of As(V) adsorbed onto ferrihydrite (Saalfield and Bostick, 2010), perhaps by forming soluble Ca-arsenate complexes, but did not seem to affect As(III) adsorption in the columns, varying

among different depth intervals independently of Ca levels. Relatively high alkalinity in the influent shallow groundwater (Table 4.3) might have limited the adsorption of As to some extent (Norrman et al., 2008), due to the competition of bicarbonate and arsenite for sorption sites, but the effect is probably minimal (Radu et al., 2005; Stollenwerk et al., 2007). Phosphate is a more significant adsorption competitor of arsenite (Dixit and Hering, 2003; Stollenwerk et al., 2007), and was clearly scavenged from the dissolved phase by all columns (Fig. 4.9 in Appendix), thus it must have adversely affected the adsorption of As to some extent. Although the influent concentration of 0.4 mg/L P was relatively modest compared to other shallow wells in the area (Dhar et al., 2008; Zheng et al., 2005), it was still above the levels found in most deep, low-As wells. The roughly similar Si concentrations in the initial column pore water and the shallow groundwater inflow mean that silica is unlikely to have affected the adsorption portion of As BTCs, although it is known to marginally compete with As for sorption sites (Stollenwerk et al., 2007).

4.4.6 Implications for As mobility and low-As aquifer sustainability

The study demonstrated that the brown, low-As sand from a Bangladeshi aquifer can adsorb As from infiltrating shallow groundwater, even under rather fast flows compared to the natural groundwater velocities. The estimated As retardation coefficient of ~20-40 offers a significant amount of protection to low-As aquifers from As contamination that might occur with increased pumping, in agreement with other recent studies on the Pleistocene sediment (McArthur et al., 2010; McArthur et al., 2008; Radloff et al., 2011; Stollenwerk et al., 2007; van Geen et al., 2013). A distinguishing

characteristic of this study is that while it was performed under nearly *in situ* conditions, with results more representative than the classic batch or column methods, it also avoided the limitations associated with field experiments, such as complex heterogeneities, preferential flows, and tracer loss/dispersion (Radloff et al., 2011), and the complex modeling formulations required to interpret the obtained data from those approaches (Radloff et al., 2011; Stollenwerk et al., 2007). This simple technique also circumvented the difficulty of finding field sites where geology and hydrology align in a way that makes it possible to track As breakthrough and the degree of retardation (McArthur et al., 2010; McArthur et al., 2008; van Geen et al., 2013). Thus, the results from this approach could be easily transferred to other locations requiring contaminant transport studies to initiate simple comparisons – for example, arsenic retardation in other Southeast Asian Holocene deltaic and riverine sediments.

The retardation of As might have been underestimated due to the relatively high column flow rates, however the kinetic limitations could indeed be applicable to faster vertical flows occurring within or around deep wells with mechanical failures subject to a downward hydraulic gradient. The applicability of our As sorption estimates to the transport of As in low-As aquifers in the context of natural groundwater and sediment variability was not explicitly explored here. The groundwater used in our study was enriched with soluble reduction products or species (As, Fe, Mn) and with known As adsorption competitors (HCO_3, and moderate amounts of PO_4 and H_4SiO_4), but was also unusually SO_4-rich for a reducing environment (Buschmann and Berg, 2009), which could have enhanced the observed retention of As on sediment. Despite these uncertainties, the agreement between this and other recently published studies with brown

sand indicates that the natural variability mentioned may not cause large differences in As retardation. Stratigraphic variability instead may turn out to be more of a controlling factor for the sustainability of low-As aquifers. The heterogeneity in sediment distribution, including the locations of grey and orange sands hosting low-As groundwater, is not well understood (BGS and DPHE, 2001; Burgess et al., 2010; Zheng et al., 2005) and requires more study. Gray sands might also have a significant, but slightly lower, capacity for adsorbing As (BGS and DPHE, 2001; Radloff et al., 2011; van Geen et al., 2008). Aquitard distribution also requires further characterization, as it can greatly impact the way shallow contaminants infiltrate deeper parts of the aquifer (Michael and Voss, 2009b).

Another variable needing investigation in the evaluation of low-As aquifer sustainability is the reactive organic matter (OM) that might arrive with shallow groundwater intrusion. If reactive, the OM can reduce the brown sediment, cause an additional release of As, and limit its capacity to adsorb As due to a reduction in surface area of Fe minerals, much like what happens in the shallow, reduced aquifer, whether the organic matter be sourced from the surface or co-deposited with the sediment (Harvey et al., 2002; Mailloux et al., 2013; Neumann et al., 2010; van Geen et al., 2004). Reductive changes and/or the release of As have already been reported in brown, Pleistocene sediment studies in the field (McArthur et al., 2010; van Geen et al., 2013) and upon addition of electron donors in batch (Dhar et al., 2011) or column systems (Robinson et al., 2011). The reactivity of brown sands observed within the low pore velocity columns in this study, however, implied that the reduction of Fe oxyhydroxides in the presence of high SO_4 and Fe(II) levels may, at least initially, limit the mobility of As. Iron mineral

rearrangements under such conditions might actually help sequester As and reduce the risk of As contamination, as previously observed on model laboratory materials (Kocar et al., 2010; Saalfield and Bostick, 2009; Tufano and Fendorf, 2008). The characteristics of the formed mineral phases warrant further research to determine their stability with respect to As retention, although the importance of this mineralogical pathway may be of limited scope in Southeast Asian aquifers due to the rare occurrence of groundwater high in both As and SO_4.

4.5 Conclusions

Column experiments performed with freshly cored sediment and shallow high-arsenic groundwater can be used to closely mimic *in situ* studies of As transport retardation without physically being performed in a low-As aquifer. The migration of As was delayed by adsorption on aquifer sediments by a factor of 20-40 times compared to the flow of groundwater, providing an estimate within the same range as those made by representative field studies. Other, non-sorptive reactions also impact As retention by aquifer material and warrant further study to predict the long-term behavior of As in low-As aquifers. This relatively simple method, although it cannot accurately represent dispersion processes in the aquifer, requires only routine analytical effort and is transferrable to other locations where the basic retardation properties of contaminants need characterization in a sedimentary aquifer setting.

Acknowledgements

A fellow graduate student, Karen Wovkulich, was instrumental in getting me started on the column experimental design, and we would not have made it in the field without the fraction collector built by Thomas Protus. I am also grateful to Raymond Sambrotto for letting me use his centrifuge and to Stephen Barten for great laboratory assistance and companionship. Special thanks go to the family of Shahidullah Shahud for letting us use their yard to set up experiments, sleep in their house, and for taking a great care of us day and night. Thanks also to our driver, Razzak, for spending a few sleepless nights when we needed to go out to monitor the experiment at odd times.

4.6 References

Ahmed, M.F., Ahuja, S., Alauddin, M., Hug, S.J., Lloyd, J.R., Pfaff, A., Pichler, T., Saltikov, C., Stute, M., van Geen, A., 2006. Epidemiology - Ensuring safe drinking water in Bangladesh. Science 314, 1687-1688.

Argos, M., Kalra, T., Rathouz, P.J., Chen, Y., Pierce, B., Parvez, F., Islam, T., Ahmed, A., Rakibuz-Zaman, M., Hasan, R., Sarwar, G., Slavkovich, V., van Geen, A., Graziano, J., Ahsan, H., 2010. Arsenic exposure from drinking water, and all-cause and chronic-disease mortalities in Bangladesh (HEALS): a prospective cohort study. Lancet 376, 252-258.

Bednar, A.J., Garbarino, J.R., Ranville, J.F., Wildeman, T.R., 2002. Preserving the distribution of inorganic arsenic species in groundwater and acid mine drainage samples. Environmental Science & Technology 36, 2213-2218.

BGS and DPHE, 2001. Arsenic Contamination of Groundwater in Bangladesh, in: Kinniburgh, D.G., Smedley, P.L. (Eds.). British Geological Survey and Department of Public Health Engineering, BGS Technical Report WC/00/19. British Geological Survey, Keyworth, UK.

Burgess, W.G., Hoque, M.A., Michael, H.A., Voss, C.I., Breit, G.N., Ahmed, K.M., 2010. Vulnerability of deep groundwater in the Bengal Aquifer System to contamination by arsenic. Nature Geoscience 3, 83-87.

Burnol, A., Charlet, L., 2010. Fe(II)-Fe(III)-Bearing Phases As a Mineralogical Control on the Heterogeneity of Arsenic in Southeast Asian Groundwater. Environmental Science & Technology 44, 7541-7547.

Buschmann, J., Berg, M., 2009. Impact of sulfate reduction on the scale of arsenic contamination in groundwater of the Mekong, Bengal and Red River deltas. Applied Geochemistry 24, 1278-1286.

Cheng, Z., Zheng, Y., Mortlock, R., van Geen, A., 2004. Rapid multi-element analysis of groundwater by high-resolution inductively coupled plasma mass spectrometry. Analytical and Bioanalytical Chemistry 379.

Darland, J.E., Inskeep, W.P., 1997. Effects of pore water velocity on the transport of arsenate. Environmental Science & Technology 31, 704-709.

Dhar, R.K., Zheng, Y., Saltikov, C.W., Radloff, K.A., Mailloux, B.J., Ahmed, K.M., van Geen, A., 2011. Microbes Enhance Mobility of Arsenic in Pleistocene Aquifer Sand from Bangladesh. Environmental Science & Technology 45, 2648-2654.

Dhar, R.K., Zheng, Y., Stute, M., van Geen, A., Cheng, Z., Shanewaz, M., Shamsudduha, M., Hoque, M.A., Rahman, M.W., Ahmed, K.M., 2008. Temporal variability of groundwater chemistry in shallow and deep aquifers of Araihazar, Bangladesh. Journal of Contaminant Hydrology 99, 97-111.

Dixit, S., Hering, J.G., 2003. Comparison of arsenic(V) and arsenic(III) sorption onto iron oxide minerals: Implications for arsenic mobility. Environmental Science & Technology 37, 4182-4189.

Dixit, S., Hering, J.G., 2006. Sorption of Fe(II) and As(III) on goethite in single- and dual-sorbate systems. Chemical Geology 228, 6-15.

Gran, G., 1952. Determination of the equivalence point in potentiometric titrations .2. Analyst 77, 661-671.

Harter, R.D., Naidu, R., 2001. An assessment of environmental and solution parameter impact on trace-metal sorption by soils. Soil Science Society of America Journal 65, 597-612.

Harvey, C.F., Gorelick, S.M., 2000. Rate-limited mass transfer or macrodispersion: Which dominates plume evolution at the Macrodispersion Experiment (MADE) site? Water Resources Research 36, 637-650.

Harvey, C.F., Swartz, C.H., Badruzzaman, A.B.M., Keon-Blute, N., Yu, W., Ali, M.A., Jay, J., Beckie, R., Niedan, V., Brabander, D., Oates, P.M., Ashfaque, K.N., Islam, S., Hemond, H.F., Ahmed, M.F., 2002. Arsenic mobility and groundwater extraction in Bangladesh. Science 298, 1602-1606.

Hoque, M.A., Hoque, M.M., Ahmed, K.M., 2007. Declining groundwater level and aquifer dewatering in Dhaka metropolitan area, Bangladesh: causes and quantification. Hydrogeology Journal 15, 1523-1534.

Horneman, A., Van Geen, A., Kent, D.V., Mathe, P.E., Zheng, Y., Dhar, R.K., O'Connell, S., Hoque, M.A., Aziz, Z., Shamsudduha, M., Seddique, A.A., Ahmed, K.M., 2004. Decoupling of As and Fe release to Bangladesh groundwater under reducing conditions. Part 1: Evidence from sediment profiles. Geochimica Et Cosmochimica Acta 68, 3459-3473.

Islam, F.S., Gault, A.G., Boothman, C., Polya, D.A., Charnock, J.M., Chatterjee, D., Lloyd, J.R., 2004. Role of metal-reducing bacteria in arsenic release from Bengal delta sediments. Nature 430, 68-71.

JICA and DPHE, 2010. Report on Situation Analysis of Arsenic Mitigation, 2009. Dept. of Public Health Engineering, Bangladesh and Japan International Cooperation Agency, Local Government Division, Government of Bangladesh, DPHE, JICA.

Jonsson, J., Sherman, D.M., 2008. Sorption of As(III) and As(V) to siderite, green rust (fougerite) and magnetite: Implications for arsenic release in anoxic groundwaters. Chemical Geology 255, 173-181.

Jung, H.B., Bostick, B.C., Zheng, Y., 2012. Field, Experimental, and Modeling Study of Arsenic Partitioning across a Redox Transition in a Bangladesh Aquifer. Environmental Science & Technology 46, 1388-1395.

Jung, H.B., Zheng, Y., 2006. Enhanced recovery of arsenite sorbed onto synthetic oxides by L-ascorbic acid addition to phosphate solution: calibrating a sequential leaching method for the speciation analysis of arsenic in natural samples. Water Research 40, 2168-2180.

Keon, N.E., Swartz, C.H., Brabander, D.J., Harvey, C.F., Hemond, H.F., 2001. Validation of an arsenic sequential extraction method for evaluating mobility in sediments. Environmental Science & Technology 35, 2778-2784.

Kocar, B.D., Borch, T., Fendorf, S., 2010. Arsenic repartitioning during biogenic sulfidization and transformation of ferrihydrite. Geochimica Et Cosmochimica Acta 74, 980-994.

Mailloux, B.J., Trembath-Reichert, E., Cheung, J., Watson, M., Stute, M., Freyer, G.A., Ferguson, A.S., Ahmed, K.M., Alam, M.J., Buchholz, B.A., Thomas, J., Layton, A.C., Zheng, Y., Bostick, B.C., van Geen, A., 2013. Advection of surface-derived organic carbon fuels microbial reduction in Bangladesh groundwater. Proceedings of the National Academy of Sciences of the United States of America 110, 5331-5335.

McArthur, J.M., Banerjee, D.M., Hudson-Edwards, K.A., Mishra, R., Purohit, R., Ravenscroft, P., Cronin, A., Howarth, R.J., Chatterjee, A., Talukder, T., Lowry, D., Houghton, S., Chadha, D.K., 2004. Natural organic matter in sedimentary basins and its relation to arsenic in anoxic ground water: the example of West Bengal and its worldwide implications. Applied Geochemistry 19.

McArthur, J.M., Banerjee, D.M., Sengupta, S., Ravenscroft, P., Klump, S., Sarkar, A., Disch, B., Kipfer, R., 2010. Migration of As, and H-3/(3) He ages, in groundwater from West Bengal: Implications for monitoring. Water Research 44, 4171-4185.

McArthur, J.M., Ravenscroft, P., Banerjee, D.M., Milsom, J., Hudson-Edwards, K.A., Sengupta, S., Bristow, C., Sarkar, A., Tonkin, S., Purohit, R., 2008. How paleosols influence groundwater flow and arsenic pollution: A model from the Bengal Basin and its worldwide implication. Water Resources Research 44.

Meng, X.G., Korfiatis, G.P., Jing, C.Y., Christodoulatos, C., 2001. Redox transformations of arsenic and iron in water treatment sludge during aging and TCLP extraction. Environmental Science & Technology 35, 3476-3481.

Michael, H.A., Voss, C.I., 2008. Evaluation of the sustainability of deep groundwater as an arsenic-safe resource in the Bengal Basin. Proceedings of the National Academy of Sciences of the United States of America 105, 8531-8536.

Michael, H.A., Voss, C.I., 2009a. Controls on groundwater flow in the Bengal Basin of India and Bangladesh: regional modeling analysis. Hydrogeology Journal 17, 1561-1577.

Michael, H.A., Voss, C.I., 2009b. Estimation of regional-scale groundwater flow properties in the Bengal Basin of India and Bangladesh. Hydrogeology Journal 17, 1329-1346.

Mukherjee, A., Fryar, A.E., Scanlon, B.R., Bhattacharya, P., Bhattacharya, A., 2011. Elevated arsenic in deeper groundwater of the western Bengal basin, India: Extent and controls from regional to local scale. Applied Geochemistry 26, 600-613.

Neumann, R.B., Ashfaque, K.N., Badruzzaman, A.B.M., Ali, M.A., Shoemaker, J.K., Harvey, C.F., 2010. Anthropogenic influences on groundwater arsenic concentrations in Bangladesh. Nature Geoscience 3, 46-52.

Norrman, J., Sparrenbom, C.J., Berg, M., Nhan, D.D., Nhan, P.Q., Rosqvist, H., Jacks, G., Sigvardsson, E., Baric, D., Moreskog, J., Harms-Ringdahl, P., Van Hoan, N., 2008. Arsenic mobilisation in a new well field for drinking water production along the Red River, Nam Du, Hanoi. Applied Geochemistry 23, 3127-3142.

Panaullah, G.M., Alam, T., Hossain, M.B., Loeppert, R.H., Lauren, J.G., Meisner, C.A., Ahmed, Z.U., Duxbury, J.M., 2009. Arsenic toxicity to rice (Oryza sativa L.) in Bangladesh. Plant and Soil 317, 31-39.

Radloff, K.A., Zheng, Y., Michael, H.A., Stute, M., Bostick, B.C., Mihajlov, I., Bounds, M., Huq, M.R., Choudhury, I., Rahman, M.W., Schlosser, P., Ahmed, K.M., van Geen, A., 2011. Arsenic migration to deep groundwater in Bangladesh influenced by adsorption and water demand. Nature Geoscience 4, 793-798.

Radu, T., Subacz, J.L., Phillippi, J.M., Barnett, M.O., 2005. Effects of dissolved carbonate on arsenic adsorption and mobility. Environmental Science & Technology 39, 7875-7882.

Raven, K.P., Jain, A., Loeppert, R.H., 1998. Arsenite and arsenate adsorption on ferrihydrite: Kinetics, equilibrium, and adsorption envelopes. Environmental Science & Technology 32, 344-349.

Ravenscroft, P., Brammer, H., Richards, K.S., 2009. Arsenic pollution: a global synthesis. Wiley-Blackwell.

Ravenscroft, P., McArthur, J.M., Hoque, M.A., 2013. Stable groundwater quality in deep aquifers of Southern Bangladesh: The case against sustainable abstraction. Science of the Total Environment 454, 627-638.

Robinson, C., von Bromssen, M., Bhattacharya, P., Haller, S., Biven, A., Hossain, M., Jacks, G., Ahmed, K.M., Hasan, M.A., Thunvik, R., 2011. Dynamics of arsenic adsorption in the targeted arsenic-safe aquifers in Mat lab, south-eastern Bangladesh: Insight from experimental studies. Applied Geochemistry 26, 624-635.

Saalfield, S.L., Bostick, B.C., 2009. Changes in Iron, Sulfur, and Arsenic Speciation Associated with Bacterial Sulfate Reduction in Ferrihydrite-Rich Systems. Environmental Science & Technology 43, 8787-8793.

Saalfield, S.L., Bostick, B.C., 2010. Synergistic effect of calcium and bicarbonate in enhancing arsenate release from ferrihydrite. Geochimica Et Cosmochimica Acta 74, 5171-5186.

Stollenwerk, K.G., Breit, G.N., Welch, A.H., Yount, J.C., Whitney, J.W., Foster, A.L., Uddin, M.N., Majumder, R.K., Ahmed, N., 2007. Arsenic attenuation by oxidized aquifer sediments in Bangladesh. Science of the Total Environment 379, 133-150.

Stute, M., Zheng, Y., Schlosser, P., Horneman, A., Dhar, R.K., Datta, S., Hoque, M.A., Seddique, A.A., Shamsudduha, M., Ahmed, K.M., van Geen, A., 2007. Hydrological control of As concentrations in Bangladesh groundwater. Water Resources Research 43.

Tufano, K.J., Fendorf, S., 2008. Confounding impacts of iron reduction on arsenic retention. Environmental Science & Technology 42, 4777-4783.

van Geen, A., Bostick, B.C., Trang, P.T.K., Lan, V.M., Mai, N.-N., Manh, P.D., Viet, P.H., Radloff, K.A., Aziz, Z., Mey, J.L., Stahl, M.O., Harvey, C.F., Oates, P., Weinman, B., Stengel, C., Frei, F., Kipfer, R., Berg, M., 2013. Retardation of arsenic transport through a Pleistocene aquifer. Nature in press.

van Geen, A., Cheng, Z.Q., Jia, Q., Seddique, A.A., Rahman, M.W., Rahman, M.M., Ahmed, K.M., 2007. Monitoring 51 community wells in Araihazar, Bangladesh, for up to 5 years: Implications for arsenic mitigation. Journal of Environmental Science and Health Part a-Toxic/Hazardous Substances & Environmental Engineering 42, 1729-1740.

van Geen, A., Rose, J., Thoral, S., Garnier, J.M., Zheng, Y., Bottero, J.Y., 2004. Decoupling of As and Fe release to Bangladesh groundwater under reducing conditions. Part II: Evidence from sediment incubations. Geochimica Et Cosmochimica Acta 68, 3475-3486.

van Geen, A., Zheng, Y., Goodbred, S., Horneman, A., Aziz, Z., Cheng, Z., Stute, M., Mailloux, B., Weinman, B., Hoque, M.A., Seddique, A.A., Hossain, M.S., Chowdhury, S.H., Ahmed, K.M., 2008. Flushing history as a hydrogeological control on the regional distribution of arsenic in shallow groundwater of the Bengal Basin. Environmental Science & Technology 42, 2283-2288.

van Genuchten, M.T., Alves, W.J., 1982. Analytical solutions of the one-dimensional convective-dispersive solute transport equation, USDA ARS Technical Bulletin 1661. U.S. Salinity Laboratory, Riverside, CA.

Wasserman, G.A., Liu, X.H., Parvez, F., Ahsan, H., Factor-Litvak, P., Kline, J., van Geen, A., Slavkovich, V., Lolacono, N.J., Levy, D., Cheng, Z.Q., Graziano, J.H., 2007. Water arsenic exposure and intellectual function in 6-year-old children in Araihazar, Bangladesh. Environmental Health Perspectives 115, 285-289.

Winkel, L.H.E., Pham Thi Kim, T., Vi Mai, L., Stengel, C., Amini, M., Nguyen Thi, H., Pham Hung, V., Berg, M., 2011. Arsenic pollution of groundwater in Vietnam exacerbated by deep aquifer exploitation for more than a century. Proceedings of the National Academy of Sciences of the United States of America 108, 1246-1251.

Wood, W.W., Kraemer, T.F., Hearn, P.P., 1990. Intergranular diffusion - an important mechanism influencing solute transport in clastic aquifers. Science 247, 1569-1572.

Yu, W.H., Harvey, C.M., Harvey, C.F., 2003. Arsenic in groundwater in Bangladesh: A geostatistical and epidemiological framework for evaluating health effects and potential remedies. Water Resources Research 39, 17.

Zhang, H., Selim, H.M., 2005. Kinetics of arsenate adsorption-desorption in soils. Environmental Science & Technology 39, 6101-6108.

Zhang, H., Selim, H.M., 2006. Modeling the transport and retention of arsenic (V) in soils. Soil Science Society of America Journal 70, 1677-1687.

Zheng, Y., van Geen, A., Stute, M., Dhar, R., Mo, Z., Cheng, Z., Horneman, A., Gavrieli, I., Simpson, H.J., Versteeg, R., Steckler, M., Grazioli-Venier, A., Goodbred, S., Shahnewaz, M., Shamsudduha, M., Hoque, M.A., Ahmed, K.M., 2005. Geochemical and hydrogeological contrasts between shallow and deeper aquifers in two villages of Araihazar, Bangladesh: Implications for deeper aquifers as drinking water sources. Geochimica Et Cosmochimica Acta 69, 5203-5218.

4.7 Appendix

4.7.1 Column porosity and dispersion estimated by Br breakthrough and the 1-dimensional advection-dispersion model

Bromide breakthrough curves (BTCs) from the two columns prepared in the field and run later in the laboratory (Fig. 4.8) resulted in estimated column porosities of 0.29 and 0.33 (Table 4.2). For the simplicity of calculations, and because the true variability of the porosity is unknown, all pore volumes (PV) and pore velocities in PV/day for column experiments in the field were calculated assuming a porosity of 0.33 (Table 4.2). The two measured column porosities were utilized, however, to obtain the exact column linear velocity (v), a necessary input parameter for a 1-dimensional advection-dispersion model to estimate the longitudinal dispersivity in the two columns. A simple analytical solution (van Geen et al., 2013; van Geen et al., 2008; van Genuchten and Alves, 1982) was used to fit the model to observed Br concentrations C at time t for a point at distance x along the flow path (i.e. the column length for column effluent), assuming that no Br is initially present in the columns because they were pre-conditioned with Br-free water:

$$C(x,\ t) = C_0 \left[\frac{1}{2} erfc \frac{(Rx - vt)}{2(DRt)^{\frac{1}{2}}} + \frac{1}{2} \exp(vx / D) erfc \frac{(Rx + vt)}{2(DRt)^{\frac{1}{2}}} \right] \quad \text{(eq. 4)}$$

where C_0 is the inflowing Br concentration (170 mg/L or 1 in case of the dimensionless C/C_0), R is the retardation factor (set to 1 in case of Br), and D is the hydrodynamic dispersion coefficient. The molecular diffusion in negligible in this case, resulting in the hydrodynamic dispersion expression of $D = \alpha_L v$, where α_L is the longitudinal dispersivity.

The values of α_L estimated from the rising flank of Br BTCs are 0.5 and 0.7 cm in the columns containing the sand from 42 and 66 ft bgl, respectively (Fig. 4.8 and Table 4.2).

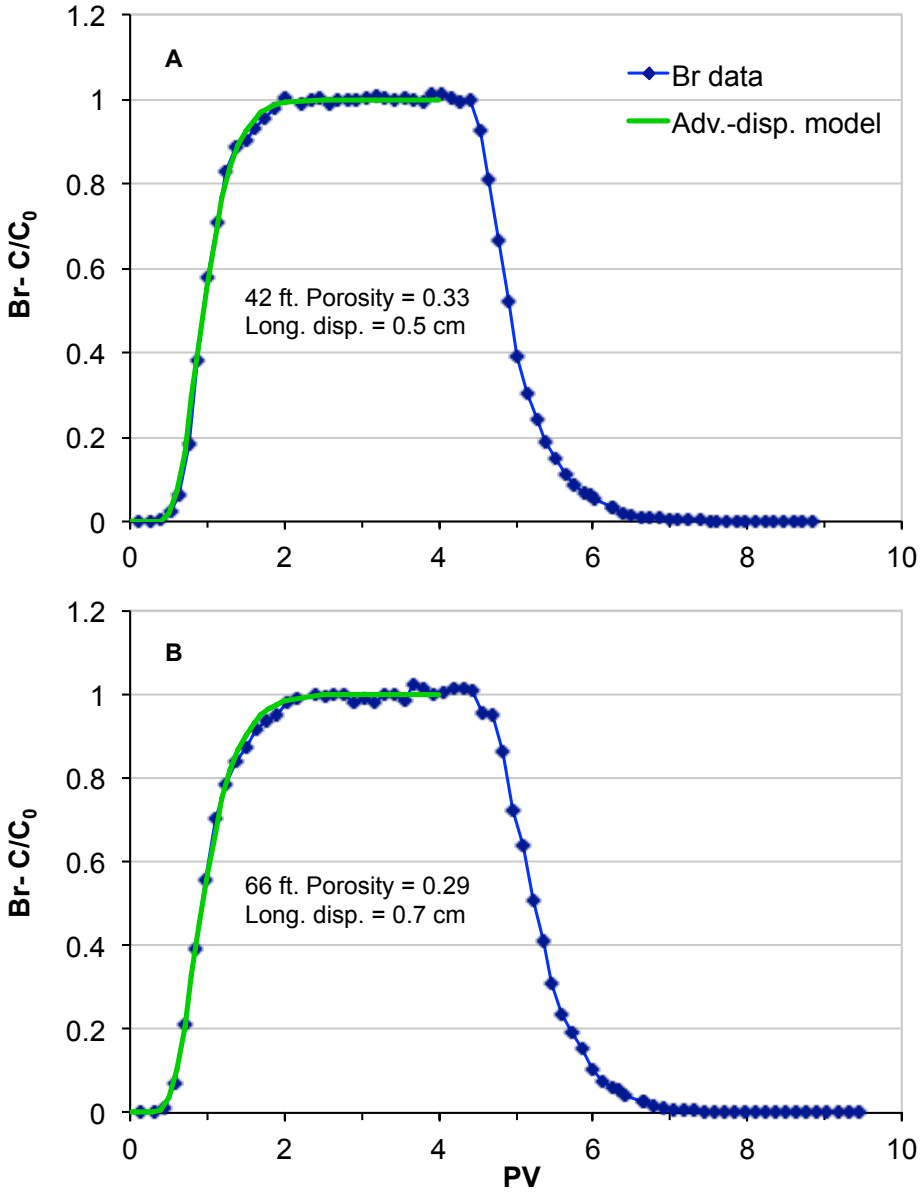

Figure 4.8. Bromide breakthrough curves (normalized to C_0 of 170 mg/L) from (a) 42 ft sediment and (b) 66 ft sediment. Br BTCs were used to estimate column porosity (PV = 1 where $C/C_0 = 0.5$) and advection-dispersion model fits (van Genuchten, 1982), shown as green lines, were employed to estimate longitudinal dispersivity. The resulting porosity and longitudinal dispersivity are indicated on the panels.

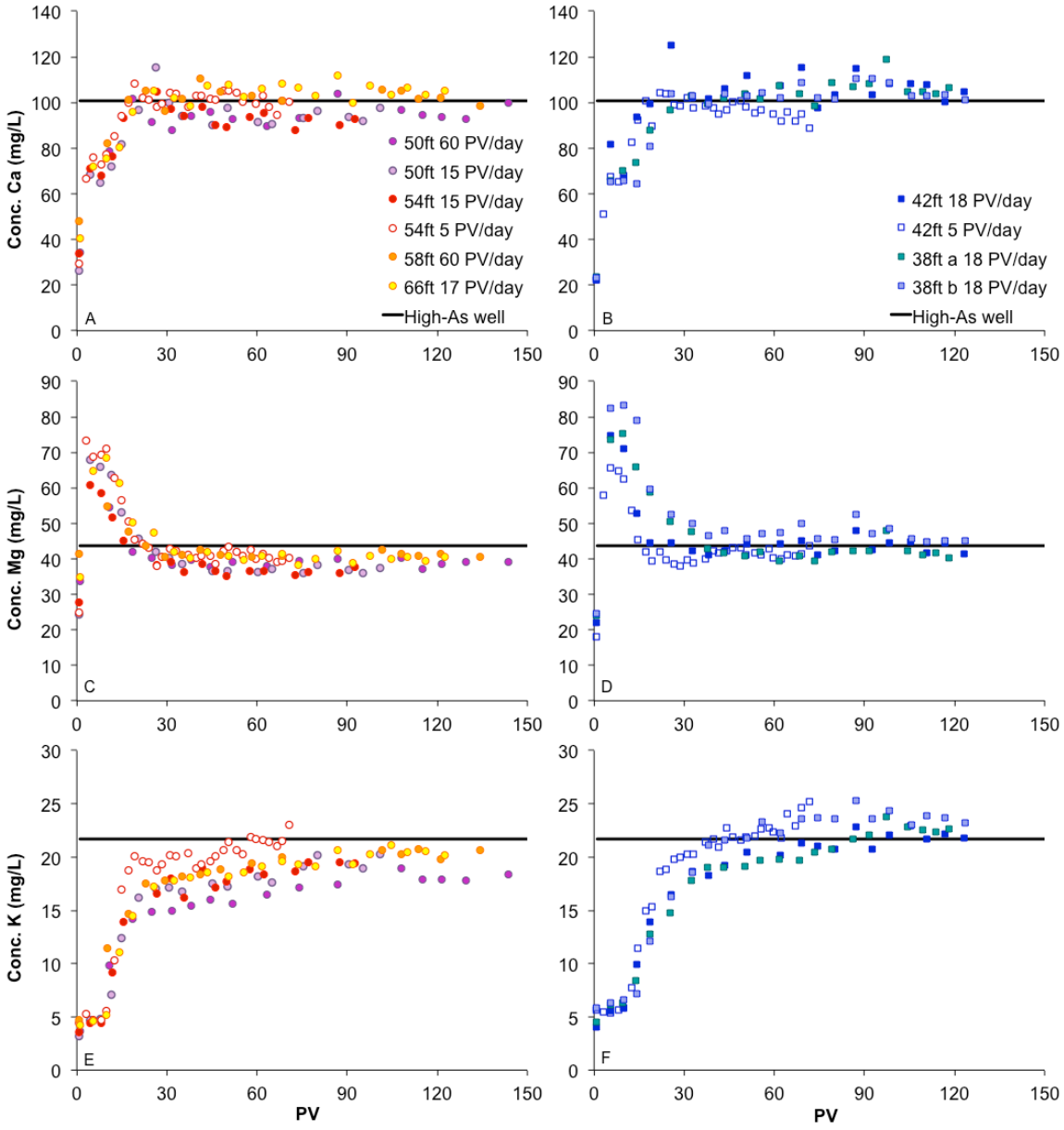

Figure 4.9. (part I): Breakthrough curves of (a,b) Ca, (c,d) Mg, and (e,f) K in columns from 50-66 ft bgl (left side panels) and 38-42 ft bgl (right side panels). Note that the cations reached steady-state concentration by PV~20, regardless of the sediment depth, in contrast to the sorption of As (Fig. 4.2) and Mn (this figure, part III).

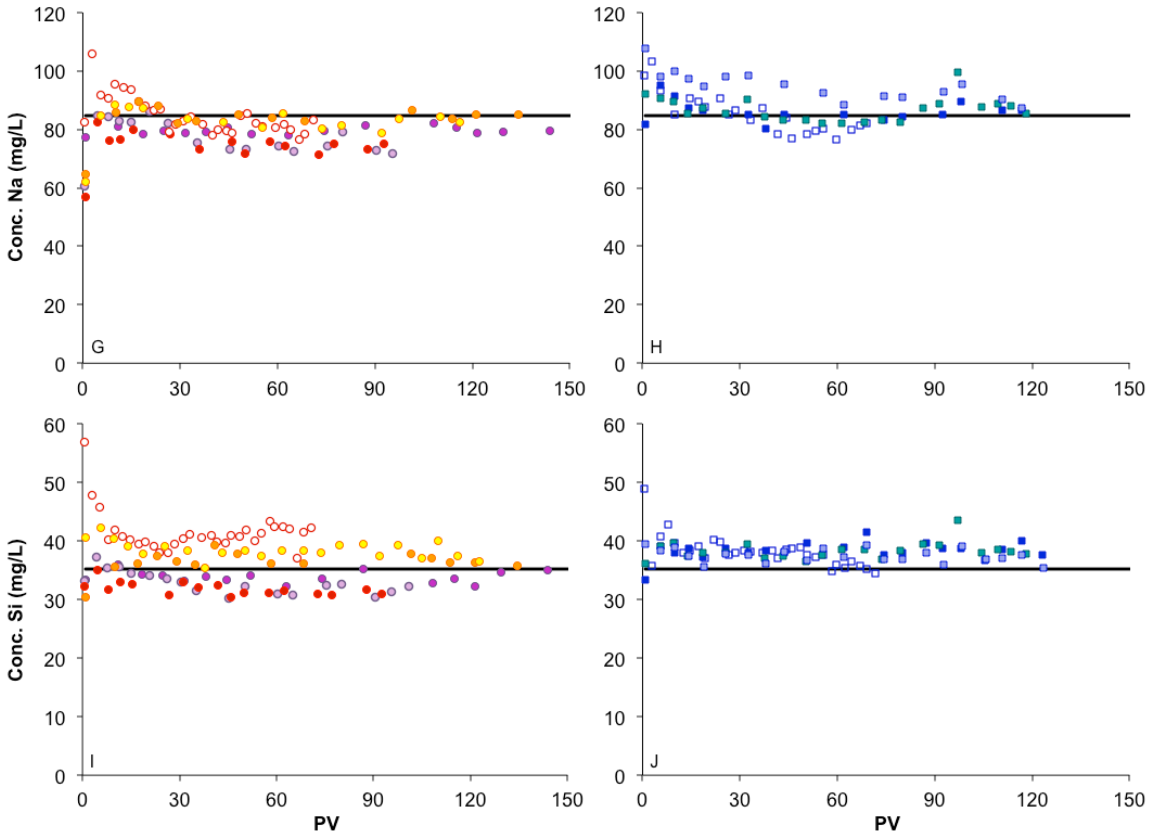

Figure 4.9. (part II): Breakthrough curves of (g,h) Na, and (i,j) Si in columns from 50-66 ft bgl (left side panels) and 38-42 ft bgl (right side panels).

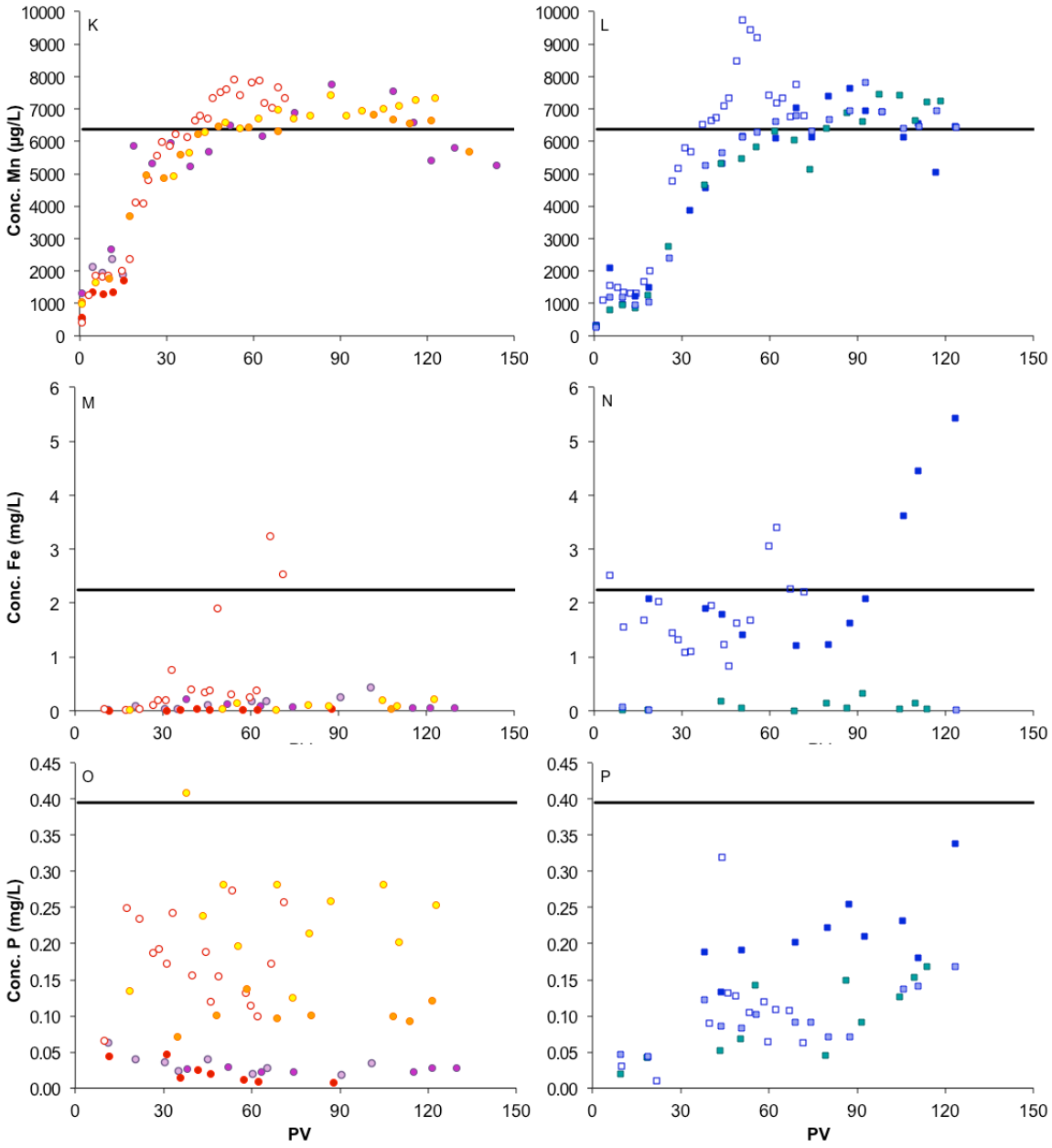

Figure 4.9. (part III): Breakthrough curves of (k,l) Mn, (m,n) Fe, and (o,p) P in columns from 50-66 ft bgl (left side panels) and 38-42 ft bgl (right side panels). Note that the breakthrough of Mn followed a similar pattern to that of As (Fig. 4.2) with more retardation in the sediment from 38-42 ft. More dissolved Fe and consistenly higher P

(proxy for PO_4) were present in the 38-42 ft range. Only the 5 PV/day column from 54 ft bgl released some Fe.

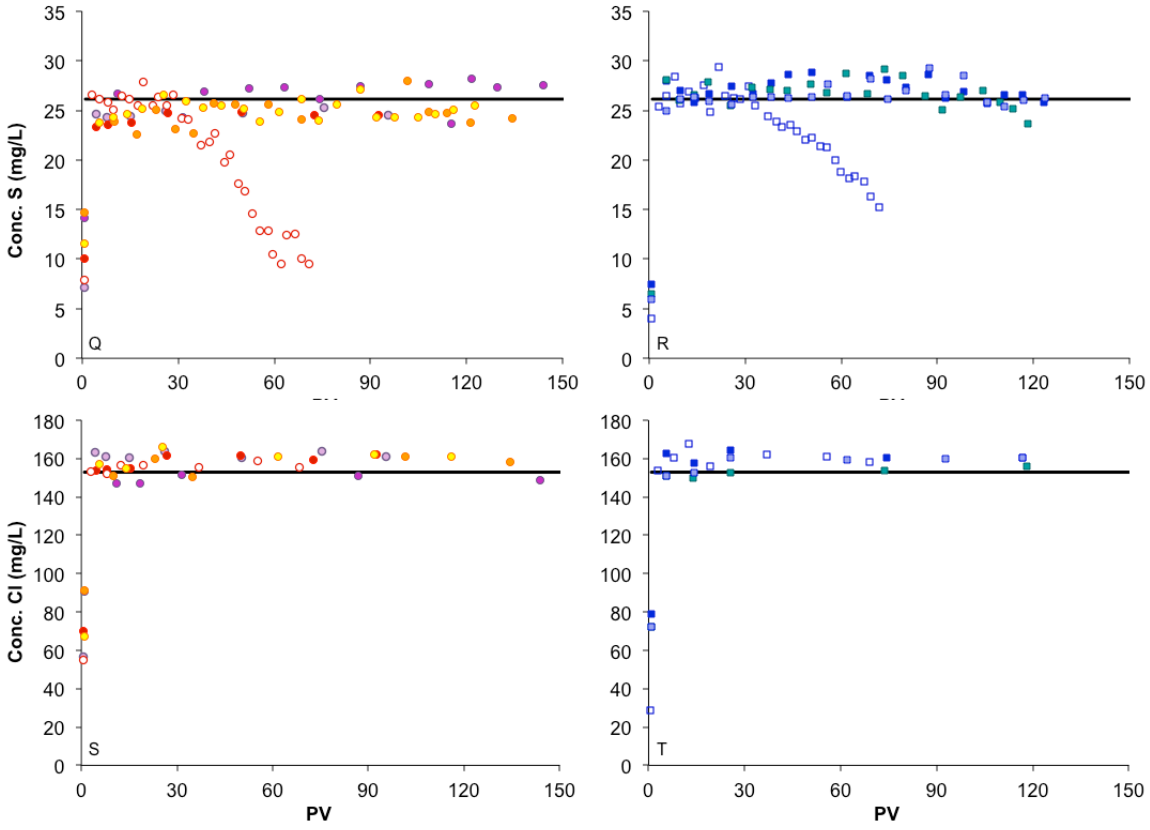

Figure 4.9. (part IV): Breakthrough curves of (q,r) S, and (s,t) Cl in columns from 50-66 ft bgl (left side panels) and 38-42 ft bgl (right side panels). Note that S (proxy for SO_4) and Cl broke through immediately, as expected from anions. SO_4, however, was reduced in the slow-flowing columns (5 PV/day).

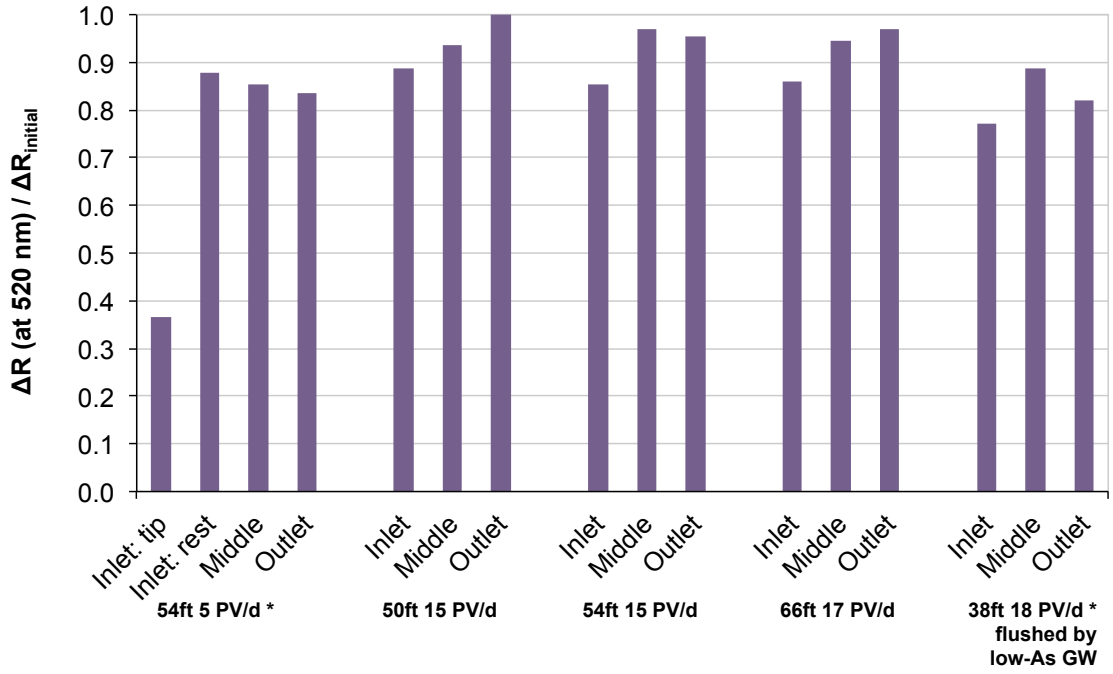

Figure 4.10. Diffuse spectral reflectance (ΔR) between 530 and 520 nm (or 550 and 500 nm in samples with *) normalized to the ΔR of the initial sediment in each column. The lower the ΔR, the more grey the sediment color is, indicating a change of the Fe speciation towards more reduced Fe species, Fe(II). The initial ΔR of the sediment was 1.25-1.31 (530-520 nm) or 6.3-6.9 (550-500 nm), typical of the Pleistocene brown sediment in the area.

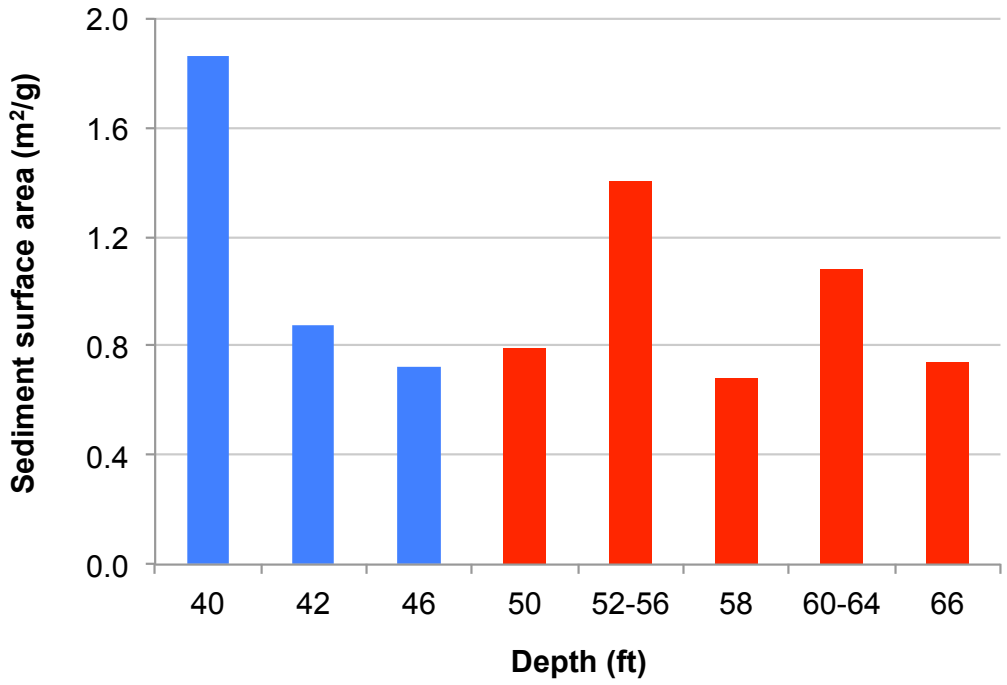

Figure 4.11. Sediment surface area based on the grain size analysis and assuming the particles are shaped as platelets.

Table 4.1. Reversibility of As sorption: percentage of As removed by flushing with low-As groundwater and/or PO_4 extractions.

Depth (ft)	Pore velocity PV/day	Total As (final)* ppm	Flush with low-As GW?	% As removed by GW Flush	Field PO_4 ext.	Lab. PO_4 ext.^	Lab. HCl ext.
54	5	5.7	NO	-	-	45.6	7.4
66	17	5.5	NO	-	63.1	64.9	7.3
38 a	18	7.6	YES	51.8	-	30.2[$]	6.7[$]
38 b	18	7.0	NO	-	70.9	-	-
42	18	4.7	YES	71.6	-	-	-

* Includes initial PO_4-ext. As + column mass balance with high-As groundwater (GW)

^ Laboratory extraction performed 4 months later. Includes As extractable by MilliQ water

[$] % total As, in addition to the flush with low-As GW

Table 4.2. Column test parameters.

Depth / borehole ft	Length cm	Pore volume* mL	Pore velocity mL/min	Pore velocity PV/day	Flush with low-As GW?	Br test pore vel. PV/day	Br test porosity	Br test long. disp.[$] cm
42 b	10.00	8.40	0.027	4.7	-	-	-	-
42 a	9.70	8.15	0.103	18.2	Yes	35.2	0.33	0.5
38 a	9.70	8.15	0.100	17.8	Yes	-	-	-
38 b	9.75	8.19	0.105	18.5	-	-	-	-
54 b	10.00	8.40	0.027	4.6	-	-	-	-
54 a	9.50	7.98	0.085	15.3	-	-	-	-
66 a	9.80	8.23	0.105	18.4	-	-	-	-
66 b ^	10.35	8.69	-	-	-	37.4	0.29	0.7
50 a	9.90	8.31	0.087	15.1	-	-	-	-
50 b	10.00	8.40	0.363	62.2	-	-	-	-
58 a	10.00	8.40	0.339	58.1	-	-	-	-

* Pore volume (PV) calculated from column dimensions by assuming a porosity of 0.33 for all columns.

^ Column from 66 ft depth, borehole b was only used for the Br tracer test

[$] Longitudinal dispersivity (this value is multiplied by velocity to get the longitudinal dispersion for advection-dispersion model)

Table 4.3. Groundwater chemistry of the source wells for the column experiments. Values shown are averages of daily sampling over the duration of column experiments. Low-As well was used for flushing the two columns from 38 and 42 ft depth and for the sorption isotherm and kinetics experiments (with added As(III) spikes).

Measurement	Unit	Source Well	
		High-As	Low-As
Na	mg/L	84.7	51.0
Mg	mg/L	43.6	6.0
Si	mg/L	35.1	69.5
P	mg/L	0.40	0.22
S	mg/L	26.1	1.0
K	mg/L	21.7	1.5
Ca	mg/L	100.7	17.5
Mn	µg/L	6372	62
Fe	mg/L	2.24	0.05
As	µg/L	593.7	0.3
AsIII	µg/L	585.4	0.4
Cl	mg/L	153	28
Temp.	°C	25.67	26.32
Cond.	mS/cm	1.398	0.388
ORP	-	-89.9	20.5
DO kit	µg/L	<5	<5
pH	-	6.70	6.37
Alkalinity	mM	7.62	2.72

Table 4.4. Grain size analysis.

Size fraction (< xx µm)	Sediment Depth (ft) ===> 40 % of total sed	42 % of total sed	46 % of total sed	50 % of total sed	52-56 % of total sed	58 % of total sed	50-64 % of total sed	66 % of total sed
2500	2.7	1.4	12.0	11.1	8.9	3.0	1.2	2.9
500	34.8	70.4	63.3	66.1	65.1	74.6	74.2	73.1
150	42.0	13.0	9.0	8.0	10.8	10.5	9.8	10.6
70	0.2	0.0	0.1	0.1	0.0	0.1	0.0	0.1
62	2.7	1.1	2.1	1.0	1.0	0.5	0.5	1.1
31	3.1	2.5	2.6	2.8	1.0	2.0	1.6	3.2
16	3.7	3.6	3.4	4.0	1.9	2.6	3.3	3.6
8	2.9	2.8	3.4	2.7	2.4	2.6	3.4	2.3
4	2.9	2.5	2.4	2.2	3.9	1.9	2.5	1.6
2	1.5	1.3	0.5	0.6	2.1	0.9	1.7	0.6
1	0.6	0.8	0.5	0.7	1.2	1.1	0.7	0.1
0.8	2.9	0.6	0.5	0.7	1.5	0.3	1.0	1.0
	Surface area (m^2/g), assuming spheres ===>							
Total sediment	0.25	0.12	0.10	0.11	0.19	0.09	0.15	0.10
	Surface area (m^2/g), assuming platelets (thickness = 1/20 length) ===>							
Total sediment	1.86	0.87	0.73	0.79	1.40	0.68	1.08	0.74

The following Tables and Figures are NOT referred to in the text

Table 4.5. Time series of the input well groundwater composition; constituents measured by IC (Cl) and ICP-MS (all else)

Date	Na mg/L	Mg mg/L	Si mg/L	P mg/L	S mg/L	K mg/L	Ca mg/L	Mn µg/L	Fe mg/L	As µg/L	AsIII µg/L	Cl mg/L	Exp. End pt.
SHALLOW HIGH-As WELL													
8-Jan-10													Start: all
9-Jan-10 am	80.5	42.1	35.6	0.38	24.1	17.2	95	5223	2.06	608	598	150	
9-Jan-10 pm	81.0	41.1	34.2	0.47	24.7	18.4	99	5944	2.00	589	651	150	
10-Jan-10	84.7	44.3	35.9	0.44	26.4	21.7	101	6564	2.10	613		151	
11-Jan-10	86.0	43.3	35.6	0.36	26.5	22.3	102	6748	2.46	596	589	153	High-vel. end
12-Jan-10	85.8	45.0	34.7	0.34	26.9	23.0	100	6661	2.26	602		155	
13-Jan-10	86.6	44.5	34.6	0.32	26.6	23.8	102	6357	2.26	572	591	152	
14-Jan-10	87.6	44.5	35.1	0.45	26.2	23.5	104	6664	2.36	583		155	
15-Jan-10	85.3	43.9	35.1	0.41	27.6	23.5	103	6812	2.44	586	564	156	Med-vel. end
16-Jan-10	88.5	45.0	34.7	0.42	26.9	24.3	101	6715	2.65	577		156	
17-Jan-10	89.0	46.0	34.5	0.42	27.7	24.6	100	6867	2.57	588	492	158	
18-Jan-10	86.6	43.6	35.2	0.34	26.7	25.1	104	6969	2.78	601			
19-Jan-10	87.0	45.8	35.7	0.33	26.9	26.2	102	7001	2.77	578	521	155	
20-Jan-10	86.5	44.9	37.1	0.40	26.4	25.9	104	6917	3.04	563		155	
21-Jan-10	89.1	44.8	35.4	0.36	25.9	26.9	101	7269	3.06	565	528	156	
22-Jan-10	87.1	45.6	35.4	0.38	26.6	27.7	100	7201	3.00	590		154	
23-Jan-10	83.1	43.4	35.0	0.51	25.3	26.4	97	6959	3.09	558	510	155	
24-Jan-10	86.4	45.1	35.1	0.47	25.9	27.8	96	6881	3.12	532		151	Low-vel. end
DEEP LOW-As WELL													
15-Jan-10	51.1	6.0	71.3	0.22	1.1	1.7	18	70	0.08	0.3	0.4	28	Start
16-Jan-10	51.9	6.1	69.5	0.23	1.0	1.5	17	68	0.08	0.4		28	(Med-vel. only)
17-Jan-10	51.1	5.8	66.2	0.21	1.0	1.5	17	62	0.03	0.1		28	
18-Jan-10												28	
19-Jan-10	50.9	6.1	70.1	0.24	1.1	1.5	18	61	0.17	0.4		28	
20-Jan-10	51.7	6.0	71.5	0.22	1.1	1.5	18	61	0.02	0.3		28	
21-Jan-10	51.4	5.9	70.4	0.23	1.1	1.5	17	62	0.01	0.1		27	
22-Jan-10	50.1	6.0	68.9	0.22	1.0	1.5	17	60	0.02	0.2		28	
23-Jan-10	49.4	5.8	71.0	0.21	1.0	1.4	18	55	0.01	0.1		28	
24-Jan-10	51.7	5.9	66.2	0.23	1.0	1.5	17	61	0.01	0.3		28	End

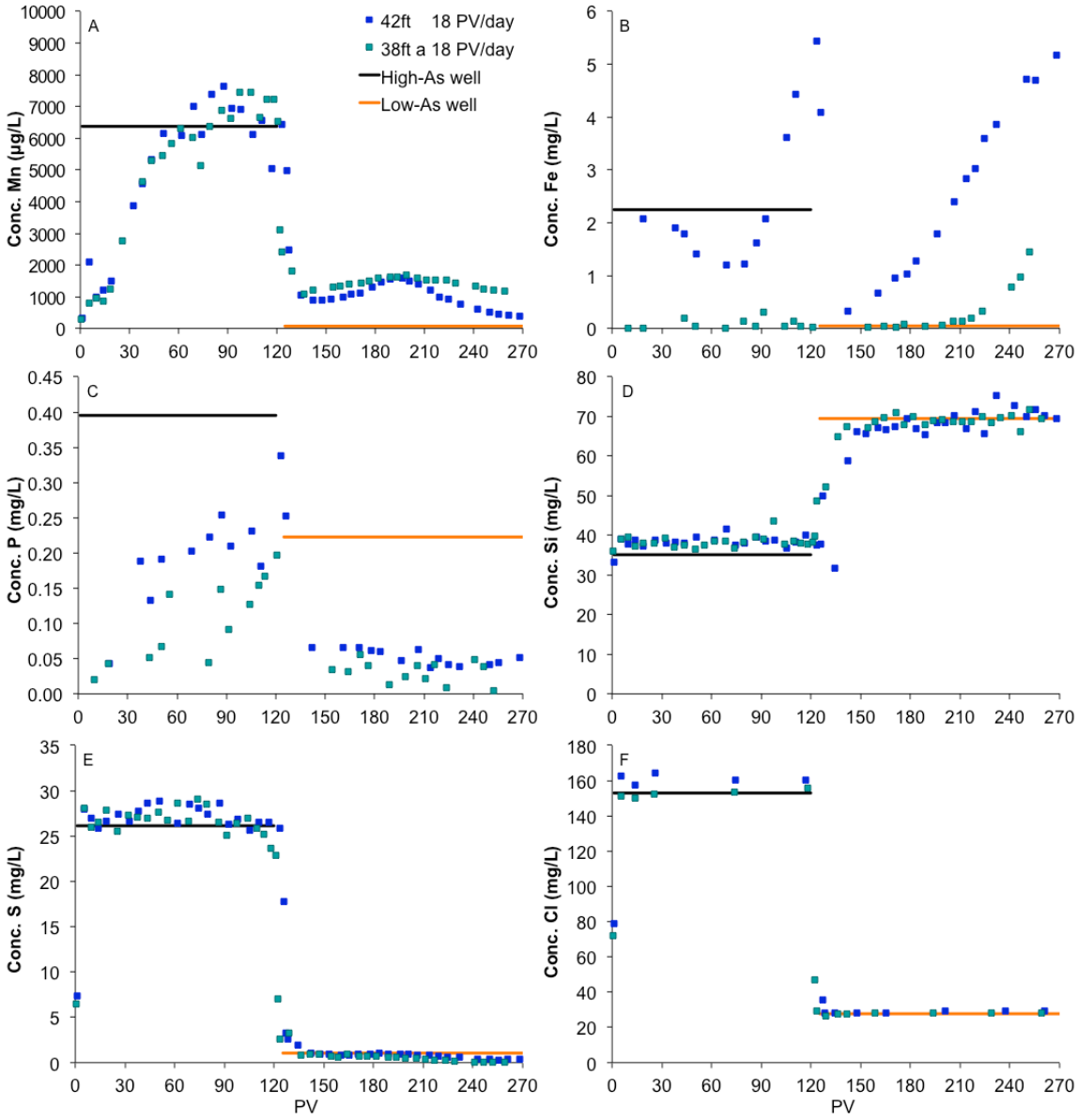

Figure 4.12. (part I): Breakthrough curves from the columns flushed by deep, low-As groundwater after 120-125 PV of shallow, high-As groundwater inflow. Elements shown: (a) Mn, (b) Fe, (c) P, (d) Si, (e) S, and (f) Cl.

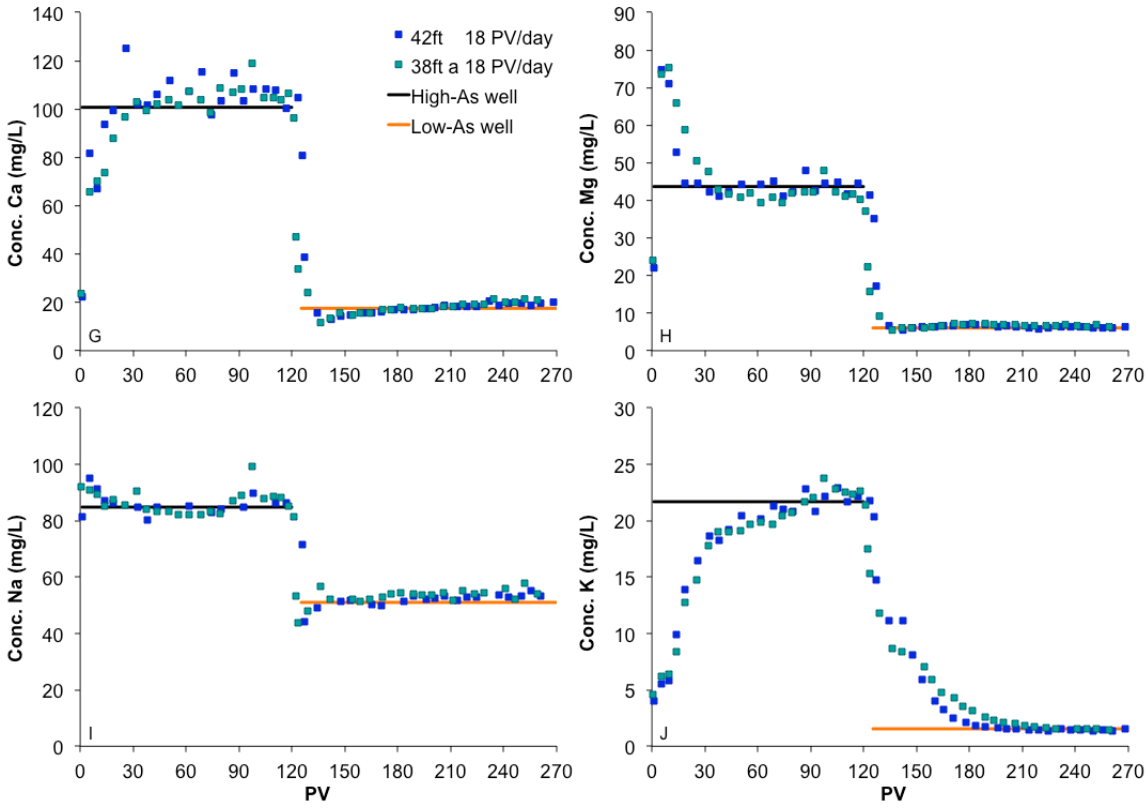

Figure 4.12. (part II): Breakthrough curves from the columns flushed by deep, low-As groundwater after 120-125 PV of shallow, high-As groundwater inflow. Elements shown: (g) Ca, (h) Mg, (i) Na, and (j) K.

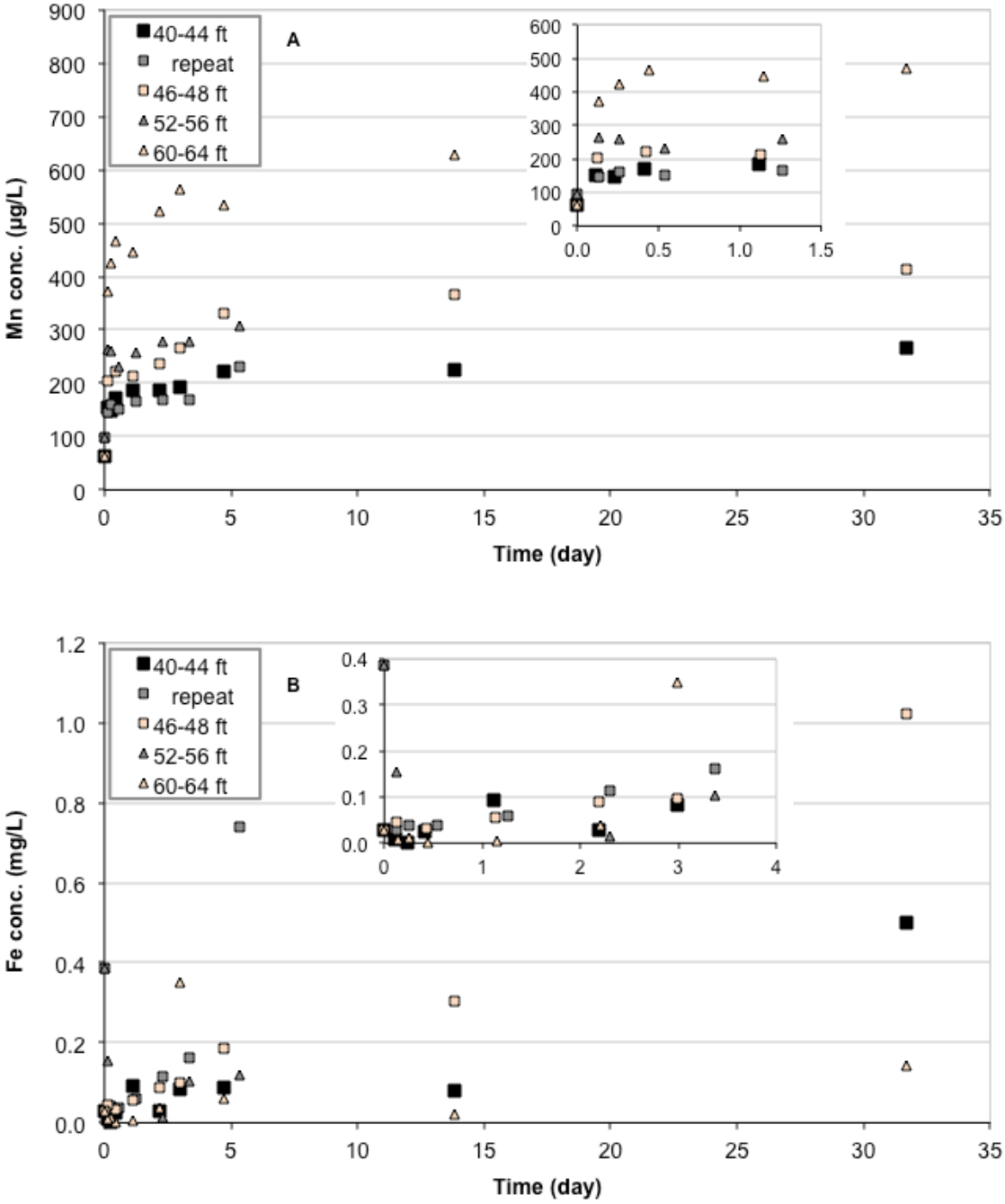

Figure 4.13. Dissolved (a) Mn and (b) Fe in batch kinetic experiments.

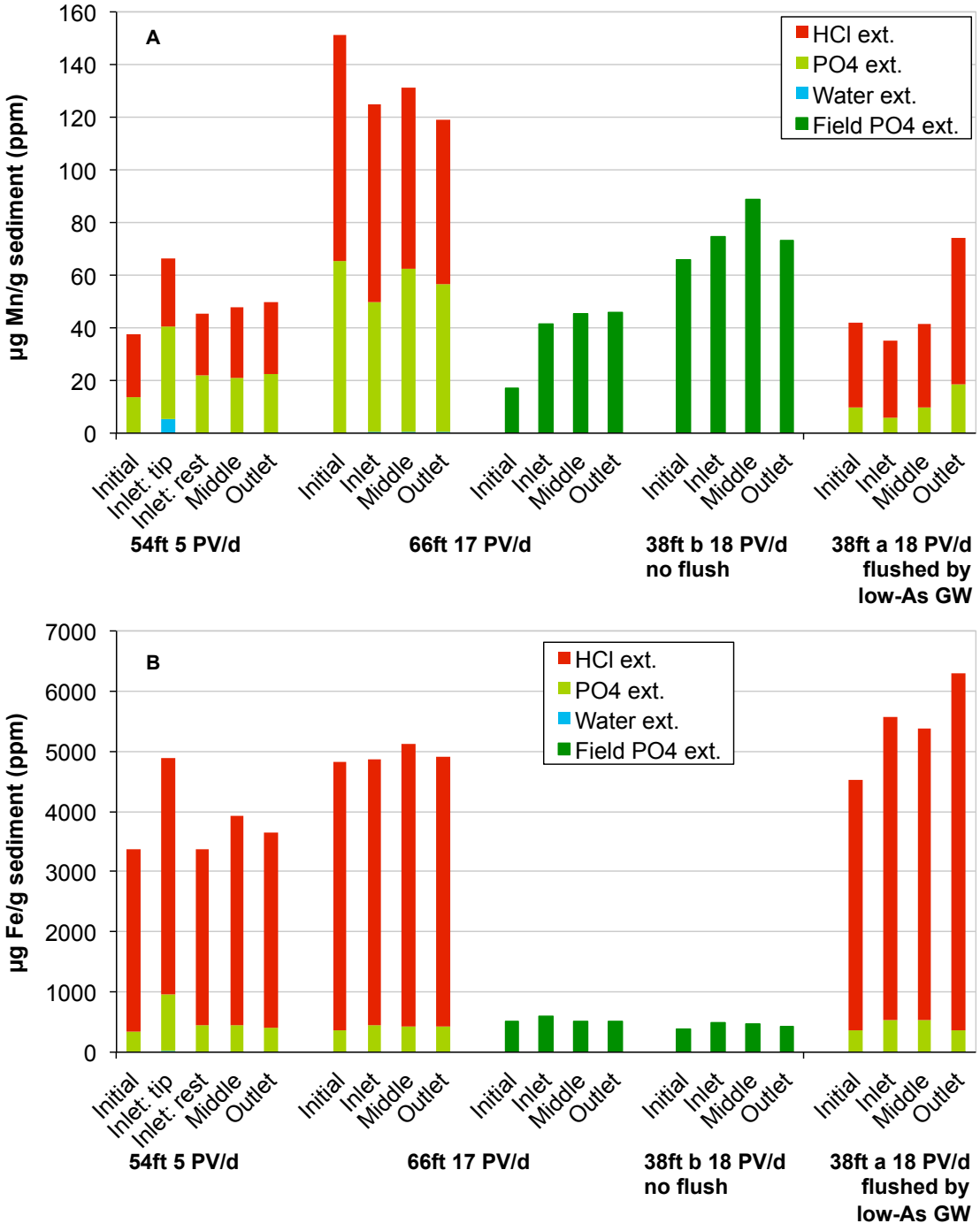

Figure 4.14. (a) Mn and (b) Fe extracted from the column sediment.

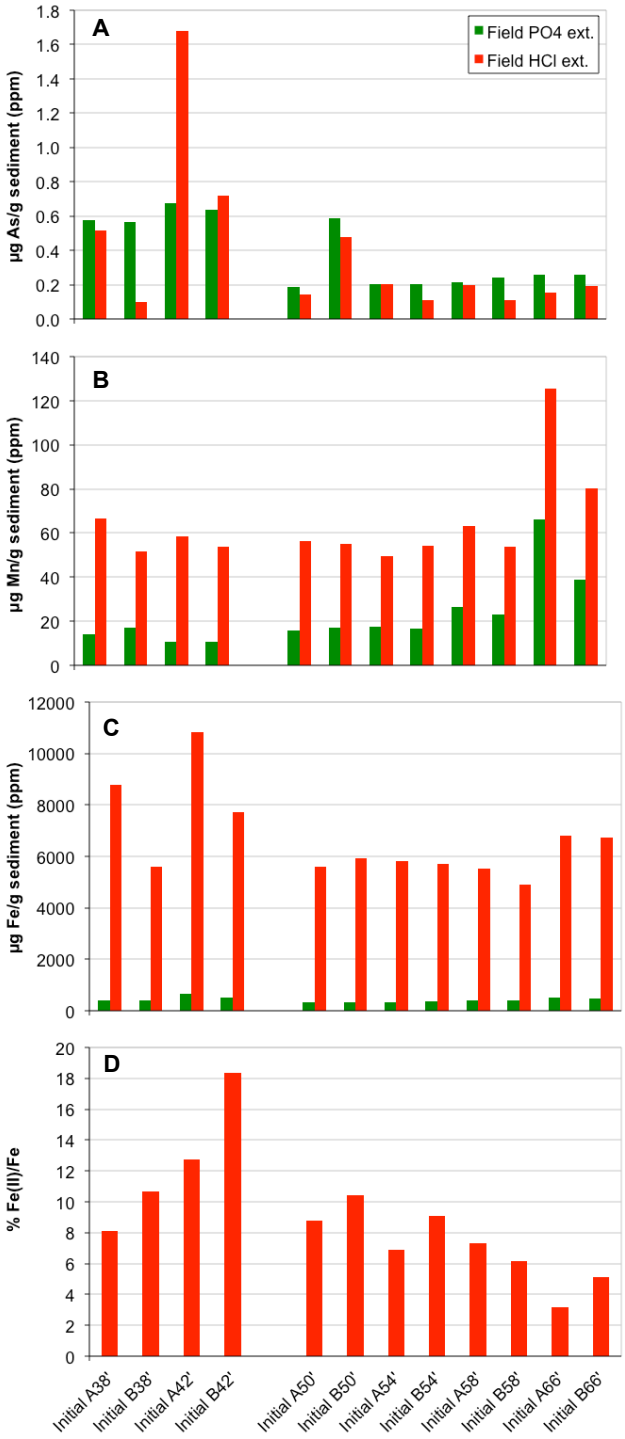

Figure 4.15. Non-sequential, field extractions of the initial column sediment with PO_4 and HCl. Results are shown for (a) As, (b) Mn, (c) Fe, and (d) Fe speciation.

Chapter 5:

Conclusions

5.1 General overview

The research presented here focused on the vulnerability of low-As aquifers in Bangladesh by investigating their hydrologic and geochemical properties across several spatial and temporal scales. The question of sustainability of these aquifers, located beneath the shallow aquifers with peaking As concentrations, is intimately coupled to the changing patterns of groundwater abstraction and the implications these changes will have on As contamination. The continued rise in pumping of these aquifers, and the drawdown of shallow groundwater with As and organic matter seem inevitable with further development. Some researchers (see Ravenscroft et al., 2013 in Introduction) have argued that the low-As aquifers should also be exploited for food production to maintain the quantity and quality of crop yields, despite the risks of contaminating this source of drinking water in the future. My work does not necessarily argue against such a view on resource development. Although we currently see no evidence of widespread contamination of deep or intermediate aquifer in our field area, the findings presented here could help better understand the associated risks and inform the future resource management.

5.2 Main findings and their implications

5.2.1 Groundwater recharge and residence times in intermediate (35-120 m) and deep (>120 m) low-arsenic aquifers east of Dhaka, Bangladesh

Broader-scale patterns in groundwater geochemistry and residence times at depth were characterized across a 25 km^2 study area in Chapter 2. The variability of groundwater chemistry and ages in the intermediate depth zone of low-As aquifers (35-120 m bgl) demonstrated that a portion of these low-As aquifers is subject to recharge with shallow groundwater. However, the intrusion of shallow groundwater to this depth, indicated by elevated concentrations of bomb-released ^{3}H (>0.3 TU) or $^{14}C_{DIC}$ (>0.9 FM), did not correlate with increased groundwater As levels, which is a reassuring finding for the long-term stability of groundwater quality. The recharge from shallow aquifers might preferentially originate from low-As zones and/or low-As aquifer sediment has enough capacity to retard As transport, both of which could contribute to the observed robustness of the intermediate aquifers. The results from these aquifers also reinforced the fact that the distribution of confining clay layers is patchy, and that despite their presence in well lithologs, they do not necessarily protect the wells from shallow groundwater intrusion that can happen at some lateral distance where the clay capping is absent.

Groundwater at depth >120 m bgl has a fairly constant signature of low Na and dissolved inorganic carbon (DIC), high Si, and a ^{14}C age of ~10 kyr. The consistent relationship between radiocarbon and stable isotopes, ^{13}C in DIC, and ^{2}H and ^{18}O in water, is compatible with the recharge of deep groundwater at the transition from

Pleistocene to Holocene when the summer monsoon was intensifying and the dominant vegetation was changing from that adapted to more arid conditions (e.g. C4 grasses) to the vegetation more successful in wetter environments (e.g. C3 bushes and mangroves). Besides being the first report, to our knowledge, of a paleoclimatic record contained within the groundwater of Bengal basin, the importance of this finding lies in the possibility that groundwater was trapped or rapidly recharged at the onset of the Holocene and has not been subject to significant flows since. If groundwater at this depth had been more or less stagnant, increasing deep groundwater abstraction by installing large mechanized urban supply systems, such as the one in Dhaka, could dramatically increase the recharge rate from lateral or vertical leakage and alter the residence time of groundwater in these aquifers. As the connectivity of deep aquifers to the sources of lateral recharge, such as the rivers or the hilly basin edges, is not well known, increased exploitation might induce more infiltration along vertical flowpaths and possibly along preferential flow pathways with as yet unclear consequences for As contamination.

A linear relationship was found between ^{14}C in DIC and the radiogenic He modeled from noble gas concentrations in groundwater from all depths in this study. The noble gas record could, thus, be used to approximate groundwater ages based on the accumulation of radiogenic He in groundwater elsewhere in the basin and at greater depths where the ^{14}C technique might not work, as well as in other sandy aquifers. The key to using this dating technique would be to better constrain the release rates of He from aquifer sediment, perhaps by measuring U and Th directly in the studied sediment.

5.2.2 Arsenic contamination exacerbated by clay layers in a low-arsenic aquifer in Bangladesh

The dominant notions of low-As aquifer vulnerability were challenged by the work presented in Chapter 3. A confining clay layer may not always protect the underlying aquifer from contamination, whereas a contact with shallow aquifer via recent recharge may not always adversely affect the low-As aquifer. At the studied location near a community well with documented failures despite a sound well construction, the pore water seeping out of the capping clay layer introduced As, Fe, and NH_3 into the aquifer, as well as the organic matter that helps reduce aquifer sediment near the clay layer and release additional As. The groundwater age in this zone is >60 years, and clay pore water may enter due to a combined effect of downward hydraulic gradient across the clay and the stresses that squeeze the compressible clay, such as the long-term compaction and the short-term pressure pulses when irrigation pumps turn on and off.

The deeper part of the aquifer is well flushed by recent recharge, but there is no evidence of the recharge bringing reactive DOC, as the sand here is still orange and host groundwater with <10 μg/L As. A discontinuity in the clay layer south of the site likely allows the penetration of younger groundwater, but more complex flow paths are also possible because the downward hydraulic gradient can drive vertical flows across any other clay discontinuities that might exist. It appears that the faster recharge at depth of the orange sand currently protects this portion of the aquifer from contamination seeping downward from the clay and upper part of the aquifer, but it is not clear if this lack of contamination with As is due to a low-DOC content of the intruding groundwater, or if the arrival of shallow organics and As to the site is presently delayed by sediment

adsorption. Unfortunately, the migration of As is observed within the vertical dimension when a frequently pumped community well is installed in the thin orange sand layer, and As is transported from the upper, reduced part of the aquifer to the well screen within 1-2 years.

The results of this study call for a re-evaluation of the sustainability concepts for the low-As aquifer to include the possibility that (1) pore water within deeper clay layers, and not just peats or surface clay deposits, might exacerbate the As contamination, and that (2) more rapid recharge might protect the aquifers when the infiltrating groundwater contains low As or organic matter levels. Another major implication of the study is that the wells in low-As aquifers might be prone to failures if the aquifer is too thin to provide flowpaths sufficiently long for As sorption to occur, or if the well is too close to the base of the edge of a confining unit to avoid mixing with the clay pore water. Caution is necessary when installing future wells, and the importance of regular testing of water quality and hydraulic heads is further underscored in order to detect potential problems within the formation chosen for installation.

5.2.3 Arsenic transport through columns of brown low-arsenic aquifer sand eluted in the field with shallow groundwater

A novel set-up of the column experiments with fresh sediment cores converted into columns, and elution with high-As shallow groundwater while the columns were submerged and maintained anoxic, allowed for a simulation of *in situ* conditions, while at the same time providing a simple and controlled flow system for this sorption study. The transport of As under flow rates explored in the experiment was described by

hydrodynamic dispersion, measured with Br tracer, and equilibrium adsorption of As, resulting in a range of retardation coefficients of ~20-40. A large amount of the adsorbed As could be desorbed by flushing with low-As groundwater and/or by sediment extractions targeting the pools of adsorbed As and As incorporated in less crystalline Fe minerals, however at least 10-30% of the adsorbed As was retained on column sediments. The retention of As on column sediment by adsorption was likely limited by the relatively fast flow conditions imposed, but also enhanced by non-sorptive reactions occurring, particularly in low pore velocity columns. The longer residence time in these columns allowed for a greater impact of SO_4 and Fe reduction on Fe mineral rearrangements that likely incorporated some As scavanged from the dissolved phase.

The retardation of As varied by a factor of 2 within the cores we studied, collected at a single borehole location, but various types of sediment (e.g. grey sand) are present in low-As aquifers throughout the basin. The groundwater composition, although highly reducing, atypically included both high As and high SO_4, so the reactions occurring under such conditions might not be geographically representative. Nevertheless, the estimates of As retardation made in the column experiments are within the range of those reported in other studies, both *in situ* and experimental, thus validating the relevance of this approach. Furthermore, the method described in our study is relatively simple to execute, it does not rely on the availability of specific subsurface flow geometries that often make field studies more difficult to locate, and the results can be interpreted in a straightforward manner. Thus, barring the availability of sediment cores, the column experimental method described here is easily transferrable elsewhere and could be employed to initially and simply characterize the general retardation and reactions of As

and other contaminants on diverse aquifer sediments with various groundwater compositions in the areas of concern worldwide.

5.3 Future work

While the research performed as a part of this thesis has shed light on certain aspects surrounding the flow of groundwater and transport of arsenic between and within sandy aquifers in Bangladesh, the findings also raise new questions. The groundwater age reported in Chapter 2 for low-As aquifers 120-240 m deep, located roughly in the central part of Bengal basin, was ~10,000 years, however the residence times of groundwater at greater depths or along the basin edges are unknown. Surveying the ages systematically across the basin might be able to answer the question whether recharge from basin edges to deeper parts of the aquifer continues at present; if so, faster recharge from the basin-margin highlands with more dilute low-arsenic groundwater might be able to protect the aquifer to a certain degree from vertical intrusion of contaminated shallow groundwater.

As downward vertical gradients grow larger in the region, it would be of interest to verify if direct vertical recharge and shallow groundwater leakage occur at depths >100 m bgl in the areas most affected by deep pumping, such as in Dhaka city. The drawdown cone under Dhaka might have already impacted the groundwater chemistry and tracers, such as stable isotopes, ^{3}H, and ^{14}C, but this has not been documented yet. Large rivers, such as the Ganges, the Brahmaputra, and the Meghna surround Dhaka city, thus the recharge of increasingly exploited deep aquifers could also be occurring from the rivers. Whether this indeed occurs can be explored by detailed hydraulic head monitoring

in vicinity of the rivers, as well as by sampling groundwater tracers and chemistry within the area potentially affected. The goal would be to document what effect the river recharge, if it occurs, might have on local aquifer redox status. It could bring in additional organic matter present in the river water or mobilized from the fresh riverbank sediments, promoting reduction and As release in the deep aquifer. Alternatively, active recharge with river water could actually improve water quality in the aquifer if it carries a negligible content of organic matter and lowers total dissolved solids of the groundwater.

The finding in Chapter 3 that organic matter leaching from clay layers can reduce aquifer sediments calls for the assessment of the impact that clay layers have at greater depths in the low-As aquifer, in particular in the zone >150 m bgl where many wells are currently being installed. Older clay units, perhaps predating Pleistocene, could supply As and reductants to the deep aquifers as they are squeezed by ongoing subsidence in the Bengal basin due to both the natural processes of compaction and tectonic plate tilting at the convergence boundary, and the anthropogenic effect of deep pumping near major cities (see Erban et al., 2013 in Chapter 3). Deep drilling for sediment recovery, coupled to geologic studies of subsidence and deep well sampling campaigns, may be necessary in the region to elucidate this topic.

Other questions were also raised by the observations that intermediate aquifer hydraulic heads both decrease and experience less dry season disturbance from the shallow irrigation pumping as the lateral distance from a recharge window increases. It is not clear, for example, what hydrological conditions and aquifer hydraulic properties exactly control the lower hydraulic heads in the intermediate aquifer and how they respond to various stressors. It is also not clear whether more isolation from the shallow

aquifer, and presumably recharge and contaminant inputs, leads to lower As levels and better groundwater quality for human consumption. It would be of interest, therefore, to expand the area of study laterally to include more potential recharge windows, identified by a combination of drilling, high ^{3}H levels, and geophysical techniques, such as borehole logging and cross-hole resistivity imaging. The study could also be expanded to a slightly greater depth below the Pleistocene clay layers to evaluate the deep aquifer hydraulic pressure forcing. A flow model of 1-2 km scale might be able to identify exactly how distal deep pumping affects the transfer of hydraulic pressure to the intermediate aquifer and how it affects the flow between the shallow and intermediate aquifers. A clear picture of flow in the intermediate aquifer might also help answer other questions of both geochemical and hydrologic significance: how is the intermediate aquifer As and redox status affected by the penetration of recharge from the surface? Can a simple deployment of transducers simultaneously collecting pressure data from the shallow and intermediate aquifers be used to identify vulnerable areas of the intermediate aquifers? Could a close hydraulic connection to the shallow aquifer be easily identified by observing the water level difference between the aquifers and the amount of high-frequency pressure variations?

Lastly, the novel column method of studying As transport through aquifer sediments presented in Chapter 4 can be deployed in any area considered vulnerable to As intrusion. Low flow velocities should be used to avoid the concerns of kinetic limitations, while at the same time adequate experimental monitoring should be performed to ascertain no oxidative artifacts occur due to the longer residence time in columns. The estimates of As retardation based on our column experiments appear to be

in agreement with the field studies in West Bengal, central Bangladesh, and Vietnam, thus a generalizable As retardation could be used in some local assessments of aquifer sustainability. However, at locations where sediment or groundwater compositions are sufficiently different to raise reasonable doubts about the applicability of general As sorption parameters, As retardation could be assessed fairly efficiently with the column technique. For example, grey Pleistocene (and older) sediments in the basin have not been examined for their As sorption properties. As another example, groundwater might contain high levels of PO_4 that could compete with arsenite for adsorption sites, or unusually high concentrations of DOC could both interfere with As adsorption on Fe oxides and cause Fe mineralogical changes due to reductive processes.

In addition, the column method could be used for scientific purposes in general because of the ready availability of the sediment for characterization upon the elution-induced changes. For instance, one could study in real time and in more detail the mineral transformations of oxidized aquifer sediment caused by the inflow of groundwater with a significant reducing power. Such transformations have been suggested in numerous field studies, for example, in Vietnam (see van Geen et al, 2013) or in the upper intermediate aquifer of site M, both discussed in Chapter 3. In another example, the Fe mineral phase that formed under sulfate-reducing conditions, and that helped retain As in the low pore velocity columns of Chapter 4, could be better characterized and its stability and As sequestration properties better understood.

5.4 Final remarks

The ultimate question that drove my research was to what extent and how we can predict the vulnerability and sustainability of a low-As sedimentary aquifer in topographically flat river basins or deltas. My best answer would be to assess the factors that we currently know are the most important in determining the As status of sandy aquifers subject to a reducing environment: the subsurface geology, the patterns of groundwater flow to the aquifer in question, and the sources of organic matter (OM).

The source of OM is necessary to supply electron donors and cause anoxia coupled to reductive release of As from the sediment; without the organics, there would not be a problem, unless the location suffered from an unusual accumulation of arsenic-bearing minerals like sulfides. The OM could originate from the surface features such as the ponds filled with human waste, landfills, biologically productive wetlands or lowlands accumulating fresh sediment. For the surface sources of OM to matter, we also need a mode of delivering these organics to the depth via groundwater flow, i.e. downward hydraulic gradients and conductive sediments. However, the OM could also be sourced from an underground deposit, such as peats, organics in clay layers, or dispersed particulate matter in the aquifer. Some knowledge of the subsurface geology is thus necessary and a primary requirement in every case because it both determines the underground flow patterns and potentially hides additional sources of organic matter.

A particular attention should be paid to the low-conductivity units such as clays and peats. They could help on the one hand by diverting groundwater flow derived from the surface OM sources away from the aquifer, but on the other they could also contribute

organics to the system and cause or exacerbate sediment reduction. Thus, the lateral extent of clays, and their properties, such as the organic content and the potential modes of its delivery to the aquifer, must be evaluated. The absence of low-conductivity units could be beneficial in certain well-defined cases, for example if the surface sources of recharge would introduce oxic groundwater low in organics and As to the aquifer. Finally, the status of aquifer sediment is also important – if the source of OM and As and a method of their delivery have been identified, less reduced brown/orange sand might have potential to withstand the intrusion for a longer time. In such a case, if an unusual or extreme groundwater type is present, for example containing very high PO_4, DOC, SO_4, or HCO_3 concentrations, the retardation of As could also be experimentally determined to better inform the assessment.